Molecular studies of Stiff skin-causing mutations in fibrillin-1

Sarah Iqbal
Wolfson College
University of Oxford

A thesis submitted for the degree of
Doctor of Philosophy
Hilary Term 2011

Sarah Iqbal, Wolfson College, University of Oxford

A thesis submitted for the degree of Doctor of Philosophy, Hilary term 2011

ABSTRACT

Fibrillin-1 is the main component of the 10-12 nm microfibrils, which are found in several elastic and non-elastic tissues. Human fibrillin-1 contains multiple calcium-binding epidermal growth factor-like (cbEGF) domains interspersed with transforming growth factor β-binding protein-like (TB) domains. TB4 domain contains a flexible RGD loop which mediates cell adhesion *via* αVβ3, α5β1 and αVβ6 integrins. Mutations which introduce amino acid substitutions into TB4 are associated with a wide spectrum of diseases such as Marfan syndrome (MFS), ectopia lentis, Stiff skin syndrome (SSS). Amino acid substitutions such as W1570C, C1564S and C1577G in the TB4 domain have been found to cause SSS. The upstream TB5 domain has been predicted to modulate integrin binding and a deletion in the domain has been found in Weill-Marchesani syndrome (WMS), phenotype of which is similar to SSS (skin fibrosis and short stature), thereby suggesting that the underlying pathogenic mechanism might be similar.

This study has used cellular, biochemical and biophysical methods to investigate the effects of SSS substitutions C1564S and W1570C on domain structure and function and compared it to a MFS substitution C1564Y in the TB4 domain and WMS deletion in the TB5 domain. Effects of the SSS mutations on structure of the domains were studied using limited proteolysis, nuclear magnetic resonance spectroscopy and calcium chelation experiments. Subsequently, the ability of human fibroblasts to secrete wild-type and mutant fibrillin-1 was examined to identify the effect of the mutations on the trafficking of the protein. Finally, cell binding assays and SPR was employed to investigate the effect of disease-causing mutations on fibrillin-1/integrin interactions.

The results demonstrate that the SSS mutations affect TB4-cbEGF23 interface and calcium-binding to cbEGF23 but do not alter secretion of recombinant fibrillin-1 mutant fragments from the cell. On the other hand, intracellular retention was observed for MFS substitution C1564Y which was shown to be more susceptible to proteolysis than SSS substitution C1564S. WMS deletion also gives rise to partial retention of the recombinant fragment, suggesting a different pathogenic mechanism for these disorders. Cell binding assays and surface plasmon resonance (SPR) experiments show that SSS mutations affect binding to αvβ3 integrin, but not αvβ6 integrin suggesting that selectively impaired integrin interactions may contribute to pathogenesis of SSS.

Declaration

I declare that this work is entirely my own except where stated in the text:

- Assistance with recording the NMR spectra and resonance assignments was provided by Dr. Christina Redfield.
- DNA sequencing was carried out by the Department of Biochemistry Sequencing Facility.

Acknowledgements

I would like to express my deep and sincere gratitude to my supervisor, Prof Penny Handford for giving me the opportunity to work in her lab for my DPhil. Her wide knowledge and her logical and critical way of thinking have been of great value for me. Her understanding, encouragement and personal guidance have provided a good basis for the present thesis.

I owe my sincere gratitude to Dr Christina Redfield for her immense help with NMR and otherwise, during my DPhil.

I would like to thank Professor Helen Mardon for allowing me to work in her lab to carry out cell-binding experiments and for giving useful inputs for my project.

I am extremely grateful to Dr Sacha Jensen, for his undaunted supervision throughout my DPhil, for spending endless hours answering my naïve questions, fostering my biochemistry knowledge and without whom my DPhil would have been impossible. My heartfelt thanks to Dr Chandramouli Chillakuri for helping me with the cell-binding experiments and for always being there for scientific discussions.

I would really like to thank all the past and present members of Handford lab for making lab a great place to work and learn, and for their friendship and support. Special thanks to Pat, Jelena, Juliana, Joyce, Ralf, David, Paul, Philip, Shaoyan, Ian and Bun.

I would also like to thank the department DGS, Dr Mary Gregoriou for her help and advice and the department for funding my DPhil.

Finally, huge thanks to those without whom I could not have kept going. Thanks to all my lovely friends at Oxford who made my experience here at Oxford a really special and memorable one. Thanks to my friends and family in India and US for their love and cheer. My brother, Aman, for all his love, support, advise and without whom life at Oxford would not have been the same. Finally, I would like to thank my wonderful parents for their unconditional love, support and encouragement all throughout my DPhil and for helping me follow my dream, and without whom this would not have been possible. Love you all a lot.

Sarah Iqbal

CONTENTS

ABBREVIATIONS

APS	ammonium persulphate
ATP	adenosine triphosphate
bp	base pairs
A	adenine
Br_2BAPTA	5,5'-dibromo-1,2-bis-(2-aminophenoxy)ethane-N,N,N',N'-tetraacetic acid
BSA	bovine serum albumin
cbEGF	calcium-binding pidermal growth factor-like domain
cDNA	complementary DNA
Da	daltons
DNA	deoxyribonucleic acid
dNTP	deoxynucleoside 5' triphosphates
DTT	dithiothreitol
ECM	Extracellular matrix
EDTA	ethylenediaminetetraacetic acid
EGF	Epidermal growth factor
ELISA	Enzyme-Linked Immuno Sorbent Assay
ESI-MS	Electrospray ionisation mass spectral analysis
FBN	human fibrillin gene
FPLC	Fast Protein liquid chromatography
Gdn	guanidine
HPLC	high performance liquid chromatography
I	ionic strength
IPTG	isopropyl-β-D-thiogalactopyranoside
IPTG	Isopropyl β -thiogalacto-pyranoside
kb	kilobase

K_d	dissociation constant
kDa	kilo Dalton
LTBP	Latent TGF- β binding protein
mA	milliamp
mRNA	messenger RNA
MAGP	icrofibril associated glycoprotein
MFS	Marfan Syndrome
NMR	Nuclear Magnetic Resonance
NOE	nuclear Overhauser effect
NOESY	nuclear Overhauser effect spectroscopy
PAGE	polyacrylamide gel electrophoresis
PBS	phosphate buffered saline
PCR	Polymerase chain reaction
RGD	Arginine-Glycine-Aspartic acid, putative cell binding site
rpm	revolutions per minute
ppm	Parts per million
SA	Streptavidin
SDS PAGE	Sodium dodecyl sulphate polyacrylamide gel electrophoresis
SPR	surface plasmon resonance
SSS	Stiff Skin Syndrome
TBE	Tris-Borate-EDTA
TBS	Tris buffered saline
TB	Transforming growth factor □ binding protein-like domain
TFA	trifluoroacetic acid
Tsk	Tight Skin mouse
TGF-β	Transforming growth factor β
Tris	tris (hydroxymethyl) aminomethane
QH_2O	distilled water
1D	one dimensional

2D	two dimensional
UV	ultra-violet
V	volts
WMS	Weill-Marchesani syndrome
WT	wild type

Single letter code for amino acids

A	Alanine
C	Cysteine
D	Aspartic acid
E	Glutamic acid
F	Phenylanaline
G	Glycine
H	Histidine
I	Isoleucine
K	Lysine
L	Leucine
M	Methionine
N	Asparagine
P	Proline
Q	Glutamine
R	Arginine
S	Serine
T	Threonine
V	Valine
W	Tryptophan
X	Any amino acid
Y	Tyrosine

CHAPTER 1 Introduction

1.1 Introduction to Extracellular Matrix and the Fibrillin-rich Microfibrils

The extracellular matrix (ECM) is a complex entity found within all metazoan tissues that surrounds and supports cells. The ECM provides the architectural framework that establishes the organisational and physical properties of different tissues. It supplies structural signals that impart positional information to the surrounding cells and it regulates and modulates a variety of developmental and homeostatic events. The ECM has an active role in determining cellular fate and behaviour. Cell-matrix interactions have been implicated as a regulatory component in nearly every fundamental cellular activity including survival, growth, migration and differentiation. Therefore, cell-matrix interactions play key roles in physiological and pathological processes including embryonic development, wound healing, immune response, hemostasis and tumorigenesis (Bissell *et al.,* 1982; Ramirez *et al.,* 2007, 2009 & 2010).

The extracellular matrix is comprised of a complex mixture of different glycoproteins e.g. fibronectin, fibrillin, collagens and glycosaminoglycans (e.g. hyaluronan, dermatan sulphate, heparan sulphate etc.) and proteoglycans (e.g. aggrecan, perlecan, versican). Many of the ECM proteins are structurally related, as they share modules or domains that are associated with their multifunctional nature, such as epidermal growth factor (EGF)-like, complement-like, immunoglobulin-like, laminin-type EGF-like and fibronectin I, II and III-like domains. Modularity provides biological systems with a convenient way of presenting binding sites on a stable protein scaffold in the correct position for function and it also allows regulation by module rearrangement (Hohenester and Engel, 2002; Campbell, 2003). Any inherited or acquired defect to ECM components or metabolic disturbance in the ECM may cause cellular and tissue alterations leading to the development or progression of a disease.

The 10-12 nm diameter microfibrils are a class of ubiquitous extracellular filaments with a pivotal role in organising and connecting matrix components (Low, 1961, Low 1962). These microfibrils are a major constituent of elastic fibres, which also contain elastin, lysyl oxidase and accessory proteins such as the fibulins and microfibril-associated glycoproteins (MAGP) (Gibson MA *et al.,* 1986 & 1991). Elastic fibres are found in the skin, lungs, arteries, veins, elastic cartilage, periodontal ligament, foetal tissue and other structures. The 10-12 nm microfibrils are located primarily around the periphery of the amorphous elastin component of the elastic fibres, but can also occur independently in the absence of elastin (ciliary zonule and kidney) (Figure 1.1 A). They confer tensile strength to connective tissues, contribute to cell–matrix (with integrins; Pffaf *et al.,* 1996 and Sakamoto *et al.,* 1996) and matrix-matrix (with fibulins, heparan sulphate, fibronectin etc., Kinsey *et al.,* 2008; Cain *et al.,* 2005; El Hallous *et al.,* 2007) interactions and act as a store of cytokines *via* their interactions with the latent transforming growth factor β-binding proteins (LTBPs) and bone morphogenetic proteins (BMPs) (Isogai *et al.,* 2002, Gregory *et al.,* 2005) (Figure 1.1 B). Fibrillin-1 and fibrillin-2 are the major structural components of microfibrils (Sakai *et al*., 1986; Zhang *et al*., 1994). These heavily cross linked, insoluble macromolecular structures are proposed to be made up of a complex assembly of several proteins in addition to the fibrillin, including MAGPs and LTBPs, although fibrillin and MAGP-1 are thought to be the core components (Cain *et al.,* 2006). When viewed by rotary shadowing electron microscopy, microfibrils have a characteristic 'beads on a string' appearance with an average but variable inter-bead periodicity of ~56 nm (Bruns, 1984; Sakai *et al*., 1986; Keene *et al*., 1991; Kielty *et al*., 1991) (Figure 1.2).

Calcium plays a key role in maintaining the organisation of the fibrillin monomer (Reinhardt *et al.,* 1997) and fibrillin-rich microfibrils. This has been demonstrated by

removal of calcium from extracted microfibrils, which causes a reversible disruption in the structure of the inter-bead region. This region becomes diffuse and the bead-to-bead periodicity of the microfibrils decreases significantly despite the bead remaining intact. In addition, treated microfibrils display a marked increase in flexibility, frequently appearing curled in contrast to the extended appearance of untreated microfibrils. These are calcium-specific effects since they are only reversed upon re-introduction of calcium and not magnesium (Kielty and Shuttleworth 1993a; Cardy and Handford 1998; Wess *et al.,* 1998) (Figure 1.2). A study using a micro-needle technique performed on isolated microfibrils noted a 50% decrease in length and a reduction in stiffness of the microfibril in the absence of calcium, reinforcing the importance of calcium in microfibril assembly and integrity (Eriksen *et al.* 2001).

1.2 Fibrillins

Fibrillins are calcium-dependent glycoproteins which assemble to form connective tissue 10-12 nm microfibrils that provide structural support to the tissues. Fibrillin-1 and fibrillin-2 are the major structural components of 10-12 nm microfibrils. Three functional fibrillin genes have been identified in metazoan genomes. The function of fibrillin-3 is yet to be determined and it has been shown that a rodent homologue of the fibrillin-3 gene has been inactivated (Corson *et al.,* 2004). All three proteins have a similar modular structure with the only major sequence differences between the fibrillins residing in an internal domain, that is enriched with either proline residues (fibrillin-1) or glycine residues (fibrillin-2), or both proline and glycine residues (fibrillin-3). Furthermore, they vary in the number of integrin-binding Arg-Gly- Asp (RGD) sequences and putative glycosylation sites (Kielty *et al.,* 2005; Hubmacher *et al.,* 2006; Ramirez *et al.,* 2007). Gene expression data indicate that fibrillin-2 is generally produced during organ development

and tissue remodelling, but consistently in lower amounts than fibrillin-1, which continues to be produced throughout postnatal growth and in the adult organism (Zhang *et al.,* 1995; Quondamatteo *et al.,* 2002; Kelleher *et al.*, 2004). Many mutations in the fibrillin-1 gene lead to heritable connective tissue disorder such as the Marfan syndrome (MFS; McCusick 1993) which affects the cardiovascular, ocular and skeletal systems of the body and other fibrillinopathies with striking variations in phenotypes. Mutations affecting fibrillin-1 TB4 domain have recently been found in patients with Stiff skin syndrome (Loeys *et al.,* 2010). The clinical phenotype of this disorder is the opposite of MFS, where SSS patients have thickened skin, short stature and no cardiovascular, ocular or skeletal defects. Mutations found in fibrillin-2 gene give rise to Congenital Contractural Arachanodactyly (CCA) which affects the cardiovascular, skeletal and muscular systems. Recent studies have suggested a possible role of fibrillin-3 in the pathogenesis of Polycystic Ovary Syndrome (PCOS) (Jordan *et al.,* 2010)

1.2.1 Fibrillin-1 and its domain organisation

Fibrillin-1 is a large (350 kDa) extracellular glycoprotein that is the main component of the 10-12 nm microfibrils. The fibrillin-1 gene (*FBN1*) is found on chromosome 15 in humans and is expressed by connective tissue producing cells such as fibroblasts. Fibrillin-1 undergoes extensive post-translational modifications including disulphide bond formation, glycosylation and the N- and C- termini are processed and fibrillin-1 is secreted most likely as a monomer into the matrix where it forms 10-12 nm microfibrils (Figure 1.4). Human fibrillin-1 contains multiple calcium-binding epidermal growth factor-like (cbEGF) domains interspersed with transforming growth factor β-binding protein-like (TB) domain (Figure 1.3).

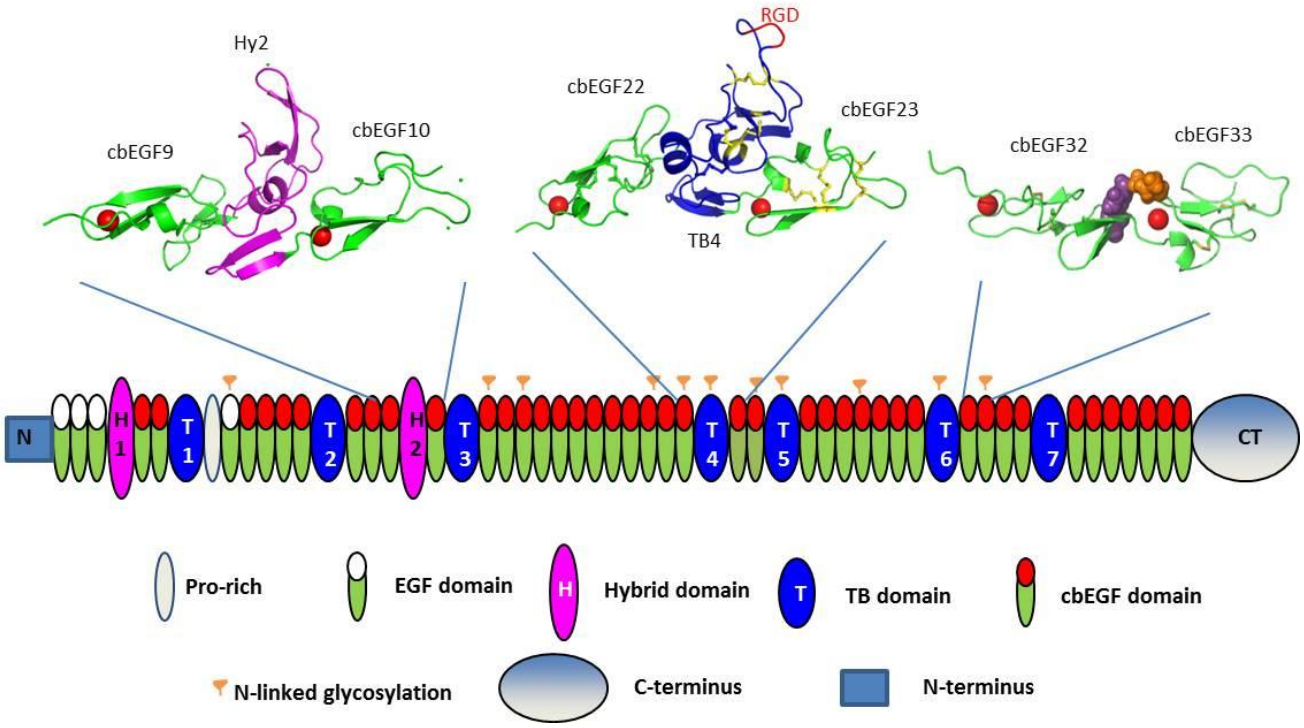

Figure 1.3 Modular organisation of fibrillin-1. *Above are known tertiary structures of cbEGF9-hyb2-cbEGF10, cbEGF22-TB4-cbEGF23 and cbEGF32-33 which were determined by X-ray crystallography and NMR (Jensen et al., 2009; Lee et al., 2004; Downing et al., 1996). Calcium ions are shown as a red spheres. The integrin binding RGD sequence in TB4 is also indicated. Multiple tandem repeats of cbEGFs are stabilised by calcium-binding sites located in the interdomain region. A range of biophysical and biochemical assays have demonstrated that calcium rigidifies the interdomain region, resulting in polypeptides that are resistant to proteolytic degradation. Figure was created using PyMOL software using the cbEGF22-TB4-cbEGF23 (PDB ID 1UZJ), cbEGF9-hyb2-cbEGF10 (PDB ID 2W86) and cbEGF32-33 construct coordinates.*

Each of the cbEGF domains contain three disulphide bonds, and the calcium binding consensus sequence (Handford *et al*., 1991; Mayhew *et al*., 1992). Each TB domain is folded into a compact globule with a significant hydrophobic core which is further stabilised by four disulphide bonds. Additional domains in fibrillin-1 are two hybrid domains, a unique proline-rich region and N- and C-terminal domains which have homology to domains in the LTBP family (Corson *et al.*, 1993; Pereira *et al.*, 1993; Saharinen *et al.*, 1999).

1.2.1.1 Epidermal growth factor-like domains

The EGF domain is a common structural motif found in cell surface and extracellular matrix proteins (Campbell *et al.,* 1993). Fibrillin-1 contains 47 EGF domains, 43 of which are of calcium binding (cbEGF) type. Figure 1.5 A illustrates the secondary structures of typical EGF and cbEGF domains. Each of the cbEGF domains contain six cysteine residues, forming three disulphide linkages in a 1-3, 2-4, 5-6 arrangement, and the calcium binding consensus sequence **D/N-X-D/N-E/Q-X$_m$-D*/N*-X$_n$-Y/F** (where *m* and *n* are variable and * indicates possible post-translational β-hydroxylation) (Handford *et al*., 1991; Mayhew *et al*., 1992). The secondary structure of a cbEGF module consists of a major and a minor double stranded anti-parallel β-sheet, located at the N-terminus and the C-terminus, respectively. A loop between the first and the second cysteine residues is sometimes observed to have α-helical character (Downing *et al*., 1996; Rao *et al*., 1999) (Figure 1.5 A). The biological importance of the EGF domains is highlighted by the widespread occurrence of these modules in functionally diverse proteins, where they are often arranged as multiple tandem repeats. These include ECM proteins (fibrillins 1 and 2, fibulins 1-5, LTBPs 1-4, nidogen), proteins involved in the control of blood coagulation (factors IX and X, proteins C and S, thrombomodulin) and cholesterol uptake (low density lipoprotein (LDL) receptor), and proteins involved in the specification of cell fate (Notch, Delta and Serrate). Calcium plays a pivotal role in the structure of fibrillin-1 and the supramolecular structure of the fibrillin-rich microfibrils (Kielty and Shuttleworth, 1993; Cardy and Handford, 1998). A major role of calcium binding in fibrillin is structural: ^{15}N backbone relaxation data for a fibrillin-1 cbEGF pair have shown that binding Ca^{2+} to the interdomain region between adjacent cbEGF repeats causes stretches of tandemly repeated cbEGF repeats to adopt a rigid, rod-like conformation (Downing *et al*., 1996;

Knott *et al*., 1996). Calcium binding also stabilises fibrillin-1 against proteolytic degradation (Reinhardt et al., 1997), and calcium is important for some of the recently described protein–protein interactions of fibrillin-1 (Reinhardt *et al.,* 2000; Jensen *et al*., 2001). MFS-causing mutations which alter calcium binding consensus residues can disrupt the rod-like organisation of tandem cbEGFs resulting in enhanced susceptibility to proteolysis or impaired protein-protein interactions and can affect the proper folding of the domain and secretion of fibrillin-1 (Knott *et al.,* 1996; Reinhardt *et al.,* 1997a; Whiteman *et al.,* 2003).

Calcium dissociation constants of the various heterologous and homologous cbEGF domain pairs of fibrillin-1 have been determined using techniques such as NMR, fluorimetry, chromophoric calcium chelation competition assays and equilibrium dialysis. It was evident from these studies that the calcium affinities of different cbEGF domains can vary markedly (Handford, 2000; Jensen *et al.,* 2005) and that the affinity of a particular cbEGF for calcium can be modulated by its local domain context (McGettrick *et al.,* 2000). cbEGFs at the C-terminus of a cbEGF-cbEGF pair were found to have much higher Ca^{2+} affinities compared to isolated cbEGF domains, probably because of the stabilisation of the Ca^{2+}- binding site by the presence of a preceding domain (Smallridge *et al.,* 1999; Werner *et al.*, 2000; Glanville *et al.*, 1994).

1.2.1.2 Transforming growth factor β (TGFβ)-binding protein-like domains

The transforming growth factor β (TGFβ)-binding protein-like (Bork *et al*., 1996) domain contains eight cysteine residues and is found in two protein families: the fibrillins and the LTBPs. These are both localised to extracellular matrix fibrils which are involved in extracellular matrix architecture and storage of latent TGF-β (Sakai *et al*., 1991; Dallas

et al., 1995; Taipale *et al*., 1996). The TB domain is composed of ~ 80 amino acids folded into a compact globule with a significant hydrophobic core and further stabilised by four disulphide bonds paired in a 1-3, 2-6, 4-7, 5-8 arrangement. The available solution and crystal structures of TB modules reveal the secondary structure to be comprised of four-stranded and two-stranded antiparallel β-sheets, and two α-helices (Figure 1.5 B) (Yuan *et al.,* 1998; Lee *et al.,* 2004).

The TB4 domains of fibrillin-1 and -2 contain an RGD (Arg-Gly-Asp) motif, which has been implicated as the major cell-binding epitope in the specific interaction between fibrillins and cell surface receptors of the integrin family (Pfaff *et al*., 1996; Sakamoto *et al*., 1996). The association of LTBP-1 with latent TGF-β1 is also mediated by a TB domain in LTBP-1(Gleizes *et al*., 1996; Saharinen *et al*., 1996). The discovery of MFS and Stiff skin-causing mutations affecting TB domains in human fibrillin-1 emphasises the biological significance of this module (reviewed in Dietz and Pyeritz, 1995; Ades *et al*., 1996; Collod-Béroud *et al*., 1997; Loeys *et al.,* 2010). The structural effects of these disease-causing mutations are not understood although it is plausible they could disrupt intra- or intermolecular associations either during microfibril assembly or, if properly assembled, with other components of the ECM. TB5 domain, which is in close proximity to the RGD-binding TB4 domain has been shown to bind to heparin sulphate and support cell adhesion (Bax *et al.,* 2007).

1.2.1.3 TB-cbEGF domain interactions

Previous investigations of the TB-cbEGF linker regions have suggested that they might have particular biological functions as their sequences are conserved between fibrillin-1 and -2. Fibrillin-1 contains 34 cbEGF-cbEGF, seven cbEGF-TB and six TB-cbEGF

linkages. Comparative alignments of linker regions from cbEGF-TB pairs within fibrillin-1 suggest that the relative orientation of cbEGF22-TB4 (Lee *et al.,* 2004) is preserved at homologous sites within fibrillin-1. On the other hand, the variation in amino acid number and composition of TB-cbEGF linkers suggests that these pairs may adopt different orientations with respect to one another within fibrillin-1 and may contribute to the biomechanical properties of microfibrils (Jensen *et al.,* 2005). Jensen *et al.* have shown that calcium affinity determination of the TB-cbEGF pairs is a more reliable method of measuring interdomain flexibility than analysing linker length alone. They also showed that most TB-cbEGF pairs bind Ca^{2+} more tightly than previously observed and therefore, most of the cbEGF domains in TB-cbEGF pairs will be fully saturated under physiological conditions (pH=7.4, $[Ca^{2+}]_{free}$~1.5 mM and *I*=0.15) and may impart rigidity to the native protein. This observation holds true for all the TB-cbEGF pairs in fibrillin-1 except for TB6-cbEGF32, which has low calcium affinity and greater flexibility and may contribute to the extensibility and elasticity of the microfibrils (Kettle *et al.,* 1999; Yuan *et al.,* 1997; Werner *et al.,* 2000). The crystal structure of cbEGF22-TB4-cbEGF23 (Lee *et al.,* 2004) and work performed on the TB4-cbEGF23 pair (Jensen *et al.,* 2005), gave an insight into the molecular basis for the unexpectedly high calcium affinity associated with the TB4-cbEGF23 fragment. Through the stabilisation of the calcium-binding site was achieved through extensive hydrophobic domain–domain interactions (Figure 1.5 B). These observations have major implications for the proposed models of fibrillin arrangement in microfibrils, since they restrict the number of possible conformations.

1.3 Fibrillin-1 assembles to form 10-12 nm microfibrils

The organisation of fibrillin-1 within microfibrils has been a topic of debate for several years because of the difficulty in developing *in vitro* assays to identify assembly

stages and the difficulty of extracting microfibrils in their native state from ECM. Structural analyses, epitope mapping and transglutaminase cross-link identification support a parallel alignment of fibrillin monomers within the microfibril, but do not distinguish between the currently proposed models of either a staggered or unstaggered arrangement (Reinhardt *et al*., 1996; Downing *et al*., 1996; Baldock *et al*., 2001; Lee *et al.,* 2004) (Figure 1.6 A).

The original ‘‘pleated’’ model by Baldock *et al.* (2001) proposed that the untensioned fibrillin monomer has an observed length of 150-180 nm, and the bead periodicity in microfibrils is just ~56 nm. The bends proposed in this model at TB7-cbEGF37 and at TB3-cbEGF11 by Baldock *et al.* (2001) seem improbable as both the pairs show high calcium affinities of cbEGF domains (Jensen *et al.,* 2005) and are likely to have significant interdomain interactions that make them more likely to show the extended structure as seen in the cbEGF22-TB4-cbEGF23 structure. A simpler staggered model described by Lee *et al*. (2004), does not require this folding. This model suggests a head-to-tail arrangement with an overlap of ~12 nm between successive molecules with a 1/3 staggered alignment, which would give the observed bead periodicity of ~56 nm. Another model of fibrillin-1 organisation in microfibrils proposed by Baldock *et al.* (2006) supersedes their previous “pleated” model which showed bends in the molecule and uses a new length of 90 nm for fibrillin-1 (Figure 1.6 B). The new model was derived using techniques such as SAXS (Small Angle X- ray Scattering) and MALLS (Multi Angle Laser Light Scattering) and suggests that the N- and C-termini overlap and reside at the beads, and domains TB4 to TB6 have a compact arrangement. The structural information gained in their previous model about the proline-rich region having a hinge-like structure, allowing the N-terminus of the fibrillin-1 molecule to fold back (Baldock *et al.,* 2001), is

reinforced by this model. This model proposes a mechanism for the molecular basis of extensibility of the microfibrils. Domain-domain conformational rearrangements could allow some regions like TB4 to TB6 to become more linear upon imposed force, which would enable the extension within the interbead region of microfibril. However, extensibility is accounted for in the Lee *et al.* (2004) model by reversible extension at TB-cbEGF linker. A more recent half-staggered model based on non-enzymatically extracted microfibrils whose periods are only rarely extended to 80 nm, proposes that fibrillins are half staggered with the N-terminal halves forming an outer surface on the microfibrils that mediates binding to multiple proteins (Figure 1.6 C; Kuo *et al.,* 2007). These studies underscore the importance of the highly conserved fibrillin-1 TB domains in microfibril assembly and further structural analysis and the study of their interaction with other ECM molecules might shed some light on how those interactions might be involved in microfibril assembly.

1.3.1 Involvement of other ECM molecules in microfibril assembly

Various extracellular matrix macromolecules and cell surface molecules associate with fibrillin-1 (Table 1.1). The functions of these macromolecules in the fibrillin-rich microfibrils can be of structural support to stabilise the interaction of fibrillin molecules within the microfibril; mediation of the interaction of adjacent microfibrils within bundles; assembly of elastin on the surface of the microfibrils; interfacing between the microfibrils and other structural elements of different matrices; modulation of the interaction of the microfibrils with cells to influence the deposition, orientation and organisation of microfibrils and elastic fibres in different tissue environments; provision and modulation of non-structural functions of the microfibrils e.g. TGF-β storage;

enzymatic activity, e.g. lysyl oxidase (involved in the cross-linking of tropoelastin monomers); and specific interactions with fibrillin-2-containing microfibrils (Marfan Syndrome: A Primer for Clinicians and Scientists by Mark Gibson).

Microfibril-associated glycoprotein-1 (MAGP-1) and -2 are well characterised and are specifically associated with microfibrils but have different issue distributions (Gibson *et al.,* 1998; Trask *et al.,* 2000). They have been shown to be covalently linked by disulphide bonds and transglutaminase cross-links to fibrillin-containing microfibrils. MAGP-2 has been shown to be involved in elastic fibre assembly (Lemaire *et al.,* 2006). A study by Cain *et al.* (2005) described how heparin and heparan sulphate glycosaminoglycans (HSPGs) regulated fibrillin-1 interactions with MAGP-1 and tropoelastin. HSPGs and fibronectin have been implicated in driving the initial pericellular steps of microfibril assembly *in vitro* (Kinsey *et al.,* 2008).

Depletion of fibronectin matrix assembly has shown to result in diminished fibrillin-1 microfibril assembly (Kinsey *et al.,* 2008). siRNA knockdown experiments have also demonstrated that the assembly of fibrillin-1 is strictly dependent on the presence of extracellular fibronectin fibrils (Sabatier *et al.,* 2009). Fibronectin is not present in lower metazoans, suggesting that fibrillin is not always dependent on these proteins for assembly (Robertson *et al.,* 2010)

Some studies have shown that a heparin-binding site of fibrillin-1 in TB5 domain synergises with the proximate RGD sequence in the TB4 domain and that inhibition of heparan sulphate attachment to core proteins or glycosaminoglycan sulphation disrupts microfibril assembly (Tiedemann *et al.,* 2001; Ritty *et al.,* 2003; Cain *et al.,* 2005; Bax *et al.,* 2007; Cain *et al.,* 2008).

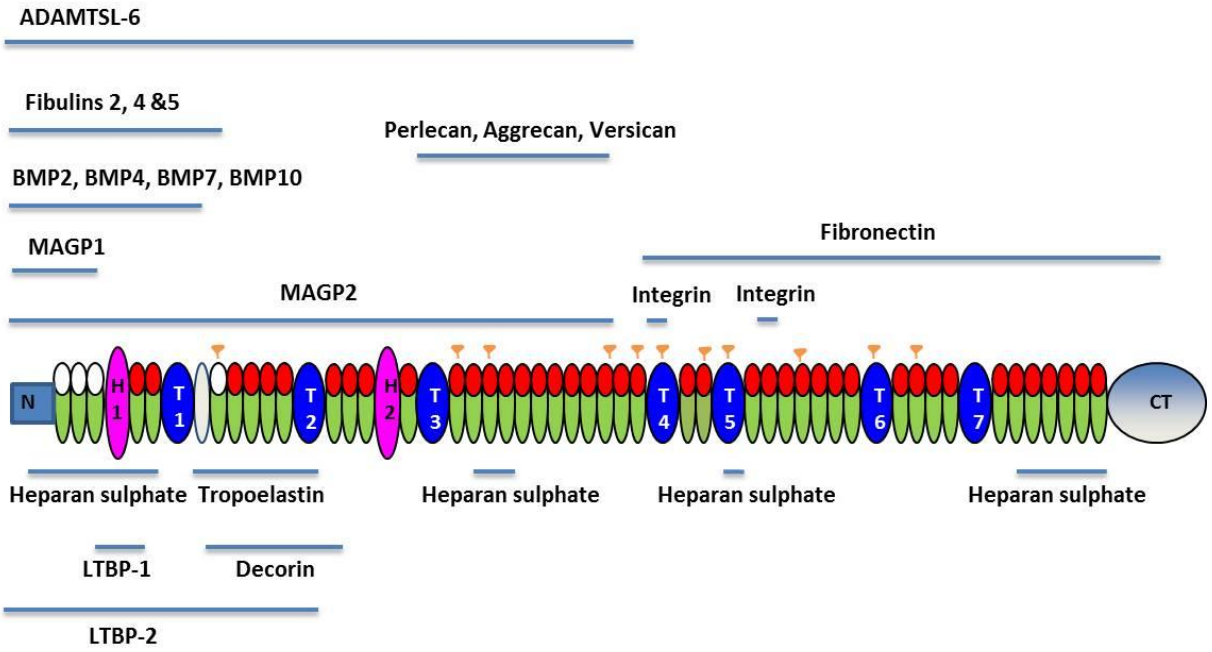

Figure 1.7 *Fibrillin-1 domain organisation showing different regions on the protein which interact with different ECM molecules. Blue bars represent the regions of fibrillin-1 to which the interactions have been mapped to. Minimal binding epitopes have not yet been identified in most cases and the region of fibrillin-1 indicated is a function of the construct used.*

Various A disintegrin And Metalloproteinase with Thrombospondin motifs-like (ADAMTSL) and ADAMTS proteins have been shown to associate with ECM molecules (Hirohata *et al.,* 2002). ADAMTS-1 and -4 are capable of binding to sulphated glycosaminoglycan chains and ADAMTSL-2 was recently shown to bind to LTBP-1 (Le Goff et al., 2008). Recent studies have shown ADAMTSL-6 to associate with fibrillin-1 microfibrils and promote microfibril assembly *in vitro* and *in vivo* (Tsutsui *et al.,* 2009*)*.

1.4 Fibrillin-1 microfibrils sequester cytokines in the matrix

Transforming growth factor β (TGF-β) is a pleiotropic cytokine which promotes fibroblast proliferation, differentiation, migration, adhesion and survival, induces cytokine secretion and upregulates synthesis of collagen and other extracellular matrix components. Increased TGF-β signalling has been implicated in many fibrotic and non-fibrotic disorders.

Fibrillin-rich microfibrils contribute to the extracellular regulation of endogenous TGFβ activity by providing a structural platform that controls the bioavailability of these ligands. TGFβ-1, −2, and −3 are each secreted either as a small latent complex (SLC) that consists of the bioactive homodimer non-covalently associated with its pro-peptide (latency-associated protein; LAP) or as a large latent complex (LLC) in which the SLC is covalently bound to LTBP−1, −3, or −4 (Rifkin 2005). LTBPs are structurally similar to fibrillins containing EGF, cbEGF and TB domains. Four N-terminal domains of fibrillin-1 have been shown to interact with three C-terminal domains *in vitro* and also with LTBP-4, in a tissue specific manner (Isogai *et al.,* 2002, 2003). Recent studies have shown that LTBP-1 associates with fibrillin during the assembly of microfibrils and that LTBP-1-associated microfibrils colocalise with fibronectin during the formation of higher-order networks (Dallas et al., 2000; Massam-Wu *et al.,* 2010). LTBP-1 association with fibrillin-1 is dependent on pericellular heparan sulphate (Massam-Wu *et al.,* 2010). Genetic studies in mice demonstrated that a deficiency of fibrillin microfibrils causes dysregulation of TGF-β activation and signalling, resulting in apoptosis in the developing lung (Neptune *et al*., 2003).

A reduction in the number of functional microfibrils significantly changes the targeting and sequestration of latent TGF- β. This leads to the pronounced TGF- β activation as seen in Marfan syndrome (MFS), a disease associated with mutations in fibrillin-1. Habashi *et al.* (2006) showed that aortic aneurysm in a mouse model of MFS is also associated with increased TGF- β signalling and can be prevented by TGF- β antagonists such as TGF- β -neutralizing antibody or the angiotensin II type 1 receptor (AT1) blocker, losartan. Collectively these studies, suggest a strong role for microfibrils in the regulation and storage of TGF- β.

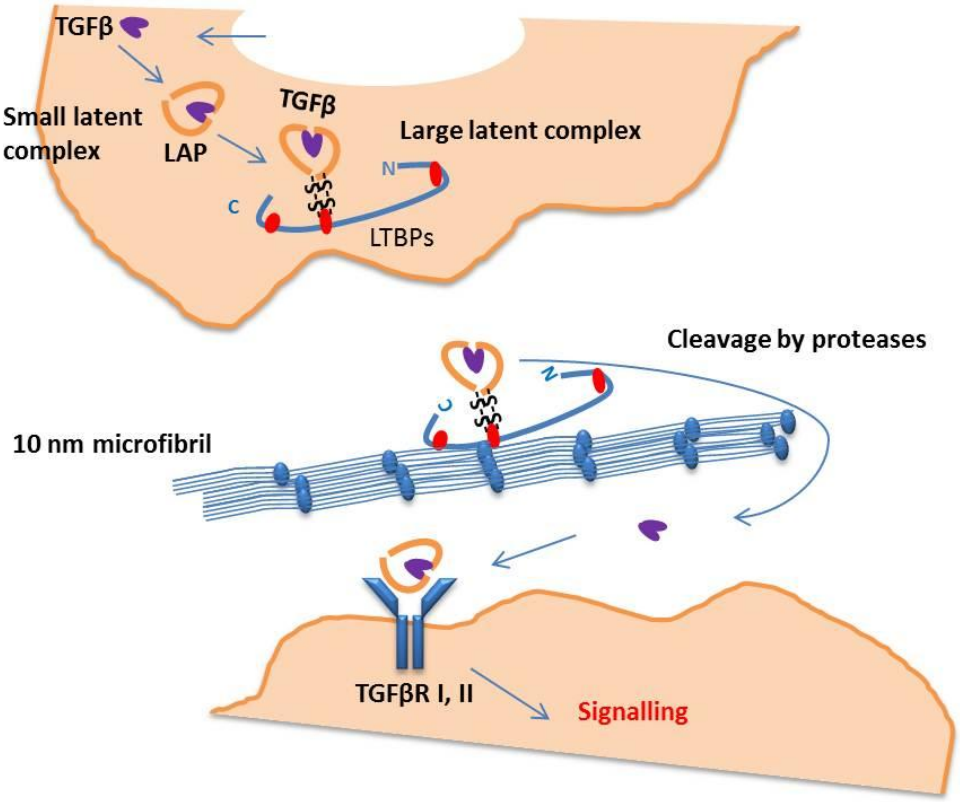

Figure 1.8 TGF-β sequestration by fibrillin-1 microfibrils and activation by ECM proteases. *The TGF-β activation process involves the release of the LLC from the matrix, followed by further proteolysis of the LAP to release TGF-β to its receptors. TGF-β can also be activated by integrins, reactive oxygen species and by pH changes. But the exact activation mechanism is still not known. Symbols: TGF-β- Transforming growth factor β; TGFβR- Transforming growth factor β receptor; LTBP- Latent transforming growth factor β-binding protein LAP- Latency associated peptide; LLC- Large latent complex*

BMPs are also stored in the ECM and synthesized as complexes containing pro-domains associated with bioactive dimers (Koenders *et al.,* 2009). These are targeted directly to microfibrils through noncovalent interactions between their pro-domains and the N-terminal regions of fibrillin-1 and −2 (Figure 1.7; Sengle *et al.,* 2008a). Microfibril-bound BMPs require proteolytic or non-proteolytic release from fibrillins in order to signal. BMP signalling can also be activated simply through the competitive displacement of the pro-domain by type II receptors (Sengle *et al.,* 2008b). BMP-7 and -4 have been shown to bind to fibrillin-1 *in vitro* (Gregory *et al.,* 2005). Several ECM molecules and

their binding to fibrillin-1 appear to influence fibrillin-directed control of endogenous TGF-β and BMP signalling, for e.g., fibronectin and different LTBPs bind fibrillin-1 and TGF-β with varying affinities.

1.5 Role of fibrillin-1 microfibrils in cell-matrix interactions

1.5.1 TB4 domain mediates cell adhesion to microfibrils

Apart from acting as structural scaffolds for elastogenesis and BMP/TGF-β storage, fibrillin-rich microfibrils have been found to be involved in cell adhesion (Pfaff *et al.*, 1996; Sakamoto *et al.*, 1996). Fibrillins contain an Arg-Gly-Asp (RGD) tripeptide which is a putative cell attachment motif (Pereira *et al.* 1993) (Figure 1.9). Integrins are heterodimeric transmembrane receptors that mediate cell adhesion to the ECM, usually through the characteristic RGD motif. They have widespread essential functions in development, tissue organisation, and the immune system (Humphries *et al.,* 2002; Shattil *et al.,* 2010). Integrin-mediated cell interactions regulate cell adhesion and migration and initiate signalling pathways that lead to reorganisation of the actin cytoskeleton, cellular proliferative and secretory responses, growth, differentiation and apoptosis. Integrin interactions are likely to be particularly important in tissues where microfibrils are in close proximity to cells, such as in the elastic lamellae of arteries, and may play a role in the assembly of the microfibril network.

Fibrillin-1 contains one RGD sequence in the fourth TB module (Pereira *et al.,* 1993). Fibrillin-2 contains two RGD sequences, one in the fourth TB module as in fibrillin-1 and the other in the third TB module where it is surrounded by hydrophobic amino acids (Zhang *et al*., 1994).

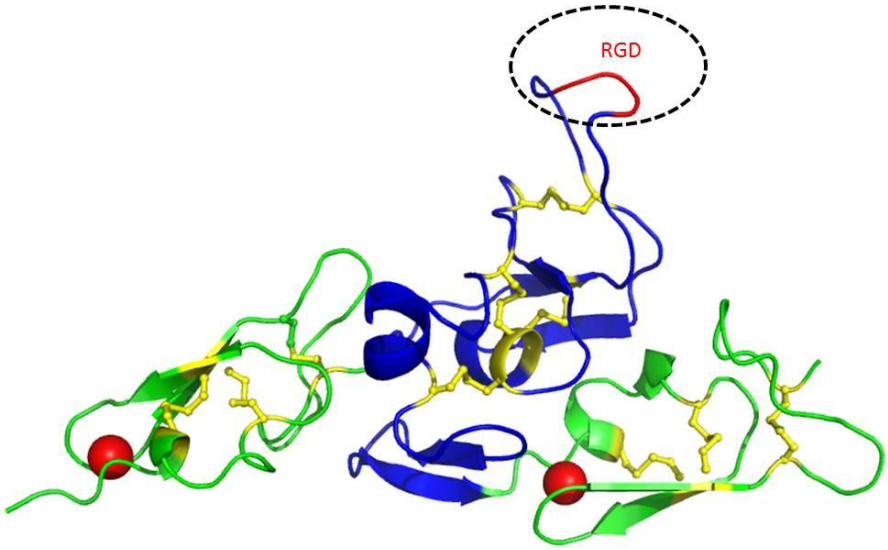

Figure 1.9 *Crystal structure of cbEGF22-TB4-cbEGF23 showing the integrin binding RGD motif present on the flexible loop (Lee et al., 2004). This motif has been shown to interact with αVβ3, αVβ6 and α5β1 integrins with varying affinities. Figure was created using PyMOL software using the cbEGF22-TB4-cbEGF23 triple domain construct coordinates (Lee et al., 2004).TB4 domain is coloured blue and the cbEGF22 and 23 domains are shown in green. Integrin binding RGD motif is shown in red.*

A recently found fibrillin-3 also has two RGD sequences, one in the 19th cbEGF repeat and a second in the fourth TB module (Nagase *et al*., 2001). In fibrillin-1 the RGD motif in TB4 domain lies in a 10 residue flexible loop, which makes it available for cellular interactions (Lee *et al.,* 2004). The RGD in the third TB motif in fibrillin-2 does not mediate cell adhesion, probably due to its inaccessibility (Sakamoto *et al.,* 1996; Yuan *et al.,* 1997).

The triple domain fragment of fibrillin-1 cbEGF22-TB4-cbEGF23 has been shown to bind αVβ3, αVβ6 and α5β1 integrins with varying affinities (Figure 1.9; Lee *et al.,* 2004; Jovanovic *et al.,* 2007) with αVβ3 having the highest affinity (K_d~40 nM). These integrins display different substrate specificity. For example, αVβ3 requires TB4 to be presented as a cbEGF22-TB4 domain pair to achieve a high affinity interaction, whereas αVβ6 does not require cbEGF22 (Jovanovic *et al.,* 2007). Epithelial restricted integrin αVβ6 integrin and its interaction with fibrillin-1 in the dermal-epidermal junction is likely to be important in

anchoring epidermal cells to the dermis during development (Jovanovic *et al.,* 2007). These interactions may influence cellular functions *via* signalling pathways controlled by the integrins. Although there are no naturally found mutations which directly change RGD, mutations affecting residues within the TB4 domain might directly affect integrin binding.

1.5.1.1 Integrin signalling: cell adhesion formation

An integrin molecule is composed of two noncovalently associated transmembrane glycoprotein subunits called α and β. A variety of human integrin heterodimers are formed from 9 types of β subunits and 24 types of α subunits. This diversity is further increased by alternative splicing of some integrin RNAs. The same integrin molecule in different cell types can have different ligand-binding specificities.

Three different integrin conformations have been identified so far; inactive, bent conformation (Xiong, *et al.,* 2001; Zhu *et al.,* 2008), active (or primed), an extended form with a closed headpiece, and ligand bound, extended form with an open headpiece, respectively (Takagi *et al.,* 2002). The opening of the headpiece is predicted to induce separation of the integrin subunit legs that allows intracellular signalling molecules to bind during the process of outside-in signalling (Mould *et al.,* 2003; Xiao *et al.,* 2004; Puklin- Faucher *et al.,* 2006). After the integrin binds to its ligand in the matrix, the cytoplasmic tail of the β subunit binds to several intracellular anchor proteins, including talin, α-actinin, and filamin. These proteins bind directly to actin or to other anchor proteins such as vinculin, thereby linking the integrin to actin filaments in the cell cortex. Given the right conditions, this linkage leads to a clustering of the integrins and the formation of focal adhesions between the cell and the extracellular matrix. The specific binding of the extracellular domains of integrins to ECM proteins which support cell

adhesion, is crucial for embryonic development, tissue maintenance and repair, host defence and haemostasis. These processes depend on the linkage of integrins to the intracellular cytoskeleton through the generally short integrin cytoplasmic tails; such linkage permits the bi-directional transmission of force across the plasma membrane (Figure 1.10 Calderwood *et al.,* 2000; Evans and Calderwood, 2007). In addition to their mechanical roles in cell anchorage, integrins transmit chemical signals into the cell (outside-in signalling), providing information on its location, local environment, adhesive state and surrounding matrix (Hynes, 2002; Miranti and Brugge, 2002). These signals determine cellular responses such as migration, survival, differentiation and motility. In addition to outside-in signalling, integrins can regulate their affinity for extracellular ligands. They do this by undergoing conformational changes in their extracellular domains that occur in response to signals that impinge upon the integrin cytoplasmic tails – a process that is termed inside-out signalling or activation (Calderwood, 2004; Wegner *et al.,* 2007).

Integrin activation comprises triggering events, intermediate signalling events and, finally, the interaction of integrins with cytoplasmic regulators, which changes an integrin's affinity for its ligands (Shattil *et al.,* 2010). When cells attach to ECM, lateral diffusion and clustering of integrins promote the assembly of actin-associated signalling complexes: focal complexes and focal adhesions, which are visible by light microscopy (Kucik *et al*., 1996; Zamir and Geiger, 2001). One of the first integrin signalling molecules to be identified was focal adhesion kinase (FAK), which acts as a phosphorylation-regulated signalling scaffold and is important for adhesion turnover, Rho-family GTPase activation, cell migration and cross-talk between growth-factor signalling and integrins (Mitra *et al.,* 2005). When integrins cluster at sites where the cell and matrix contact, FAK

is recruited to focal adhesions by intracellular anchor proteins such as talin, which binds to the integrin β subunit, or paxillin, which binds to one type of integrin α subunit. The clustered FAK molecules cross-phosphorylate each other on a specific tyrosine, creating a phosphotyrosine docking site for members of the Src family of cytoplasmic tyrosine kinases. These kinases then phosphorylate FAK on additional tyrosines, creating docking sites for a variety of intracellular signalling proteins; they also phosphorylate other proteins at focal adhesions. In this way, the signal is transmitted into the cell. ECM-integrin interactions through the formation of FAKs are extremely crucial in regulating cell polarity, survival and proliferation, cytoskeletal structure and expression of different genes.

Specialised cells are surrounded by different combinations of ECM proteins and express an array of tissue-specific integrin receptors and this diversity may present one way to generate unique intracellular signals that give rise to tissue-specific phenotypes.

1.5.1.2 Implications of Integrin/TGF-β interactions for ECM organisation

TGF-β controls the transcription of genes that encode numerous integrins (Table 1.2) in several cell types and tissues, as well as in various human cancers and fibrotic disorders (Margadant *et al.,* 2010). The LAPs of TGF-β1 and TGF-β3—but not of TGF-β2—contain an RGD motif that can potentially be bound by the five αv-containing integrins and αIIbβ3, α5β1 and α8β1. Integrin binding to LAP has been demonstrated formally for α8β1 and all αv-integrins, although binding of α8β1 does not seem to lead to activation, and whether αvβ1 can activate TGF-β is also unclear (Table 1.2; Munger *et al,* 1999; Lu *et al,* 2002; Ludbrook *et al,* 2003). Whether activation of TGF-β is *via* its interaction with integrins or *via* its proteolytic release from LTBP-1 (Figure 1.8), is still not very well

understood. αvβ3-mediated or αvβ5-mediated TGF-β activation could be important in pathological conditions, as increased expression of both of these integrins is observed in the dermis of scleroderma patients, and these integrins elicit autocrine TGF-β signalling in patient fibroblasts *in vitro* (Asano *et al,* 2005a, 2006a). TGF-β-induced collagen expression through p42/p44 MAPK (Mitogen-Activated Protein Kinase) requires integrin-mediated FAK activation in mesangial cells (Hayashida *et al,* 2007). Since, fibrillin-1 mediates cell adhesion *via* binding to integrins and also acts as a store for cytokines, understanding these various protein-protein interactions would be useful in understanding mechanisms underlying different pathologies involving these molecules.

Table 1.2 *Integrin* αvβ3, αvβ6 and α5β1 *mediated activation of TGF*-β.

Integrin	Cell-type	Regulation of TGF-β activation or signalling	Context
αvβ3	Fibroblasts, carcinoma cells, endothelial cells	TGF-β activation *in vitro*, modulation of TGF-β signalling by physical association with TGF-βRII, control of expression of TGF-βRI and II	Regulation of granulation tissue during wound healing, carcinoma cell migration and invasion, possible role in systemic sclerosis/scleroderma
αvβ5	Keratinocytes, fibroblasts	TGF-β activation *in vitro* and *in vivo*, enhancement of TGF-β signalling by physical association with TGF-βRII	Pulmonary fibrosis, possible role in Systemic sclerosis/scleroderma
αvβ6	Keratinocytes, fibroblasts, carcinoma cells,	TGF-β activation *in vitro* and *in vivo*	Development, idiopathic pulmonary fibrosis, kidney and renal fibrosis, systemic sclerosis, wound healing, epithelial-to-mesenchymal transition, carcinoma migration and invasion
αvβ8	---	TGF-β activation *in vitro* and *in vivo*	Development, suppression of T-cell-mediated immunity, possible role in COPD or wound healing
α5β1	Keratinocytes, fibroblasts, carcinoma cells, endothelial cells	Control of TGF-βRII expression, binding and activation of LAP	Re-epithelialization during wound healing, epithelial-to-mesenchymal transition, cancer cell migration and invasion, endothelial cell migration and tube formation

Adapted from Margadant *et al.,* 2010

1.5.2 Interaction with cell surface proteoglycans

In addition to interacting with integrins, fibrillin-1 has been shown to mediate cell-matrix interactions through heparin sulphate proteoglycans (HSPGs) such as members of the syndecan or glypican families. Four heparin/heparan sulphate-binding sites have been mapped in fibrillin-1 (Figure 1.7). Syndecans are type I transmembrane proteins present in both invertebrates and vertebrates and contain a core protein modified with glycosaminoglycan chains, most commonly heparan sulphate. They can interact with heparan sulphate, collagens and glycoproteins of the extracellular matrix and a range of other molecules in the ECM. They are referred to as co-receptors because they generally work along with other molecules, mainly integrins (Morgan *et al.,* 2007). Syndecans are considered to have important roles during development, wound healing, inflammation and tumour progression. There are four known syndecans present in vertebrates, namely, -1, -2, -3 and -4 (Bernfield et al., 1992; Carey *et al.,* 1997). Out of the four syndecans syndecan-4 has a wide distribution and has been studied extensively. Syndecan-4 null mouse fibroblasts are defective in focal adhesion formation on fibrillin-1 fragments that encompass the TB4 and TB5 modules, indicating the similarity of responses to integrin and heparin-binding sites to those seen in fibronectin (Bax *et al.,* 2007). On the other hand, syndecan-4 null mouse fibroblasts can form some adhesion plaques on fibrillin-1 N- and C- terminal fragments which contain high affinity heparin-binding sites (Cain *et al.,* 2008). Heparin-binding to fibrillin-1 N- and C- terminal might be involved in fibrillin assembly in microfibrils and elastic fibres.

1.6 Diseases caused by mutations in fibrillin-1

1.6.1 Marfan Syndrome

Mutations in the fibrillin-1 (*FBN1*) gene have been found to cause Marfan Syndrome, a pleiotropic autosomal dominant disorder of the fibrous connective tissue with highly variable clinical manifestations including aortic dilation and dissection, ectopia lentis, skeletal anomalies such as scoliosis, pectus deformities, arachanodactyly and a characteristic Marfan syndrome habitus dolichostenomelia (long, thin extremities) (Figure 1.11). The different pathogenic mechanisms proposed that could contribute to MFS, includes reduction in the amount of fibrillin produced from the cell, inhibition of microfibril assembly, and production of abnormal microfibrils (Figure 1.12).

A central region of fibrillin-1 (exons 24 –32), often referred to as the "neonatal region", is a hotspot for mutations which give rise to the early lethal neonatal form of Marfan syndrome (nMFS) (Tiecke *et al*., 2001). The neonatal region interacts with elastin (Rock *et al.* 2004), and has been suggested to localise to the microfibril interbead region (Mecham *et al.,* 1994; Sherrat *et al*., 2003). However the precise cause of nMFS has not been proven and some mutations affecting this region cause classic disease.

Most missense mutations in cbEGF modules lead to a substitution of one of the six highly conserved cysteine residues and the second most common missense mutation affects residues of the calcium binding consensus sequence. Mutations affecting the conserved cysteine residues disrupt one of the three disulphide bonds of affected cbEGF modules and cause domain misfolding and loss of calcium binding with secondary deleterious effects on the structure and proteolytic susceptibility of fibrillin (Suk *et al.,* 2004; Reinhardt *et al.,* 1997). Mutations resulting in changes to residues implicated in

calcium binding result in loss of rigidity and increased protease susceptibility and may abrogate specific protein-protein interactions. Furthermore, they may also affect domain folding (Whiteman et al., 1998, 2001, 2003). Mutations affecting other residues of cbEGF domain are rarer, including those predicted to create a novel N-glycosylation site (Lonnqvist *et al.,* 1996), a mutation affecting a conserved glycine involved in domain–domain packing between two cbEGF modules (Downing *et al.*, 1996), and a number of mutations of non-conserved residues (Collod-Béroud *et al*., 1997).

Booms *et al.* (2004) suggested that *FBN1* mutations that an increase in the susceptibility of entire microfibrils to proteolytic degradation can then in turn lead to fragmentation of microfibrils in affected tissues. This hypothesis is supported by studies which have given clear evidence of microfibrillar fragmentation in tissues of MFS patients (Fleischer *et al*., 1997), and an increase in concentration of matrix metalloproteinase (MMP). Fibrillin-1 is susceptible to digestion by several MMPs and various studies have shown that fibrillin-1 fragments containing an RGD binding site can upregulate the expression and production of MMPs (Booms *et al.,* 2005). Therefore, the constant presence of fibrillin-1 fragments could lead to increased MMP production which in turn could be involved in the progressive breakdown of microfibrils and play a role in MFS.

Haploinsufficiency can contribute to reaching the threshold loss of microfibril function needed for clinical expression of MFS (Hutchinson *et al.,* 2003; Judge *et al.,* 2004). While imposed reduction in microfibril abundance may or may not be sufficient, in isolation, to lead to classic MFS, it appears critical to the context within which a dominant negative effect can achieve clinical significance (Robinson *et al.,* 2006). These studies give rise to the possibility of boosting fibrillin-1 expression, which may be a useful therapeutic strategy.

Mouse models of MFS have been instrumental in modifying the long-held belief that MFS is a classic dominant-negative disorder, in which the abnormal protein derived from the mutant allele functionally "neutralises" the normal protein produced from the wild type allele. They have revealed other functions of ECM microfibrils in orchestrating critical cellular and morphogenetic functions *via* TGFβ and BMP sequestration/regulation (Section 1.5). Studies on mouse models show that a normal amount of fibrillin-1 is needed for elastic fibre homeostasis, rather than formation and may be needed to initiate productive microfibrillar assembly (Pereira *et al.,* 1997 and 1999, Bunton *et al.,* 2001). Excess TGFβ signalling drives aortic aneurysm in MFS, while its attenuation by TGFβ neutralizing antibody (TGFβNAb) or losartan (an angiotensin II receptor antagonist drug) prevents aneurysm progression (Matt *et al.,* 2009).

1.6.1.1 Other MFS-related fibrillinopathies

In addition to mutations found in patients with classical MFS-phenotypes, *FBN1* mutations have been found in a series of related connective tissue disorders which are termed Type I fibrillinopathies (Table 1.3). Mutations have been found in the closely related LTBP family of proteins and in TGFβ receptor type I or II (Loeys-Dietz aortic aneurysm syndrome), giving rise to disease whose clinical features overlap with the MFS phenotype (Loeys *et al*., 2006; Singh *et al.,* 2006). Patients with homocystinuria (HC), a metabolic disorder that affects methionine metabolism, often exhibit phenotypic abnormalities similar to MFS. It was suggested that the HC phenotype is caused by chemical reduction of disulphide bonds within fibrillin-1 domain, due to high circulating concentration of HC, resulting in the loss of native structure (Hutchinson *et al.,* 2005). Also, mutations in ADAMTSL4 have recently been associated with ectopia lentis which is a

one of the main features of Marfan syndrome (Ahram *et al.,* 2009). Because of this overlap in clinical features, diagnosis is made according to strict clinical criteria (Revised Ghent criteria; Loeys *et al.,* 2010).

1.6.2 Stiff skin syndrome

Apart from MFS, mutations in fibrillin-1 have recently been associated with Stiff Skin Syndrome (SSS; MIM #184900; Table 1.4), which is a congenital autosomal dominant form of scleroderma. *FBN1* mutations resulting in substitutions W1570C, C1564S and C1577G within the TB4 domain of fibrillin-1 have been described (Loeys *et al.,* 2010). TB4 is the only domain within fibrillin-1 which contains an RGD sequence that mediates integrin binding. The domain-specific nature and unique phenotypic outcome of SSS mutations suggests a different pathogenic mechanism from that of MFS. In MFS, a "loss-of-function" mechanism of fibrillin-1 mutations is seen resulting in effects on the cardiovascular, skeletal or ocular systems. In contrast SSS has no observed effect on these organ systems but is skin-specific and suggestive of a "gain-of-function" mechanism which results in over-production of the ECM. Fibrosis is a process in which excess fibrous connective tissue forms and is characterized by the accumulation of fibrillar collagens although other ECM components are also over produced. Fibrosis is initiated and maintained by different mechanisms in various tissues involving organ-specific mechanisms and cell type specific signalling events. The molecular pathogenic mechanisms of lung fibrosis (Fernandes *et al.,* 2006) are, for example, different from renal fibrosis (Pozzi *et al.,* 2009).

First described by Esterly and McKusick in 1971, SSS is characterised by stony-hard skin, mild hypertrichosis, and limitation of joint mobility as a result of an accumulation of

ECM (fibrosis). In SSS patients indurations usually appear on the buttocks, and slowly involve the limbs and trunk (Figure 1.13). Other occasional findings include focal lipodystrophy and muscle weakness. About forty cases have been reported in the literature (DiRocco 2001; Loeys *et al.,* 2010). SSS skin shows disorganized macroaggregates of fibrillin-1 that fails to contact neighbouring cells at the dermal-epidermal junction similar to that in Systemic Sclerosis (SSc). Skin biopsies from patients with SSS revealed increased deposition of both fibrillin-1 and elastin in the dermis, when compared to age- and gender-matched control samples. Although both patients and controls showed accumulation of microfibrils at the dermal-epidermal junction, these microfibrillar bundles had a stubby appearance in SSS, without the deep projections into the underlying dermis seen in controls (Figure 1.14). Dermal deposition of elastin was seen immediately adjacent to the epidermis in SSS, a zone that shows relative exclusion of elastin in controls (Figure 1.14). These data suggest that pathogenic events in SSS may alter the amount and architecture of microfibrillar deposits and are abnormally permissive for the association of fibrillin-1 and elastin at the dermal-epidermal junction (Loeys *et al.,* 2010).

Excessive TGF-β activity is a common feature of a number of fibrotic disorders (Branton & Kropp 1999). An increased nuclear accumulation of phosphorylated Smad2 (pSmad2) and expression of connective tissue growth factor (CTGF), a direct effector and a target of TGF-β signalling, respectively, was observed in the dermis of SSS patients compared to controls (Loeys *et al.,* 2010). Blocking the TGF-β pathway might have adverse effects on immunity and tissue repair and therefore looking at other molecules involved in the disease-causing mechanism as therapeutic targets might be useful in these disorders.

1.6.3 Fibrillin-1 in other fibrotic disorders

Fibrillin-1 has also been shown to be involved in other fibrotic disorders including systemic sclerosis (SSc) or scleroderma (Table 1.4) where fibrillin-1 autoantibodies were seen in patients. A genetic association study suggested a link between variation at the *FBN1* locus and scleroderma in Choctaw Indians (Tan FK *et al.,* 1999), however no pathogenic mutation has been identified. The autosomal dominant form of Weill-Marchesani Syndrome (WMS; MIM #277600) is a fibrotic disorder caused by a small deletion in the TB5 domain of fibrillin-1 (Faivre *et al.,* 2003). This domain has heparan sulphate binding residues which were shown to modulate integrin binding to the TB4 domain of fibrillin-1 (Bax *et al.,* 2007). The recessive form of WMS is caused by mutations in the gene encoding ADAMTS10 (Faivre *et al.,* 2003). The phenotype of WMS is similar to that of SSS patients, short stature, thick skin, joint stiffness, brachydactyly but with the exception of ocular defects involving, anterior dislocation of the ocular lens with severe glaucoma, which is also a feature of MFS. Mutations in another gene encoding ADAMTSL2 have been found in patients of geleophysic dysplasia, an autosomal recessive disorder characterized by short stature, brachydactyly, thick skin, and cardiac valvular anomalies (Le Goff *et al.,* 2009). These similarities in phenotype strongly suggest that there might be a functional link between ADAMTS proteins and microfibril networks containing fibrillin-1. The SSS phenotype is also very similar to the phenotype of the *Tsk* mouse (thickened skin), which has a naturally occurring in-frame duplication of exons 17-40 of the murine fibrillin-1 gene. The mutant fibrillin molecule contains an extra RGD cell recognition site as well as duplicated flanking regions, as shown in figure 1.15.

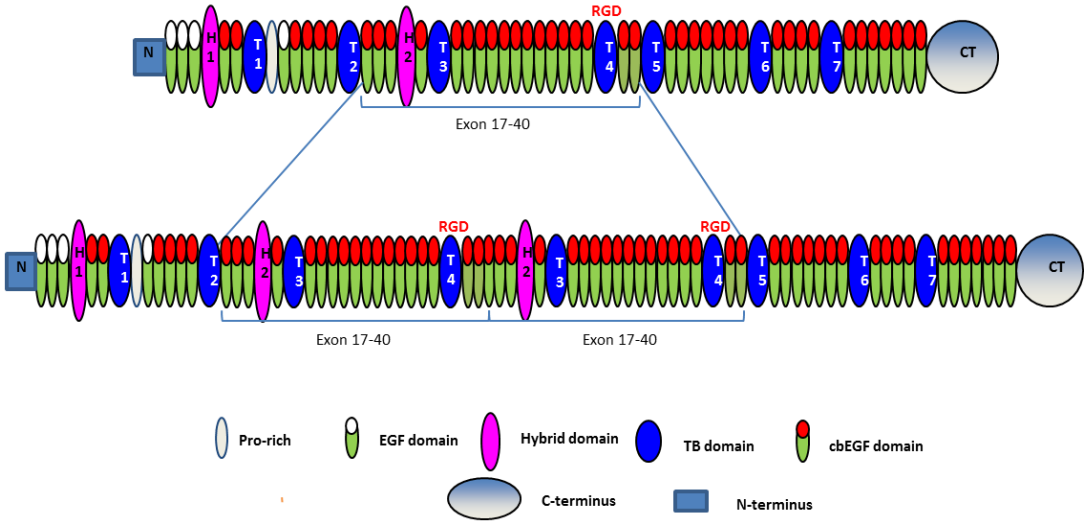

Figure 1.15 *Murine fibrillin-1 domain organisation showing duplication of region encompassing domains cbEGF7-cbEGF24 (exon 17-40) which gives rise to Tsk phenotype (Siracuse et al., 1996)*

The similarity in the phenotypes of the *Tsk* mouse (skin fibrosis) with WMS patients (skin fibrosis and short stature) and SSS suggests that the pathogenic mechanisms involved might be related and may be due to disturbed cell-matrix interactions rather than a loss of microfibrils. Immunohistochemical analysis of stained tissue samples of SSS patients, show that fibrillin-1 fails to contact neighbouring cells at the dermal-epidermal junction, suggesting altered interactions with skin-specific cell matrix molecules.

Several studies have implicated aberrant integrin expression or function in SSc and other fibrotic phenotypes. In culture, integrin αvβ3 is upregulated in SSc dermal fibroblasts. Furthermore, its inhibition prevents collagen expression and reverses the myofibroblastic phenotype of SSc fibroblasts in a TGFβ-1–dependent manner (Asano *et al.,* 2005). Since, SSS missense mutations have been found to affect the integrin-binding TB4 domain of fibrillin-1, it is possible that defective interaction with integrins in SSS might induce increased integrin expression and/or bioavailability to participate in TGF-β activation, and that this might contribute to downstream events leading to tissue fibrosis. However, defective interactions of fibrillin-1 with other skin specific ECM molecules could also possibly be involved in the pathogenesis of SSS.

1.7 Thesis Aim

The aim of this thesis is to study the effects of Stiff skin syndrome-causing mutations (W1570C and C1564S) on the structure and function of TB4 domain. A Marfan syndrome-causing substitution (C1564Y) in the same domain and a Weill-Marchesani syndrome deletion in the TB5 domain which results in a clinical phenotype (fibrosis) similar to SSS, will also be investigated alongside the SSS mutations to see if there is a difference in the underlying molecular effects which might provide an explanation for the vastly different phenotypes. Various biochemical, biophysical and cell-based assays will be used to examine the effects of the SSS mutations on local structure, and the interaction with integrins. The aims of this study are as follows:

- To study local effects of mutations on structure of TB4 and adjacent regions.
- To study effects of mutations on ability of recombinant fragments to be secreted.
- To study patient cell lines and their ability to form a microfibril network.
- To study the effects of mutations on integrin binding using combination of cell based and molecular assays.

Collectively these should give insight into the molecular mechanism underlying SSS and why mutations in *FBN1* can give rise to such diverse phenotypes. Finally, these data and the potential physiological relevance of the novel findings are discussed in view of the present understanding of SSS and related disorders.

CHAPTER 2 Materials & Methods

2.1 DNA cloning

2.1.1 Amplification by the polymerase chain reaction (PCR)

PCR amplifications were carried out in 0.5 ml thin wall PCR tubes using a Biometra T3 Thermocycler. Reactions were performed with *Taq* DNA polymerase (Roche Diagnostics) or *Pfu* DNA polymerase (Stratagene) in a total volume of 50 µl containing template DNA and primers (see relevant sections for concentrations), 200 µM dNTPs, 1 × PCR buffer (Roche Diagnostics) and 2-2.5 U of the DNA polymerase. The annealing temperature for each amplification reaction corresponded to the lowest primer melting temperature (T_m) calculated using the equation below, minus 1-5°C:

$$T_m\,(°C) = 4 \times (G + C) + 2 \times (A + T) \qquad (2.1)$$

For each primer pair used further optimisation of the PCR conditions was performed to determine the appropriate hybridisation temperature and number of cycles required to obtain a sufficient amount of product. Negative controls without a DNA template were included in each experiment. 5 µl the final PCR products were analysed by agarose gel electrophoresis.

Oligonucleotide primers used for DNA sequencing and PCR amplification were synthesised by Invitrogen. The supplied lyophilised pellets containing a known quantity of DNA, were dissolved in highly purified H_2O (QH_2O) to give the concentration of ~ 200 µM. Stock solutions of ~15.0 µM were made prior to use in PCR amplification reactions. The sequence and position of all oligonucleotide primers used are listed in Appendix A.

2.1.2 Restriction digests

Digestions were performed in a total reaction volume of 200 μl, with 0.05-0.1 U of restriction enzyme per μg of DNA for 1-2 hr, using the restriction buffer and digestion temperature recommended by the enzyme manufacturer. After the restriction reaction, the DNA was purified from other reaction mixture components and buffer exchanged using QIAquick PCR purification kit (Qiagen GmbH, Germany), according to the manufacturer's instructions or gel extracted.

2.1.3 Dephosphorylation

The 5′ ends of digested DNA expression vectors were dephosphorylated through incubation with 1 unit of calf intestine alkaline phosphatase (CIP) (Roche) per 100 μl of reaction volume for 10 min at room temperature. After treatment, the CIP was removed from digested DNA, alongside the restriction enzymes by using the QIAquick PCR purification kit (Qiagen), following the manufacturer's instructions.

2.1.4 Gel electrophoresis

Agarose gels ranging from 1 to 2% and containing a final concentration of ~2 μg/ml ethidium bromide were prepared using 1 × TBE buffer (90 mM Tris-HCl, 90 mM orthoboric acid, 2.5 mM EDTA) or 1 × TAE buffer (40 mM Tris-HCl, 40 mM glacial acetic acid, 1 mM EDTA). DNA samples were mixed with 0.1 volumes of loading dye (0.25% bromophenol blue, 0.25% xylene cyanol, 30% glycerol in 10 × TBE buffer) and resolved by electrophoresis through the agarose gels alongside 0.5 μg of 1 kb DNA ladder (New England Labs) as a standard size marker. Electrophoresis was carried out in a Mini-Sub DNA Cell electrophoresis tank (Biorad) filled with 1 × TBE or 1 × TAE buffer, at 80 V until the dyes migrated the appropriate distance. The

electrophoresed DNA was visualised using an ultra-violet (UV) transilluminator (UVitech) and photographed with a video copy processor (UVitech).

2.1.5 Isolation of DNA from agarose gels

Fragments of DNA to be purified from the gel were located using a hand–held long wave UV source (UVitec) in order to minimise DNA damage, and excised from the gel as a thin slice using a razor blade. The DNA was then extracted from the agarose gel slice by using the Qiagen Gel Extraction Kit, following the manufacturer's instructions.

2.1.6 Ethanol precipitation

DNA was precipitated when necessary by addition of 0.1 volumes 3 M sodium acetate pH 5.2 and 2 volumes of 100% ethanol (-20°C). The sample was mixed thoroughly and incubated at -20°C for 5 to 10 min. Precipitated DNA was pelleted by centrifugation in a microcentrifuge at 13000 rpm for 10 min, washed with 70% ethanol and air-dried for 10 min before being re-dissolved in a suitable volume of distilled water or 10 mM Tris-HCl at pH 8.5

2.1.7 DNA ligation

DNA ligations were performed using the Roche Rapid ligation kit (according to manufacturer's instructions). Ligation reactions were then transformed into *E. coli* NM554 [pREP4] competent cells (section 2.1.9) and the colonies screened for positive clones.

2.1.8 Preparation of competent cells

A single colony of *recA*$^{-}$ NM554 *E.coli* host strain (Raleigh *et al*. 1988) with (or without) a *lac* repressor plasmid (pREP4, Qiagen) was used to inoculate 2.5 ml of 2x

TY medium (1.6% tryptone, 1% yeast extract, 85 mM NaCl, pH 7.4) with or without 25 μg/ml kanamycin and the culture grown with vigorous shaking at 37°C overnight. 100 ml of sterile 2x TY medium was inoculated with 1ml of overnight culture and grown with shaking at 37°C until A^{600} reached 0.4. The culture was poured into sterile chilled 50ml tubes (Greiner) and the cells harvested by centrifugation at 5,000 rpm at 4°C for 10 min. The cells were gently resuspended in 50 ml sterile, ice-cold Tfb buffer (10 mM PIPES, 50 mM $CaCl_2$, 15% glycerol pH 6.0), placed on ice for 30 min and then re-pelleted by centrifugation as before. The pelleted cells were gently re-suspended in 5 ml sterile, ice-cold Tfb buffer before aliquoting and flash freezing in liquid N_2.

2.1.9 Transformation of competent cells

Prokaryotic expression vector ligations were transformed into competent NM554 *E. coli* cells containing pREP4 (NM554 [pREP4]) and eukaryotic expression vector ligations were transformed in NM544 cells. 100 μl competent cells and 5 μl DNA ligation mix were pipetted into ice-cold eppendorf tubes, gently mixed and incubated on ice for 20 min. The cells were heat shocked at 42°C for 90 s followed by addition of 100 μl sterile 2x TY medium and incubation at 37°C for 30 min. Cells containing pREP4 were plated onto pre-warmed agar plates containing 25 μg/ml kanamycin and 100 μg/ml ampicillin (K/A).When dry, the plates were inverted and incubated at 37°C overnight.

2.1.10 Site- directed mutagenesis

The desired mutations were introduced into wild-type plasmid DNA by overlapping PCR mutagenesis (Jensen *et al.,* 2005) using primers with the required

mutations. PCR was performed in a 50 μl reaction volume containing 10 ng wild-type plasmid DNA, 0.2 mM dNTPs, 0.2 μM primers, 1x *Pfu* reaction buffer (Stratagene) and 1.25 U *Pfu* DNA polymerase (Stratagene). The thermal profile comprised of an initial denaturation step for 3 min at 95°C followed by 30 cycles of denaturation for 30 s, annealing at the appropriate T_m for 30 s and extension at 72°C for 7 min. After cycling a final extension step of 72°C for 10 min was carried out. Following amplification the reaction was held at 4°C until required. All primer sequences can be found in the appendix.

2.1.11 PCR based colony screening

Colonies were picked into 50 μl sterile QH_2O using sterile pipette tips and vortexed briefly. To determine whether the vector of an individual colony contained a DNA fragment of the expected size an aliquot of each bacterial suspension was included in a PCR reaction with primers specific for the vector present (Appendix A, sequencing primers). PCR reactions were carried out in a volume of 50 μl containing 10 μl bacterial suspension, 0.17 μM primers, 0.2 mM dNTPs, 1x PCR buffer (50 mM KCl, 10 mM Tris-HCl pH 9, 0.1% Triton X-10, 1.5 mM $MgCl_2$) and 2.5 U *Taq* DNA polymerase. The thermal profile consisted of an initial denaturation for 3 min at 95°C followed by 30 cycles of denaturation at 95°C for 30 s, annealing at 50°C for 30 s and extension at 72°C for 1 min. After cycling a final extension step of 72°C for 10 min was carried out. Reaction products were visualised following agarose gel electrophoresis (Section 2.4). Positive colonies were cultured for plasmid DNA preparation (Section 2.8).

2.1.12 Preparation of plasmid DNA

Plasmid DNA for sequencing and transformations was prepared using the Plasmid Midi Kit (Qiagen) for culture volumes of 100 ml. The Qiagen Kit procedure uses the modified alkaline lysis method of Birnboim and Doly (1983). Bacteria from a single colony were used to inoculate 100 ml 2x TY medium containing appropriate concentrations of selective antibiotics and the culture grown with shaking at 37°C overnight. Cells were harvested by centrifugation. Plasmid DNA was isolated using the appropriate Qiagen kit according to the manufacturer's instructions.

2.1.13 Quantitation of DNA and RNA

DNA and RNA samples were diluted as required in a total volume of 100 µl and the absorbance at 260 nm (A^{260}) was measured in a 100 µl quartz cuvette (Hellma) using a Shimadzu mini UV 1240 spectrophotometer. The concentration of the undiluted DNA sample was calculated on the basis that a 50 µg/ml solution of double-stranded DNA gives an A^{260} reading of 1.0. The concentration of the RNA samples was calculated on the basis that a 40 µg/ml solution of single-stranded RNA gives an A^{260} reading of 1.0. Readings of 0.1 to 1.0 were accepted since they are in the linear range of the calculation.

2.1.14 DNA sequencing

Sequencing was performed by Geneservice Ltd., using plasmid DNA prepared as described (2.1.12).

2.2 Prokaryotic protein production and purification

2.2.1 Expression of recombinant domain constructs

Single colonies of bacteria harbouring the appropriate constructs were used to inoculate 2 x 100 ml 2 x TY plus antibiotic cultures, which were grown overnight at 37°C. 22 to 24 ml of an overnight starter culture (see 2.1.12) was used to inoculate 8x 500ml of 2x TY media containing 100 μg/ml ampicillin and 25 μg/ml kanamycin. The expression cultures were incubated with shaking at 200 rpm at 37°C until the absorbance at 600 nm (A^{600}) reached 0.8 to 1.0, corresponding to the end of the log phase of bacterial growth. Expression of the protein was induced by addition of IPTG (isopropyl-β-D-thiogalactopyranoside) to a final concentration of 2 mM. After induction, the growth was continued for another 3 to 4 hr. The culture was harvested by centrifugation in 500 ml centrifuge bottles by centrifugation at 5,000 rpm for 15 min (Beckman J-2, JLA-10.500 rotor). Bacterial pellets were frozen at -20°C and used within one month.

2.2.2 Nickel-affinity chromatography

The frozen bacterial pellet was lysed by scraping into ~30 ml guanidine buffer (6 M guanidine-HCl, 50 mM sodium phosphate, 5 mM β-mercaptoethanol, pH 7.4) at room temperature. Solid guanidine-HCl was added during lysis to maintain the guanidine concentration at ~6 M as the pellet lysed. The cell lysate was sonicated for 1 min at 20 W (Jencons Ultrasonic Processor) to reduce viscosity and then clarified by ultra-centrifugation at 40,000 rpm for 30 min (Beckman L7-55 Ultracentrifuge, 60Ti rotor).

A column containing 2-3 ml fast flow chelating Sepharose (Amersham

Pharmacia) was prepared for affinity purification of the recombinant His-tagged protein. 10 ml of 1 M $NiSO_4$ was passed through the column which was then washed with 50 ml QH_2O to remove excess $NiSO_4$ before equilibration with 10ml guanidine buffer. The cleared supernatant was loaded onto the column and unbound protein was washed off with 10 ml guanidine buffer before elution of His-tagged protein with 25 ml guanidine buffer containing 50 mM EDTA. The eluted protein pool was adjusted to 0.1 M DTT, 0.1 M Tris-HCl pH 8.3 and left for at least 1 hr at room temperature to allow for full reduction of the protein to take place. Reduced His-tagged protein was further purified from contaminating bacterial proteins by reverse phase high performance liquid chromatography (HPLC, see Section 2.10.2). In preparation for HPLC the reduced protein solution was acidified to pH 2-3 with 1 M HCl and dialysed overnight at room temperature against 2 L of 0.1% trifluoroacetic acid (TFA) to remove guanidine-HCl.

2.2.3 Reverse-phase HPLC purification

All HPLC purifications were carried out using a Beckman Gold system equipped with a reverse-phase C8 semi-preparative column (Rainin). All samples were acidified to pH 2-3 prior to loading. A 20-80% gradient of buffer B was applied over 40 min (buffer A = 0.1% trifluoroacetic acid; buffer B = 80% acetonitrile, 0.1% trifluoroacetic acid) and the elution profile monitored continuously at 280 nm.

2.2.4 *In vitro* refolding and purification

HPLC purified reduced protein was refolded *in vitro.* The procedure used is based on an oxido-shuffling system that contains L-cysteine and L-cystine in a 10:1 (3

mM cysteine and 0.3 mM cystine) molar ratio at pH 8.3; conditions which favour disulphide bond exchange (Knott *et al.,* 1996). The optimal concentration of Ca^{2+} required for refolding was determined by carrying out small scale refolds with varying concentrations of Ca^{2+}, using a control sample containing 10 mM EDTA. Following at least 36 hr under refolding conditions the oxidised protein solution was acidified to pH 2-3, and purified on a semi-preparative reverse phase HPLC column (section 2.2.3). HPLC profiles gave a qualitative idea of how well the cbEGF domain refolded assuming that a single sharp peak reflects the presence of a single protein conformer in solution. Optimal conditions were used for refolding of the bulk reduced material.

2.2.5 Site specific biotinylation of BirA-tagged fibrillin-1 constructs

Fibrillin-1 constructs expressed from the pQE30 BirA vector contain a 15 amino acid C-terminal BirA tag (a variant of the sequence identified by Schatz, 1993). These were biotinylated *in vitro* using a biotin-protein ligase enzyme kit (BirA; Avidity, L.L.C). Fibrillin-1 substrate at 40 µM was incubated with BirA at an enzyme: substrate ratio of 1 µg : 50 nmoles. The reaction mixture contained 1 volume of Biomix-A (0.5 M Bicine buffer, pH 8.3), 1 volume of Biomix-B (100 mM ATP, 100 mM magnesium acetate, 500 µM biotin), and 8 volumes of substrate in 10 mM Tris-HCl, pH 8. Following overnight incubation at room temperature, biotinylated protein was purified from the reaction mixture by reverse-phase HPLC and analysed by mass spectrometry to verify that biotinylation had taken place.

2.2.6 Determination of protein concentration

HPLC peaks were collected and lyophilised before being dissolved in water and the protein concentration measured using the optical absorption at A^{280} and the equation (2.1).

$$\text{Protein concentration (mg/ml)} = \frac{A^{280} \times \text{protein molar mass (g/mol)}}{\varepsilon\ (M^{-1}\ cm^{-1}) \times \text{length of the light path (cm)}} \quad (2.1)$$

Where ε is the extinction coefficient of the protein calculated using the Protein Parameters tool (http://ca.expasy.org/cgi-bin/protparam) based on the number of tyrosine and tryptophan residues in the protein, and oxidation state of its cysteines (Gill and von Hippel, 1989).

2.2.7 SDS-PAGE

Protein samples were analysed by SDS-PAGE in a 1.5 mm thick polyacrylamide gel composed of a 16% separating gel [16% of 29:1 acrylamide : bisacrylamide, 0.1% SDS, 0.38 M Tris-HCl pH 8.8, 0.2% ammonium persulphate (APS) w/v, 0.2% N,N,N`,N`-tetramethylethylenediamine (TEMED)] v/v and a 6% stacking gel (6% 29:1 acrylamide : bisacrylamide, 0.25 M Tris-HCl pH 6.8, 0.1% SDS, 0.2% APS, 0.2% TEMED) as previously described by Laemmli, 1970.

Prior to loading, protein samples were boiled with an equal volume of loading buffer (50 mM Tris pH 6.8, 10% glycerol, 3% SDS, 0.2% bromophenol blue) with or without β -mercaptoethanol (β-ME).The gels were run in Tris-glycine buffer (30 mM Tris-HCl, 250 mM glycine pH 8.3, 0.1% SDS) and stained with Coomassie brilliant blue (Sigma)(Appendix B) for 1 hr at 50°C. Destaining was usually carried out overnight at

room temperature in 10% methanol, 10% acetic acid with gentle agitation. The gel was visualised on a light box and photographed with a video copy processor (UVitech).

2.2.8 Mass spectrometry analysis

Purified proteins were subjected to Electrospray Ionisation Mass Spectral analysis (ESI-MS) to confirm the correct mass. Freeze-dried proteins were dissolved in 1:1 (v/v) acetonitrile: water containing 0.1% formic acid to achieve a protein concentration of 10 µM. Approximately 10 µl sample was loaded onto the autosampler of an A Micromass Platform-II equipped with Agilent HP100 Sample Handling system and analysed.

2.3 Eukaryotic protein production and analysis

2.3.1 Maintenance of cell lines

MSU1.1 cells (human dermal fibroblasts; Morgan *et al.,* 1991) were used for cell trafficking experiments, were maintained in minimum essential medium (MEM, Invitrogen), supplemented with 10% (v/v) fetal bovine serum (FBS, Invitrogen), 50 U/ml penicillin, 50 µg/ml streptomycin and 2 mM glutamine (Sigma-Aldrich) (complete MEM).

Human dermal fibroblasts established from foreskin (FS2) and human squamous carcinoma VB6 cell line were used for cell adhesion assays. FS2 cells were maintained in DMEM supplemented with 10% (v/v) FBS, 50 U/ml penicillin, 50 µg/ml streptomycin and 2 mM glutamine (Sigma-Aldrich) (complete DMEM). Human squamous carcinoma VB6 cell line was obtained by transfecting the parental cell line, αV-negative oral squamous carcinoma cells (H357, Prime *et al*., 1990) with αV and β6

cDNA (Thomas *et al*., 2001). VB6 cells were maintained in DMEM supplemented with 10% FBS, 180 µ M adenine, 0.5 µg/ml hydrocortisone, 0.1 nM cholera toxin, 5 µg/ml insulin and 1 ng/ml EGF. Human embryonic kidney cells deficient in N-acetylglucosaminyltransferase I (HEK 293S), were used for eukaryotic protein production, were maintained in complete DMEM. Primary patient dermal fibroblasts used for immunostaining and cell binding assays were also maintained in complete DMEM

2.3.2 Subculturing of cells

Confluent monolayers of cells were rinsed with 2 to 3 ml PBSE (0.02% w/v EDTA in phosphate-buffered saline (PBS) and detached by incubation with 2 ml 0.17% trypsin in PBSE at 37°C for 1 to 3 min. Trypsination was terminated by adding 4 ml of complete MEM/DMEM. The cells were pelleted by centrifugation at 1000 rpm for 3 min (ALC centrifuge PK120, T534 rotor), resuspended in an appropriate volume of fresh medium and re-seeded at a density of 1:3 to 1:10 of that of the original culture.

2.2.3 Freezing and thawing of cells

Cells from a ~90% confluent monolayer were detached from a 75 cm^2 flask as described above. Following centrifugation, the pelleted cells were resuspended in 90% FBS containing 10% (v/v) dimethyl sulphoxide (DMSO) at a concentration of ~$3x10^6$ cells/ml. 1 ml aliquots of the cell suspension were pipetted into cryotubes (Nunc) and slowly frozen to -80°C using a Stratacooler cryofreezer before being transferred to liquid nitrogen for long-term storage.

Frozen cells were rapidly thawed by transferring the cryotube into warm sterile water at 37°C. Once thawed, the cells were transferred into a sterile 50 ml Falcon tube (Greiner Bio-one) and gradually diluted with 10 ml of MEM/DMEM containing appropriate antibiotics. Cells were pelleted by centrifugation as described above and resuspended in 4 to 5 ml fresh medium and placed in a fresh tissue culture flask.

2.3.4 Stable transfection

Transfection of MSU-1.1 cells was performed using LipofectAMINE 2000 (Invitrogen). 24 µg of purified circular plasmid DNA was added to 1.5 ml of serum-free Opti-MEM I medium (Invitrogen) and gently mixed. Another 1.5 ml of Opti-MEM I was mixed with 60 µl of LipofectAMINE 2000 reagent. After incubation at room temperature for 5 min, the DNA and LipofectAMINE containing media were combined and incubated at room temperature for another 20 min to allow for the formation of DNA-liposome complexes. A ~90% confluent monolayer of MSU cells in a 75 cm^2 flask was rinsed twice with 5 ml Opti-MEM I medium and incubated for ~10 min with 12 ml Opti-MEM I containing 10% FBS. The DNA and LipofectAMINE mix was added to the cells and incubated o/n at 37°C in a humidified atmosphere containing 5% (v/v) CO_2.

The next day, the cells were split 1:2 into complete MEM additionally containing 2.5 µg/ml puromycin (Sigma). This selective medium was changed twice per week until more than fifty individual clones of about 3 mm diameter were observed.

2.3.5 Transient transfection-HEK293 cells

24 µg plasmid DNA was added to 1.5ml serum-free DMEM and mixed well. 75 µl Lipofectamine 2000 solution was added and solution mixed. DNA-Lipofectamine 2000 complex formation was allowed to proceed for 20 min. Medium from the 175 cm^2 flask was discarded and replaced with 25 ml fresh DMEM (without serum), and the 3 ml DNA-Lipofectamine 2000 mix was added. Cells were incubated for 4-6 days for protein expression. Medium was collected and recombinant protein expressed by the cells was purified using a Ni^{2+} affinity column followed by HPLC. 25 µl of medium sample was taken for western blot analysis.

2.3.6 Glycosylation assays

Conditioned media and cell lysates from a confluent monolayer of a transfected pool of clones in a 25 cm^2 flask were denatured at 100°C for 10 min and then treated with Peptide: N-Glycosidase F (PNGase F) and Endoglycosidase H (EndoH) for 1 hr according to the manufacturer's instructions (New England BioLabs Inc.). Digested samples were then analysed by western blot as described in the previous sections.

2.3.7 Sample preparation for western blot analysis

Two 75 cm^2 tissue culture flasks were prepared for each transfected cell line preparation. The cells of one flask were frozen down for long-term storage and the other was aliquoted into usually four 25 cm^2 flasks containing selective medium in a total volume of 4 ml. The cells typically reached confluency by the second day. Medium samples were taken each day and centrifuged for 5 min at 13,000 rpm (Heraeus pico Biofuge) to remove cell debris. 150 µl of medium sample was

supplemented with 60 µl 4x reducing SDS-PAGE loading dye and boiled for 10 min. Cells were harvested as described earlier, resuspended in 500 µl 2x reducing SDS-PAGE loading dye and immediately boiled for 10 min. Medium and cell lysate samples for SDS-PAGE were stored at -20°C until required. To avoid protein degradation, the storage did not exceed one month before analysis by Western blotting. 40 µl of the medium sample and 10 µl of the cell lysate sample were loaded onto a 10 well 4–15% precast gradient gel (Biorad) and separated by SDS-PAGE alongside 10 µl of Full-Range Rainbow Molecular Weight Markers (Amersham).

2.3.6 Western blotting

Proteins were transferred by electrophoresis for 90 min at 100 V onto a nitrocellulose membrane (Whatman Protran) using a Mini Trans-Blot Cell (Biorad) and transfer buffer containing 25 mM Tris, 190 mM glycine, 20% (v/v) methanol and 0.02% (w/v) SDS. The nitrocellulose membrane was then placed in blocking buffer (5% w/v dried skimmed milk powder in PBS (Sigma) containing 0.1% (v/v) Triton X-100 (Sigma) (PBST) overnight at 4°C with gentle shaking. The blocking buffer was removed the next day and the membrane washed 5 x 5 min in PBST before incubation of the membrane for up to 2 hr with primary antibody (Kettle *et al.*, 2000) diluted 1:500 in fresh blocking buffer. The membrane was then washed 5 x 3 min in PBST before adding the secondary antibody (anti-rabbit IgG whole molecule peroxidase conjugate, Sigma) in a 1:1000 dilution in blocking buffer for up to 2 hr. After washing 5 x 3 min in PBST and rinsing twice in deionised water, the blot was developed using Amersham ECL Plus Western Blotting Detection Reagents (GE Healthcare) following the manufacturer's instructions. Excess reagent was drained

off by using Whatman paper (Schleicher & Schuell); the nitrocellulose was placed betwemen two sheets of transparency film and placed in a film cassette. In a dark room, Amersham Hyperfilm ECL (GE Healthcare) was laid on top of the film and exposed for 1 to 10 min before developing through an automatic Compact-X4 developer (Xograph Imaging systems).

2.4 Cell adhesion assay

Cell attachment assay were conducted essentially as published previously (Mardon and Grant, 1994). Briefly, 96-well plates (MaxiSorp^{c}) were coated with doubling dilutions of recombinant fibrillin-1 fusion proteins and fibronectin controls in Tris buffered saline (TBS; 10 mM Tris-HCl, pH 7.4, 150 mM NaCl) containing 2 mM calcium chloride, and incubated overnight at 4^{0}C. The wells were rinsed three times with TBS and blocked with 100 μl of 1% (w/v) BSA in TBS for 1 hr at 37°C, followed by three additional washes with TBS. Meanwhile, sub-confluent FS2 or VB6 cells were washed with warm PBS, trypsinised in trypsin-EDTA (Sigma), and neutralised with an equal volume of 1 mg/ml trypsin inhibitor. Cells were collected by centrifugation at 1500 rpm for 3 min, washed in warm PBS and spun again. Cells were then re-suspended in 4 ml of serum-free medium, an aliquot was taken for counting and the remainder incubated at 37°C, 5% CO_2 for 10 min. Serum-free medium was used to dilute the cells to 2 ×10^5 /ml and 50 μl of this suspension added to each well with gentle mixing to disperse any cell clumps. The plates were incubated for 2 hr (FS2) or 1.5 hr (VB6) at 37°C, 5% CO_2. Following incubation, adherent cells were gently washed with warm PBS and fixed with 100 μl of 4% (v/v) formaldehyde in PBS. After 30 min, the fixative was removed and adherent cells quantified by staining the nuclei

with 0.1% (w/v) crystal violet in 10% ethanol for 1 hr. The dye was solubilised with methanol for 10 min and A^{595} measured. Background attachment to BSA was subtracted from the OD values for test wells. All data points in cell adhesion experiments described here were obtained from two or three identical wells.

Adherent cells were scored for spread morphology according to the criteria of Mardon and Grant (1994). A Leitz Labovert FS inverted microscope (Leica Mikroskopie and Systeme GmbH, Wetzlar, Germany) was used for this purpose. Cells were considered spread if non-refractile with an increased surface area and visible nucleoli. Rounded cells with a refractile appearance were scored as non-spread. In each well, 200 cells were counted in at least four separate fields.

2.5 Immunocytochemistry

2.5.1 Preparation of cells for immunostaining

Sterile glass coverslips were coated with 100 µg/ml of His-tagged fibrillin-1 fragments at 10 µg/ml in TBS overnight at 4°C. Coverslips were washed with TBS and blocked for 1 hr with 1% (w/v) BSA. Cells to be analysed by immunocytochemistry were prepared as described for the cell adhesion assay (Section 2.16.1). 6×10^3 cells were plated on fibrillin-1 coated coverslips for 1 hr (VB6) and 2 hr (FS2) at 37°C, 5% CO_2. The coverslip cultures were then washed with warm PBS, fixed with 3% (w/v) paraformaldehyde in PBS, and permeabilised with the permeabilisation buffer (0.25% (v/v) Triton X-100). Assembly of focal contacts was demonstrated by staining with mAb in 0.1% (w/v) BSA in to human integrins αVβ3, αVβ6 and α5β1 and visualised using corresponding mAbs at 10 µg/ml. Incubation with primary antibody was followed by staining with FITC-conjugated donkey anti-mouse antibody (Jackson

Immunoresearch Laboratories), at 13.3 μg/ml in 0.1% (w/v) BSA in PBS, for 1 hr at room temperature. Actin was visualised with phalloidin conjugated to Texas red dye (1:1000). Stained coverslip cultures were subsequently mounted on microscope slides over a drop of Vectashield mounting medium (Vector Laboratories, Peterborough, U.K.) containing the nuclear dye 4', 6-diamidino-2-phenylindole (DAPI) (Vector Laboratories). Slides were stored in the dark at 4°C.

2.5.2 Immunostaining fibrillin-1 microfibrils

Fibroblast cell strains were seeded at 5×10^5 cells/well on 8-chamber slides for 72 hr in DMEM containing 10% FBS. The cells were rinsed with PBS, fixed with 4% (v/v) formaldehyde for 10 minutes, and then washed with PBS. Following a 30 min incubation with blocking buffer containing 3% bovine serum albumin, the slides were incubated using a rabbit polyclonal antibody recognising proline-rich region of fibrillin-1 for 1 hr at room temperature. The slides were then washed 3 times for 5 min each in PBS. The slides were incubated with secondary antibody Texas Red Goat anti-rabbit IgG (Invitrogen/Life Tech) diluted 1:100 at room temperature for 1 hr, and the wash step was repeated. Coverslips were applied with Vectashield mounting medium containing DAPI.

2.5.3 Image capturing and analysis

Images of adherent cells prepared as described in the previous sections were captured with a computer-controlled Hamamatsu Orca C4742-95 digital camera attached to either a Leica DM IRB inverted microscope or to a Leica DM RBE microscope equipped with a set of light filters for viewing fluorescence (both

microscopes manufactured by Leica, UK). Images were subsequently processed and overlaid with the OpenLab software, version 2.0.6 (Improvision, Coventry, UK).

2.6 Chromophoric calcium competition assays

Calcium binding affinity was determined by competition with the chromophoric Ca^{2+} chelator 5, 5'-Br_2BAPTA (Linse *et al.,* 1991). Lyophilised protein was resuspended in Ca^{2+} -free buffer (5 mM Tris-HCl, 150 mM NaCl, pH7.5) to a final concentration of 25-30 µM in the presence of 25-30 µM Br_2BAPTA and titrated with Ca^{2+} - containing stock buffers (5 mM $CaCl_2$, 5 mM Tris-HCl, 135 mM NaCl, pH 7.5). All titrations were performed at 23 ± 2 °C using a Shimadzu UV mini 1240 spectrophotometer to monitor absorbance at 263 nm; at this wavelength the absorbance of the chelator shows maximum Ca^{2+}-dependence. Background Ca^{2+} levels in the protein-containing samples were determined by extrapolating the initial linear region of each titration curve back to the *y*-axis. The initial Ca^{2+} concentration of each curve was adjusted so that the *y*-intercept was equivalent to that of a "chelator-only" control.

2.7 Proteolytic cleavage of protein samples

Aliquots (50 µg) of recombinant domain pairs in 50 mM Tris-HCl pH 7.5 were supplemented with 10 mM EDTA or 1 mM or 50 mM $CaCl_2$ and adjusted to equivalent ionic strength with NaCl (I = 0.15). Peptide aliquots were incubated at 37°C for 60 min with different ratios of peptide to protease and the reaction stopped by addition of 50 µl loading buffer with 2-mercaptoethanol added to 5% (v/v) and

heating to 95°C for 5 min. 10 µl of each digestion was analysed by SDS-PAGE using a 16% polyacrylamide gel.

2.8 Enzyme-linked immunosorbent assay (ELISA)

The surfaces of MaxiSorp 96-well plates were coated with 100 µl 5 µM of each His-tagged protein in 200 mM $NaHCO_3$ pH ~ 8 and incubated at 4°C overnight. Series of doubling dilutions of primary antibody (Anti-TB4RGD rabbit polyclonal) were made from the stock. Samples were analysed in triplicate. After washing and blocking the plate three times for 20 minutes with blocker solution (see Appendix B), the plate was incubated with the primary antibody in TBS for 2 hr at room temperature. Wells were then washed three times with blocker solution. The secondary antibody (goat anti-rabbit IgG-peroxidase conjugate) solution (1:1000 in TBS) was added at 100 µl per well for 1 hr. Wells were then washed twice with Blocker solution and once with TBS. Developer solution (see appendix) was added at 50 µl per well and after 45 min 100 µl of 1% (w/v) SDS was added to each well to stop the development reaction. The absorbance readings were made at A^{405} on a Labsystems MULTISKAN ELISA reader.

2.9 NMR data acquisition

2.9.1 Sample preparation

Recombinant domain constructs for nuclear magnetic resonance (NMR) analysis were dissolved in 280 µl of 99.9 % D_2O, 5 mM Tris pH 6.5, 150 mM NaCl to yield a 300 µM protein solution. The pH was adjusted to 6.5 with the addition of 0.1-0.5 M NaOD or 0.1-0.5 M DCl aliquots. Spectra were acquired on a home-built NMR spectrometer (Oxford Instrument Magnets), operating at 500 MHz. All NMR

experiments were performed with the assistance of Dr. C. Redfield (Oxford University).

2.9.2 1D ^{1}H NMR

One dimensional NMR data were collected at 37°C with a spectral width of 6666.67 Hz and a block size of 4 K. The number of acquisitions collected was typically 256 scans. Data were processed using Felix 2.3 (Accelrys, Inc.). Spectra were referenced with respect to residual water at 4.65 ppm and zero-filled to 8192 points, yielding a digital resolution of 0.0016 ppm/point.

2.9.3 2D ^{1}H-NMR

Two dimensional spectra were recorded at 37°C. Water suppression was achieved by saturation of the residual water resonance during recycle delay. The spectral width in each dimension was 6666.67 Hz. In all cases, 1024 complex points were acquired in F_2 for each experiment.

NOESY (nuclear Overhauser effect spectroscopy) spectra were recorded with a mixing time of 150 ms. Number of acquisitions were 96 scans, and the number of complex points collected in F_1 was 256. TOCSY (total correlation spectroscopy) spectra were recorded with a mixing time of 40 ms. Typically, 64 scans were collected, with 400 complex points in F_1. The number of acquisitions in COSY (correlated spectroscopy) experiments was 80 scans with 400 complex points collected in F_1.

All acquired NMR data were processed using Felix 2.3 (Accelrys, Inc.). Spectra were referenced with respect to residual water at 4.65 ppm and were zero- filled to

2048 complex points in both F_1 and F_2 dimensions, to yield a digital resolution of 0.0066 ppm/point.

2.10 Surface plasmon resonance

Integrin/fibrillin complex formation was monitored in real time on a Biacore T100 instrument (Biacore, GE Healthcare Life Sciences). All experiments were performed at 25°C, using TBS (25 mM Tris, 150 mM NaCl, pH 7.4) containing $CaCl_2$, $MgCl_2$ and $MnCl_2$ at 2 mM each as a running buffer. Air bubbles or other particles, which could disrupt the measurements, were eliminated from the flow system by filtering (0.2 µm) and degassing the buffers and samples.

Two different ligand immobilisation procedures were employed. Initially, between 1000 and 2000 RU of fibrillin-1 fragments were directly bound to the surface of a CM5 (carboxymethylated dextran) sensor chip *via* amine coupling, according to the manufacturer's instructions (Biacore Handbook). 0.4 M EDC [1-ethyl-3(3-dimethylaminopropyl)-carbodiimide hydrochloride] was mixed 1:1 (v/v) with 0.1 M NHS (*N*-hydroxysuccinimide) and injected over the sensor surface in order to activate the carboxymethyl groups of the CM5 chip to react with amine groups on proteins. Immediately after activation, fibrillin-1 fragments (0.1-0.3 mg/ml) in 0.1 M NaOAc pH 5.5 were injected to drive the coupling reaction. The remaining activated carboxymethyl groups were then blocked with 50 µl of 1M ethanolamine, pH 8.0.

Alternatively, fibrillin-1 fragments with C-terminal biotin tags were immobilised indirectly *via* streptavidin in a two-step procedure. In the first step, ~1000-1500 RU of streptavidin was amine coupled to the sensor surface by injecting 0.05 mg/ml streptavidin in acetate buffer pH 5.0 over the activated CM5 surface. After blocking

the unreacted carboxymethyl groups with 1 M ethanolamine, a short pulse of 50 mM NaOH was used to elute any noncovalently bound material. Biotinylated fibrillin-1 fragments were then captured on streptavidin-coated surfaces at densities of ~ 800-1300 RU, by injection of ~4 µM fibrillin-1 diluted in 25 mM Tris pH 7.4 containing 300 mM NaCl.

Recombinant human αvβ3 (Takagi *et al*., 2001) or αVβ6 integrins (Weinacker *et al*., 1994) were used as analytes. Dilution series of αvβ3 integrin (120-32 nM) were injected at 10 µl/min for 4 min, and allowed to dissociate over 10 min. In cases where analyte did not dissociate completely within the stipulated time, the ligand was regenerated by injecting 40 µl of TBS containing 10 mM EDTA. EDTA is a mild regenerant, which acts as divalent cation chelator and abolishes integrin-ligand interactions without affecting the activity of the ligand. For kinetic analysis of αVβ6 interactions with fibrillin, dilutions of the integrin (600-30 nM) in the running buffer were injected at 10 µl/min for 4 min, and allowed to dissociate over 10 min before injecting the regeneration solution for 4 min.

Data were analysed using the BIAevaluation T100 software (Biacore). All measurements were baseline corrected by subtracting the sensorgram obtained from the control flow cell containing the RGA mutant. The kinetic parameters were derived by fitting the data onto a simple 1:1 Langmuir binding model. At least three independent experiments were performed for each integrin-ligand pair.

CHAPTER 3 Structural consequences of Stiff skin syndrome substitutions in fibrillin-1

3.1 INTRODUCTION

The X-ray crystal structure of cbEGF22-TB4-cbEGF23 has provided a good insight into the positions of some key residues in the TB4 domain, which are involved in domain packing and integrin-binding (Figure 1.5 B; Figure 3.3) and contribute to a very high calcium affinity site at the TB4-cbEGF23 interface. Also, the presence of a heparan sulphate binding site in TB5, in close proximity to the TB4 domain, suggests this region may be extremely important for cell matrix interactions and for microfibril assembly (Chapter 1, section 1.4.1). Various MFS-causing missense mutations including C1564Y, C1564F, C1577G, V1580G, C1589F, and E1605K, affect the TB4 domain but the disease-causing mechanism underlying these mutations is still unknown. Stiff skin syndrome (SSS) mutations have also been recently mapped to the TB4 domain (Table 3.1; Figure 3.1; Loeys *et al.,* 2010). Mutations in the TB4 domain, affecting the 5th and 7th cysteine residues (C1564S and C1577G) and at the highly conserved W1570 residue (W1570C) result in SSS, but mutations occurring at the same residues in TB5 and TB6 domains result in MFS (Figure 3.2). This suggests that the TB4 domain might have a unique role in microfibril assembly and the cell-matrix interactions that regulate ECM organisation.

Interdomain hydrophobic contacts between TB-cbEGF domains make a significant contribution in stabilising the calcium-binding pocket of the corresponding cbEGF domain (Jensen *et al.,* 2005; Yuan *et al.,* 2002). The absence of any interdomain contacts, between TB6-cbEGF32, as demonstrated by NMR and the observed low calcium affinity of the cbEGF32 domain highlighted this fact (Yuan *et al.,* 2002). Determination of the crystal structure of cbEGF22-TB4-cbEGF23 (Lee *et al.,* 2004) and previous work done on the TB4-cbEGF23 pair (Jensen *et al.,* 2005),

established that the molecular basis for the unexpectedly high calcium affinity associated with the TB4-cbEGF23 fragment was the stabilisation of the calcium-binding site through extensive hydrophobic domain–domain interactions (Figure 3.3). Therefore, any substitutions in a TB domain could indirectly affect the calcium-binding properties of the adjacent cbEGF domain by altering the interdomain interfaces, as well as affecting TB4 structure alone.

SSS-causing missense mutations W1570C and C1564S in TB4 domain were investigated in this chapter using a range of molecular techniques designed to probe TB4 and cbEGF23 structure and function. W1570 and C1564 are structurally important residues in the TB4 domain, involved in stabilising the hydrophobic core and fold of the domain. Residue W1570 is highly conserved and plays an important structural role in the TB4 domain hydrophobic core (Yuan *et al.,* 1997; Lee *et al.,* 2004). C1564 residue forms one of the disulphide bridges in the TB4 domain. Amino acid substitutions W1570C and C1564S both result in the creation of free cysteine residues in the domain.

In addition to SSS-causing mutations, another disease-causing mutation in TB4 domain was studied with the aim of understanding the genotype-phenotype relationships of the mutations. The effect of a MFS-causing mutation, C1564Y on calcium-binding was also investigated in this chapter in the context of cbEGF22-TB4-cbEGF23. This substitution occurs at the same position which, when substituted with a serine results in SSS. Collectively W1570C (SSS), C1564S (SSS) and C1564Y (MFS) were investigated for their effects on structure and interactions of TB4. Initially each substitution was analysed in either pair or triple domain fragments expressed in bacteria and refolded *in vitro* using a well-established method.

3.2 Expression and purification of TB4-containing fibrillin-1 wild-type and mutant fragments

3.2.1 Cloning of TB4-cbEGF23 and cbEGF22-TB4-cbEGF23 wild-type and mutant constructs

Construct cbEGF22-TB4-cbEGF23 encompasses residues 1486-1647 (nucleotides 4456-4941) of fibrillin-1 and TB4-cbEGF23 construct encompasses residues 1527-1647 (nucleotides 4579-4941; numbering according to Pereira *et al.,* 1999). The two SSS substitutions W1570C and C1564S were introduced into cbEGF22-TB4-cbEGF23 construct by PCR- based mutagenesis and mutant fragments were cloned into the pQE30 BirA vector (Figure 3.4). Similarly the MFS-causing substitution C1564Y was also introduced into the cbEGF22-TB4-cbEGF23 fragment and cloned into pQE30 BirA vector. A 6xHis tag was present at the N-terminus of each construct to allow the purification of the recombinant proteins by nickel chelation chromatography. Cloning of TB4-cbEGF23 mutant constructs was performed by David Stoddart and Sacha Jensen.

3.2.1.1 Prokaryotic expression and purification of wild-type and mutant triple and pair constructs

Expression of the recombinant fragments was performed in *E.coli* NM544 cells containing a lac repressor plasmid (pRep4) (see Materials & Methods). The plasmid encoding the desired fibrillin-1 fragment in the pQE30 BirA vector was transformed into chemically competent NM554 [pREP4] cells. Purification and expression was carried out as outlined in chapter 2. A flow chart of the purification procedure is shown in figure 3.5.

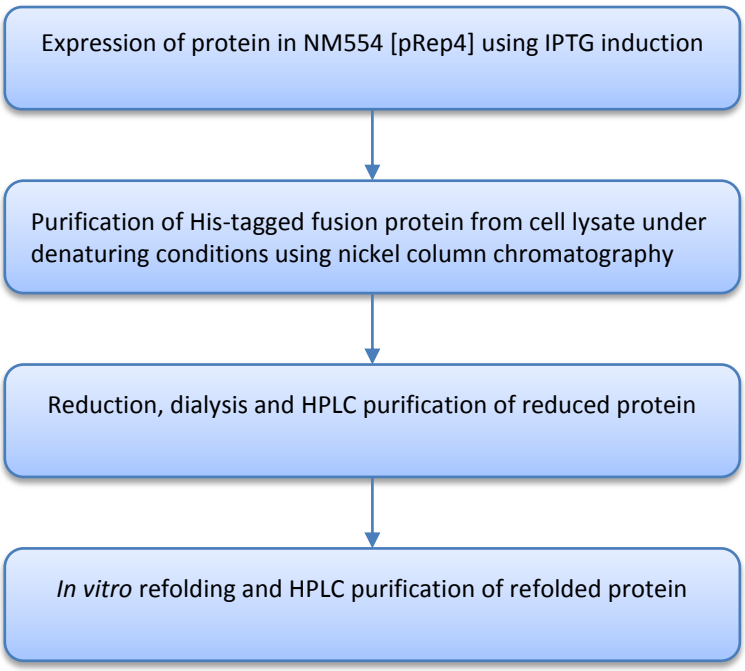

Figure 3.5. *Schematic overview of the expression, purification and refolding procedure for the prokaryotic TB4-containing fibrillin-1 fragments.*

Following Ni^{2+} purification, reduced His-tagged protein was further purified from contaminating bacterial proteins by reverse phase high performance liquid chromatography (HPLC). In preparation for HPLC, the reduced protein solution was acidified to pH 2-3 with 1 M HCl and dialysed overnight at room temperature against 2 L of 0.1% (v/v) trifluoroacetic acid (TFA) to remove guanidine-HCl. HPLC-purified reduced protein was refolded *in vitro.* A well-established *in vitro* refolding system was used to produce the native disulphide-bonded structure (Knott *et al.,* 1996). The procedure used is based on an oxido-shuffling system that contains L-cysteine and L-cystine in a 10:1 (3 mM cysteine and 0.3 mM cystine) molar ratio at pH 8.3; conditions that favour disulphide bond exchange. Addition of calcium to the refolding mix facilitates refolding of cbEGF-containing constructs. The optimal concentration of Ca^{2+} required for refolding was determined by carrying out small

scale refolds with varying concentrations of Ca^{2+}, which were then compared to a control sample containing EDTA. Following at least 36 hr under refolding conditions, the oxidised protein solution was acidified and purified on a semi-preparative reverse phase HPLC column. HPLC profiles provided qualitative information on how well the cbEGF domain refolded. Optimised conditions were used for large-scale preparations.

As observed previously, effect of calcium on protein refolding was evident by the significant sharpening of peaks, suggesting a major conformer was present. In the presence of EDTA the peaks were broader, suggesting a mixture of non-native species (Figure 3.6 A). Since Ca^{2+} improved the HPLC profiles of oxidized proteins, 10 mM Ca^{2+} was routinely added to the refolding mix. The final purified product was analysed by non-reducing and reducing SDS-PAGE, to investigate purity (Figures 3.6 and 3.7). Mass spectrometry analysis revealed that the mutant proteins had an increased mass (~121 Da) consistent with the formation of a disulphide bond between the protein and a free cysteine from the refolding buffer.

Table 3.2 Electrospray mass spectrometry analysis of purified fibrillin-1 WT and mutant triple and pair constructs.

His_6- TB4-cbEGF23	Theoretical mass (Da)	Experimental mass (Da)
Wild-type	15444.2	15665.4 ± 1.2[1]
W1570C	14789.5	14910.6 ± 0.71[1]
C1564S	14858.5	14980.2 ± 1.51[1]
His_6-cbEGF22-TB4-cbEGF23		
Wild-type	21581.2	21580.3±0.23
W1570C	21497.1	21618.2±0.91[1]
C1564S	21566.1	21687.3±1.02[1]
C1564Y	21642.2	21763.4±1.56[1]

[1] A free cysteine has been covalently attached to the protein during *in vitro* refolding as has been observed previously for constructs with an unpaired cysteine (Suk *et al.,* 2004).

Overall, each stage of the purification revealed striking similarities between the three mutant constructs with the wild-type. These similarities and the presence of a major species at each stage of the purification suggested that the disease-causing substitutions do not produce grossly misfolded proteins, even though they all alter residues required to stabilize the native TB fold.

3.3 Ca^{2+}-binding to TB4-containing constructs

Ca^{2+} binding to fibrillin-1 cbEGF domains have important structural and functional consequences: it rigidifies the linkage between contiguous cbEGF domains (Downing *et al*., 1996; Werner *et al*., 2000), confers protection from digestion by tissue proteases (Reinhardt *et al*., 2000; McGettrick *et al*., 2000) and is required for protein-protein interactions. The importance of Ca^{2+} binding for cbEGF function is highlighted by the large number of pathogenic *FBN1* mutations affecting conserved Ca^{2+}-binding residues, which are predicted to cause reduction or abrogation of Ca^{2+} binding to the affected domain (Dietz *et al*., 1993; Kainulainen *et al*., 1994). Such amino acid changes have also been detected in cbEGF domains from other proteins, giving rise to diseases such as haemophilia B (Diuguid *et al*., 1986) and familial hypercholesterolaemia (Hobbs *et al*., 1992).

The first crystal structure of a cbEGF domain from human clotting factor IX revealed that the Ca^{2+}-binding site has pentagonal bipyramidal geometry, with six out of seven ligands provided by intradomain oxygen atoms (Rao *et al*., 1995). The identity of Ca^{2+} ligands can however vary, as evidenced by the somewhat different Ca^{2+}-coordination pattern seen in the cbEGF22-TB4-cbEGF23 crystal structure (Lee *et al*., 2004) (Figure 3.8). This structure identified the backbone carbonyl of a highly

conserved serine as the seventh intradomain Ca^{2+}-binding ligand in cbEGFs 22 and 23. The side chain of this residue forms a hydrogen bond with a nearby arginine and stabilises the Ca^{2+}-binding pocket. The structure provided a rationale for the potential pathogenic mechanism of MFS mutations affecting this serine residue, conserved in thirty-one of the forty-three human fibrillin-1 cbEGF domains.

A number of studies demonstrated that affinity for calcium depends on the native geometry of the metal-binding site (Handford *et al*., 1991b; Mayhew *et al*., 1992; Hughes *et al*., 1993). Furthermore, *in vitro* studies of MFS-causing mutations affecting cbEGF cysteines showed that a cysteine substitution disrupts native disulphide bond formation, giving rise to intradomain misfolding and the loss of Ca^{2+} binding (Suk *et al*., 2004). Therefore, Ca^{2+} binding to a cbEGF domain depends on intact disulphide bonds and can be considered an important criterion in determining whether a cbEGF domain is correctly folded. The wild-type and mutant constructs produced here were analysed for their Ca^{2+}-binding properties using limited proteolysis and chromophoric chelator competition assays. This analysis provides evidence for proper folding of cbEGF23 in wild-type construct and also assesses whether or not the pathogenic substitutions impair high affinity Ca^{2+}-binding.

3.3.2 Limited proteolysis of wild-type and mutant constructs

Several studies have shown that recombinant fragments of fibrillin-1 are protected against proteolysis by Ca^{2+}. Disruption of the cbEGF Ca^{2+}-binding fold by introducing a mutation was shown to increase the susceptibility of these fragments to proteolytic cleavage (Reinhardt *et al.,* 1997; Whiteman *et al.,* 1998; Ashworth *et al.,* 1999; Booms *et al.,* 2000; McGettrick *et al.,* 2000; Reinhardt *et al.,* 2000b;

Whiteman *et al.,* 2001). In this section, the low-resolution method of limited proteolysis was used to compare the Ca^{2+}-binding properties of wild-type and mutant proteins.

Purified His-tagged proteins were analysed for Ca^{2+}-binding by carrying out limited digestions using trypsin in the presence of either Ca^{2+} or EDTA. Ca^{2+} binding to cbEGF domains affords protection against proteolysis due to rigidification of the cbEGF domain linkage. Samples were analysed by reducing SDS-PAGE to assess the calcium protection from proteolysis (Figure 3.9, 3.10).

cbEGF22-TB4-cbEGF23 wild-type, SSS mutants W1570C and C1564S and MFS mutant C1564Y fragments were used in this study. As expected, the wild-type fragment showed more protection against proteolysis in Ca^{2+} compared to in EDTA consistent with presence of some native cbEGF fold. There is evidence of intact protein both in 1 mM and 50 mM Ca^{2+} at T_{60} compared to EDTA where the wild-type fragment appears to have degraded. The W1570C and C1564S mutant fragments showed a change in digest pattern in EDTA indicating either a change in structure or change in the ability of protease to bind substrate. Irrespective of this, these fragments also displayed some Ca^{2+} protection (Figure 3.9 B, C). Therefore, SSS mutations do not abrogate Ca^{2+}-binding completely. The MFS substitution C1564Y on the other hand, showed almost no Ca^{2+} protection as the protein is degraded to the same extent in the presence of Ca^{2+} and in EDTA. TB4-cbEGF23 W1570C and C1564S mutant fragments showed similar pattern of digestion to the triple domain fragments (Figure 3.10 B, C).

3.3.1 Chromophoric chelator competition assay on cbEGF22-TB4-cbEGF23 and TB4-cbEGF23 wild-type and SSS mutant fragments

Chromophoric chelator competition assays were performed on purified TB4-cbEGF23 and cbEGF22-TB4-cbEGF23 fragment containing the SSS substitutions to investigate the effects of these mutations on Ca^{2+} binding to the two cbEGF domains flanking the TB4 domain. The chromophoric chelation method is based on the competition for added Ca^{2+} between the chelator of known Ca^{2+} affinity and the protein (Linse *et al.*, 1991). The change in the chelator absorbance is monitored as a function of added Ca^{2+} at 263 nm, where absorption is Ca^{2+}-dependent. All titrations are performed with 20-30 µM protein and 20-30 µM chelator at 23±2°C using a Shimadzu UV mini 1240 spectrophotometer to monitor absorbance at 263 nm. Background calcium levels in the protein-containing samples were determined by extrapolating the initial linear region of each curve back to the Y-axis. A K_d value for the chelator was determined independently from chelator-only control experiments.

The chromophoric chelator Br_2BAPTA [5, 5'-dibromo-1, 2-bis (2-aminophenoxy) ethane-N, N, N', N'-tetraacetic acid] was used in the determination of Ca^{2+}-dissociation constants of cbEGF domains within the cbEGF22-TB4-cbEGF23 fragment. The calcium dissociation constant (K_d) of Br_2BAPTA was found to be 1.3 µM (Jensen *et al.,* 2005).The calcium dissociation constant (K_d) for cbEGF23 of both triple and pair wild-type constructs has been determined previously using this assay and have been found to be ~5.5 nM and ~16 nM respectively. High-affinity Ca^{2+} binding to cbEGF22-TB4-cbEGF23 fragment is indicative not only of native disulphide arrangement in cbEGF23, but also of the large interface between TB4 and cbEGF23 in solution similar to that observed in the crystal structure.

The different shapes of the titration curves of protein with Ca^{2+} reflect the different degrees of competition for added Ca^{2+} between the protein and chelator (Figure 3.11). Protein samples with a high affinity for Ca^{2+} (wild-type) relative to the chelator show an initial lag in the decrease of absorbance *versus* Ca^{2+}, because the protein binds most of the added Ca^{2+} (Figure 3.11 C, Figure 3.12 A, Figure 3.13 A). Protein samples with a lower Ca^{2+} affinity (mutant constructs), relative to that of the chelator, show a decrease in absorbance at low Ca^{2+} concentration, because both protein and chelator bind the added Ca^{2+} (Figure 3.11 A,B; Figure 3.12 B,C; Figure 3.13 B,C). From the Ca^{2+} titration curves it is evident that the Ca^{2+}-binding affinity of the mutants is significantly lower compared to the wild-type constructs and a K_d could not be determined using this assay.

3.4 1D and 2D ^{1}H-NMR analysis of SSS-causing mutations W1570C and C1564S on TB fold, Ca^{2+} binding and TB4-cbEGF23 interface

Limited proteolysis of the wild-type and mutant constructs has suggested that the introduction of the SSS substitutions into triple and pair cbEGF constructs reduces but does not completely abrogate calcium protection. To investigate this further, 1D and 2D ^{1}H-NMR analyses were performed to describe precisely the extent of the effect of each mutation on TB4 domain fold, calcium-binding and on the TB4-cbEGF23 domain interface. The TB4-cbEGF23 fragment was used in this study as it has less complicated NMR spectra.

There are several distinctive resonances in a 1D ^{1}H-NMR spectrum that are indicative of correctly folded cbEGF domains and TB domains, and these peaks act as

markers for various structural motifs in these domains (Yuan *et al.,* 2002; Jensen et al., 2005).

- W1570 and C1534 residues in the antiparallel β-sheet in the globular TB4 domain give rise to downfield shifted H^{α} peaks in the spectrum. However, if TB4 is not folded in the native state, part of the β -sheet may not form and there may be no peaks in this region of the spectrum (see sections 1.2.3 & 1.2.4, chapter 1).
- In a misfolded protein, protons on the aromatic ring of Phe residues give peaks at about 7.3 ppm. The crystal structure of the wild type cbEGF22-TB4-cbEGF23 shows that Phe1595 of TB4 packs against Phe1626 of cbEGF23 at the interdomain interface (Figure 3.3). This interaction causes these Phe peaks in the 1D and 2D spectrum to shift as a result of aromatic ring current effects. The Phe1626 shifts downfield to 7.5 ppm and the Phe1595 shifts upfield to about 6.6 ppm in presence of calcium. Peaks at these positions are therefore markers that suggest that the interface region has formed, and provide a measure of the structural integrity of the interface region and TB4 domain.
- A dramatically upfield shifted peak at -0.75ppm in the TB4 spectrum is assigned to the Hβ of the conserved K1559, by homology with K2080 in TB6. This explains the packing of K1559 side chain against the aromatic ring of W1570, as seen in the cbEGF22-TB4-cbEGF23 X-ray crystal structure.
- There are several upfield shifted methyl resonances at around 0.6-0.7 ppm, due to methyl groups packing against a tyrosine in TB4. Peaks within this

region suggest that the corresponding residues in the TB4 domain are in a correctly folded environment.

- Calcium dependent peak shifts within the TB4-cbEGF23 spectrum indicate calcium binding to the protein confirming presence of a native cbEGF fold.

These resonances were used to investigate the structural effects of these SSS-substitutions in a TB4-cbEGF23 fragment which has been discussed in the next section.

3.4.1 Assessment of TB4 fold, TB4-cbEGF23 interface and Ca^{2+} binding to cbEGF23 by 1D ^{1}H-NMR

To assess the fold of the TB domain, TB4-cbEGF23 interface and Ca^{2+} binding to cbEGF23, 1D ^{1}H-NMR spectra of the TB4-cbEGF23 wild-type and SSS mutant constructs were collected. Spectra were recorded in 99.9% D_2O (5 mM Tris-DCl, pH 6.5, 150 mM NaCl and *I* = 0.15). In each case, spectra were collected in the presence and absence of calcium using a protein concentration of ~300 µM. The apparent chemical shifts of the different constructs were indicative of a defined tertiary structure. This would not be expected from a random coil peptide because the chemical shifts of identical amino acids approach one another and the lines become narrower due to increased mobility.

TB4 fold: A dramatically-upfield shifted peak at -0.75 ppm in wild-type and TB4-cbEGF23 C1564S spectrum was assigned to the H^{β} of the conserved K1559 (Figure 3.14). This upfield shift arises from the packing of K1559 side chain against the aromatic ring of W1570. In the wild-type and C1564S mutant fragments two of the

downfield shifted H^{α} resonances were assigned to the conserved C1534 and W1570 residues which reside on a β sheet in the TB4 domain (Figure 3.15 A & B). These resonances were absent in the spectra of the W1570C mutant fragment because the W1570 residue has been substituted to a cysteine residue in this fragment. Upfield shifted methyl resonances at around 0.6 ppm (Figure 3.14 A), due to methyl groups packing against a tyrosine in TB4 are seen in spectra of the wild-type, C1564S and W1570C mutants, suggesting that these residues are in a more native-like environment in TB4 domain. There are calcium dependent changes seen in these spectra which suggest they may partly arise from cbEGF23 methyls and/or TB4-cbEGF23 interface.

Calcium binding to cbEGF23: In both the C1564S and W1570C TB4-cbEGF23 spectra, there are clear Ca^{2+}-dependent peak shifts similar to the wild-type. On the addition of Ca^{2+}, notable changes are observed at 7.5 ppm, 5.9 ppm in the aromatic region (Figure 3.15) and in the upfield shifted region (Figure 3.14) suggesting that cbEGF23 binds Ca^{2+} in both the mutants but the Ca^{2+} affinity of the mutants must be lower than wild-type.

TB4-cbEGF23 interface: On addition of 5 mM Ca^{2+} to TB4-cbEGF23 wild-type, peak for F1626 (cbEGF23) is downfield-shifted to 7.5 ppm and a peak at 6.6 ppm for F1595(TB4) resonances resulting from the formation of Ca^{2+}-dependent interdomain interface were observed (Figure 3.15) indicating interface formation. Peaks at similar positions in C1564S spectra indicate some interface formation. In W1570C spectra, no peaks were observed at 6.6 ppm but peak at 7.5 ppm for F1626 was present suggesting that it might be due to calcium-binding and not because of interface

formation. A 2D ^{1}H-NMR spectra would give a better insight into the interface formation for the mutants.

1D ^{1}H-NMR spectra of the mutant fragments indicated that the substitutions do affect the overall tertiary structure of the TB4 domain and the TB4-cbEGF23 interface, but do not completely abrogate calcium-binding in the mutant fragments. 2D ^{1}H-NMR spectra were recorded to give clear insights into interface formation in these mutant constructs.

3.4.2 Structural information of the TB4-cbEGF23 W1570C and C1564S mutant from 2D ^{1}H-NMR

Two-dimensional NOESY spectra of the TB4-cbEGF23 wild-type and SSS mutants were collected to determine the structural effects of the W1570C and C1564S substitutions (Figure 3.16). Spectra were recorded in 99.9% D_2O (5 mM Tris-DCl , pH 6.5, 150 mM NaCl and *I* = 0.15). Resonances in the spectra were assigned by Dr Christina Redfield. In the wild-type spectra, the large upfield-shift of F1595 in TB4 is consistent with a significant change in the environment of this residue, and is most likely a consequence of its packing interactions with F1626 from cbEGF23 (Jensen *et al.,* 2005). These data are consistent with the formation of a stable interface between the TB4 and cbEGF23 domains in saturating Ca^{2+}. There are also many calcium-dependent peak shifts seen in the spectra. In neither the W1570C nor the C1564S mutant spectra were calcium dependent upfield-shifts of residue F1595 in TB4 domain were observed. Residue F1626 in cbEGF23 domain, which packs with F1595 in wild-type TB4, does not show as large a movement in the presence of calcium as that seen for the wild-type construct and the shift might just be due to calcium-binding. These results imply that the SSS substitutions do affect the TB4-

cbEGF23 interface. There are calcium-dependent shifts observed in the spectra for the mutants, however, suggest that calcium binding has not been completely abolished in these mutants. In order to determine the calcium affinity of the mutants by NMR, calcium titrations will have to be performed.

3.5 Discussion

The results in this chapter demonstrate the successful production of cbEGF22-TB4-cbEGF23 and related fragments harbouring SSS substitutions W1570C and C1564S and the MFS substitution C1564Y (MFS) using an *in vitro* refolding system. Free cysteine residues present in the mutant proteins as a result of the SSS substitutions were inactivated by oxidation, with the addition of a cysteine residue from the refolding mix and were therefore not available for intra/intermolecular disulphide bonding. When subjected to limited proteolysis, the mutant proteins showed a large increase in susceptibility to digestion compared to the wild-type. The MFS substitution C1564Y showed more susceptibility to proteolysis compared to the SSS substitution C1564S, suggesting a more severe effect of the MFS substitution on the structure of the domains. It was not possible however to determine the calcium binding affinity (K_d) of these mutant constructs using a chromophoric calcium chelator as unlike the wild-type protein the mutant protein did not compete with the chelator. This suggests that these substitutions had a dramatic effect on calcium binding but did not completely abolish it. High resolution structural studies using NMR were performed on the TB4-cbEGF23 pair construct containing the SSS substitutions. 1D and 2D ^{1}H-NMR data show that these substitutions affect the

extensive interface between the TB4 and cbEGF23 domains but there is still calcium binding seen for the SSS mutants.

W1570 and C1564 are structurally important residues in TB4 domain stabilising the hydrophobic core and tertiary structure of the domain. A variety of assays used in this chapter show that W1570C and C1564S substitutions identified in SSS patients, affect the structural integrity of the TB4 domain but the native fold of cbEGF23 is likely to be preserved.

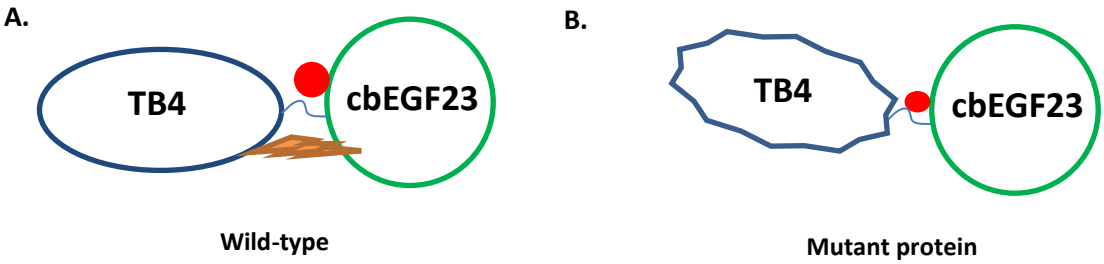

Figure 317 A. *Folding at the TB4-cbEGF23 interface in wild-type is supported by extensive interdomain hydrophobic interactions (orange bar) which stabilises the cbEGF23 calcium binding pocket and also gives rise to high calcium affinity of that domain.* ***B.*** *A mutation in TB4 domain can lead to misfolding of that domain, resulting in impaired interdomain interface and reduced calcium affinity (denoted by a smaller red sphere), as seen in the SSS mutant fragments. Since* Ca^{2+} *binding is observed in the mutants it is likely that the cbEGF fold is preserved.*

The MFS-causing substitution C1564Y studied in this chapter alongside the SSS mutations had a dramatic effect on domain fold and calcium binding, more severe than the SSS mutations as seen by proteolytic digests. Due to low calcium affinity of cbEGF22 domain compared to the cbEGF23 domain, it was not possible to predict the effect of these mutations on calcium-binding to cbEGF22 domain or on the cbEGF22-TB4 interface using a triple domain fragment. These assays could be used further to elucidate the effect of these mutations on cbEGF22-TB4 domain interface by using a pair fragment instead of a triple domain fragment. To determine whether these structural consequences of the mutations effect the secretion of the mutant

protein from the cell, as has been seen previously in the case of some MFS mutations, cell trafficking experiments were performed.

CHAPTER 4 Trafficking of Stiff skin & Marfan syndrome-causing substitutions in TB4 domain of fibrillin-1 in a human fibroblast line

4.1 Introduction

Pulse chase studies of MFS patient fibroblast have shown three different cellular phenotypes of (i) normal, (ii) delayed secretion and (iii) retention of fibrillin-1. In cases where retention is observed, the mechanism of pathogenesis is likely to be haploinsuffuciency whereas in (i) there is likely to be a dominant negative effect (Aoyama *et al.,* 1994; Schrijver *et al.,* 1999; Suk *et al.,* 2004; Whiteman *et al.,* 2003, 2007). In this chapter, secretion studies were carried out to investigate whether or not the disease-causing mutations in the TB domains secrete out of the cell. The effect of the substitutions on protein secretion was analysed using a human fibroblast cell line MSU-1.1 which has been shown to assemble extracellular microfibrils and contains all the cellular factors required for fibrillin-1 folding, processing, secretion and assembly (Kettle *et al.,* 2000). By expressing the construct in MSU-1.1, any dominant negative effect of recombinant expression on the processing and secretion of full-length fibrillin-1 could also be determined. A well-established cellular system has been used which has previously given insights into the effects of various MFS-causing mutations on cell trafficking and has also been used to study the trafficking profile of mutant fibulin-5 proteins (Schneider *et al.,* 2010). These studies should provide an insight into the mechanism underlying these different diseases associated with the mutations in the same protein, fibrillin-1. Furthermore, this is the first study where substitutions affecting TB domains have been investigated for cell trafficking.

Stiff skin-causing amino acid substitutions C1564S and W1570C affect the fold of the domain and calcium binding as shown by NMR, calcium chelation assays and proteolytic digests in the previous chapter. A Marfan syndrome-causing substitution,

C1564Y, was also investigated for trafficking in this study as it occurs at the same cysteine residue which when substituted to a serine results in SSS (Figure 4.1 A). An eight amino acid deletion in the TB5 domain of fibrillin-1 which has been found in patients suffering from a dominant-form of Weill-Marchesani syndrome (WMS) was also investigated in this chapter because of its phenotypic similarity (thickened skin and short stature) with SSS. This deletion creates a free cysteine in the TB5 domain similar to the SSS and MFS substitutions that are being investigated in this study (Figure 4.1 B). All the three disorders are autosomal dominant conditions, which means the patient will have one mutant and one wild-type copy of *FBN1* gene.

Pulse-chase analysis radioactively labels both wild-type and mutant fibrillin-1 within the cell and follows the fate of the labelled protein over time. Since one cannot distinguish between wild-type and mutant protein using pulse chase analysis, it is not possible to conclude if there is a reduction in the amount of mutant protein and if the mutant allele in any way affects the secretion of the wild-type protein. Further cell trafficking experiments using truncated forms of fibrillin-1 recombinant protein will provide an insight into the pathogenic mechanisms underlying these different disorders involving fibrillin-1. Furthermore, primary fibroblasts obtained from SSS patients will be examined for their ability to produce a microfibril network.

4.2 Construction of cbEGF18-26 wild-type and mutant recombinant fragments

A fibrillin-1 cDNA fragment encoding the N-terminus to the proline rich region (NterPro) had previously been cloned into the pKG52 (polyA) expression vector and a system established for expressing regions of fibrillin containing mutant domains (Whiteman *et al.,* 2003). DNA fragments encoding wild-type cbEGF18-26 and

cbEGF18-26 containing the disease-causing substitutions C1564S, W1570C (Stiff skin syndrome), C1564Y (MFS) in the TB4 domain and the Weill-Marchesani deletion in TB5 domain were cloned downstream of the N-terminal fragment (Figure 4.2). The wild-type cbEGF18-26 fragment containing a *XhoI* restriction site in its sequence was first ligated into the *SalI* site of the pBluescript II KS+ vector. This was used as a template to carry out site directed mutagenesis to make the mutant fragments. These fragments were then ligated in frame into the *XhoI* site of the pKG52 (polyA) expression vector (Figure 4.2). Successful construction of each mutant in pBluescript, and subsequent orientation analysis of the recombinant fragment were confirmed by sequencing (Geneservice, Oxford).

4.3 Gene expression analysis

Following transfection of MSU-1.1 cells and stable selection in puromycin (see Materials & Methods), RNA levels of recombinant fibrillin constructs from different pools of clones were analysed using reverse transcription-PCR (RT-PCR) and compared with endogenous fibrillin-1 RNA levels. For RT-PCR, reverse primer cbEGF24-R was used followed by two PCR reactions which amplified both recombinant as well as endogenous fibrillin-1 (Figure 4.3). The primer pair used to amplify endogenous fibrillin-1 RNA was expected to produce a fragment similar in size (~1.2 kb) to that produced by RT-PCR amplification of recombinant fibrillin-1 RNA (~1.4 kb) (Figure 4.3). The number of PCR cycles was varied to check for any large differences between the RNA levels of the constructs. Results show bands of the expected size were successfully amplified and that RNA levels are similar for all the recombinant fragments (Figure 4.3).

4.4 Analysis of pools of wild-type and mutant clones from stable transfection

Pools of clones resulting from a stable transfection of MSU-1.1 cells with each of the plasmids encoding cbEGF18-26 wild-type and mutant constructs were analysed by immunoblotting for the expression of the recombinant fibrillin-1 fragment (Materials and Methods) by using a polyclonal antibody targeted at the proline-rich region (Kettle *et al.,* 2000). The expression of wild-type and mutant constructs was compared using pools of clones, rather than isolated clones, to eliminate the effects of clonal variability on the level of expression. Recombinant fibrillin-1 construct (~110 kDa) could be easily distinguished from the endogenous fibrillin-1 (~350 kDa) on the western blot, as has been shown in previous studies analysing recombinant fibrillin-1 fragments in MSU-1.1 (Kettle *et al.,* 2000; Whiteman *et al.,* 2003; Suk *et al.,* 2004). Transfection for each recombinant fibrillin-1 fragment was carried out thrice and similar results were seen for all of them.

4.4.1 Wild-type and SSS-causing mutations W1570C and C1564S secrete out of the cell

Western blot analysis of the conditioned medium from pools of clones obtained after transfection with NterPro-cbEGF18-26 wild-type and the same construct containing amino acid substitutions W1570C and C1564S is shown in figure 4.4. The wild-type fragment and the W1570C and C1564S containing fragments were always detectable in the medium and not inside the cells. The band corresponding to the recombinant protein is absent in the western blot of untransfected MSU-1.1 cells, confirming that it is derived from the recombinant construct. All samples showed good expression of endogenous fibrillin-1. Two bands indicated by the

asterisks in the figure, are seen in the medium of both mutant and wild-type samples and are also recognised in the medium of untransfected MSU-1.1 cells (Figure 4.4), suggesting cross-reaction of the anti-Pro antibody with non-specific proteins or with breakdown products derived from full-length fibrillin-1.

4.4.2 MFS-causing mutation C1564Y appears to be retained inside the cell and not secreted into the ECM

Western blot analysis of the media samples of C1564Y substituted recombinant construct showed a gradual increase of endogenous fibrillin-1 over three days, but no recombinant protein was observed as is seen in figure 4.5. A band of ~ 110 kDa was detected inside the cells, which corresponds to the recombinant fibrillin-1 fragment and is distinct from the additional products recognised by anti-Pro antibody (Figure 4.5). The results suggest that the MFS-causing mutation causes retention of the protein inside the cell.

4.4.3 Weill-Marchesani deletion (WMSdel) in TB5 domain appears to be both secreted and retained within the cell

The WMS deletion in TB5 domain of fibrillin-1 which results in a phenotype similar to SSS, creates an extra cysteine in the TB5 domain (Figure 4.1, section 1.6.3, chapter 1). The immunoblotting profile of the WMSdel fragment showed the recombinant protein is present both inside the cell and in the medium (Figure 4.5). To further investigate whether the protein retained inside the cell is in the endoplasmic reticulum (ER) or in another cellular compartment, endoglycosidase assays were performed on WMSdel and the MFS substitution C1564Y. These blots were carried from three different transfections.

4.4.4 Endoglycosidase treatment of C1564Y and WMSdel fragments

NterPro-cbEGF18-26 fragment containing the MFS substitution C1564Y appears to be retained inside the cell and NterPro-cbEGF18-26 containing the WMS deletion in the TB5 domain is seen both inside as well as outside the cell. To determine whether the mutant protein retained inside the cell is in the ER or in the Golgi apparatus, the type of carbohydrate modification on the protein was investigated using two different endoglycosidases, PNGase F and Endo H. When proteins enter the ER, the quality control mechanisms inspect conformation and ensure that only correctly folded and assembled proteins are transported further to the Golgi apparatus. Misfolded protein is retained and eventually degraded inside the cell (Ellgard *et al.,* 2001). Proteins are glycosylated in the ER but further modification of the chitobiose core of the sugar on the protein takes place in the in the Golgi apparatus where folded protein is transported to from the ER. PNGase F removes all types of N-linked (Asn linked) glycosylation; high mannose, hybrid, bi, tri, and tetra antennary, whereas Endo H removes only high mannose and some hybrid types of N-linked carbohydrates, i.e. only simple sugars, not the more complex glycosylation structures. The use of these two enzymes can indicate the compartment in which the protein is retained since only simple sugar modification occurs in the ER and more complex modifications takes place in the Golgi (Figure 4.6).

Endoglycosidase-treated samples were run on a Western blot to analyse the migratory pattern of the protein retained inside the cell compared to the untreated sample. The retained NterPro-cbEGF18-26 C1564Y fragment treated with PNGase resulted in a reduction in molecular weight of the fragment inside the cell (Figure

4.7). Endo H digested recombinant fragment co-migrated with the PNGase treated fragment suggesting that the secreted mutant protein does not have complex modification and is therefore retained in the ER. Glycosylation assays performed on the retained and secreted cbEGF18-26 WMSdel protein compared to the secreted NterPro-cbEGF18-26 wild-type fragment showed that the mutant protein is sensitive to PNGase F but not Endo H (Figure 4.7). PNGase and Endo H digests showed that protein retained inside the cell does not have complex sugar modifications and therefore is in the ER. The secreted fragment on the other hand showed resistance to Endo H because it has more complex sugar modifications similar to the wild-type. These assays show therefore, that the recombinant WMSdel fragment gets partly retained in the ER.

4.5 Immunofluorescence of fibrillin-1–containing microfibrils assembled by SSS patient fibroblasts

Since production of recombinant fragments containing SSS substitutions was shown to be similar to the wild-type fragment, fibrillin-1 microfibrils produced by SSS patient-derived fibroblasts were visualised *in situ* by immunofluorescence (IF) using a polyclonal antibody recognising the proline-rich region of fibrillin-1. IF studies were performed on three SSS cell lines, along with a cell line from a MFS patient containing a C1589F substitution in the TB4 domain because patient cell line harbouring the C1564Y substitution was unavailable. These experiments were performed three times to obtain reliable data. Three normal neonatal and adult dermal fibroblasts were used as controls. All the control fibroblasts displayed a prominent meshwork of immunostainable microfibrils (Figure 4.8). The MFS fibroblast culture showed greatly diminished immunostainable microfibrils (Figure

4.8). In contrast, each of the SSS patient cell lines displayed a pronounced array of microfibrils, similar to that observed in the control fibroblasts (Figure 4.8). These results, although qualitative rather than quantitative, indicate that SSS fibroblasts can assemble a normal fibrillin-1 microfibril meshwork, as has been observed in other primary fibroblast lines. These data suggest but do not prove that the MFS cells are deficient in microfibril assembly but taken together with recombinant trafficking analysis do show a reduced secretion of mutant fibrillin-1 protein in case of the MFS substitutions in the TB4 domain.

4.6 Discussion

Cellular trafficking experiments were carried out in order to investigate whether or not the introduced *FBN1* mutation affects protein trafficking. Despite the disruptive effects of the W1570C and C1564S substitutions on domain folding as shown in chapter 3, and thus possible intracellular retention of mutant proteins, secretion was seen in the case of the SSS mutants (Figure 4.4). The trafficking experiments performed on SSS proteins exclude the possibility of cellular retention as a major disease-causing mechanism in SSS but they do not rule out minor effects on secretion since only steady-state levels of protein were analysed. In the case of the Marfan syndrome-causing substitution C1564Y, cellular retention was seen (Figure 4.5). The studies on the differential effects of the glycosidase enzymes PNGase F and Endo H indicate the observed accumulation of the NterPro-cbEGF18-26 C1546Y mutant fragment is likely to be in the ER where a further modification of the core carbohydrate structures does not occur and the mutants fail to be targeted to the Golgi complex. Retention within an incorrect cellular compartment as a result

of misfolding of multi-domain proteins has been characterized for a number of diseases and previous studies on MFS-causing mutations have shown retention of the mutant protein can be associated with the pathogenesis of the disease (Suk *et al.,* 2004). It is interesting to note in this new DPhil study that the same cysteine residue when substituted to two different residues can result in diseases with a totally opposite phenotype, MFS (loss of function) and SSS (gain of function). Previous studies have shown that some MFS mutations result in a more lethal form of the disease than the others even when they occur at the same residue or in a particular region (neonatal) of fibrillin-1 but it has never been reported to result in two totally opposite clinical phenotypes. These results suggest that the difference in phenotype seen for these two diseases might arise due to misfolding and subsequent retention of the C1564Y MFS mutant protein, i.e., a functional haploinsufficiency, unlike the SSS C1564S substitution which is secreted effectively.

A TB5 domain deletion construct of fibrillin-1 was also investigated in this chapter as this deletion (WMSdel) has been found in patients demonstrating a phenotype similar to SSS. The secretion profile of the NterPro-cbEGF18-26 fragment containing WMS deletion indicated that there is partial retention of the mutant protein. Although there is reduced level of mutant protein seen in the ECM, it appears to confer a 'gain of function' phenotype. Treatment with endoglycosidases, PNGase and Endo H, as for C1564Y, also suggested that the retained protein contains simple sugars as it was Endo H sensitive but the secreted protein had more complex carbohydrate modifications. Pulse-chase analysis of WMSdel patient samples will further elucidate whether the retention observed is due to a delay in secretion.

Collectively, these results show that the effect of different substitution within the TB domain results in a variety of trafficking profiles, which are not easily predictable.

Analysis of RNA transcripts derived from cDNA transfections of MSU-1.1 cells did not reveal any differences that would account for the absence of C1564Y recombinant fragment in media samples in the western blot analysis compared to the wild-type, SSS and WMS fragments. This suggested that the effects of the different disease-causing substitutions are asserted at the protein level and not at the RNA level. Therefore, the use of the human fibroblast line MSU-1.1, which efficiently secretes ECM proteins, the western blot analysis, combined with the knowledge that the gene expression of the SSS-causing substitution-containing recombinant constructs was similar to wild-type, suggests that there is no major effect of these substitutions on trafficking.

Immunostaining of *Tsk* mouse fibroblasts and SSc fibroblasts have shown difference in microfibril staining, even though both are fibrotic disorders. In the case of the former, a very faint network of microfibrils was seen. SSc fibroblast cultures on the other hand, were shown to assemble similar amounts of fibrillin-1-containing microfibrils compared with control fibroblasts (Wallis *et al.,* 2003). In this study however, immunostaining of the microfibrils secreted by control and SSS patient cell lines showed an extensive microfibril network. In contrast, a MFS patient cell line (containing C1589F substitution in TB4) showed a diminished network consistent with a functional haploinsufficiency caused by cellular retention of mutant protein, or disruption of microfibril assembly. These studies also suggest that mutant fibrillin-1 is secreted and assembled into microfibrils in SSS.

In summary, the effect of disease-causing mutations on cell trafficking has been investigated for the first time for TB domains in fibrillin-1 and show pleiotropic effects which might explain the very different phenotypes that arise. The effects of these different mutations now need to be studied in the extracellular environment, in relation to microfibril assembly and interaction with other ECM molecules to further understand the difference in disease-causing mechanism.

CHAPTER 5 Cell binding properties of WT and mutant RGD-containing fibrillin-1 fragments

5.1 Introduction

TB4 domain of fibrillin-1 contains a flexible RGD loop that mediates cell adhesion *via* αVβ3, αVβ6 and α5β1 integrins (Lee *et al.,* 2004; Bax *et al.,* 2005; Jovanovic *et al.,* 2007). The RGD motif is present at the tip of a flexible loop in TB4 domain and is stabilised by a disulphide bridge (Figure 4.1). The presence of an RGD motif in TB4 and the high affinity calcium binding site formed between TB4 and cbEGF23 are likely to confer unique functional properties to this TB domain within fibrillin-1 and hence specific phenotypic consequences upon disruption of domain structure and function. Integrin αVβ3 requires TB4 to be presented as a cbEGF22-TB4 domain pair to achieve a high affinity interaction, whereas αVβ6 does not require cbEGF22 (Jovanovic *et al.,* 2007). This is most likely due to an indirect effect of cbEGF22 on RGD loop stabilisation since substitution of cbEGF22 by another cbEGF domain does not perturb the αVβ3-fibrillin-1 interaction (unpublished data). SSS substitutions W1570C and C1564S are structural mutations that affect the TB4 fold, TB-cbEGF interface and calcium binding to cbEGFs flanking the TB4 domain as shown in chapter 3 of this thesis. Although fibroblast cultures of SSS patients show microfibril network formation (Chapter 4), SSS skin shows disorganized macroaggregates of fibrillin-1 that fail to contact neighbouring cells at the dermal epidermal junction, a condition similar to that seen in the skin in systemic sclerosis (Loeys *et al.,* 2010). Since fibrillin-1 microfibrils are important component of the extracellular matrix which contribute to the regulation of ECM-cell interactions, an explanation for this pathology might be defective fibrillin-1/integrin interactions due to structural perturbation of TB4 domain.

In this chapter, biological assays have been employed to identify any effect of SSS mutations on integrin binding. Initially cell binding assays were performed to check whether the integrins on the patient dermal fibroblasts are functional and have the ability to communicate with its ECM. Following this, SSS patient cell morphology was investigated and compared to normal and MFS patient cells, as it is an important indicator of efficient integrin signalling.

In addition to testing cell binding on the triple cbEGF22-TB4-cbEGF23 prokaryotic fragments, these assays were also performed on a larger cbEGF22-25 fragment which may be more 'native-like', containing four downstream domains of TB4 domain as well as TB5 domain have been included in the glycosylated fragments as these have been shown to potentially modulate integrin binding in various studies (Bax *et al.,* 2007). To make a larger fragment using a prokaryotic expression system would have been difficult as it would be hard to assess the fold of the refolded protein; therefore, a mammalian expression system to make this fragment was a preferred choice containing post-translational modifications. This chapter outlines the successful expression and purification of a larger cbEGF22-25 eukaryotic wild-type and mutant fragments. Both non-glycosylated (cbEGF22-TB4-cbEGF23) and glycosylated fibrillin-1 fragment (cbEGF22-25) were subsequently used in this study to compare fibrillin-1/integrin interactions (Figure 5.1). SSS mutations were introduced in these fragments and cell spreading and attachment assays were then performed on cell lines expressing the αVβ3, αVβ6 and α5β1 integrins, to investigate whether or not the SSS mutations disrupt interactions with a particular integrin resulting in defective cell adhesion.

Along with the SSS substitutions, a deletion in TB5 domain was also studied in this chapter for its effect on the protein structure. An eight amino acid deletion (R-S-L-C-Y-R-N-Y) in TB5 domain of fibrillin-1 has been found in patients with Weill-Marchesani syndrome (WMS). The clinical phenotype of this disorder is similar to SSS (skin fibrosis, short stature) (Chapter 1, Section 1.6.3) but WMS deletion had a more pronounced effect on trafficking than SSS substitutions (Chapter 4). Since, Bax *et al.,* (2007) showed TB5 domain to have a heparan sulphate binding site which is predicted to modulate integrin binding, it will be interesting to see if this deletion construct results in any defective fibrillin-1 mediated integrin signalling. This deletion was analysed for its effect on cellular trafficking in the previous chapter (Chapter 4) and showed that although the deletion must introduce structural change in the domain, due to removal of a consensus cysteine residue, some protein was delivered to ECM.

5.2 Production and purification of cbEGF22-25 fibrillin-1 wild-type and mutant fragments

5.2.1 Cloning of cbEGF22-25 wild-type and mutant eukaryotic fragments

DNA fragments encoding wild-type cbEGF22-25 wild-type and mutant were amplified by PCR using fibrillin-1 cDNA and ligated into eukaryotic secretion vector pSectag (Invitrogen) (Figure 5.1). For cloning into the eukaryotic expression vector pSecTag forward primers contained a *Sfi*I restriction enzyme site and reverse primers had a *Sal*I restriction enzyme site and non-hybridizing nucleotides encoding six histidine residues and two stop codons. PCR mutagenesis was performed on the

wild-type fragment to introduce SSS mutations in the TB4 domain and WMS deletion in the TB5 domain (see appendix for primer sequences).

5.2.2 Eukaryotic expression and purification of cbEGF22-25 wild-type and mutant fibrillin-1 constructs

The wild-type and mutant fragments were expressed with a C-terminal His-tag and were transfected into HEK293S cells, which have been shown to lack N-acetylglucosaminyltransferase I (GnTI) activity, and are consequently unable to synthesize complex N-glycans (Reeves *et al.,* 2002). These cells express homogeneously glycosylated protein compared to recombinant proteins expressed from HEK293 cells, which can be highly heterogeneous. Conditioned medium was collected four days after transfection and recombinant protein was purified using Ni^{2+} affinity chromatography followed by HPLC.

Eukaryotically expressed constructs were analysed by western blot using an antibody directed against C-terminal His-tags (anti-His (Cterm); Invitrogen). The final purification product was analysed by SDS-PAGE (Figure 5.2). Only the WMS deletion containing fragment showed a faint higher molecular weight band most likely corresponding to a dimer. Treatment with endoglycosidases suggested that the recombinant protein is glycosylated (data not shown). All the recombinant constructs showed similar purification profile.

5.3 Limited proteolysis of cbEGF22-25 wild-type and mutant constructs

cbEGF22-25 wild-type, W1570C, C1564S and WMSdel fragments were studied for Ca^{2+} protection. Wild-type protein seems to display Ca^{2+} protection as is shown by the presence of intact protein in 1 mM and 50 mM Ca^{2+} at T_{60} compared to that in

EDTA (Figure 5.3 A), consistent with the presence of a native-like fold. C1564S and W1570C mutants also displayed some Ca^{2+} protection as is evidenced by the presence of some intact protein in Ca^{2+} samples at T_{60}, but not to the extent seen in the wild-type fragment (Figure 5.3 B,C). This indicates that, although C1564S and W1570C are structural mutations in TB4 domain they do affect Ca^{2+}-binding to the cbEGFs. This observation is very similar to what was seen in the case of the prokaryotically-expressed triple domain construct with the SSS substitutions and its corresponding wild-type (Figure 3.9). The WMS deletion which is in the TB5 domain, renders the protein more susceptible to proteolysis even in the presence of Ca^{2+} (Figure 5.3 D) suggesting that this deletion also affects Ca^{2+} binding to cbEGFs.

5.4 Enzyme-Linked Immuno Sorbent Assay (ELISA) to examine RGD loop exposure

The integrin-binding RGD loop in the TB4 domain is exposed in the native structure. To investigate the possibility that the disease-causing mutations may affect integrin binding by reducing the accessibility of the RGD loop, ELISAs were used to analyse whether or not the RGD motif of W1570C, C1564S and WMS deletion fragments was able to be bound by an anti-fibrillin-1 RGD antibody. This antibody recognises the loop in the TB4 domain which contains the RGD motif. To check for the availability of the RGD loop in the immobilised mutant fragments, a polyclonal antibody raised against a 14 amino acid-peptide representing the RGD loop of fibrillin-1 was used (a kind gift from Prof C. Kielty, University of Manchester).

Initially ELISAs were performed to determine whether the amount of His-tagged protein bound to the wells of MaxiSorp^{c} plate was the same for all the constructs. The primary detection antibody used in this ELISA was mouse anti-RGS His antibody

and the secondary antibody was anti-mouse IgG horseradish peroxidase conjugate. The ELISA curves show that similar amounts of mutant and wild-type proteins bind to the wells for both the triple domain fragments and six domain fragments (Figure 5.4) and thus a direct comparison of constructs could be made using an "RGD" antibody. A His_6-TB3-cbEGF11 fibrillin-1 fragment was used to compare the extent of coating to plastic in this assay and it is clear from the curves that this construct does not bind to the wells in a similar manner.

A second ELISA was performed using the anti fibrillin-RGD antibody and showed that the RGD loop is exposed in both W1570C and C1564S mutant fragments and binds the antibody at least as well as the wild-type protein (Figure 5.5). cbEGF22-25 WMSdel construct also showed similar binding to the fibrillin-1 antibody compared to the wild-type and SSS mutants indicating that the RGD loop in this fragment is also exposed. The triple domain mutant fragments also showed similar RGD loop exposure compared to the corresponding wild-type. A His_6-TB3-cbEGF11 fibrillin-1 fragment was used as a negative control in this assay, as it does not contain a RGD tripeptide sequence and as expected did not bind the fibrillin antibody.

In summary, all constructs, wild-type, W1570C, C1564S and WMSdel fragments immobilise on plastic in a similar manner and contain an exposed RGD loop which is recognised by a fibrillin-1 antibody. These assays are important in order to compare cell attachment and spreading data of different fibrillin-1 recombinant fragments, which has been described in the subsequent sections.

5.5 Effect of Stiff Skin-causing mutations on RGD-dependent cell attachment and spreading using cell lines expressing different integrins

To investigate the integrin/fibrillin-1 interaction in using protein constructs containing SSS substitutions, cellular assays were carried out. Cell spreading and attachment assays were performed using prokaryotically and eukaryotically expressed recombinant His-tagged TB4-containing wild-type and mutant constructs that were characterised in the previous chapter (see chapter 4). Cell binding experiments were performed as described by Jovanovic *et al.,* 2007, first with the shorter prokaryotic cbEGF22-TB4-cbEGF23 wild-type and SSS mutant fragments. To determine whether glycosylation and the presence of the downstream TB5 domain which has been shown to modulate integrin binding has any effect on integrin binding, eukaryotically expressed cbEGF22-25 wild-type and mutant fragments were then used in this assay. Two different cell lines human dermal fibroblasts and keratinocytes were used to check the interaction of the RGD motif-containing wild-type and mutant fragments, with different integrins expressed by these cell lines. A D1543A substitution in the cbEGF22-TB4-cbEGF23 construct (RGA mutant) used previously by Jovanovic *et al.,* (2007) and BSA were used as negative controls in this assay.

5.5.1 Immunostaining of integrins on human squamous carcinoma keratinocytes (VB6) and dermal fibroblasts (FS2)

VB6 cells were generated by transfection of the αV-, β6-negative oral squamous carcinoma cell line with human cDNAs for these integrins subunits (kind gift of Dr J Marshall). Immunostaining using antibodies against αVβ6, αVβ3 and α5β1 in VB6 cells on cbEGF22-TB4-cbEGF23 showed αVβ6 in the focal contacts. In contrast

α5β1 had a diffused staining pattern in the VB6 cells and was not shown to localise to focal contacts (Figure 5.6). Flow cytometry has previously shown αvβ6 as the most abundant integrin on VB6 cells along with α5β1. Immunostaining showed that human foreskin dermal fibroblasts (FS2 cells) express both α5β1 and αvβ3 integrins, with only the latter localising to focal adhesions (Figure 5.6).

Together, these data demonstrate that in cells adherent on fibrillin-1, integrins αVβ3 and αVβ6 are recruited to focal contacts where they colocalise with actin, in contrast integrin α5β1 does not get recruited to focal contacts but might contribute to overall adhesion to fibrillin-1 due to its abundance.

5.5.2 VB6 spreading and attachment on wild-type and mutant fragments

As shown by immunostaining assay, αVβ6 is the most abundant integrin on the surface of VB6 keratinocytes and the main mediator of their adhesion to fibrillin-1. Epithelial restricted integrin αVβ6 has been found to be a moderately high affinity receptor for fibrillin-1 and it is known that interaction in the dermal-epidermal junction is likely to be important in anchoring epidermal cells to the dermis (Jovanovic *et al.,* 2007).

The extent of cell attachment as the primary integrin-mediated event in the process of cell adhesion was estimated by attachment assay of VB6 cells on recombinant fibrillin-1 fragments. VB6 cells were added to microtiter plates precoated with recombinant cbEGF22-25 and cbEGF22-TB4-cbEGF23 fusion proteins. The cell attachment data were derived from the intensity of the crystal violet stain taken up specifically by attached cells.

The ability of the fibrilin-1 constructs to induce secondary changes in cell morphology was evaluated by quantifying the proportion of VB6 cells that adopt spread morphology on these substrates within 1.5 hr using phase contrast microscopy. Cells were shown to secrete their own matrix by 1.5 hr as was evidenced by attached and spread cells on the BSA control after 1.5 hr. The spreading assay was performed by counting 200 cells from each well of a 96-well plate, and grading them as “spreading” or “non-spreading” cells based upon morphology. Background cell attachment and spreading activity was observed for the RGA control, as expected. The data are presented as the % of cells showing a spreading morphology indexed to the total number of attached cells. All constructs were found to be similarly potent in inducing cell attachment and spreading as shown in Figure 5.7 & 5.8 and no difference between the smaller unglycosylated cbEGF22-TB4-cbEGF23 fragment and larger glycosylated cbEGF22-25 fragment was observed.

5.5.3 FS2 spreading and attachment on wild-type and mutant fragments

Since SSS patients show only skin fibrosis, dermal fibroblasts were used to study the effect of the SSS-causing mutations in fibrillin-1 on cell attachment and spreading. Immunochemical studies have shown that in dermal fibroblasts, RGD-dependent adhesion to recombinant fibrillin-1 RGD fragments is mediated through αvβ3 integrin which localises to the focal adhesions (section 5.4.1).

Fibrillin-1 constructs were pre-coated on microtitre wells and FS2 cells were added and left to incubate at 37°C for 2 hr. Number of cells attached and spread were determined in the same way as for the VB6 cells (see section 5.4.2 and Materials & Methods). The result of the FS2 cell attachment and spreading assay is

shown in Figure 5.9. SSS mutant constructs showed considerably reduced cell attachment and spreading compared to the wild-type, but C1564S substitution showed less impairment compared to W1570C (Figure 5.9 & 5.10). There was no difference seen in attachment and spreading on corresponding glycosylated and non-glycosylated fibrillin-1 wild-type and mutant proteins. These data suggest that neither glycosylation nor heparin-binding effects cell adhesion, as determined by these assays. Glycosylation might be important for the overall stability of intact protein and may modulate other fibrillin-1 interactions. Previous studies (Lee *et al.* 2004, Jovanovic *et al.* 2007) show a requirement for cbEGF22 covalently linked to TB4 for signalling through αvβ3 but not αvβ6. So it is possible that misfolding mutations in TB4 might disrupt the cbEGF22-TB4 interface in addition to any effects on TB4-cbEGF23 interface and would therefore be predicted to affect interaction with αvβ3, rather than with αvβ6. Alternatively, it may be that αvβ3 is more sensitive to the conformation of the RGD loop within TB4.

5.6 VB6 and FS2 cell attachment and spreading on Weill-Marchesani deletion (WMSdel) construct

The Weill-Marchesani deletion in TB5 domain was also tested for its effect on cell attachment and spreading. VB6 and FS2 cells plated on the WMS deletion construct showed normal cell attachment and spreading similar to the wild-type (Figures 5.11 and 5.12) suggesting that this deletion has little effect on integrin binding. This deletion also results in removing one of the potential heparan sulphate binding residue (R1691) in TB5 domain but from the cell attachment and spreading data the deletion of this residue does not seem to affect binding to integrin which leads to cell attachment and spreading. This supports the comparative wild-type

data collected for cbEGF22-25 and cbEGF22-23 which showed no impact of larger fragment on cell attachment and spreading and suggests that the pathogenic mechanism underlying WMSdel is different to that of SSS mutations.

5.7 Cellular assays on Stiff skin syndrome patient dermal fibroblasts

5.7.1 Cell attachment assay using SSS patient fibroblasts

To check whether the integrins present on the SSS patient cells have the capability of recruiting intracellular adhesion molecules and can bind to its ECM ligands, cell spreading and attachment assays were performed with SSS dermal fibroblasts and control dermal fibroblasts. SSS fibroblasts could assemble a normal fibrillin-1 microfibril meshwork similar to wild-type fibroblasts, which is in contrast to an MFS cell strain used in the experiment in the previous chapter (Section 4.5).

In this assay, cells were plated on tissue culture 96-well plates in the absence of serum, in the presence of serum and on a wild-type integrin binding cbEGF22-25 fibrillin-1 fragment which has already been shown to induce cell attachment and spreading in the previous sections. Serum contains various growth factors and ECM components that help cells to attach and spread properly and faster compared to when the cells are left to secrete their own components. It was observed that the control dermal fibroblasts grown in medium without serum start secreting their own matrix by 2 hr and consequently start spreading. Both cell types were incubated at 37°C for 72 hr to give enough time for matrix secretion and microfibril deposition (Section 4.6, Chapter 4).

The cell attachment data were derived from the intensity of the crystal violet stain taken up specifically by attached cells (see Materials & Methods). The signal

intensity at OD 620 is directly proportional to the number of adherent cells as described previously (Jovanovic *et al*., 2007). Control dermal fibroblasts showed similar attachment and spreading in all conditions, but SSS patient cells showed normal attachment and spreading only when exogenous matrix components (serum and/or wild-type fragment) were provided. MFS fibroblasts also showed normal cell attachment and spreading similar to the control cells in all the conditions (Figure 5.13).

These results suggest that the integrins expressed on the cell surface of SSS patient fibroblasts are functional and capable of binding to wild-type ECM ligands when provided exogenously, e.g., serum or recombinant RGD fragment. However, the cells secrete defective ECM which fails to induce proper cell attachment and spreading. In the next section the cell morphology of the fibroblasts derived from SSS patients has been investigated as it is an indicator of proper integrin signalling.

5.7.2. Cell morphology of SSS patient cells

Alterations in ECM and integrin signalling result in changes in cell shape and behaviour. Cell morphology is determined by the organization of the intracellular actin cytoskeleton, which is influenced by events inside and outside the cell. Focal adhesions are sites at which the actin cytoskeleton is linked to the extracellular matrix by integrin receptor complexes as described in the first chapter (section 1.4.1). Actin is present in cells in its globular form (G-actin) and in its filamentous form (F-actin). When a cell spreads, mechanical forces at the focal adhesions induce actin polymerisation and form long F-actin filaments. Therefore, if there is defective integrin signalling in a disease state, cell shape and morphology would be affected.

To test if this is the case in SSS patient fibroblasts, cells were stained for F-actin in the absence of any exogenous ECM component and in the presence of a wild-type TB4-containing fibrillin-1 ligand.

SSS, MFS and control dermal fibroblasts were plated on a four-well tissue culture plate. In one well they were plated in the absence of any serum/exogenous ECM component and on the second well they were plated on cbEGF22-25 fibrillin-1 fragment. After incubating for 72 hr at 37°C, cells were stained for F-actin using a fluorescently labelled phalloidin conjugate. SSS patient cells, in the presence of their own matrix, but in the absence of any exogenous ECM component showed diffused actin staining indicative of defective spread morphology, but the morphology was rescued when a wild-type ligand (or serum) was present (Figure 5.14) and prominent long actin filaments were observed. Control and MFS cells on the other hand, showed long actin bundles indicative of a spread cell both when on their own matrix and in the presence of wild-type fibrillin-1 cbEGF22-25 fragment. The difference in the way the control and patient cells stained for actin suggested that there might be defective ECM-integrin interactions in case of SSS.

These preliminary results on SSS patient fibroblasts suggest that there is likely to be a defective ECM-cell interaction in SSS but not in MFS.

5.5 DISCUSSION

In this chapter, the effect of the SSS substitutions on structure was investigated in a large glycosylated fragment in preparation for its use in comparative cell spreading assays. W1570C and C1564S substitutions were introduced in the cbEGF22-25 six domain construct, which included a downstream

heparin/heparan sulphate binding TB5 domain. An eight amino acid deletion in TB5 domain which results in Weill-Marchesani syndrome was also introduced in this fragment and all the mutants were checked for their proteolytic susceptibility. These recombinant fragments were expressed in HEK293S cells and eluted as a single sharp peak on HPLC purification after Ni^{2+} affinity chromatography. SDS-PAGE analysis showed that samples were homogenous on the basis of presence of single sharp band. There was very little calcium protection from proteolysis seen for the SSS mutants compared to the wild-type. This observation is similar to calcium protection from proteolysis demonstrated by these SSS substitutions in prokaryotically expressed cbEGF22-TB4-cbEGF23 triple domain fragments. The WMSdel fragment showed more proteolytic susceptibility compared to the SSS mutants suggesting that this deletion has a marked effect on calcium binding and domain folding. ELISA experiments showed that the RGD loop is exposed in both mutant recombinant peptides, despite their observed effect on structure and is therefore available for integrin interactions (Figure 5.5). This was also the case for the cbEGF22-25 WMSdel construct.

In order to test the hypothesis that SSS mutations alter integrin binding, fibrillin-1 fragments were prepared that encode TB4 and adjacent calcium-binding epidermal growth factor-like domains and TB5 domain containing a heparin/heparan sulphate binding site (cbEGF22-TB4-cbEGF23 and cbEGF22-25) as described before. Prokaryotic and mammalian expression systems were used to make the recombinant proteins to check if presence of downstream heparin/heparan sulphate-binding TB5 domain had any effect on cell spreading and attachment compared to prokaryotically expressed non-glycosylated protein.

Immunochemical studies showed that in human dermal fibroblasts (FS2 cells), RGD-dependent adhesion to recombinant fibrillin-1 RGD fragments is mediated through αvβ3 integrins with a possible contribution from α5β1, whereas in VB6 keratinocytes, a keratinocyte cell line expressing high levels of integrin αvβ6, it is largely dependent on αvβ6 (Jovanovic *et al.,* 2007) (Figure 5.6). Human foreskin dermal fibroblasts (FS2 cells) express both α5β1 and αvβ3 integrins, with only the latter localizing to focal adhesions (Figure 5.6). Therefore, we assessed integrin-mediated events when different cell types were plated on dishes coated with either wild-type or mutant recombinant fibrillin-1 fragments. VB6 keratinocytes showed normal attachment and spreading when plated on mutant as well as wild-type substrates, consistent with preserved αvβ6 integrin-fibrillin-1 interactions in this system (Figure 5.7 & 5.8). In contrast, both SSS mutations induced a dramatic loss of both attachment and spreading of FS2 cells, suggesting impairment of interaction with αvβ3 integrins and may be to some extent to α5β1 (Figure 5.9 & 5.10). A contribution from α5β1 in these cell lines cannot be ruled out even though it is not present in focal adhesions because this integrin has been found to modulate cell adhesion and morphology in a 3D matrix (Zamir and Geiger, 2001; Yamada *et al.,* 2003). A contribution from other integrins, such as α8β1, αvβ5, αvβ8 etc. also cannot be ignored and will be investigated in the future. These findings support the skin-specific phenotype of the disease where no other organ system is affected, indicating that specific fibrillin-1/integrin interactions might be affected in this disorder.

No difference in cell attachment and spreading was observed for glycosylated wild-type and mutant cbEGF22-25 constructs compared to the non-glycosylated

cbEGF22-TB4-cbEGF23 constructs. This suggests that glycosylation and presence of a heparan sulphate-binding TB5 domain downstream of the TB4 domain, does not have an effect on integrin binding in case of both wild-type and the mutants as has been presented in a study by Bax *et al.,* 2007.

FS2 and VB6 cells on fibrillin-1 cbEGF22-25 fragment containing the WMS deletion did not show any difference in cell attachment and spreading compared to the wild-type fragment (Figure 5.11). This suggests that the disease-causing mechanism in case of WMS disorder is likely to be different from SSS, even though it has some phenotypic similarity with SSS. Since, the WMS deletion is in the TB5 domain of fibrillin-1, it is unlikely to affect the structure of TB4 domain as much as the SSS mutations which are present in this domain, however, other cell-matrix interactions may be affected. These findings highlight the importance of this region and possibility of other ECM-fibrillin-1 interactions that have not yet been studied.

In this chapter cell-based assays were also performed on SSS patient dermal fibroblasts to investigate their cell morphology which is an indicator of integrin signalling. Integrins present on patient cells were also checked for their ability to induce cell spreading and attachment, an indicator of functionality. Patient and control cell lines were used for these assays as they had shown normal microfibril networks for SSS patient cells (Chapter 4). This assay showed that the integrins on the cell surface of the SSS patient fibroblast have the capability to bind to wild-type ECM components and could mediate events leading to cell attachment and spreading. In the absence of any exogenous ECM component, patient cells showed defective spreading and diffuse F-actin staining (Figures 5.13 & 5.14). A MFS cell line was also used in these assays to study the difference in the spread morphology

compared to SSS patient cells. MFS patient cells showed normal cell attachment and spreading similar to the control cells even though they appear to secrete less fibrillin-1 microfibrils (Chapter 4). Cultured dermal fibroblasts from patients with SSS have also shown reduced amounts of the activated (phosphorylated) form of focal adhesion kinase (pFAK), an event mediated by the interaction of RGD ligands with integrins concentrated at focal adhesions (Loeys *et al.,* 2010). Reduced levels of FAK in SSS indicate defective integrin signalling. These preliminary data using patient dermal fibroblasts suggest that the matrix produced by SSS dermal fibroblasts is defective and leads to impaired ECM-cell interactions, despite the fact that a fibrillin network can be observed by immunocytochemistry (Chapter 4).

Taken together, these data suggest that *FBN1* mutations that cause SSS can impair binding to selective integrins establishing this as a plausible mechanism for the isolated phenotype. Defective integrin binding does not underlie the pathology of WMS.

CHAPTER 6
Quantitative analysis of wild-type and Stiff skin mutant RGD-containing fibrillin-1 fragments/ αVβ6 and αVβ3 integrin interactions

6.1 Introduction

Cell adhesion assays (Chapter 5) showed that the SSS mutant fibrillin-1 fragments disrupt cell attachment and spreading in the case of human dermal fibroblasts (FS2) but not in keratinocytes (VB6). A fibrillin-1 fragment containing the Weill-Marchesani deletion (WMSdel) allowed for normal cell attachment and spreading in both cell lines. To investigate the effect of each mutation on the stability of the fibrillin-1/integrin complex, the surface plasmon resonance (SPR) technique was employed. SPR technology is an extremely useful technique in quantifying the effect of mutations on the thermodynamics and kinetics of weak protein/ligand interactions and for this reason it has been employed to study the effect of the SSS mutations on the fibrillin-1/integrin interactions. SPR has been used previously to investigate the binding interaction between fibrillin-1 and integrins αVβ3 and αVβ6 (Jovanovic *et al*., 2007) and these studies showed that domain cbEGF22, which is immediately N-terminal to the RGD-motif containing TB4 domain is essential for binding in case of the αVβ3 binding, but not for αVβ6. The kinetics of α5β1-fibrillin-1 complex formation has not been reliably measured by SPR due to its very low affinity and the consequent requirement for the large amounts of analyte (Jovanovic *et al*., 2007).

Triple domain cbEGF22-TB4-cbEGF23 wild-type and mutant constructs produced in a prokaryotic system, and six domain cbEGF22-25 wild-type and mutant constructs expressed in a eukaryotic expression system, were used to study the effect of the SSS mutations on the kinetics of fibrillin-1/integrin complex formation (Figure 6.1). These are the same TB4-containing fragments that were investigated for cell attachment and spreading previously (Chapter 5). Fibrillin constructs were

immobilised on the CM5 surface by amine-coupling (see Materials & Methods). This study also investigated whether glycosylation and the presence of domains downstream of the TB4 domain has any effect on fibrillin-1/integrin complex stability or affinity compared to the non-glycosylated cbEGF22-TB4-cbEGF23 fibrillin-1 fragments.

6.2 Surface Plasmon Resonance

Biacore biosensors, which are currently the most widely used SPR-based instrument, have been used in this study to investigate fibrillin-1/integrin interactions. Biacore technology allows biomolecular interactions to be monitored in real time and is suitable not only for the determination of the thermodynamic parameters (association and dissociation constants, K_a and K_d respectively) but also individual rate constants of the association (k_a) and the dissociation reaction (k_d). Real time binding data is important to understand the dynamic interactions between proteins and other biomolecules that drive and regulate biological processes.

In Biacore, binding events are monitored at the solution/metal interface where one molecule (ligand) is immobilised onto the sensor surface and its binding partner (analyte) is injected in aqueous solution (sample buffer) through the flow cell, also under continuous flow. When the analyte binds to the ligand the accumulation of protein on the surface results in an increase in the refractive index. This change in refractive index is measured in real time, and the result plotted as resonance units (RUs) versus time as a sensorgram. A background response is also generated if there is a difference in refractive indices of the running and sample buffers. This background response is subtracted from the sensorgram to obtain the actual binding

response. The background response is recorded by injecting the analyte through a control or reference flow cell, which has no ligand or an irrelevant ligand immobilized to the sensor surface. One RU represents the binding of approximately 1 pg protein/mm^2 (Surface plasmon resonance, P. Anton van der Merwe).

6.2.1 Physical basis of Surface Plasmon Resonance

SPR-based biosensors measure the intensity (I) of the light reflected from the conducting film at the interface between two media of different refractive indexes (n) as a function of the angle of the incident beam of light (θ) (Figure 6.2). When a beam of light passes from material with a high refractive index into material with a low refractive index some light is reflected from the interface. When the angle at which the light strikes the interface (θ) is greater than the critical angle (θc), the light is completely reflected (total internal reflection). If the surface of the glass is coated with a thin film of a noble metal (e.g. gold), this reflection is not total; some of the light is lost into the metallic film. The angle at which this loss is greatest and at which the intensity of reflected light reaches a minimum or 'dip' is called the surface plasmon resonance angle (θspr). It is a result of the oscillation of mobile electrons (or 'plasma') at the surface of the metal film which are known as surface plasmons. When the wave vector of the incident light matches the wavelength of the surface plasmons, the electrons 'resonate', hence the term surface plasmon resonance. The 'coupling' of the incident light to the surface plasmons results in a loss of energy and therefore a reduction in the intensity of the reflected light. It is because the amplitude of the wave vector in the plane of the metallic film depends on the angle at which it strikes the interface that a θspr is observed. A momentary (decaying)

electrical field associated with the plasma wave travels for a short distance of ~300 nm into the medium from the metallic film. Because of this, the resonant frequency of the surface plasma wave (and thus θspr) depends on the refractive index of this medium. If the surface is immersed in an aqueous buffer (refractive index or μ ~1.0) and protein (μ ~1.33) binds to the surface, this results in an increase in refractive index which is detected by a shift in the θspr. The Biacore instrument uses a photo-detector array to measure very small changes in θspr. The change is quantified in resonance units or response units (RUs) with 1 RU equivalent to a shift of 10-4 degrees. Empirical measurements have shown that the binding of 1 ng/mm^2 of protein to the sensor surface leads to a response of ~1000 RU. Apart from the refractive index, temperature also affects θspr and therefore it is important to have a precise temperature control (Surface plasmon resonance, P. Anton van der Merwe; Biacore).

6.2.2 Biacore sensor chips

In the Biacore system a sensor chip houses four separate sensor surfaces (composed as described above), each of which forms the floor of a flow cell through which the running buffer continuously flows. Injections can be made over individual or combinations of flow cells during an experiment and real time detection of the SPR signal occurs in all cells or selected cells only. These capabilities enable the immobilization of different ligand molecules on each sensor surface in preparation for comparative experiments in which analyte injections are allowed to flow over all four flow cells. The responses of each different ligand molecule to the same analyte solution can therefore be seen in real time. One of the four sensor

surfaces should always be used as the control surface for determination of the background SPR signal associated with each analyte injection.

6.2.3 Kinetics and affinity measurements using Biacore

The affinity of an interaction can be represented in a number of ways, the most common of which is as a dissociation constant or K_D. This is simply the ratio at equilibrium of product and reactant concentrations during the dissociation of two molecules. Thus for:

$$AB \longleftrightarrow A + B \qquad K_D = [A]\,[B] / [AB]$$

The K_D of an interaction can be determined in one of two ways using the Biacore system. The first involves a kinetic approach in which the association and dissociation rate constants (k_a and k_d respectively) are determined through analysis of the association and dissociation phases of binding curves obtained when different concentrations of analyte are injected over the ligand surface. The dissociation constant can then be calculated from these two rate constants:

$K_D = k_d / k_a$

A drawback of this approach is the problem of mass transport. Because of the high surface density of ligand on the sensor surface, the rate at which analyte binds ligand can exceed the rate at which it is delivered to the surface (referred to as mass transport). In this situation binding is said to be mass transport limited. They can be reduced by increasing the flow rate and, most importantly, lowering the level of immobilised ligand. Kinetic measurements can give a reliable estimate of the stability of a complex.

Another approach to determine the affinity of an interaction is equilibrium binding analysis. This method involves the injection of a series of analyte solutions of varying concentrations over the ligand surface with each injection being sufficiently long for the interaction to reach equilibrium. Non-linear curve fitting can then be used to fit the equilibrium binding data to an appropriate binding model. The Langmuir model is applicable in most cases. This assumes that the analyte (A) is both homogenous and monovalent and that the ligand (L) is also homogenous. Thus for the interaction,

$A + L \leftrightarrow AL$

$RU = ([A] * RU^{Max}) / ([A] + K_D)$

where RU is the equilibrium binding response obtained at analyte concentration [A]. RU^{Max} represents the binding response at saturation and K_D has the same units as [A].

In this chapter, a kinetics approach has been adopted to investigate stabilities of the mutant fibrillin-1/integrin complexes, as Biacore generates real-time binding data making it suitable to analyse binding kinetics of protein complexes. It is also less time consuming compared to equilibrium binding analysis. Mass transport effect has been negated by using a low level of immobilised ligand and high flow rate.

6.3 Results

6.3.1 Preparation of active surface

In this study, fibrillin ligands were initially immobilised on the carboxymethyldextran-modified gold surface of a CM5 sensor chip (Biacore Inc.), using two different approaches; direct amine coupling and indirect coupling *via*

streptavidin. A representative sensorgram obtained during amine coupling of a fibrillin-1 ligand to the dextran surface of a CM5 chip is shown in Figure 6.3. Amine-coupling yields a very stable, although heterogeneous surface and often decreases or completely abrogates analyte binding. To check for this, the cbEGF22- TB4-cbEGF23 fragments were constructed with a C-terminal BirA tag which allowed site-specific biotinylation. Streptavidin was coupled to the CM5 chip *via* amine-coupling and fibrillin-1 ligands were flowed over it. It was observed that there was no significant difference in the K_D in case of both amine-coupled and indirect streptavidin-coupled wild-type and mutant constructs (data not shown) and therefore amine-coupled ligands were used for the subsequent SPR experiments.

6.3.2 Quantitative analysis of SSS mutants and wild-type fibrillin-1 fragments with αVβ6 integrin

Keratinocytes plated on either wild-type or SSS mutant fibrillin-1 fragments showed normal cell attachment and spreading behaviour, with focal adhesions in these cells formed by interactions involving αVβ6 (Chapter 5). These interactions were investigated by SPR using recombinant truncated αVβ6 integrin (Weinacker *et al*., 1994) expressed and purified by Dr. N. Abrescia, CIC bioGUNE, Spain. SDS-PAGE analysis of integrins demonstrated that the heterodimer was purified to > 95% homogeneity (see Appendix C).

Kinetic measurements were performed by immobilising fibrillin ligands on a CM5 chip at low density to reduce mass transport effects, and monitoring αVβ6 binding at a wide range of concentrations (75-700 nM) in the presence of Ca^{2+}, Mg^{2+} and Mn^{2+} at 2 mM each in the running buffer to ensure that integrins are in the

extended conformation optimal for ligand binding (Shimaoka *et al.,* 2002; Jovanovic *et al.,* 2007) (Figure 6.4 & 6.5). Both non-glycosylated and glycosylated fibrillin-1 recombinant fragments were tested. The soluble integrin was injected through each Biacore flow cell with fibrillin fragments bound to CM5 sensor surface at several concentrations. Only a bulk refractive index change was observed in the control flow cell with the control non-glycosylated cbEGF22-TB4-cbEGF23 RGA mutant (see chapter 5), which was subsequently subtracted from the sensorgrams obtained with test proteins to give the actual binding response. The dissociation phase of binding curves was found to fit well to a simple one-step Langmuir model. Biacore T100 evaluation software was employed to determine the different rate constants. The dissociation rates of αVβ6 integrin for the different fibrillin-1 constructs were found to be almost identical, suggesting equivalent stability of the wild-type and mutant fibrillin-1/integrin complexes. Excellent fits were obtained when fitting the association and dissociation phase of sensorgrams onto a 1:1 Langmuir binding model (χ^2 values <0.1) (Figure 6.4 & 6.5). The chi-squared (χ^2) value was used to judge the quality of fit between experimental data and that derived from binding models. The smaller the χ^2 value, the smaller their variation. Typically, good fittings derive χ^2 values less than 10 (Baglia *et al.,* 2000). SPR data obtained for the wild-type cbEGF22-TB4-cbEGF23/αvβ6 interactions is in agreement with binding studies done by Jovanovic *et al.,* (2007) on prokaryotic cbEGF22-TB4-cbEGF23 wild-type fragment with recombinant integrin αvβ6.

Table 6.1 *SPR-derived kinetic parameters and apparent K_D values for αVβ6 binding to WT and mutant fibrillin-1 fragments, immobilised via amine-coupling. Values represent mean ± S.D. from three different experiments using recombinant fibrillin-1 constructs from three different protein preparations.*

Ligand (Amine-coupled)	k_a x10 ^{4} $M^{-1}s^{-1}$	k_d x10^{-4} s^{-1}	K_D (x 10^{-7} M) (k_d/k_a)
Non-glycosylated			
cbEGF22-TB4-cbEGF23 WT	3.53 ± 0.05	57.7 ± 0.31	1.6 ± 0.2
cbEGF22-TB4-cbEGF23 W1570C	3.74 ± 0.01	52.59 ± 0.55	1.4 ± 0.15
cbEGF22-TB4-cbEGF23 C1564S	3.34 ± 0.01	60.2 ± 0.01	1.8 ± 0.01
Glycosylated			
cbEGF22-25 WT	1.2 ± 0.11	26.44 ± 0.61	2.2 ± 0.05
cbEGF22-25 W1570C	1.61 ± 0.54	56.17 ± 0.13	3.48 ± 0.15
cbEGF22-25 C1564S	2.5 ± 0.06	58.4 ± 0.40	2.33 ± 0.31

6.3.3 Quantitative analysis of SSS mutants and wild-type fibrillin-1 fragments with αVβ3 integrin

The real-time kinetic parameters of the fibrillin-1/αVβ3 complex formation were monitored using truncated recombinant αVβ3 integrin (a generous gift from Professor J. Takagi, Osaka University, Japan; Takagi *et al.,* 2002, Appendix C) and fibrillin-1 fragments amine-coupled to the surface of a CM5 sensor chip at equivalent density. Binding of injected soluble αVβ3 of various concentrations (32-120 nM) was monitored in the presence of Ca^{2+}, Mg^{2+} and Mn^{2+} at 2 mM each (Figure 6.6 & 6.7). Dissociation and association phases were analysed separately as described in the previous section.

The wild-type cbEGF22-TB4-cbEGF23 fragment and cbEGF22-25 fragment showed similar kinetics. Kinetic analysis of the sensogram yielded a K_D of 43 ± 2.3 nM for cbEGF22-TB4-cbEGF23 wild-type/ αVβ3 and a K_D of 38 ± 3.1 nM for cbEGF22-25 wild-type/ αVβ3 interactions. The K_D value obtained for these fragments is in

agreement with previous values obtained by SPR using TB4-containing fibrillin-1 fragments performed earlier (Jovanovic *et al.,* 2007). Each mutant was subsequently tested and all showed weaker binding with a ~20 fold difference in K_D for cbEGF22-TB4-cbEGF23 W1570C/αVβ3 and an ~ 8 fold difference for cbEGF22-TB4-cbEGF23 C1564S/αVβ3 interactions was observed compared to the wild-type (Figure 6.6 & 6.7; Table 6.2). Similarly, a ~ 15 fold difference in K_D of glycosylated cbEGF22-25 W1570C/ αVβ3 and a ~13 fold difference for cbEGF22-25 C1564S/ αVβ3 interactions compared to cbEGF22-25 wild-type was recorded. Therefore overall, a significant difference in K_D compared to the wild-type fragment was seen for the triple domain mutant fragments and six domain mutant fragment, all mutants showing a reduced affinity for αVβ3 integrin.

Even though the association constants (k_a) of the wild-type and mutant cbEGF22-TB4-cbEGF23 constructs were comparable, the dissociation constants (k_d) showed that the mutant fibrillin-1/ αVβ3 complex was very unstable and dissociated faster than the wild-type construct (Table 6.2). The same result was observed for glycosylated fibrillin-1 cbEGF22-25 fragments containing the SSS mutations. A similar difference in dissociation constants has been observed previously between the interactions of cbEGF22-TB4 and TB4-cbEGF23 wild-type fragments with αVβ3 (Jovanovic *et al.,* 2007), with the former establishing a more stable complex with the integrin compared to TB4-cbEGF23, thereby highlighting the importance of the presence of upstream cbEGF22 domain for interaction with αVβ3. It is therefore possible that the cbEGF22-TB4 interface has been disrupted by the SSS substitutions, which makes the complex unstable compared to the wild-type, although the

conformation of RGD loop may have been altered independent of the cbEGF22-TB4 interface.

Table 6.2 *SPR-derived kinetic parameters and apparent K_D values for αVβ3 binding to WT unglycosylated and glycosylated fibrillin-1 fragments, immobilised via amine-coupling. Values represent mean ± S.D. from three different experiments using recombinant fibrillin-1 constructs from three different protein preparations.*

Ligand (Amine-coupled)	k_a x10 ^{4} $M^{-1}s^{-1}$	k_d x10^{-5} s^{-1}	K_D (x 10^{-8} M) (k_d/k_a)
Unglycosylated			
cbEGF22-TB4-cbEGF23 WT	1.2 ± 0.01	0.52 ± 0.22	4.3 ± 0.23
cbEGF22-TB4-cbEGF23 W1570C	0.80 ± 0.23	6.44 ± 0.34	80.4 ± 0.54
cbEGF22-TB4-cbEGF23 C1564S	1.8 ± 0.04	6.53 ± 0.1	34.9 ± 0.3
Glycosylated			
cbEGF22-25 WT	3.7 ± 0.05	1.40 ± 0.52	3.8 ± 0.31
cbEGF22-25 W1570C	6.5 ± 0.21	39.13 ± 0.41	60.2 ± 0.31
cbEGF22-25 C1564S	4.7 ± 0.02	22.59 ± 0.45	50.2 ± 0.33

6.3.4 Kinetic analysis of SSS mutants and wild-type fibrillin-1 fragments with α5β1 integrin

α5β1 integrin fails to be recruited into the focal contacts in both dermal fibroblasts and keratinocytes. The kinetic data obtained for a series of concentrations of α5β1 (recombinant integrin, kind gift by Prof J Takagi, Japan, Appendix C) flowed over wild-type as well as mutants, did not fit the 1:1 Langmuir binding model and had a very high χ^2 value, making it impossible to determine a reliable K_D for this interaction. Determining kinetics of α5β1-fibrillin-1 complex formation by SPR has been unsuccessful in the past due to its low affinity and the consequent requirement for the large amounts of analyte. However, this interaction has been studied in a reverse orientation by enzyme-linked immunosorbent assay

and K_D >1 μM when it was fitted in a simple 1:1 Langmuir binding model (Jovanovic *et al.,* 2007). This integrin was tested for its activity by flowing it over FNIII 9-10 fragment, which has already been shown to be a strong ligand for this integrin, amine-coupled to the SPR chip and a K_D of 13.2±1.2 nM was recorded. This value is in agreement with already published data for this interaction (Takagi *et al.,* 2003; Altroff *et al.,* 2003; Jovanovic *et al.,* 2007) therefore showing that this integrin is active and functional.

6.3.5 Weill-Marchesani deletion (WMSdel)-containing cbEGF22-25 fragment shows normal binding to both αVβ3 and αvβ6 integrins

Interaction of purified αVβ3 and αvβ6 integrins with the cbEGF22-25 WMSdel fragment was also assessed by SPR to determine whether this deletion alters the stability of fibrillin-1/integrin complex. This WMS deletion is present in the TB5 domain which is three domains downstream of the integrin binding TB4 domain. This domain has been shown to modulate integrin binding in a cell binding study by Bax *et al.,* (2007) but the WMSdel fragment was found to induce cell attachment and spreading similar to the wild-type fragment (Chapter 5). This result indicated that this deletion in TB5 does not have a significant effect on cell binding, suggesting that integrin binding to TB4 is unaffected by the change to TB5 domain structure. Quantitative kinetic parameters of αvβ6/WMSdel cbEGF22-25 interactions were found to be similar to the wild-type construct (Table 6.3). This suggests that this deletion does not affect the αvβ6 interaction with fibrillin-1 and the complex is as stable as that for the wild-type.

Table 6.3 *SPR-derived kinetic parameters and apparent K_D values for αVβ6 binding to cbEGF22-25 wild-type and WMSdel fibrillin-1 fragments, immobilised via amine-coupling. Values represent mean ± S.D. from three different experiments using recombinant fibrillin-1 constructs from three different protein preparations.*

Ligand (Amine-coupled)	k_a x10^4 $M^{-1}s^{-1}$	k_d x10^{-4} s^{-1}	K_D (x 10^{-7} M)
cbEGF22-25 WT	1.2 ± 0.11	26.44 ± 0.61	2.2 ± 0.05
cbEGF22-25 WMSdel	1.3 ± 0.11	27.84 ± 1.11	2.1 ± 0.56

SSS mutants showed reduced affinity for αvβ3 integrin and formed less stable complexes with the integrin. Association and dissociation constants of αvβ3/WMSdel cbEGF22-25 interactions suggested that unlike the SSS mutants, the affinity and stability of the complex in case of the WMS deletion are similar to the wild-type (Table 6.4). The kinetic parameters for this interaction are given below.

Table 6.4 *SPR-derived kinetic parameters and apparent K_D values for αVβ3 binding to cbEGF22-25 wild-type and WMSdel fibrillin-1 fragments, immobilised via amine-coupling. Values represent mean ± S.D. from three different experiments using protein from three different preparations.*

Ligand (Amine-coupled)	k_a x10^4 $M^{-1}s^{-1}$	k_d x10^{-5} s^{-1}	K_D (x 10^{-8} M)
cbEGF22-25 WT	3.7 ± 0.05	1.47 ± 0.52	3.8 ± 0.31
cbEGF22-25 WMSdel	2.3±0.36	13.7±0.08	5.96±0.10

These findings support the cell binding data of this fragment (Chapter 5) which demonstrates that WMSdel is indistinguishable from wild-type in supporting attachment and spreading.

6.4 DISCUSSION

Results in this chapter support the findings of the previous chapter where both glycosylated and non-glycosylated SSS mutant fragments failed to induce attachment and spreading on dermal fibroblasts *via* αVβ3 integrin but showed normal attachment and spreading on keratinocytes expressing αVβ6 integrin. α5β1 did not localise to the focal contacts in either of the cell lines and has been shown to have a very low affinity for fibrillin-1 (Jovanovic *et al.,* 2007).

Quantitative analysis of wild-type and mutant fibrillin-1 interactions with αVβ6 exhibited similar K_D values for all the constructs, showing that SSS mutations do not significantly affect the fibrillin-1/ αVβ6 interaction. On the other hand, SSS mutants showed a much weaker interaction with αVβ3 compared to the wild-type. Non-glycosylated cbEGF22-TB4-cbEGF23 wild-type protein amine-coupled to the chip showed higher stability of the fibrillin-1/ αVβ3 complex compared to the W1570C and C1564S substitutions containing cbEGF22-TB4-cbEGF23 fragments, since K_D values for mutants were ten folds larger than wild-type. Similarly, glycosylated cbEGF22-25 wild-type fragment also showed higher affinity for the αVβ3 integrin compared to the SSS mutants due to a higher stability of the complex. This suggests that neither glycosylation nor the presence of the TB5 domain downstream of the TB4 domain stabilise the isolated fibrillin-1/integrin complex, in contrast to previously published data (Bax *et al.,* 2007). The kinetic data obtained for a series of concentrations of α5β1 did not fit the 1:1 Langmuir model and had a very high χ^2 value, making it impossible to determine a reliable K_D for this interaction.The same soluble integrin was flown over a recombinant fibronectin fragment and displayed a K_D of ~13.2 nM, which is in agreement with already published values for

this interaction (Takagi *et al.,* 2003; Altroff *et al.,* 2003; Jovanovic *et al.,* 2007). This shows that the activity of the integrin fragment

The cbEGF22-25 fragment containing the WMS deletion in the TB5 domain was shown to be capable of inducing cell attachment and spreading on both keratinocytes and dermal fibroblasts, similar to the cbEGF22-25 wild-type fragment. This fragment was investigated in this chapter for its interaction with αVβ3 and αVβ6 integrins alongside the SSS mutants. Kinetic analysis of the WMSdel fragment interaction with αVβ6 and αVβ3 integrins demonstrated a K_D similar to the wild-type, suggesting that the deletion in TB5 does not affect its interaction with either of the integrins. This again suggests that the underlying disease-causing mechanism in the case of WMS is different to that associated with SSS. It is possible that a defective fibrillin-1 interaction with some other cell matrix molecule is the primary cause. Since mutations in the ADAMTS10 gene have been found in the recessive form of WMS and ADAMTSL6 has been shown to interact with N-terminal region of fibrillin-1, it would be valuable to investigate the role of ADAMTS proteins in the dominant form of this disorder caused by the WMS deletion. Fibrillin-1/ADAMTS interaction studies could potentially give important clues for understanding the pathogenesis of AD WMS and it is interesting to speculate that defective fibrillin-1/ADAMTS interactions may underlie the phenotype.

Data in this chapter suggest that the SSS mutants form stable complexes with αVβ6 integrin, but not with αVβ3. The presence of the TB5 domain downstream of the integrin-binding TB4 domain and glycosylation does not significantly affect the stability of the fibrillin-1/integrin complex, although additional protein-protein/ GAG interactions mediated by domains in close proximity may help stabilise microfibril

interactions with cell-matrix *in vivo*. This study in a way differs with the previously published work (Bax *et al.,* 2007) on the TB5 domain which was shown to contain a heparin-binding site which was found to modulate fibrillin/integrin interactions. Bax *et al.* study however used only cell-based assays and did not study affect of the heparin-binding site on specific fibrillin-1/integrin interaction, whereas the results discussed in this chapter have been achieved by employing a combination of cellular as well as biophysical assays. Different fibrillin-1 fragments will be now used to investigate these synergistic interactions and effect of the mutations on them in more detail.

CHAPTER 7 Discussion

7.1 DISCUSSION

To date, all known mutations in the fibrillin-1 gene that result in Stiff skin syndrome have been shown to affect the gene sequence encoding TB4 domain. This is the only domain of fibrillin-1 that harbours the Arg-Gly-Asp (RGD) sequence that mediates cell-matrix interactions *via* integrins. SSS skin shows disorganised macroaggregates of fibrillin-1 that fail to contact neighbouring cells at the dermal-epidermal junction, as well as deposition of excessive elastin and collagen. This study has used cellular, biochemical and biophysical methods to investigate the effects of SSS mutations on domain structure; the secretion of fibrillin-1 from the cell and interactions with integrins. The results demonstrate that the SSS mutations affect domain structure but do not significantly alter secretion of fibrillin from the cell unlike many MFS mutations. Cell binding assays show that SSS mutations affect binding to αvβ3 integrin, but not αvβ6 integrin suggesting a specific integrin-mediated cell-matrix interaction that is essential for cell adhesion, shape and migration is disrupted. Excessive microfibrillar deposition, impaired elastogenesis, and increased TGFβ concentration and signalling in the dermis occurs in SSS patients (Loeys *et al.,* 2010) and these data suggest that selectively impaired integrin interactions may contribute to pathogenesis.

7.2 Structural effects and cell trafficking profile of the Stiff skin-causing mutations

A variety of biochemical and biophysical assays were used to show that the W1570C and C1564S substitutions identified in SSS patients affect the structural integrity of the domain (Chapter 3). The C1564Y MFS-causing substitution in cbEGF22-TB4-cbEGF23 fragment was also investigated in this assay as this

substitution occurs at the same residue which, when substituted with a serine, is found to cause SSS. The successful production of TB4-cbEGF23 wild-type, W1570C, C1564S and cbEGF22-TB4-cbEGF23 wild-type, W1570C, C1564S and C1564Y mutant constructs using an *in vitro* refolding system, demonstrated that the disruption of a disulphide bond and a highly conserved tryptophan residue in TB4 domain, did not prevent folding of the mutant constructs into defined conformational species, the majority of which was monomeric. However, all the mutant fragments showed an increase in susceptibility to protease digestion when compared with wild-type indicating that the mutations results in the instability of the protein structure. It was not possible to determine a K_D value for the binding of calcium to the mutant constructs using chromophoric calcium chelation assay with Br_2BAPTA suggesting that the K_D for both the mutants is significantly higher than the measured K_D of Br_2BAPTA (~1.6 µM; Jensen *et al.,* 2005) in contrast to K_D values of 8 nM (cbEGF22-TB4-cbEGF23) and 16 nM (TB4-cbEGF23) for the wild-type constructs. The fragment containing the MFS-causing C1564Y substitution showed more susceptibility to proteolysis compared to the C1564S substitution, indicating that this mutation may have a more dramatic effect on the domain fold compared to the SSS mutation.

SSS substitutions were also studied in a larger six-domain cbEGF22-25 recombinant fragment (Chapter 5), containing three more downstream domains to determine whether or not these domains assist in stabilising the mutant protein. Proteolytic digests showed very little calcium protection from proteolysis for either of the SSS mutant constructs compared to the wild-type construct. The triple and six domain fragments showed similar results, suggesting that presence of downstream

domains has no effect on the stability or protease susceptibility of the mutant protein. These low resolution structural studies showed that the SSS substitutions affect the domain fold but do not abrogate calcium binding completely. High resolution structural studies performed using 1D and 2D ^{1}H-NMR to investigate the effect of the SSS mutations on TB4 domain fold, the TB4-cbEGF23 domain interface and calcium binding to cbEGF23 showed that there is a very weak interface in the case of the W1570C and C1564S mutants compared to the wild-type, resulting in reduced calcium-binding. The mutants still bound calcium; however TB4 domain fold in case of C1564S does not seem to be grossly affected.

These results show that the SSS mutations have a significant effect on the structure of the protein compared to the wild-type which is consistent with the role of the affected residues in preserving the fold and their conservation in other TB domains. Since, it has been previously shown for MFS that many disease-causing mutations affect secretion of mutant protein due to misfolding, these mutations were checked for cell trafficking.

7.3 SSS and MFS mutations in TB4 have differing effects on fibrillin-1 secretion

Different disease-causing mutations in fibrillin-1 can result in either normal or delayed secretion of the mutant protein or in cellular retention. Determining whether or not the mutant protein is secreted is important in understanding the pathogenic mechanism of the mutation, as has been seen in Marfan syndrome (Suk *et al.,* 2004). The misfolded mutant protein may be recognised and targeted to degradation pathways by intracellular mechanisms and may not be secreted to the

ECM. This could lead to an intracellular dominant negative effect or functional haploinsufficiency, which might contribute to the pathogenic mechanism. On the other hand, partially misfolded fibrillin-1 may escape quality control surveillance in the cell, and on reaching the ECM, may be rapidly degraded by proteases or subsequently disrupt a specific protein-protein interaction required for the assembly of fibrillin-1 or alter the interactions of microfibrils with other cell-matrix components.

Fibrillin-1 recombinant fragments with SSS and MFS-causing mutations suggested that, although protein misfolding is an underlying defect in all cases, there was a difference in secretion observed at the protein level. Semi-quantitative RNA analysis showed that transcription of each mutant construct is unaffected relative to wild-type. Fibrillin-1 protein fragments with the SSS substitutions W1570C and C1564S showed normal levels in medium similar to the wild-type protein (Chapter 4). This observation is in agreement with the pulse-chase analysis of SSS patient fibroblasts (Loeys *et al.,* 2010) which showed normal secretion of fibrillin-1 into the ECM. The MFS-causing substitution, C1564Y, on the other hand, showed significant retention inside the cell and treatment with different endoglycosidases confirmed its retention in the endoplasmic reticulum. This functional haploinsufficiency might be the underlying disease-causing mechanism in the case of this mutation.

In preliminary experiments, SSS fibroblast cultures assembled normal quantities of fibrillin-1-containing microfibrils compared with control fibroblasts when visualized by immunofluorescence. In contrast, very few microfibrils were visualized in cell strain from patient with MFS-causing mutation C1589F in TB4 domain. This

would be consistent with either a dominant-negative pathogenesis or functional haploinsufficiency proposed for fibrillin-1 mutations associated with MFS. It would have been interesting to see if C1564Y cells gave a similar reduction in microfibrils, consistent with a large effect on domain folding seen in recombinant fragment, and the retention of a recombinant fragment containing this amino acid change, but unfortunately patient cells were not available. Further analysis of C1589F in the recombinant secretion system and in a triple domain fragment would strengthen the hypothesis that both C1564Y and C1589F result in loss of protein function.

7.4 Effects of SSS-causing mutations in fibrillin-1 on integrin binding

Several studies have implicated aberrant integrin expression or function in Systemic Sclerosis (SSc) and other fibrotic disorders (Asano *et al.,* 2008). Integrin αvβ3 has been found to be upregulated in SSc dermal fibroblasts *in situ*. Furthermore, its inhibition prevents collagen expression and reverses the myofibroblastic phenotype of SSc fibroblasts in a TGFβ-1–dependent manner (Asano *et al.,* 2005). Taking these findings into account, it is possible that defective integrin interaction with fibrillin-1 in SSS induces increased integrin expression and/or bioavailability to participate in TGFβ activation, and that this contributes to downstream events leading to tissue fibrosis. Fibrillin-1 TB4 domain is the only domain in this protein that contains an integrin binding RGD motif and has been shown to bind to αvβ3, αvβ6 and α5β1 integrins with high, moderate and low affinity, respectively. Cell-based and biophysical methods were used to investigate the effect of SSS substitutions on integrin binding.

Engagement of integrins with ECM ligands leads to receptor clustering at the plasma membrane, recruitment of structural and signalling molecules to adhesion sites, reorganisation of the actin cytoskeleton and initiation of signal transduction cascades that define cell shape and polarity (Kucik *et al*., 1996; Zamir and Geiger, 2001). F-actin is an important marker of cell shape and morphology, and preliminary investigations of cell morphology by staining for F-actin on SSS patient dermal fibroblasts showed defective spread morphology compared to control cells. SSS patient fibroblasts did not attach to their own matrix, but cell attachment and morphology could be rescued by the addition of exogenous ECM ligands (fibrillin-1 cbEGF22-25/serum). This is likely to be due to disorganised fibrillin-1 microfibril deposition by SSS patient cell lines, as they showed microfibril networks similar to the control cell strains (Chapter 4). *In vivo* experiments on skin from SSS patients show that although microfibrils form they are not localised to the correct location (Loeys et al., 2010). MFS patient cells, on the other hand, showed cell attachment and morphology similar to control cells, even though this patient cell line showed diminished microfibril network. Furthermore, cultured dermal fibroblasts from patients with SSS have been shown to have reduced amounts of the activated (phosphorylated) form of focal adhesion kinase (pFAK), an event mediated by the interaction of RGD ligands with integrins concentrated at focal adhesions (Loeys *et al.,* 2010). Taken together, these data on SSS patient fibroblast, suggest that *FBN1* mutations that cause SSS can impair ECM/integrin interactions and used to sense matrix deposition.

The specific cellular outcome of cell adhesion depends on multiple factors including the integrin repertoire, ECM ligands and the action of soluble factors that enhance adhesion-mediated events. These are tissue-specific and the combined signals from all these factors affect cell migration, proliferation and differentiation. The SSS phenotype is restricted to skin and it is possible that specific integrin/fibrillin-1 interactions are more important in skin than in other tissues.

To investigate if SSS mutations affect fibrillin-1 interactions with a specific integrin, cell binding assays were performed using recombinant fibrillin-1 fragments containing the SSS mutations in the TB4 domain. Cell attachment and spreading assays using human dermal fibroblasts (FS2) and keratinocytes (VB6) showed that focal adhesion formation is *via* αvβ3 and αvβ6 integrins, respectively. Integrin α5β1 does not localise to focal contacts in either cell lines, but its contribution to cell adhesion cannot be completely ruled out in a 3D cell matrix. However, α5β1/fibronectin interactions have a very high affinity (~10 nM); it is very unlikely that α5β1/fibrillin-1 interaction occurs in the presence of fibronectin. VB6 keratinocytes showed normal attachment and spreading when plated on mutant as well as wild-type substrates, consistent with preserved αvβ6 integrin-fibrillin-1 interaction in this system. In contrast, both SSS mutations induced a dramatic loss of both attachment and spreading of FS2 cells, suggesting an impairment of the interaction with αvβ3 integrin. Surface plasmon resonance data also supports these findings, suggesting that these mutations affect interactions with αvβ3 but not with αvβ6. The data show that it is possible to have selective disruption of integrin binding, but does not rule out other integrins which were not tested in this study

may also have defective interactions with fibrillin-1. The SSS mutations were studied in both a non-glycosylated cbEGF22-TB4-cbEGF23 fragment and in a larger glycosylated cbEGF22-25 context. The results suggested that neither glycosylation nor heparin/heparan sulphate binding have an effect on integrin binding at least in the context of a larger fragment.

Bax *et al.,* (2007) have shown that upstream cbEGF domains 19-20-21 are needed for strong α5β1-mediated adhesion. However neither did they use a fragment which has domains downstream of the TB4 domain for these studies nor did all the fragments they used in the study have the cbEGF22 domain. Also, these studies were performed using function-blocking antibodies against α5β1 and β1-activating antibody. Because specific interference of one integrin has been known to influence the behaviour of other integrins on the cell (a phenomenon called "integrin cross-talk" (Schwarz *et al.,*2002), use of these function-blocking and integrin-activating antibodies cannot by themselves be considered as a conclusive proof of integrin-ligand interactions. Therefore, in order to verify the importance of α5β1/fibrillin-1 interactions, these binding studies will have to be checked for the wild-type in a cbEGF19-25 context which has all the domain requirements for integrin binding. Cells on this fragment will also have to be immunostained specifically for α5β1 integrin to see if having those upstream domains helps this integrin to localise into the focal contacts and lastly, kinetic studies can be done to determine the stability of the fibrillin/ α5β1 complex. These studies would shed light on the possibility for the involvement of α5β1 in SSS and related disorders.

During the course of this study, a fibrillin-1 RGE mutant mouse model was found to have a phenotype similar to SSS, showing dermal thickening and replacement of subcutaneous fat with collagen (8th International Research Symposium on Marfan Syndrome abstract, Dr. Elizabeth Gerber). These recent findings in RGE mice support the results of this study which proposes defective integrin/fibrillin-1 interaction as an underlying disease-causing mechanism in the skin. It would be reasonable to propose that cells sample matrix integrity using integrins and that fibrillin-1 in the form of microfibrils acts as an indicator on the status of the matrix. Any loss of integrin-binding to fibrillin-1 might, therefore, result in a failure of communication, context-inappropriate matrix production resulting in fibrosis. Further experiments on the role of signalling pathways initiated by αvβ3/fibrillin-1, αvβ6/fibrillin-1 and α5β1/fibrillin-1 are required, to look at downstream consequences of these interactions.

7.5 Fibrillin-1 and Weill-Marchesani syndrome

Mutations in ADAMTS10 were found in the autosomal recessive (AR) form of Weill-Marchesani syndrome (Dagoneau *et al.,* 2004), which has a clinical phenotype similar to SSS (skin fibrosis and short stature). The deletion of part of fibrillin-1 domain TB5 was discovered in patients with an autosomal dominant (AD) form of WMS (Faivre *et al.,* 2003). This mutation was also investigated along with the SSS mutations. So far mutations in fibrillin-1 had only been associated with a 'loss of function' phenotype as is seen in MFS but the discovery of these mutations resulting in fibrosis underscores the importance of fibrillin-1 as an essential mediator of cell-matrix interactions and not just for maintaining the structural integrity of the ECM

and for storing cytokines. A potential heparin sulphate-binding site has been reported in the TB5 domain in fibrillin-1, assigned to two arginine residues (R1691 and R1961). This site was found to modulate integrin binding to TB4 domain by possibly binding to syndecan receptors on the cell surface (Bax *et al.,* 2007). The proximity of the TB4 and TB5 domains, the presence of sites that mediate cell-matrix interactions and discovery of mutations in these domains that result in fibrosis, suggests a unique and critical role for these domains in the ECM.

The WMS deletion investigated in this study involves the deletion of eight amino acids, including one of the two heparin-binding residues, and a highly conserved cysteine residue involved in forming one of the four disulphide bonds in the TB5 domain. This deletion also creates a free cysteine in the domain, as in the case of the SSS substitutions. To investigate whether the underlying disease-causing mechanism in WMS is similar to SSS due to their phenotypic similarity, the WMS deletion was also studied for its interaction with integrins. Protease digests of recombinant cbEGF22-25 fibrillin-1 fragment containing the WMS deletion (WMSdel) showed significant degradation even in the presence of calcium suggesting that this deletion has a considerable effect on the structure of the protein fragment, as expected. Cell secretion studies indicated that the WMSdel fragment was both retained and secreted from the cell. Pulse-chase analysis and immunostaining of WMS patient microfibrils will help shed some light on the fate of mutant fibrillin-1 in the ECM in this disorder. Cell binding assays showed that WMSdel protein fragment induced cell attachment and spreading on both keratinocytes and dermal fibroblasts. These observations were supported by surface plasmon resonance results where the

K_D of WMSdel fibrillin-1/ αvβ3 and αvβ6 interactions, was found to be similar to the wild-type. Previous studies suggest that the heparin sulphate binding site in TB5 domain modulates integrin binding (Bax *et al.,* 2007). But removal of one of the HS-binding residues (R1692) in WMS deletion does not affect its interaction with both αvβ3 and αvβ6 integrins significantly. To check whether α5β1 or interaction with any other integrins has been impaired, cell binding assays will have to be carried as described in the previous section.

These results indicate that in case of WMS the underlying disease-causing mechanism is likely to be different even though it results in a phenotype similar to SSS. The primary defect in this case might not be impairment of fibrillin-1/integrin interactions, but a reduced quantity of protein in the ECM and a defective interaction with the cell-matrix. Defective interaction with syndecan cell surface receptors could be the underlying primary defect in this case since the TB5 domain contains a heparin sulphate-binding site, and the WMS deletion results in the loss of one HS-binding amino acid residue, however unlike the Bax *et al.* (2007) study, cooperative effects on integrin binding were not observed. This may reflect specific difference in cells used since Bax et al., study was performed using mouse and rat embryonic cells.

WMS shares phenotypic similarities with hybrid syndrome (thick skin and ectopia lentis), which has recently been found in patients with a fibrillin-1 mutation (C1577G) in domain TB4 (Loeys *et al.,* 2010). Ectopia lentis is a typical clinical manifestation of Marfan syndrome. WMS also shares its phenotype with connective tissue disorders such as geleophysic dysplasia (GD) and acromicric dysplasia (AD), all

characterised by short stature, short hands, stiff joints, thick skin, delayed bone age and cone shaped epiphyses. Mutations in ADAMTS proteins have been found in autosomal recessive form of WMS (ADAMTS10) and GD (ADAMTSL2) (Dagoneau *et al.,* 2004; Le Goff *et al.,* 2008) (Table 7.1). Mutations in fibrillin-1 have been found in patients with an autosomal dominant form of ectopia lentis, but recently, mutations in *ADAMTSL4* have been found in the recessive form of this disorder (Ahram *et al.,* 2010). These intriguing phenotypic overlaps suggest a possible functional relationship of these proteins with fibrillin-1 (Table 7.1). So far, ADAMTSL6 has been shown to interact with the N-terminal region of fibrillin-1. Expression of ADAMTSL6-β has been shown to rescue microfibril disorder after periodontal ligament (PDL) injury in MFS model mice through the promotion of fibrillin-1 microfibril assembly (Tsutsui K *et al.,* 2010). ADAMTS10 has also been shown to interact with N-terminal and C-terminal half of fibrillin-1 (Kutz *et al.,* 2011). Recent studies have shown that ADAMTSL2 interacts with LTBP-1 (Le Goff *et al.,* 2010). LTBP-1 interactions with fibrillin-1 have already been mapped to the N-terminal region in fibrillin-1. These findings suggest that a contribution of any these interactions could possibly be defective in this disorder.

7.6 Concluding remarks

Various disease-causing mutations have been found in the TB domains of fibrillin-1 but the pathogenic mechanisms of these various human pathologies is not fully understood. Few pathogenic mutations have been reported in other TB-containing proteins such as the LTBPs. This is the first molecular study of pathogenic mutations in the TB domains of fibrillin-1 and the results here suggest that different

mutations in TB domains can be associated with very different disease-causing mechanisms, even if the mutations are present in the same domain, underscoring the importance of these domains in fibrillin-1. On the other hand, disorders associated with mutations in the cbEGF domain of fibrillin-1, so far have only shown to have a 'loss of function' phenotype (like, MFS, ectopia lentis, Sprintzen-Goldberg syndrome etc.).

The results in this thesis suggest an important role for integrin/ fibrillin-1 interactions in maintaining the ECM and that an impairment of this interaction can result in diseases such as SSS (Figure 7.1). Only the interactions of the αvβ3 and αvβ6 integrins with SSS mutants were investigated in this thesis, but possibility of other defective integrin/fibrillin-1 interactions that might be important in the skin cannot be ruled out, e.g., interaction with αvβ5, α8β1, αvβ8 etc. integrins. The investigation of a WMS deletion in the TB5 domain of fibrillin-1 suggested that the pathogenic mechanism underlying this disease is different and that an impairment of fibrillin-1 interactions with other ECM; or cell surface molecules might be the primary defect. Different possible pathogenic mechanisms underlying these disorders and MFS have been suggested in figure 7.1.

The clinical overlap of connective tissue disorders involving fibrillin-1, such as Tight skin mouse model and WMS, with both MFS (ectopia lentis, skeletal and cardiovascular defects) and SSS (skin fibrosis and short stature) is intriguing and also suggests a functional relationship with ADAMTS family of proteins. Mutations in ADAMTS10 have been found in the recessive form of WMS and mutations in ADAMTSL4 in a recessive form of ectopia lentis (Table 7.1). Since ADAMTSL proteins

have recently been shown to interact with fibrillin-1 and promote its deposition in extracellular matrix of cultured fibroblasts (Tsutsui *et al.,* 2010; Kutz *et al.,* 2011), a more thorough investigation of these interactions with specific domains of fibrillin-1, such as the TB5 domain, should be performed to enable us to understand the involvement of these proteins in microfibril assembly and function. The functions of some of the ADAMTSL proteins are currently unknown and these studies might shed light on their role in the ECM. A mouse model of SSS will be useful in studying and identifying the primary events leading to fibrosis and as a result, more effective drugs and therapy can be developed. A better understanding of the different pathogenic mechanisms underlying these various disorders involving fibrillin-1 will further elucidate its role and organisation into microfibrils in the ECM.

References

References

Ahram D., Sato T. S., Kohilan A., Tayeh M., Chen S., Leal S., Al-Salem M., El-Shanti H. (2009) Am. J. Hum. Genet. 84, 274–278

Arbustini E, Grasso M, Ansaldi S, Malattia C, Pilotto A, Porcu E, Disabella E, Marziliano N, Pisani A, Lanzarini L, Mannarino S, Larizza D, Mosconi M, Antoniazzi E, Zoia MC, Meloni G, Magrassi L, Brega A, Bedeschi MF, Torrente I, Mari F, Tavazzi L. (2005) Identification of sixty-two novel and twelve known FBN1 mutations in eighty-one unrelated probands with Marfan syndrome and other fibrillinopathies. Hum Mutat. Nov;26(5):494.

Arnaout, M. A. (2004). The structural basis of elasticity in fibrillin-based microfibrils. *Structure (Camb)* 12: 734-736.

Arnaout, M. A., Goodman, S. L., and Xiong, J. P. (2002). Coming to grips with integrin binding to ligands. *Curr Opin Cell Biol* 14: 641-651.

Arteaga-Solis, E., Gayraud, B., Lee, S. Y., Shum, L., Sakai, L., and Ramirez, F. (2001). Regulation of limb patterning by extracellular microfibrils. *J Cell Biol* 154: 275-281.

Asano Y, Ihn H, Yamane K, Jinnin M, Mimura Y, Tamaki K (2005a) Increased expression of integrin αvβ3 contributes to the establishment of autocrine TGF-β signaling in scleroderma fibroblasts. *J Immunol* **175**: 7708–7718

Asano Y, Ihn H, Yamane K, Jinnin M, Mimura Y, Tamaki K (2005b) Involvement ofαvβ5 integrin-mediated activation of latent transforming growth factor β1 in autocrine transforming growth factor-β signaling in systemic sclerosis fibroblasts. *Arthritis Rheum* **52**: 2897–2905

Babcock D , Gasner C , Francke U , Maslen C . A single mutation that results in an Asp to His substitution and partial exon skipping in a family with congenital contractural arachnodactyly. *Hum Genet* 1998;**103** (1) :22–8

Baglia FA, Badellino KO, Ho DH, Dasari VR, Walsh PN : A binding site for the kringle II domain of prothrombin in the apple 1 domain of factor XI. J Biol Chem 2000;41:31954-31962.

Baldock, C., Koster, A. J., Ziese, U., Rock, M. J., Sherratt, M. J., Kadler, K. E., Shuttleworth, C. A., and Kielty, C. M. (2001). The supramolecular organization of fibrillin-rich microfibrils. *J Cell Biol* 152: 1045-1056.

Baldock, C. , Veronique S, Daniel V. Bax, Stuart A. Cain, Kieran T. Mellody, Marson, A., Haston, J. L., Berry, R., Wang, M., J. Günter Grossmann, Roessle, M., Kielty, C. M., and Wess, T. J., **.**Nanostructure of fibrillin-1 reveals compact conformation of EGF arrays and mechanism for extensibility; PNAS , 2006 , vol. 103 , no. 32 , 11922-11927

Bax D.V, S. E. Bernard, A. Lomas, A. Morgan, J. Humphries, C. A. Shuttleworth, M. J. Humphries, C. M. Kielty, Cell adhesion to fibrillin-1 molecules and microfibrils is mediated by alpha 5 beta 1 and alpha v beta 3 integrins. J Biol Chem 278, 34605-34616 (2003).

Bax DV, Mahalingam Y, Cain S, Mellody K, Freeman L, Younger K, Shuttleworth CA, Humphries MJ, Couchman JR, Kielty CM. Cell adheshion to fibrillin-1: identification of an Arg-Gly-Asp-dependent synergy region and a heparin-binding site that regulates focal adhesion formation. J Cell Sci. 2007;120:1383–1392.

Bernfield M, Kokenyesi R. et al. (1992). "Biology of syndecans: a family of transmembrane heparan sulfate proteoglycans". Annu. Rev. Cell. Biol. 8: 365–393

Biery NJ, Eldadah ZA, Moore CS, Stetten G, Spencer F, Dietz HC. 1999. Revised genomic organization of FBN1 and significance for regulated gene expression. *Genomics* **56**: 70-77

Bissell MJ, Hall HG and Parry G. (1982) How does extracellular matrix direct gene expression? J Theor Biol 99:31-68. 52.

Booms P , Cisler J , Mathews KR, Godfrey M , Tiecke F , Kaufmann UC, Vetter U , Hagemeier C , Robinson PN. Novel exon skipping mutation in the fibrillin-1 gene: two 'hot spots' for the neonatal Marfan syndrome. *Clin Genet* 1999;**55** (2) :110–7

Boudreau, N. J., and Jones, P. L. (1999). Extracellular matrix and integrin signalling: the shape of things to come. *Biochem J* 339 (Pt 3): 481-488.

Branton M. H. and Kopp J. B.TGF-β and fibrosis. Microbes and Infection Volume 1, Issue 15, December 1999, 1349-1365

Brenn T, Aoyama T, Francke U, Furthmayr H. Dermal fibroblast culture as a model system for studies of fibrillin assembly and pathogenetic mechanisms: defects in distinct groups of individuals with Marfan's syndrome. Lab Invest 1996;75(3):389–402

Bunton, T. E., Biery, N. J., Myers, L., Gayraud, B., Ramirez, F., and Dietz, H. C. (2001). Phenotypic alteration of vascular smooth muscle cells precedes elastolysis in a mouse model of Marfan syndrome. *Circ Res* 88: 37-43.

Burrows, T. D., King, A., Smith, S. K., and Loke, Y. W. (1995). Human trophoblast adhesion to matrix proteins: inhibition and signal transduction. *Hum Reprod* 10: 2489-2500.

Bruns, R. R. (1984). Beaded filaments and long spacing fibrils. Relation to type-VI collagen. J Ultrastruct Res *89*, 136-145.

Butler, B., Williams, M. P., and Blystone, S. D. (2003). Ligand-dependent activation of integrin alpha vbeta 3. *J Biol Chem* 278: 5264-5270.

Cain SA, Baldock C, Gallagher J, Morgan A, Bax DV, Weiss AS, Shuttleworth CA, Kielty CM. Fibrillin-1 interactions with heparin. J Biol Chem. 2005;280:30526–30537

Cain SA, Morgan A, Sherratt MJ, Ball SG, Shuttleworth CA, Kielty CM. Proteomic analysis of fibrillin-rich microfibrils. Proteomics. 2006;6:111–122

Cain SA, Baldwin AK, Mahalingam Y, Raynal B, Jowitt TA, Shuttleworth CA, Couchman JR, Kielty CM. Heparan sulfate regulates fibrillin-1 and C-terminal interactions. J Biol Chem. 2008;283:27017–27027

Calderwood, D. A. (2004). Integrin activation. J. Cell Sci. 117, 657-666.

Calderwood, D. A., Shattil, S. J. and Ginsberg, M. H. (2000). Integrins and actin filaments: reciprocal regulation of cell adhesion and signaling. J. Biol. Chem. 275, 22607-22610.

Calderwood, D. A., Fujioka, Y., de Pereda, J. M., Garcia-Alvarez, B., Nakamoto, T., Margolis, B., McGlade, C. J., Liddington, R. C. and Ginsberg, M. H. (2003). Integrin β cytoplasmic domain interactions with phosphotyrosine-binding domains: a structural prototype for diversity in integrin signaling. Proc. Natl. Acad. Sci. USA 100, 2272-2277.

Campbell, I. D. (2003). Modular proteins at the cell surface. *Biochem Soc Trans* 31: 1107-1114.

Campbell, I. D. and Bork, P. (1993). Epidermal growth factor-like modules. *Curr Opin Struct Biol* 3: 385-392.

Campbell, I. D., and Downing, A. K. (1994). Building protein structure and function from modular units. *Trends Biotechnol* 12: 168-172.

Cardy, C. M., and Handford, P. A. (1998). Metal ion dependency of microfibrils supports a rod-like conformation for fibrillin-1 calcium-binding epidermal growth factor-like domains. *J Mol Biol* 276: 855-860.

Carey, D. J. (1997). "Syndecans: multifunctional cell-surface co-receptors". Biochem. J. 327: 1–16.

Cheresh, D. A., and Spiro, R. C. (1987). Biosynthetic and functional properties of an Arg-Gly-Asp-directed receptor involved in human melanoma cell attachment to vitronectin, fibrinogen, and von Willebrand factor. *J Biol Chem* 262: 17703-17711.

Chernushevich, I.V., Loboda, A.V., and Thomson, B.A. (2001). An introduction to quadrupole time-of-flight mass spectrometry. *J Mass Spectrom* 36: 849-865.

Collod-Beroud, G., Beroud, C., Ades, L., Black, C., Boxer, M., Brock, D. J., Holman, K. J., de Paepe, A., Francke, U., Grau, U., Hayward, C., Klein, H. G., Liu, W., Nuytinck, L., Peltonen, L., Alvarez Perez, A. B., Rantamaki, T., Junien, C., and Boileau, C. (1998). Marfan Database (3rd edition): new mutations and new routines for the software. *Nucleic Acids Res* 26: 229-223.

Collod-Beroud G , Beroud C , Ades L , Black C , Boxer M , Brock DJ, Godfrey M , Hayward C , Karttunen L , Milewicz D , Peltonen L , Richards RI, Wang M , Junien C , Boileau C . Marfan database (second edition): software and database for the analysis of mutations in the human FBN1 gene. *Nucleic Acids Res* 1997;**25** (1) :147–50.

Collod-Beroud G , Beroud C , Ades L , Black C , Boxer M , Brock DJ, Holman KJ, de Paepe A , Francke U , Grau U , Hayward C , Klein HG, Liu W , Nuytinck L , Peltonen L , Alvarez Perez AB, Rantamaki T , Junien C , Boileau C . Marfan database (third edition): new mutations and new routines for the software. *Nucleic Acids Res* 1998;**26** (1) :229–3.

Collod-Beroud G , Le Bourdelles S , Ades L , Ala-Kokko L , Booms P , Boxer M , Child A , Comeglio P , De Paepe A , Hyland JC, Holman K , Kaitila I , Loeys B , Matyas G , Nuytinck L , Peltonen L , Rantamaki T , Robinson P , Steinmann B , Junien C , Beroud C , Boileau C . Update of the UMD-FBN1 mutation database and creation of an FBN1 polymorphism database. *Hum Mutat* 2003;**22** (3) :199–208.

Cooke, R. M., Wilkinson, A. J.,Baron, M., Pastore, A., Tappin, M. J., Campbell, I. D., Gregory, H., and Sheard, B. (1987). The solution structure of human epidermal growth factor. *Nature* 327: 339-341.

Corson, G. M., Chalberg, S. C., Dietz, H. C., Charbonneau, N. L., and Sakai, L. Y. (1993). Fibrillin binds calcium and is coded by cDNAs that reveal a multidomain structure and alternatively spliced exons at the 5' end. *Genomics* 17: 476-484.

Corson, G. M., Charbonneau NL, Keene DR, Sakai LY. Differential expression of fibrillin-3 adds to microfibril variety in human and avian, but not rodent, connective tissues. Genomics. 2004;83:461–472.

Cowgill, R.W. (1967). Fluorescence and protein structure. Reappraisal of solvent and structural effects. *Biochim Biophys Acta* 133: 6- 18.

Cowgill, R.W. (1970). Fluorescence and the structure of proteins. Spatial requirements for quenching by disulfide groups. *Biochim Biophys Acta* 207: 556-9.

Dallas SL,Keene DR, Bruder SP, Saharinen J, Sakai LY, et al. Role of the latent transforming growth factor beta binding protein 1 in fibrillin-containing microfibrils in bone cells in vitro and in vivo. J Bone Miner Res. 2000;15:68–81.

Damsky, C., Sutherland, A., and Fisher, S. (1993). Extracellular matrix 5: adhesive interactions in early mammalian embryogenesis, implantation, and placentation. *Faseb J* 7: 1320-1329.

D'Arrigo C., Burl S., Withers A. P., Dobson H., Black C., and Boxer, M. (1998). TGF-beta1 binding protein-like modules of fibrillin-1 and -2 mediate integrin-dependent cell adhesion. *Connect Tissue Res* 37: 29-

Davis, E. C. (1994). Immunolocalization of microfibril and microfibril-associated proteins in the subendothelial matrix of the developing mouse aorta. *J Cell Sci* 107 (Pt 3): 727-736.

Dietz, H. C., Cutting, G. R., Pyeritz, R. E., Maslen, C. L., Sakai, L. Y., Corson, G. M., Puffenberger, E. G., Hamosh, A., Nanthakumar, E. J., Curristin, S. M., and et al. (1991b). Marfan syndrome caused by a recurrent de novo missense mutation in the fibrillin gene. *Nature* 352: 337-339.

Dietz, H. C., McIntosh, I., Sakai, L. Y., Corson, G. M., Chalberg, S. C., Pyeritz, R. E., and Francomano, C. A. (1993). Four novel FBN1 mutations: significance for mutant transcript level and EGF-like domain calcium binding in the pathogenesis of Marfan syndrome. *Genomics* 17: 468-475.

Dietz, H. C., Pyeritz, R. E., Hall, B. D., Cadle, R. G., Hamosh, A., Schwartz, J., Meyers, D. A., and Francomano, C. A. (1991a). The Marfan syndrome locus: confirmation of assignment to chromosome 15 and identification of tightly linked markers at 15q15-q21.3. *Genomics* 9: 355-361.

Dietz, H. *et al.* (1994) Marfan's syndrome and other microfibrillar diseases. In *Advances in Human Genetics*,Edited by (Harris, H. and Hirschhorn, K., eds.), Plenum Press.

Dietz, H.C. *et al.* (1993). Four novel FBN1 mutations: significance for mutant transcript level and EGF-like domain calcium binding in the pathogenesis of Marfan syndrome. *Genomics* **17**, 468-475.

M. DiRocco, Clinical images: Stiff skin syndrome. Arthritis Rheum 43, 1542 (2000).

Downing, A. K., Knott, V., Werner, J. M., Cardy, C. M., Campbell, I. D., and Handford, P. A. (1996). Solution structure of a pair of calcium-binding epidermal growth factor-like domains: implications for the Marfan syndrome and other genetic disorders. *Cell* 85: 597-605.

El-Hallous E, Sasaki T, Hubmacher D, Getie M, Tiedemann K, Brinckmann J, Batge B, Davis EC, Reinhardt DP. Fibrillin-1 interactions with fibulins depend on the first hybrid domain and provide an adaptor function to tropoelastin. J Biol Chem. 2007;282:8935–8946

Ellgaard, L. and Helenius, A. (2001) ER quality control: towards an understanding at the molecular level. Curr. Opin. Cell. Biol., 13, 431–437.

Esterly N B. and McKusick V A. (1971) Stiff skin syndrome. Pediatrics Vol. 47 No. 2, pp. 360-369

Faivre L, Gorlin RJ, Wirtz MK, Godfrey M, Dagoneau N, Samples JR, Le Merrer M, Collod-Beroud G, Boileau C, Munnich A, Cormier-Daire V. In frame fibrillin-1 gene deletion in autosomal dominant Weill-Marchesani syndrome. J Med Genet. 2003;40:34–36.

Fernandez Perez ER, Daniels CE, Schroeder DR, St Sauver J, Hartman TE, Bartholmai BJ, Yi ES, Ryu JH. Incidence, Prevalence, and Clinical Course of Idiopathic Pulmonary Fibrosis: A Population-Based Study. Chest. Jan 2010;137:129-37.

Fleischer KJ, Nousari HC, Anhalt GJ, Stone CD, Laschinger JC. Immunohistochemical abnormalities of fibrillin in cardiovascular tissues in Marfan's syndrome. Ann Thorac Surg. 1997 Apr;63(4):1012-7.

Gibson M. A, Hughes JL, Fanning JC. et al. The major antigen of the elastin-associated microfibrils is a 31kDa glycoprotein. J Biol Chem.

Gibson M. A, Sandberg LB, Grosso LE. et al. Complementary DNA cloning establishes microfibril-associated glycoprotein (MAGP) to be a discrete component of the elastin-associated microfibrils. J Biol Chem.

Gibson, M. A., Leavesley, D. I., and Ashman, L. K. (1999). Microfibril-associated glycoprotein-2 specifically interacts with a range of bovine and human cell types via alphaVbeta3 integrin. *J Biol Chem* 274: 13060-13065.

Gill, S. C. and von Hippel, P. H. (1989). Calculation of protein extinction coefficients from amino acid sequence data. *Anal Biochem* 182: 319-326.

Glanville, R.W. *et al.* (1994). Calcium binding, hydroxylation, and glycosylation of the precursor epidermal growth factor-like domains of fibrillin-1, the Marfan gene protein. *J Biol Chem* **269**, 26630-26634.

Glish, G.L. and Vachet, R.W. (2003). The basics of mass spectrometry in the twenty-first century. *Nat Rev Drug Discov* 2: 140-150.

Godfrey, M., Olson, S., Burgio, R. G., Martini, A., Valli, M., Cetta, G., Hori, H., and Hollister, D. W. (1990). Unilateral microfibrillar abnormalities in a case of asymmetric Marfan syndrome. Am J Hum Genet *46*, 661-671.

Gregory KE, Ono RN, Charbonneau NL, Kuo C-L, Keene DR, Bachinger HP, Sakai LY. The prodomain of BMP-7 targets the BMP-7 complex to the extracellular matrix. J Biol Chem. 2005;280:27979–27980.

Handford, P. A. (2000). Fibrillin-1, a calcium binding protein of extracellular matrix. *Biochim Biophys Acta* 1498: 84-90.

Handford, P. A., Baron, M., Mayhew, M., Willis, A., Beesley, T., Brownlee, G. G., and Campbell, I. D. (1990). The first EGF-like domain from human factor IX contains a high-affinity calcium binding site. *Embo J* 9: 475-480.

Handford, P. A., Mayhew, M., Baron, M., Winship, P. R., Campbell, I. D., and Brownlee, G. G. (1991). Key residues involved in calcium-binding motifs in EGF-like domains. *Nature* 351: 164-167.

Handford, P. A., Mayhew, M., and Brownlee, G. G. (1991b). Calcium binding to fibrillin? *Nature* 353: 395.

Hayashida T, Wu MH, Pierce A, Poncelet AC, Varga J, Schnaper HW (2007) MAP-kinase activity necessary for TGF-β1-stimulated mesangial cell type I collagen expression requires adhesion-dependent phosphorylation of FAK tyrosine 397. J Cell Sci 120: 4230–4240

Hirohata S., Wang L. W., Miyagi M., Yan L., Seldin M. F., Keene D. R., Crabb J. W., Apte S. S. (2002) J. Biol. Chem. 277, 12182–12189

Hobbs, H. H., Brown, M. S., and Goldstein, J. L. (1992). Molecular genetics of the LDL receptor gene in familial hypercholesterolemia. *Hum Mutat* 1: 445-466.

Hewett, D.R. *et al.* (1993). A novel fibrillin mutation in the Marfan syndrome which could disrupt calcium binding of the epidermal growth factor-like module. *Hum Mol Genet* **2**, 475-477.

Hogg, N., and Bates, P. A. (2000). Genetic analysis of integrin function in man: LAD-1 and other syndromes. *Matrix Biol* 19: 211-222.

Hohenester, E. and Engel, J. (2002). Domain structure and organisation in extracellular matrix proteins. Matrix Biol. 21: 115-128.

Hollister, D. W., Godfrey, M., Sakai, L. Y., and Pyeritz, R. E. (1990). Immunohistologic abnormalities of the microfibrillar-fiber system in the Marfan syndrome. *N Engl J Med* 323: 152-159.

Hubmacher D, Tiedemann K, Reinhardt DP. Fibrillins: from biogenesis of microfibrils to signaling functions. Curr Top Dev Biol. 2006;75:93–123.

Hubmacher D, El-Hallous EI, Nelea V, Kaartinen MT, Lee ER, Reinhardt DP. Biogenesis of extracellular microfibrils: multimerization of the fibrillin-1 C terminus into bead-like structures enables self-assembly. Proc Natl Acad Sci USA. 2008;105:6548–6553.

Humphries, J. D., Schofield, N. R., Mostafavi-Pour, Z., Green, L. J., Garratt, A. N., Mould, A. P., and Humphries, M. J. (2005). Dual functionality of the anti-beta1

integrin antibody, 12G10, exemplifies agonistic signalling from the ligand binding pocket of integrin adhesion receptors. *J Biol Chem* 280: 10234-10243.

Humphries, M. J. (2000). Integrin structure. *Biochem Soc Trans* 28: 311-339.

Hutchinson S , Furger A , Halliday D , Judge DP, Jefferson A , Dietz HC, Firth H , Handford PA. Allelic variation in normal human FBN1 expression in a family with Marfan syndrome: a potential modifier of phenotype? *Hum Mol Genet* 2003;**12** (18) :2269–76

Hutchinson S, Aplin RT, Webb H, Kettle S, Timmermans J, Boers GH, Handford PA. Molecular effects of homocysteine on cbEGF domain structure: insights into the pathogenesis of homocystinuria.J Mol Biol. 2005 Feb 25;346(3):833-44. Epub 2005 Jan 22.

Hynes, R. O., and Zhao, Q. (2000). The evolution of cell adhesion. *J Cell Biol* 150: F89-96.

Hynes, R. O. (2002). Integrins: bidirectional, allosteric signaling machines. Cell 110, 673-687

Iizuka, E., and Yang, J.T. (1966). Optical rotatory dispersion and circular dichroism of the β-form of silk fibroin in solution. *Proc Natl Acad Sci USA* 55: 1175-1182.

Isogai Z, Ono RN, Ushiro S, Keene DR, Chen Y, Mazzieri R, Charbonneau NL, Reinhardt DP, Rifkin DB, Sakai LY. Latent transforming growth factor β-binding protein 1 interacts with fibrillin and is a microfibril-associated protein. J Biol Chem. 2003;278:2750–2757.

Jaenicke, R., and Rudolph, R. (1989). *In* Protein structure: a practical approach. (Creighton, T.E., ed.) pp.208-209, IRL Press, Oxford.

Jensen, S. A., Corbett, A. R., Knott, V., Redfield, C., and Handford, P. A. (2005). Ca2+-dependent interface formation in fibrillin-1. *J Biol Chem* 280: 14076-14084.

Jordan CD, Bohling SD, Charbonneau NL, Sakai LY. Fibrillins in Human Adult Ovary and Polycystic Ovary Syndrome: Is Fibrillin-3 Affected in PCOS? J Histochem Cytochem. 2010 Jul 19.

Jovanovic, J., Takagi, J., Choulier, L., Abrescia, N.G., Stuart, D.I.,van der Merwe, P.A., Mardon, H.J., Handford, P.A. αVβ6 is a Novel Receptor for Human Fibrillin-1: Comparative studies of molecular determinants underlying integrin-RGD affinity and specificity. J. Biol. Chem., 2006. 282(9):p. 6743-6751

Judge DP, Biery NJ, Keene DR, Geubtner J , Myers L , Huso DL, Sakai LY, Dietz HC. Evidence for a critical contribution of haploinsufficiency in the complex pathogenesis of Marfan syndrome. *J Clin Invest* 2004;**114** (2) :172–81.

Kainulainen, K., Karttunen, L., Puhakka, L., Sakai, L., and Peltonen, L. (1994). Mutations in the fibrillin gene responsible for dominant ectopia lentis and neonatal Marfan syndrome. *Nat Genet* 6: 64-69.

Kao, Y. H., Lee, G. F., Wang, Y., Starovasnik, M. A., Kelley, R. F., Spellman, M. W., and Lerner, L. (1999). The effect of O-fucosylation on the first EGF-like domain from human blood coagulation factor VII. *Biochemistry* 38: 7097-7110.

Kettle, S., Yuan, X., Grundy, G., Knott, V., Downing, A. K., and Handford, P. A. (1999). Defective calcium binding to fibrillin-1: consequence of an N2144S change for fibrillin-1 structure and function. *J Mol Biol* 285: 1277-1287.

Keene DR, Maddox BK, Kuo HJ, Sakai LY, Glanville RW. Extraction of extendable beaded structures and their identification as fibrillin-containing extracellular matrix microfibrils. J Histochem Cytochem. 1991;39:441–449.

Kelleher CM, McLean SE, Mecham RP. Vascular extracellular matrix and aortic development. Curr Top Dev Biol. 2004;62:153–188.

Kielty, C. M., Cummings C., Whittaker, S. P., Shuttleworth, C. A. and Grant M.E. (1991). Isolation and ultrastructural analysis of microfibrillar structures from foetal bovine elastic tissues. Relative abundance and supramolecular architecture of type VI collagen assemblies and fibrillin. *J Cell Sci* 99 (Pt 4): 797-807.

Kielty, C. M., Baldock, C., Lee, D., Rock, M. J., Ashworth, J. L., and Shuttleworth, C. A. (2002). Fibrillin: from microfibril assembly to biomechanical function. *Philos Trans R Soc Lond B Biol Sci* 357: 207-217.

Kielty, C. M., Raghunath, M., Siracusa, L. D., Sherratt, M. J., Peters, R., Shuttleworth, C. A., and Jimenez, S. A. (1998). The Tight skin mouse: demonstration of mutant fibrillin-1 production and assembly into abnormal microfibrils. *J Cell Biol* 140: 1159-1166.

Kielty, C.M. ***et al.*** (1993). Microfibrillar assemblies of foetal bovine skin. Developmental expression and relative abundance of type VI collagen and fibrillin. *Matrix* **13**, 103-112.

Kielty, C. M., and Shuttleworth, C. A. (1993) FEBS Lett. 336, 323-326

Kieran T. Mellody, Lyle J. Freeman, Clair Baldock, Thomas A. Jowitt, Veronique Siegler, Bertrand D. E. Raynal, Stuart A. Cain, Tim J. Wess, C. Adrian Shuttleworth, and Cay M. Kielty

Kinsey R, Williamson MR, Chaudhry S, Mellody KT, McGovern A, Takahashi S, Shuttleworth CA, Kielty CM: Fibrillin-1 microfibril deposition is dependent on fibronectin assembly. J Cell Sci 2008

Kitahama, S., Gibson, M. A., Hatzinikolas, G., Hay, S., Kuliwaba, J. L., Evdokiou, A., Atkins, G. J., and Findlay, D. M. (2000). Expression of fibrillins and other microfibril-associated proteins in human bone and osteoblast-like cells. *Bone* 27: 61-67.

Knott, V., Downing, A. K., Cardy, C. M., and Handford, P. (1996). Calcium binding properties of an epidermal growth factor-like domain pair from human fibrillin-1. *J Mol Biol* 255: 22-27.

Koenders MM, Yang L, Wismans RG, Werf KO van der, Reinhardt DP, Daamen W, Bennink ML, Dijkstra PJ, Kuppevelt TH van, Feijen J (2009) Microscale mechanical properties of single elastic fibers: the role of fibrillin-microfibrils. Biomaterials 30:2425–2432

Kucik, D.F., Dustin, M.L., Miller, J.M., and Brown, E.J. (1996). Adhesion activating phorbol ester increases the mobility of leukocyte integrin LFA-1 in cultured lymphocytes. J. Clin. Invest. 97, 2139-2144

Kuo CL, Isogai Z, Keene DR, Hazeki K, Ono RN, Bachinger HP, Sakai LY (2007) Effects of fibrillin-1 degradation on microfibril structure. J Biol Chem 282:4007–4020

Lack, J., O'Leary, J. M., Knott, V., Yuan, X., Rifkin, D. B., Handford, P. A., and Downing, A. K. (2003). Solution structure of the third TB domain from LTBP1 provides insight into assembly of the large latent complex that sequesters latent TGF-beta. *J Mol Biol* 334: 281-291.

Le Goff C., Morice-Picard F., Dagoneau N., Wang L. W., Perrot C., Crow Y. J., Bauer F., Flori E., Prost-Squarcioni C., Krakow D., Ge G., Greenspan D. S., Bonnet D., Le Merrer M., Munnich A., Apte S. S., Cormier-Daire V. (2008) Nat. Genet. 40, 1119–1123

Lee, B., Godfrey, M., Vitale, E., Hori, H., Mattei, M. G., Sarfarazi, M., Tsipouras, P., Ramirez, F., and Hollister, D. W. (1991). Linkage of Marfan syndrome and a phenotypically related disorder to two different fibrillin genes. *Nature* 352: 330-334.

Lee, S. S., Knott, V., Jovanovic, J., Harlos, K., Grimes, J. M., Choulier, L., Mardon, H. J., Stuart, D. I., and Handford, P. A. (2004). Structure of the integrin binding fragment from fibrillin-1 gives new insights into microfibril organization. *Structure (Camb)* 12: 717-729.

Linse, S., Helmersson, A., and Forsen, S. (1991). Calcium binding to calmodulin and its globular domains. *J Biol Chem* 266: 8050-8054.

Liu W, Qian C, Comeau K, Brenn T, Furthmayr H, Francke U. 1996. Mutant fibrillin-1 monomers lacking EGF-like domains disrupt microfibril assembly and cause severe Marfan syndrome. *Hum Mol Genet* **5**: 1581-1587.

Liu W, Qian C, Francke U. 1997. Silent mutation induces exon skipping of fibrillin-1 gene in Marfan syndrome. *Nat Genet* **16**: 328-329.

Loeys B L *et al.* (2006), Aneurysm syndromes caused by mutations in the TGF-beta receptor. N Engl J Med. 2006 Aug 24;355(8):841-4.

Loeys B L, Gerber EE, Riegert-Johnson D, Iqbal S, Whiteman P, et al. (2010) Mutations in fibrillin-1 cause congenital scleroderma: stiff skin syndrome. Sci Transl Med

Loeys B L et al., The revised Ghent nosology for the Marfan syndrome. J Med Genet 2010;47:476-485 doi:10.1136/jmg.2009.072785

Lönnqvist L , Child A , Kainulainen K , Davidson R , Puhakka L , Peltonen L . A novel mutation of the fibrillin gene causing ectopia lentis. *Genomics* 1994 :573–6

Low FN (1961) The extracellular portion of the human blood-air barrier and its relation to tissue space. Anat Rec 139:105–123

Low FN (1962) Microfibrils: fine filamentous components of the tissue space. Anat Rec 142:131–137

Lu M, Munger JS, Steadele M, Busald C, Tellier M, Schnapp LM (2002) Integrin α8β1 mediates adhesion to LAP–TGF-β1. J Cell Sci 115: 4641–4648
Ludbrook SB, Barry ST, Delves CJ, Horgan CM (2003) The integrin αvβ3 is a receptor for the latency-associated peptides of transforming growth factors β1 and β3. Biochem J 369: 311–318

McKusick, V. A. (1993).“Mendelian Inheritance in Man,” 11th ed., Johns Hopkins Univ. Press, Baltimore, MD.
McGettrick, A.J. *et al.* (2000). Molecular effects of calcium binding mutations in Marfan syndrome depend on domain context. *Hum Mol Genet* **9**, 1987-1994.

Mecham, R. P., and Davis, E. C. (1994) in *Extracellular Matrix Assembly and Structure* (Yurchenco, P. D., Birk, D. E., and Mecham, R. P., eds) pp. 281-314, Academic Press, Inc., New York

Miranti CK, Brugge JS. Sensing the environment: a historical perspective on integrin signal transduction. Nat Cell Biol. 2002;4:E83.

Morgan M. R., Humphries M. J. & Bass M. D. Synergistic control of cell adhesion by integrins and syndecans. *Nature Reviews Molecular Cell Biology* 8, 957-969 (December 2007)

Mould A.P., Barton S.J., Askari J.A., McEwan P.A., Buckley P.A., Craig S.E., Humphries M.J. 2003a. Conformational changes in the integrin β A domain provide a mechanism for signal transduction via hybrid domain movement. J. Biol. Chem. 278:17028–17035. doi: 10.1074/jbc.M213139200.

Munger JS et al (1999) The integrin αvβ6 binds and activates latent TGF-β1: a mechanism for regulating pulmonary inflammation and fibrosis.

Nagase, T., Nakayama, M., Nakajima, D., Kikuno, R., Ohara, O. Prediction of the coding sequences of unidentified human genes. XX. The complete sequences of 100 new cDNA clones from brain which code for large proteins in vitro. DNA Res. (2001)

Neptune E R, Frischmeyer PA, Arking DE, Myers L, Bunton TE, Gayraud B, Ramirez F, Sakai LY, Dietz HC. 2003. Dysregulation of TGF-β activation contributes to pathogenesis in Marfan syndrome. *Nature Genet* **33**: 407-411.

Pereira, L., D'Alessio, M., Ramirez, F., Lynch, J. R., Sykes, B., Pangilinan, T., Bonadio, J. Genomic organization of the sequence coding for fibrillin, the defective gene product in Marfan syndrome. Hum. Mol. Genet., 1993. 2(7):p. 961-968

Puklin-Faucher E., Gao M., Schulten K., Vogel V. 2006. How the headpiece hinge angle is opened: New insights into the dynamics of integrin activation. J. Cell Biol. 175:349–360. doi: 10.1083/jcb.200602071.

Quondamatteo F, Reinhardt DP, Charbonneau NL, Pophal G, Sakai LY, Herken R. Fibrillin-1 and fibrillin-2 in human embryonic and early fetal development. Matrix Biol. 2002;21:637–646.

Raghunath, M. *et al.* (1994). Analyses of truncated fibrillin caused by a 366 bp deletion in the FBN1 gene resulting in Marfan syndrome. *Biochem J* **302**, 889-896

Ramirez F, Gayraud B, Pereira L. 1999. Marfan syndrome: new clues to genotype-phenotype correlations. *Ann Med* **31**: 202-207

Ramirez, F. and Sakai, L. Y. (2010) Biogenesis and function of fibrillin assemblies. Cell Tissue Res. **339**, 71-82

Ramirez, F., Sakai, L. Y., Rifkin, D. B. and Dietz, H. C. (2007) Extracellular microfibrils in development and disease. Cell Mol. Life Sci. **64**, 2437-2446

Ramirez, F. and Rifkin, D. B. (2009) Extracellular microfibrils: contextual platforms for TGFβ and BMP signaling. Curr. Opin. Cell Biol. **21**, 616-622

Reinhardt, D.P. *et al.* (1997a). Calcium stabilizes fibrillin-1 against proteolytic degradation. *J Biol Chem* **272**, 1231-1236.

Reinhardt, D.P. *et al.* (1996). Fibrillin-1 and fibulin-2 interact and are colocalized in some tissues. *J Biol Chem* **271**, 19489-19496.

Reinhardt, D.P. *et al.* (1997b). Calcium determines the shape of fibrillin. *J Biol Chem* **272**, 7368-7373.

Robertson I, Jensen S, Handford P. TB domain proteins: evolutionary insights into the multifaceted roles of fibrillins and LTBPs. Biochem J. 2010 Dec 22;433(2):263-76. Review.

Robinson PN, Arteaga-Solis E, Baldock C, Collod-Beroud G, Booms P, De Paepe A, Dietz HC, Guo G, Handford PA, Judge DP, Kielty CM, Loeys B, Milewicz DM, Ney A, Ramirez F, Reinhardt DP, Tiedemann K, Whiteman P, Godfrey M. ,The molecular genetics of Marfan syndrome and related disorders.
J Med Genet. 2006 Oct;43(10):769-87. Epub 2006 Mar 29. Review.

Rock MJ, Cain SA, Freeman LJ, Morgan A, Mellody K, Marson A, Shuttleworth CA, Weiss AS, Kielty CM. Molecular basis of elastic fiber formation. Critical interactions and a tropoelastinfibrillin-1 cross-link. J Biol Chem. 2004;279:23748–23758

Rommel K, Karck M, Haverich A, Schmidtke J, Arslan-Kirchner M. (2002) Mutation screening of the fibrillin-1 (FBN1) gene in 76 unrelated patients with Marfan syndrome or Marfanoid features leads to the identification of 11 novel and three previously reported mutations.
Hum Mutat. Nov;20(5):406-7.

Sabatier L, Chen D, Fagotto-Kaufmann C, Hubmacher D, McKee MD, Annis DS, Mosher DF, Reinhardt DP (2009) Fibrillin assembly requires fibronectin. Mol Biol Cell 20:846–858

Sakai L. Y, D.R Keene and E Engvall, Fibrillin, a new 350-kD glycoprotein, is a component of extracellular microfibrils, J. Cell Biol. 103 (1986)

Sakai L.Y, D.R Keene, R.W Glanville and H.P Bachinger, Purification and partial characterization of fibrillin, a cysteine-rich structural component of connective tissue microfibrils, J. Biol. Chem. 266 (1991),

Sakamoto H, T Broekelmann, D.A Cheresh, F Ramirez, J Rosenbloom and R.P Mecham, Cell-type specific recognition of RGD and non-RGD-containing cell binding domains in fibrillin-1, J. Biol. Chem. 271 (1996), pp. 4916–4922.

Schrijver I , Liu W , Brenn T , Furthmayr H , Francke U . Cysteine substitutions in epidermal growth factor-like domains of fibrillin-1: distinct effects on biochemical and clinical phenotypes. *Am J Hum Genet* 1999 1007–20.

Sengle G, Charbonneau NL, Ono RN, Sasaki T, Alvarez J, Keene DR, Bachinger HP, Sakai LY (2008a) Targeting of bone morphogenetic protein growth factor complexes to fibrillin. J Biol Chem 283:13874–13888

Sengle G, Ono RN, Lyons KM, Bachinger HP, Sakai LY (2008b) A new model for growth factor activation: type II receptors compete with the prodomain for BMP-7. J Mol Biol 381:1025–1039

Shattil S. J., Chungho Kim & Mark H. Ginsberg. The final steps of integrin activation: the end game. Nature Reviews Molecular Cell Biology 11, 288-300 (2010)

Shimaoka, M., Takagi, J., and Springer, T. A. (2002) Conformational regulation of integrin structure and function. Annu. Rev. Biophys. Biomol. Struct. 31, 485–516

Siracusa, L. D., McGrath, R., Ma, Q., Moskow, J. J., Manne, J., Christner, P. J., Buchberg, A. M. and Jiminez, S. A. (1996) *Genome Res.* **6**, 300-13

Singh et al. (2006), TGFBR1 and TGFBR2 mutations in patients with features of Marfan syndrome and Loeys-Dietz syndrome. Hum Mutat;27(8):770-7.

Smallridge RS, Whiteman P, Werner JM, Campbell ID, Handford PA, Downing AK. Solution structure and dynamics of a calcium binding epidermal growth factor-like domain pair from the neonatal region of human fibrillin-1. *J Biol Chem* 2003; (14):12199–206

Smallridge RS, Whiteman P, Doering K , Handford PA, Downing AK. EGF-like domain calcium affinity modulated by N-terminal domain linkage in human fibrillin-1. *J Mol Biol* 1999; (3) :661–8.

Suk JY, Jensen S, McGettrick A, Willis AC, Whiteman P, Redfield C, Handford PA. Structural consequences of cysteine substitutions C1977Y and C1977R in calcium-binding epidermal growth factor-like domain 30 of human fibrillin-1. J Biol Chem. 2004 Dec 3;279(49):51258 65.

Thurmond F. and Trotter J. (1996) Morphology and biomechanics of the microfibrillar network of sea cucumber dermis. Journal of Experimental Biology, Vol 199, 1817-1828

Tiedemann K, Batge B, Muller PK, Reinhardt DP (2001) Interactions of fibrillin-1 with heparin/heparin sulfate; implications for microfibrillar assembly. J Biol Chem 276:36035–36042

Takagi J, Erickson HP and Springer TA (2001) C-terminal opening mimics 'inside-out' activation of integrin 51. Nat Struct Biol, 8, 412–416.

Takagi J, Debottis DP, Erickson HP and Springer TA (2002) The role of specificity-determining loop of the integrin -subunit I-like domain in folding, association with the subunit and ligand binding. Biochemistry, 41, 4339–4347.

Tynan, K., Comeau, K., Pearson, M., Wilgenbus, P., Levitt, D., Gasner, C.,Berg, M., Miller, D. and Francke, U. (1993) *Hum. Mol. Genet.*, **2**, 1813–1821.

Wegener K. L., A.W. Partridge, J. Han, A.R. Pickford, R.C. Liddington, M.H. Ginsberg and I.D. Campbell, Structural basis of integrin activation by talin, Cell 128 (2007), pp. 171–182.

Whiteman P , Handford PA. Defective secretion of recombinant fragments of fibrillin-1: implications of protein misfolding for the pathogenesis of Marfan syndrome and related disorders. *Hum Mol Genet* 2003; 727–37.

Whiteman P, Downing AK, Smallridge R , Winship PR, Handford PA. A Gly —>Ser change causes defective folding in vitro of calcium-binding epidermal growth factor-like domains from factor IX and fibrillin-1. *J Biol Chem* 1998;**273** (14) :7807–13

Whiteman P, Smallridge RS, Knott V, Cordle JJ, Downing AK, Handford PA. A G1127S change in calcium-binding epidermal growth factor-like domain 13 of human fibrillin-1 causes short range conformational effects. *J Biol Chem* 2001;**276** (20) :17156–62

Whiteman P, Hutchinson S, Handford PA., Fibrillin-1 misfolding and disease. Antioxid Redox Signal. 2006 Mar-Apr;8(3-4):338-46. Review. PMID: 16677079

Werner JM, Knott V, Handford PA, Campbell ID, Downing AK. Backbone dynamics of a cbEGF domain pair in the presence of calcium. *J Mol Biol* 2000.

Xiao T., Takagi J., Coller B.S., Wang J.H., Springer T.A. 2004. Structural basis for allostery in integrins and binding to fibrinogen-mimetic therapeutics. Nature. 432:59–67. doi: 10.1038/nature02976.

Yamada K.M., Pankov R., Cukierman E. 2003. Dimensions and dynamics in integrin function. Braz. J. Med. Biol. Res. 36:959–966.

Yuan, X. *et al.* (1997). Solution structure of the transforming growth factor beta-binding protein-like module, a domain associated with matrix fibrils. *Embo J* **16**, 6659-6666.

Zamir E, Geiger B. Molecular complexity and dynamics of cell-matrix adhesions. J Cell Sci. 2001;114:3583

Zhang, H., Hu, W., and Ramirez, F. (1995). Developmental expression of fibrillin genes suggests heterogeneity of extracellular microfibrils. J Cell Biol *129*, 1165-76.

APPENDICES

APPENDIX A

Oligonucleotide Primers

A. Primers for cloning cbEGF18-26 wild-type in pKG52 vector

Forward primer
5'- TAG TAG GTC GAC TT ACA GAC ATC AAT GAA TGT GAA ATT -3'

Reverse primer
5'- TAG TAG GTC GAC CTA TTA GTG ATG GTG ATG GTG ATG ATT GCA CTG TCC TGT GTG CTG CCA T CT CGA G -3'

Primers for cloning cbEGF22-25 wild-type in pSecTag vector

Forward primer
5'- TAG TAG GGC CCA GCC GGC CGA TGT GAA TGA ATG CCT GGA TC-3'

Reverse primer
5'-TAG TAG GTC GAC CTA TTA GTG ATG GTG ATG GTG ATG TGC TGA TTC ACA AAC CAA CAA CTT GTC-3'

B. Primers for mutagenesis

W1570C Forward primer:
5'- GGT AAA GCC TGT GGT ACT CCT TGT GAG ATG TG -3'

W1570C Reverse primer:
5'- AGG AGT ACC ACA GGC TTT ACC CAG AGA AC-3'

C1564S Forward primer:
5'- TCC TGC TGC TCT TCT CTG GGT AAA GCC TGG GG -3'

C1564S Reverse primer:
5'- ACC CAG AGA AGA GCA GCA GGA AGC TTT GGA AAC -3'

C1564Y Forward primer:
5'- TCC TGC TGC TAT TCT CTG GGT AAA GCC TGG GG -3'

C1564Y Reverse primer:
5'- ACC CAG AGA ATA GCA GCA GGA AGC TTT GGA AAC -3'

WMSdel Forward primer
5'-TGC ATG GAT ATG AGA TAT GCT GAC AAC CAG ACC TG-3'

WMSdel Reverse primer
5'-CA GGT CTG GTT GTC AGC ATA TCT CAT ATC CAT GCA ATT ATT TCC-3'

** DNA sequence mutated has been highlighted in yellow*

Table 1.1 shows the molar extinction coefficient (ε) and Molecular mass in Da of the TB4-containing wild-type and mutant construct used for protein quantitation.

Protein	Reduced	Refolded
cbEGF22-TB4-cbEGF23 WT BirA **ε**	21602.2 17780	21581.2 18980
cbEGF22-TB4-cbEGF23 W1570C BirA **ε**	21519.1 12950	21497.1 14325
cbEGF22-TB4-cbEGF23 C1564S BirA **ε**	21586.1 18450	21566.1 19700
3x cbEGF22-TB4-cbEGF23 C1564Y BirA **ε**	21662.2 19940	21642.2 21190
TB4cbEGF23 WT **ε**	15458.2 11460	15444.2 12335
TB4cbEGF23 W1570C **ε**	14871.5 11460	14858.5 12210
TB4cbEGF2323 C1564S **ε**	14804.5 5960	14789.5 6835

Calculation of Molar extinction coefficient (using ProtParam)

The extinction coefficient (**ε)** indicates how much light a protein absorbs at a certain wavelength. It is useful to have an estimation of this coefficient for following a protein which a spectrophotometer when purifying it.

It has been shown (Pace et al. 1995) that it is possible to estimate the molar extinction coefficient of a protein from knowledge of its amino acid composition. From the molar extinction coefficient of tyrosine, tryptophan and cystine (cysteine does not absorb appreciably at wavelengths >260 nm, while cystine does) at a given wavelength, the

extinction coefficient of the native protein in water can be computed using the following equation:

ε (Protein) = **Number of (Tyr)** x **ε (Tyr)** + **Number of (Trp)** x **ε (Trp)** + **Number of (Cystine)** x **ε (Cystine)**

where **ε** (Tyr) = 1490, **ε** (Trp) = 5500, **ε** (Cystine) = 125;

The absorbance (optical density) can be calculated using the following formula:

Absorbance (Protein) = **ε** (Protein) / Molecular weight

APPENDIX B

DNA techniques

10 x PCR buffer:	100 mM KCl/ 60 mM $(NH_4)SO_4$/200 mM $MgCl_2$/1% Triton X-100/ 100 µg nuclease-free BSA.
10 x TBE buffer:	108.8 g Tris-HCl/ 55.4 g Boric acid/ 9.3 g EDTA.
3 M KOAc:	58.8 g KOAc/ 23 ml acetic acid/ to 200 ml total volume with H_2O.
5 x ligase buffer:	10 mM rATP (25 µl) 1 M Tris pH 7.5 (12.5 µl) 1 M $MgCl_2$ (2.5 µl) 1 M DTT (3.5 µl) H_2O (6.5 µl)
1% agarose:	0.5 g agarose (Roche) in 50 ml heated TBE buffer with 3 µl ethidium bromide.
6 x glycerol loading	0.25% (w/v) bromophenolblue/ 30 mM EDTA (pH 8.0)/ buffer: 30% (w/v) glycerol.

Bacterial growth

2xTy medium:	16 g Triptone/ 10 g yeast extract/ 5 g NaCl/ to 1 l total volume with H_2O, pH to 7.0-7.2
KA Plates:	Agar plates with 100 µg/ml ampicillin and 25 µg/ml kanomycin.
Ampicillin:	50 mg/ml stock solution, stored at –20 °C.
Kanamycin:	50 mg/ml stock solution, stored at –20 °C.

Protein purification

6 M guanidine buffer:	60 g guanidine-HCl/ 10 ml 0.5 M $NaPO_4$ pH 7.4, H_2O to 100 ml, add 25 µl EtSH
HPLC Buffer A:	0.1% Trifluoroacetic acid in milli-Q H_2O (pH 2.5-3).

HPLC Buffer B: 80% Acetonitrile / 0.1% Trifluoroacetic acid / milli-Q H_2O. (pH 2.5-3).

Milli-Q H_2O: Ultra pure water.

SDS-PAGE

16% polyacrylamide: 8 ml 40% acrylamide/ 4 ml 5 x separating buffer/ 8 ml resolving gel: milliQ-H_2O/ 300µl APS/ 30 µl TEMED.

6% polyacrylamide 1.5 ml 40% acrylamide/ 2 ml 5 x stacking buffer/ 6.5 ml stacking gel: milliQ-H_2O/ 200 µl APS/ 20 µl TEMED.

5 x separating buffer: 46 g Tris/ 1 g SDS/ 200 ml H_2O, pH to 8.8 with HCl

5 x stacking buffer: 30.25 g Tris/ 1 g SDS/ 200 ml H_2O, pH to 6.8 with HCl

5 x running buffer: 90 g glycine/ 18.75 g Tris/ 5 g SDS/ 1 l H_2O

Laemmli's sample 10% glycerol/ 3% SDS/ 50 mM Tris-Cl pH 6.8, trace BPB, buffer : 5% EtSH

Coomassie stain: 1.25 g Coomassie Blue R/ 10% MeOH/ 10% acetic acid

De-stain solution: 10% MeOH/ 10% acetic acid

Protein analysis

Calcium-free buffer: 1 M Tris-HCl pH 7.5 made with milli-Q H_2O containing chelex 100 Ca^{2+} chelating resin (Bio-Rad)

D_2O buffer: 100% ^2H_2O containing 5 mM Tris-DCl adjusted to pH 6.5 using DCl and NaOD

APPENDIX C

Recombinant integrins used for SPR

Recombinant αvβ3 and α5β1 integrins were a kind gift of Dr Takagi, Osaka Japan and were prepared as described in Takagi *et al.,* 2002 (αvβ3) and Takagi *et al.,* 2001 (α5β1). Soluble α5β1 and αvβ3 integrin were prepared with heterodimer extracellular fragments in which interactions between - and -subunit cytoplasmic domains were replaced with an artificial clasp.

Soluble recombinant αvβ6 integrin was a kind gift by Dr. N. Abrescia, CIC bioGUNE, Spain and purified as described in Weinacker *et al.,* 1994. The truncated integrin only contained the extracellular domains which interact with ECM ligands. FPLC (i) and SDS-PAGE (ii) profiles of purified αvβ6 recombinant integrin, which was used in SPR binding assays. αv* indicates the band that corresponds to the highly glycosylated αv (purity ~70-80%). The molecular marker is from Fermentas (Page Ruler unstained Protein ladder).

(i) (ii)

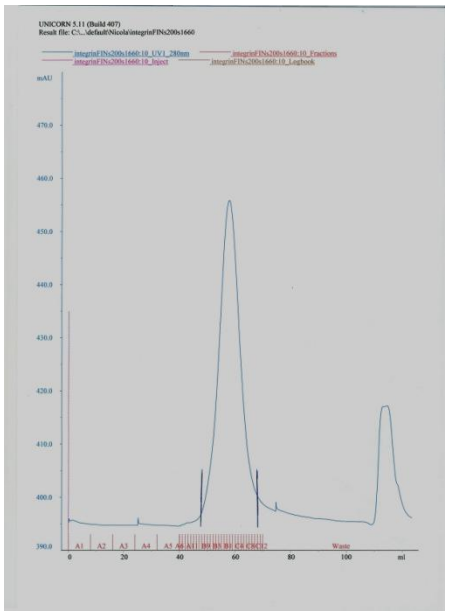

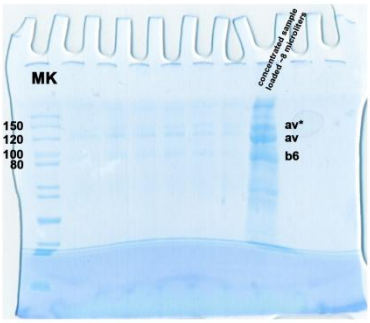

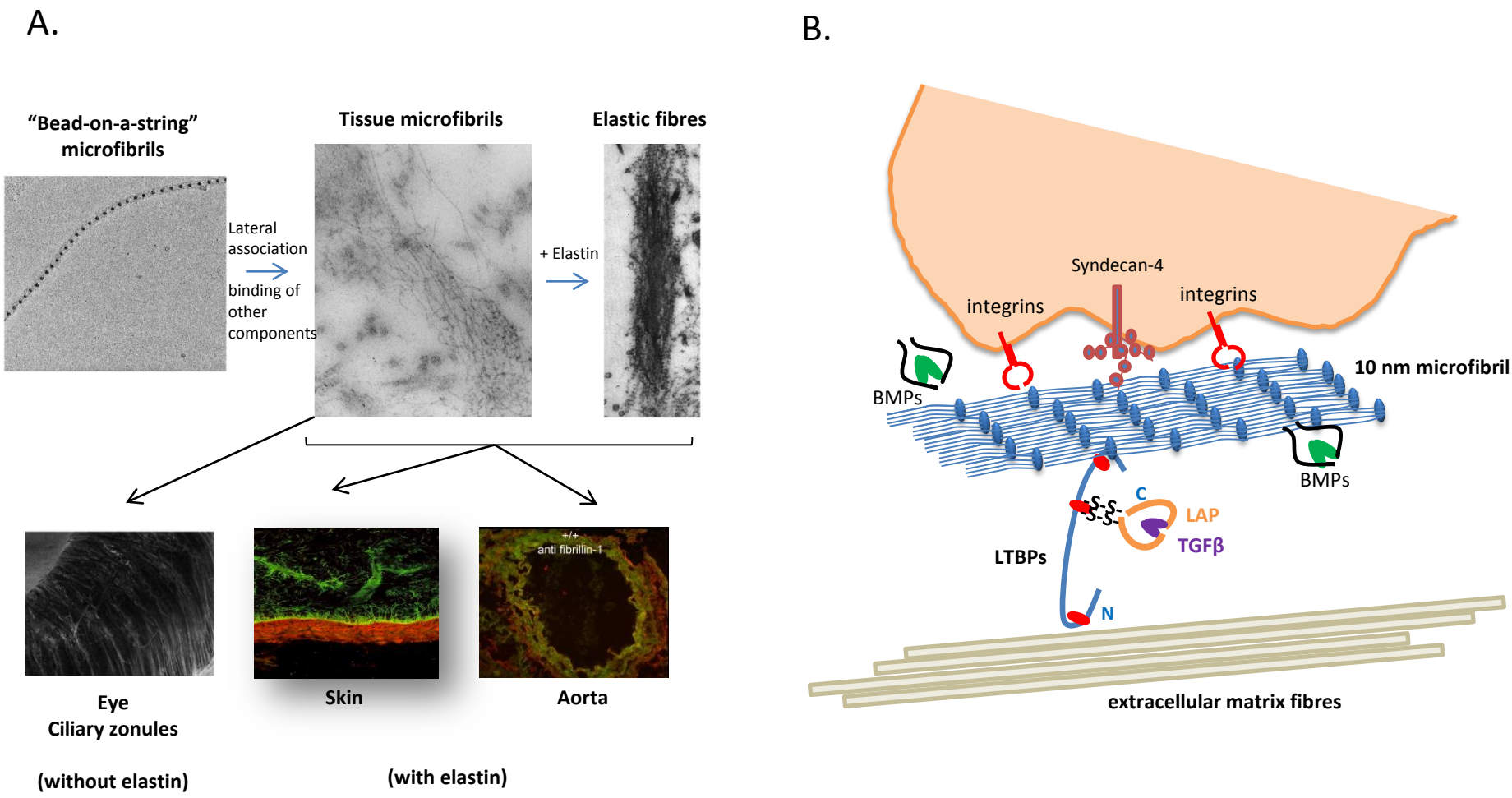

Figure 1.1 Structural and regulatory role of microfibrils: A. Fibrillin-1 microfibrils have an important structural role in the ECM and can be present in different tissues with or without elastin. Immunofluorescence of skin shows the expression of elastin (red) and fibrillin-1 (green); in aorta fibrillin-1 is present with elastin and is shown in green; and in eye fibrillin-1 microfibrils are present without elastin **B.** Apart from acting as structural scaffolds, fibrillin-1 microfibrils have also been shown to store cytokines such as TGF-β and BMPs. They have been found to mediate cell matrix interactions by binding to cell surface receptors such as integrins and syndecans. Symbols; BMP- Bone morphogenetic protein; LAP- Latency-associated peptide; LTBP- Latent transforming growth factor-β binding protein. Electron microscopy images of microfibrils, Ramirez *et al.,* 2004; image of aorta, Charbonneau *et al.,* 2010; image of skin section, Loeys *et al.,* 2010.

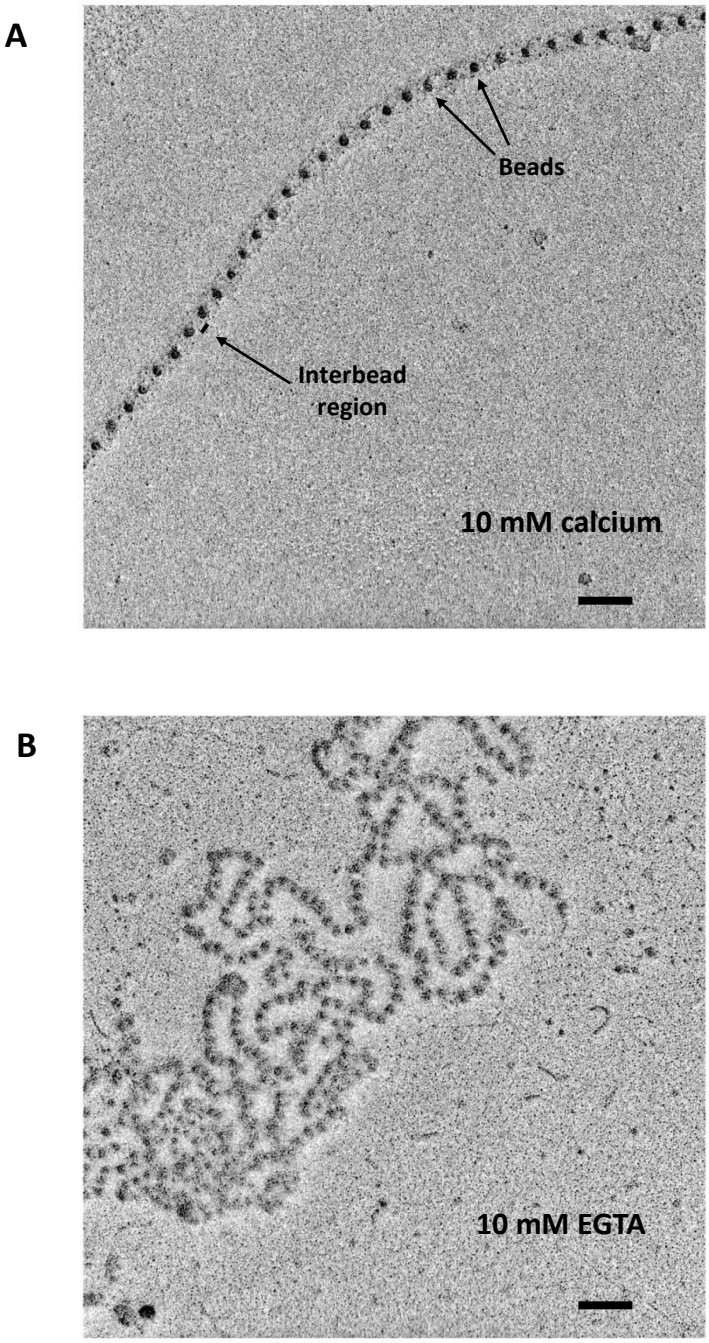

Figure 1.2. 'Bead on a string' appearance of rotary shadowed microfibrils and the importance of calcium for the organisation of fibrillin-rich 10-12 nm microfibrils. Microfibrils extracted from human dermal fibroblasts were purified in the presence of 10 mM calcium and incubated for equivalent times in the presence of A) 10mM $CaCl_2$ and B) 10mM EGTA. Note the reduction in bead to bead periodicity in the presence of EGTA and the curved appearance of the microfibril. Bar = 100 nm. Figures provided by Dr. S. Hutchinson (Cardy and Handford 1998).

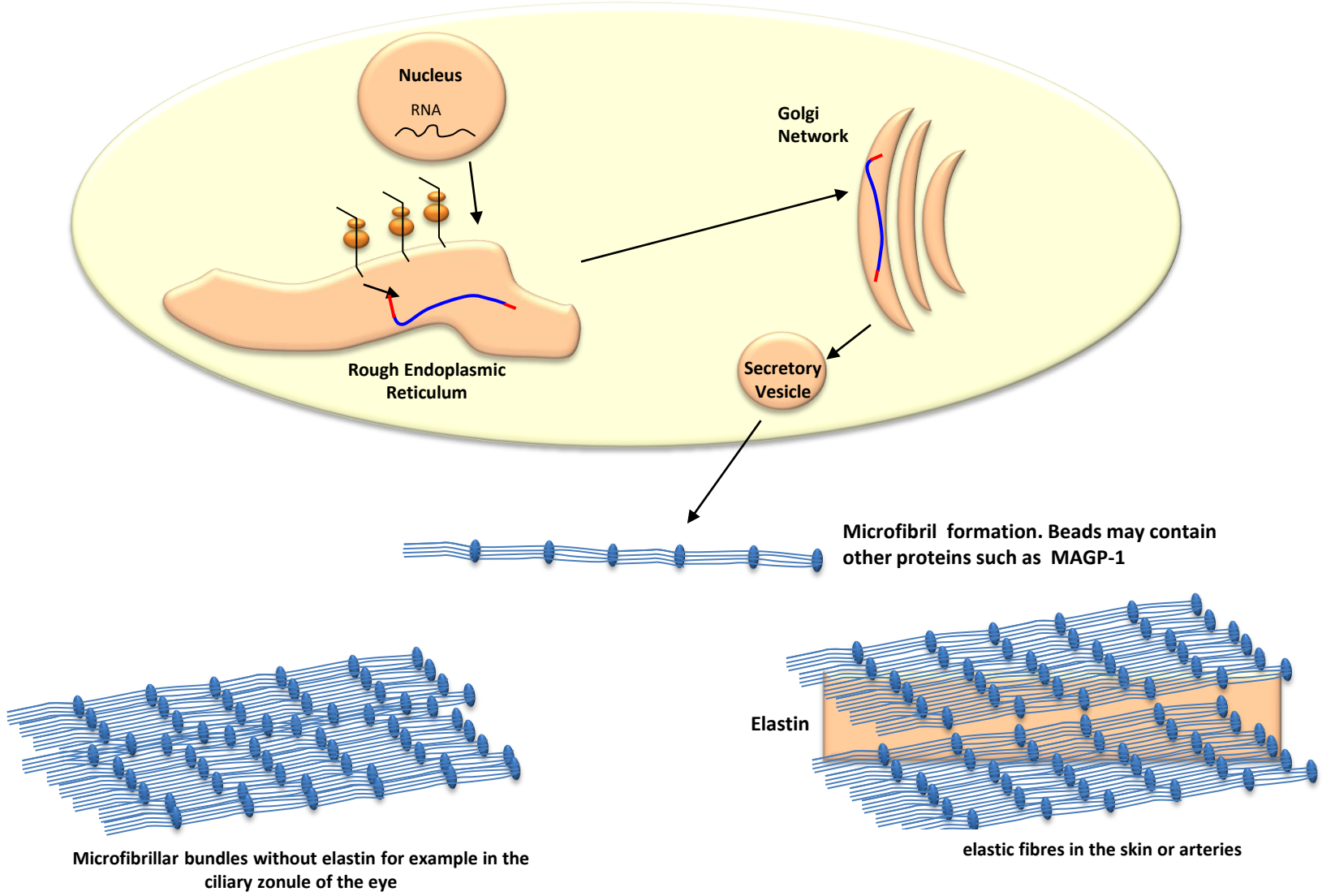

Figure 1.4 Pathway of fibrilin production, secretion and incorporation into microfibrils. *FBN1* RNA leaves the nucleus and is translated on the rough ER. In the ER disulphide bonds are formed, the protein is β-hydroxylated and undergoes N- and O- linked glycosylation. During the secretory pathway, the N- and C- termini (shown in red) are cleaved and fibrillin-1 is secreted most likely as a monomer into the matrix where it forms 10-12 nm microfibrils. In mammals, assembly of fibrillin-1 monomers to form microfibrils is dependent on fibronectin (Sabatier *et al.,* 2009), heparin/heparan sulphate (Tiedemann *et al.,* 2001) and other molecules in the matrix.

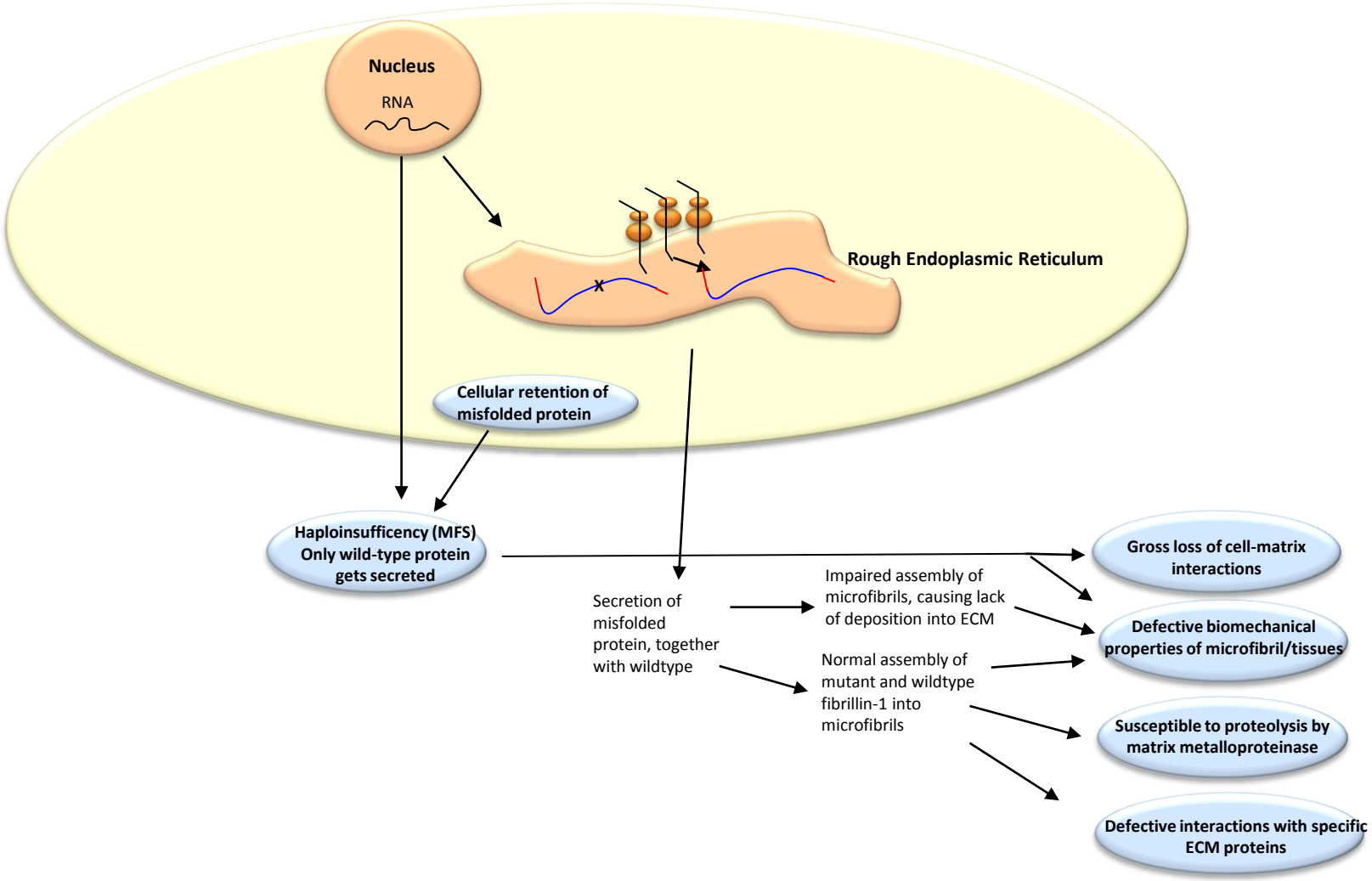

Figure 1.12 The range of pathogenic mechanisms possible as a result of *FBN1* mutations. The encircled pathogenic mechanisms are already known to be associated with MFS-causing mutations. These include haploinsufficiency and dominant–negative effects. Due to the interactive nature of fibrillin-1 with cell matrix components, it is possible that certain mutations result in amino acid substitutions which affect fibrillin-1 binding to a specific ECM component. This is a potential explanation for mutations in TB4 which cause SSS, but not MFS.

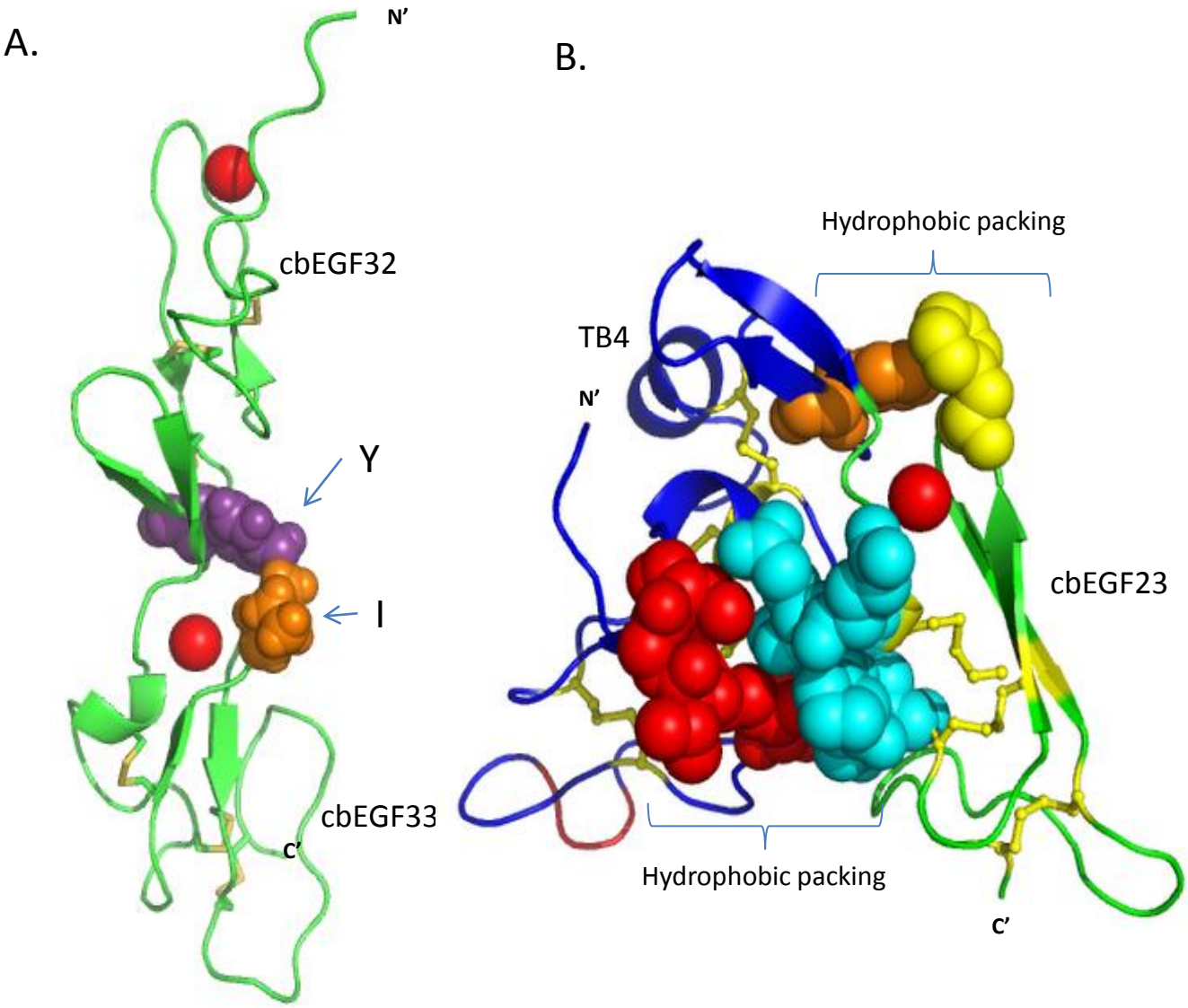

Figure 1.5 A) Tertiary structure of a typical cbEGF domain pair. Tertiary structure of cbEGF32-cbEGF33 solved by NMR (Downing *et al.* 1996). The calcium ions are shown as red spheres and the two residues Tyr (Y) and Ile (I) involved in hydrophobic interactions are shown as purple and orange spheres respectively. Disulphide linkages are shown as yellow sticks. The figure was produced by PyMol software (DeLano Scientific LLC).

B) Tertiary structure of a typical TB-cbEGF pair. Tertiary structure of TB4-cbEGF23 determined by X-ray crystallography (Lee *et al.,* 2004). The TB4 domain backbone is shown in blue, and that of the cbEGF23 domain in green. A bound calcium atom is displayed as a red sphere. TB4 and cbEGF23 domains form extensive hydrophobic interfaces as can be seen from the crystal structure which stabilises the calcium binding region and results in the observed high calcium affinity. Figure was created using PyMOL software using the cbEGF22-TB4-cbEGF23 triple domain construct coordinates (Lee *et al*., 2004).

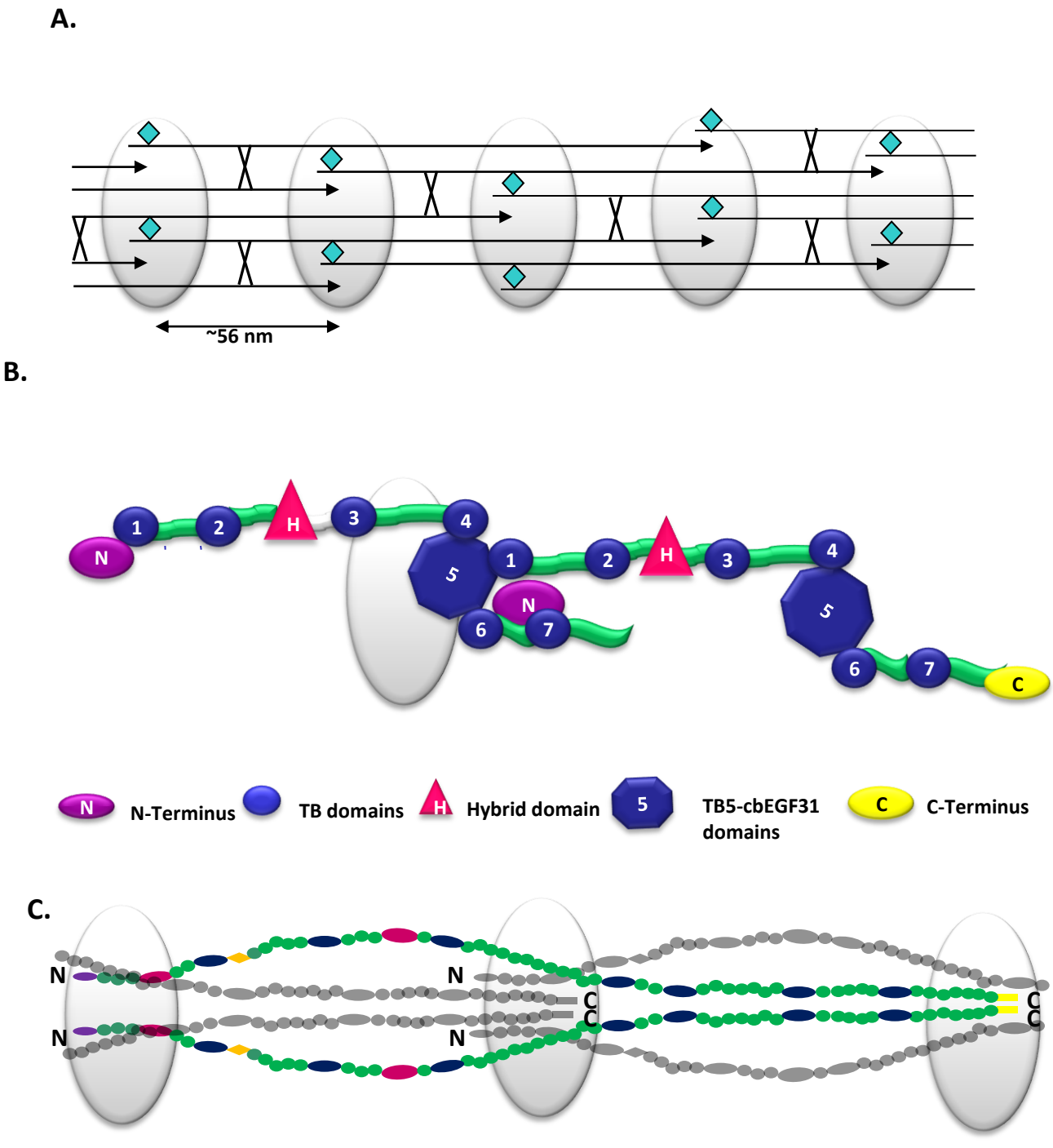

Figure 1.6. Proposed models of fibrillin-1 organisation in the microfibril. (A) A simple model of the fibrillin microfibril proposed by Lee *et al*., 2004. Monomers are arranged in a head-to-tail fashion, with ~12 nm overlap between N- and C-termini of successive molecules. Together with a 1/3 staggered alignment, this could give rise to the observed 56 nm periodicity. The intermolecular transglutaminase cross-links are shown as X and the turquoise diamonds represent MAGP-1, which is proposed to be an integral component of fibrillin microfibrils **(B)** This model by Baldock *et al.* (2006) predicts an overlap of N- and C-termini and and a molecule length of 90nm. The fibrillin-1 molecule has a compact arrangement, particularly from domains TB4 to TB6 (adapted from Baldock *et al.* 2006). **(C)** The half-staggered model with N-terminal halves on the surface of the microfibril. This model is based on antibody epitope mapping by using extracted microfibrils and on the identification of crude collagenase cleavage sites in fibrillin-1. It accommodates the findings of ligand-binding sites to N-terminal halves of fibrillin (Kuo *et al.,* 2007)

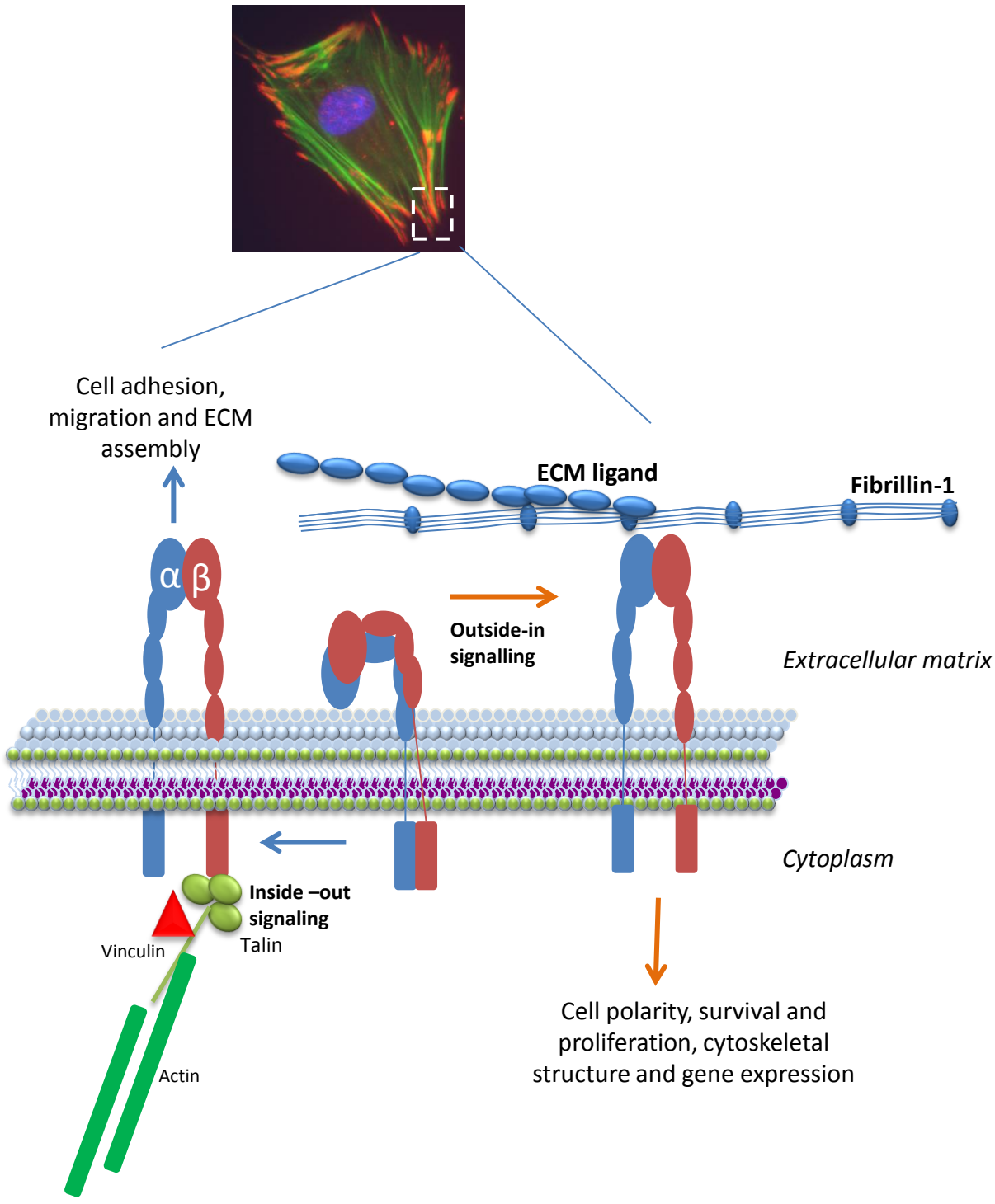

Figure 1.10 Integrin Signalling. There are two directions of integrin signalling, which have different biological consequences. During 'inside–out' signalling, an intracellular activator, such as talin, binds to the β-integrin tail, leading to conformational changes that result in increased affinity for extracellular ligands (integrin 'activation'). In outside-in signalling, binding of integrins to their extracellular ligands changes the conformation of the integrin and contributes to integrin clustering. Both these processes lead to intracellular signals that control cell polarity, cytoskeletal structure, gene expression and cell survival and proliferation. Also shown is a fluorescent micrograph of a stromal fibroblast adherent on fibrillin-1 and stained for actin (green) and αvβ3 integrin (red) showing focal adhesions or integrin clustering. (Adapted from Shattil *et al.,* 2010, Nature Reviews)

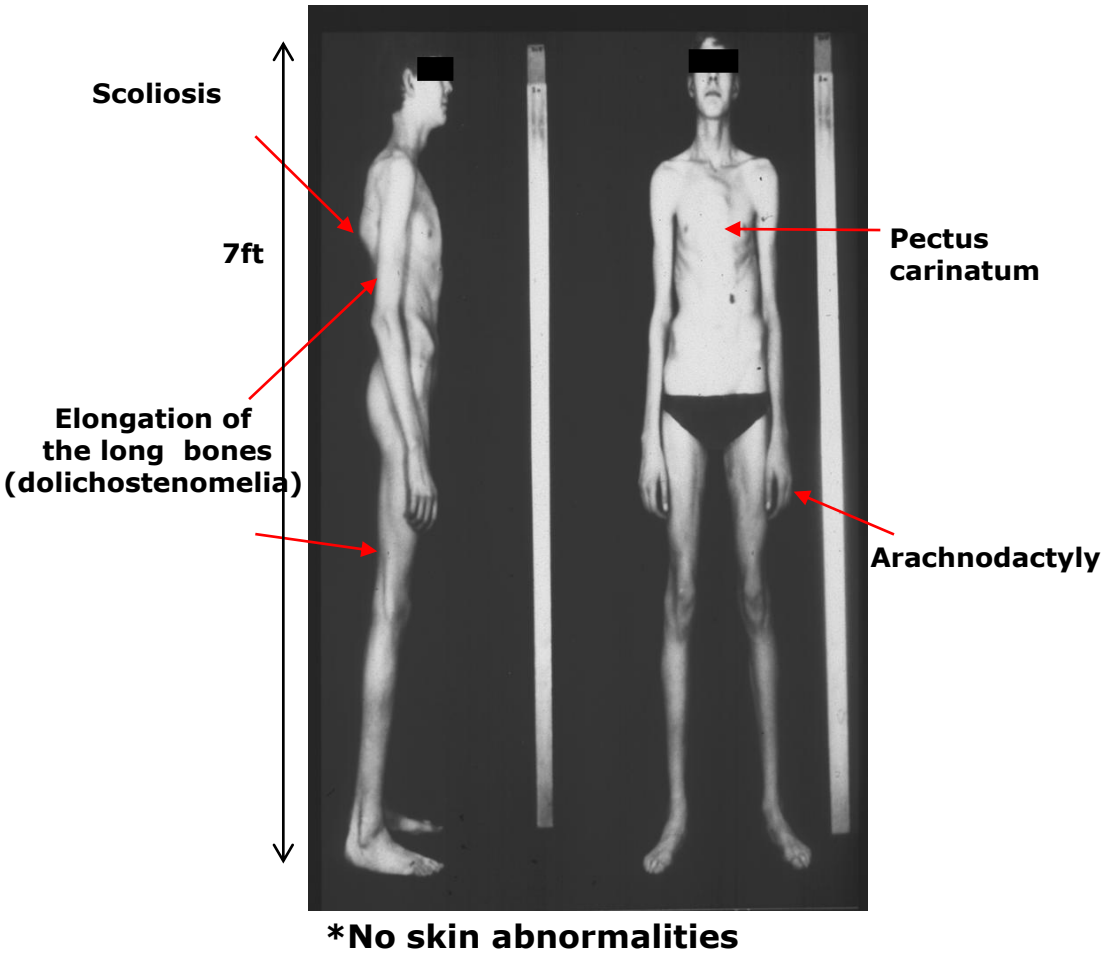

Figure 1.11. A photograph of a 17 year old youth suffering from skeletal features of MFS. MFS causes major defects in the skeleton (scoliosis, tall stature and arachnodactyly), the cardiovascular system (aortic dilation and dissection) and the ocular system (lens dislocation, myopia and retinal detachment). Note, the skin is usually normal in appearance.

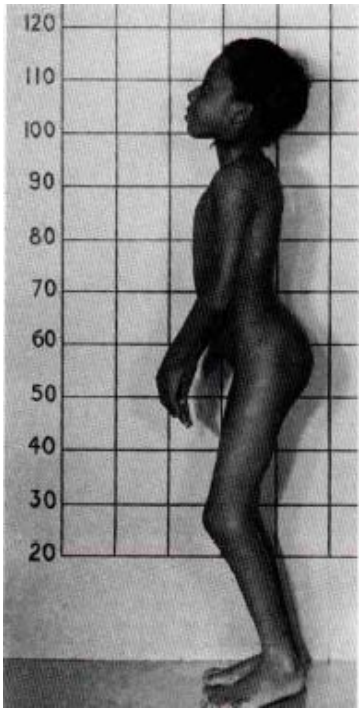

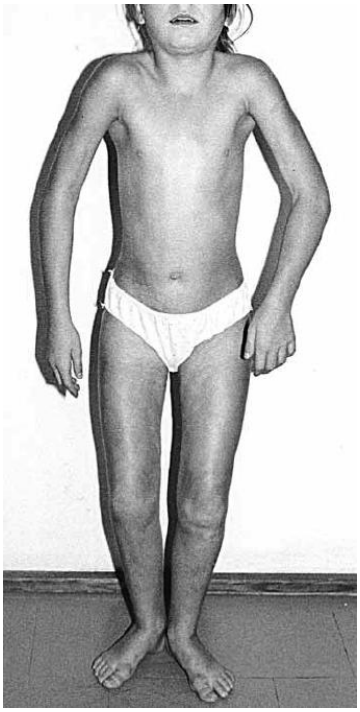

COMMON FINDINGS:

- thick and tight skin
- limitation of joint mobility
- relative short stature:
  mean adult male height 169 cm
  mean adult female height 149 cm

OCCASIONAL FINDINGS:

- cutaneous nodules
- focal lipodystrophy
- muscle weakness
- diffuse entrapment neuropathy

NO SYSTEMIC FINDINGS:

- normal eye exam
- normal cardiovascular imaging

Figure 1.13 SSS patient, L. M. at age 8 years showing lordosis (inward curvature of a portion of the vertebral column) and limited joint extension at elbows, hips, knees and 4 ankles (Esterly and McKusick, Pediatrics, 1971)

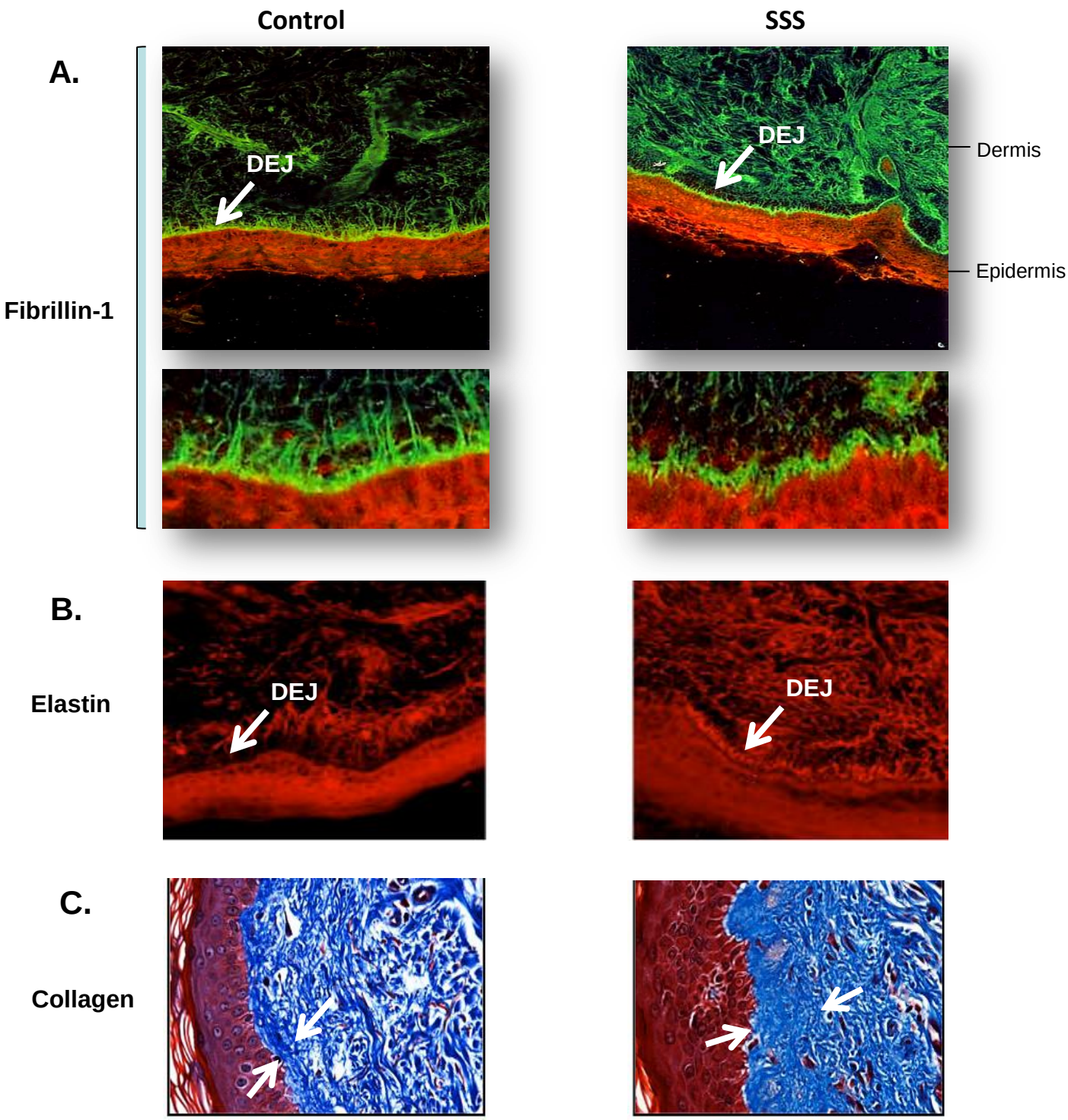

Figure 1.14 Immunochemical staining for fibrillin-1, elastin and collagen in control and SSS patient skin biopsies (A) Staining for fibrillin-1 microfibrils: Immunofluoresence of skin biopsies (10 X magnifications) from patient with SSS reveals a dramatic increase in the expression of elastin (red) and fibrillin-1 (green) in the dermis and specifically at the dermal-epidermal junction (DEJ) when compared to age-matched control. Higher magnification (40X) reveals that the microfibrillar bundles (composed of fibrillin-1) at the DEJ in patient with SSS have a stubby appearance without the deep projection into the underlying dermis seen in the control samples. **(B) Staining for elastin;** There is relative exclusion of elastin in the superficial dermis immediately adjacent to the DEJ. The SSS sample shows stubby microfibrillar deposits immediately adjacent to the DEJ that co-localize with elastin. There is also increased deposition of elastin in the deeper dermis. Scale bars = upper row of low magnification images, 50 microns; lower row of high magnification images, 20 microns. **(C) Staining for collagen;** Trichrome staining of skin biopsies (10X) from a control and a SSS patients. Note the widened zone of increased deposition of collagen (blue) in the papillary dermis of SSS patients, as delineated by white arrows (Loeys *et al.,* 2010)

Table 1.1 Molecules that can associate with fibrillin-rich microfibrils

Protein	Protein family	Potential biological role	Reference
Elastin	----------	Tropoelastin deposition	Kielty, 2002
MAGP-1,-2	Glycoprotein	Structural component of 10-12 nm microfibrils	Gibson *et al*., 2000
LTBP-1, -2, -4	Fibrillin-LTBP	Sequestering of TGFβ Structural role?	Isogai *et al*., 2003; Hirani *et al.*, 2007; Ono *et al*., 2009
Versican, Aggrecan	Proteoglycan (Hyalectin)	Link fibrillin-microfibrils to versican/hyaluronan network	Isogai *et al*., 2002
Perlecan	Proteoglycan (Hyalectin)	Anchoring microfibrils to basement membranes and in the biogenesis of microfibrils	Tiedemann *et al*., 2005
Heparin/heparin sulfate	Proteoglycan	Binding of related heparan sulfate chains may regulate cell-surface interactions assembly of fibrillin	Cain *et al*., 2005; Bax *et al*., 2007
Decorin	Small dermatan sulfate proteoglycan	Induction of fibrillin-1 expression in renal fibroblasts and mesangial cells	Hirani *et al*., 2007
Integrins (αvβ3, αvβ6, α5β1)	Integrin	Cell-matrix interactions	Pffaf *et al.,* 1996 Jovanovic *et al.,* 2006
Biglycan	Small dermatan sulfate proteoglycan	Role in elastogenesis	Schaefer *et al*., 2004
Fibulin-2, -4, -5	Fibulin	Mediate/modulate attachment of fibrillin to tropoelastin. Regulation of the initial deposition of tropoelastin on to microfibrils	El-Hallous *et al*., 2007; Ono *et al*., 2009
BMP2, 4, 7 and 10	Bone morphogenetic protein	Regulation of limb patterning	Sengle *et al*., 2008
EMILIN-1	Elastin-microfibril interface located proteins	Role in elastogenesis	Bressan *et al*., 1993; Colombatti *et al*., 2000
ADAMTSL-6	ADAMTS	Functions not known	Tsutsui *et al*., 2009
Fibronectin	---------	pericellular microfibril assembly is regulated by fibronectin fibrillogenesis	Kinsey *et al*., 2008; Sabatier *et al*., 2007

Table 1.3 Non-fibrotic disorders: Clinical manifestations of Marfan syndrome and related disorders

Syndrome	Gene	Clinical Features	References
Marfan Syndrome	*FBN1* mutation	See text	Dietz *et al.,* 1991
Neonatal MFS	*FBN1* mutation	Severe manifestation Mitral or tricuspid insufficiency Congestive heart failure Pulmonary emphysema Joint contractures Crumpled ears and loose skin. Death usually in the first year of life due to congestive heart failure	Kainulainen *et al.,* 1994
Shprintzen-Goldberg syndrome	*FBN1* mutation	Craniosynostosis and marfanoid habitus	Sood *et al.,* 1996
Familial arachnodactyly	*FBN1* mutation	Arachnodactyly Dolichostenomelia No cardiovascular manifestations	Hayward *et al.,* 1994
Ectopia lentis	*FBN1* mutation *ADAMTLS4* mutation	Bilateral ectopia lentis in some cases scoliosis No cardiovascular manifestations	Kainulainen *et al.,* 1994
Ascending aortic aneurysm and dissection without classical MFS	*FBN1* mutation	Ascending aortic aneurysm dissection No ectopia lentis No specific skeletal findings	Francke *et al.,* 1995 Milewicz *et al.,* 1996
MASS phenotype	*FBN1* mutation	Ascending aortic aneurysm and dissection No ectopia lentis No specific skeletal findings	Dietz *et al.,* 1993
New variant of the MFS	*FBN1* mutation	Skeletal features of MFS with joint contractures and knee joint effusions. Ectopia lentis No cardiovascular manifestations	Adès *et al.,* 2004
Isolated skeletal features	*FBN1* mutation	Tall stature Scoliosis Pectus excavatum Arachnodactyly	Milewicz *et al.,* 1995
Homocystinuria	Metabolic disorder: affects methionine metabolism	Arterial and venous thromboembolic events	Guisti *et al.,* 2004
Loeys-Dietz aneurysm syndrome	Mutation in TGFβ receptor I or II	Arterial tortuosity with ascending aortic aneurysm Craniosynostosis Mental retardation Congenital heart disease	Loeys *et al.,* 2006
CCA (Congenital contractural arachnodactyly)	FBN2 mutation	Marfanoid habitus Arachnodactyly Camptodactyly Crumpled ears Mild contractures in elbows, knees and hips Mild muscle hypoplasia	Tsipouras *et al.,* 1994 Park *et al.,* 1998
Ehlers-Danlos Syndrome	Mutation in TGFβ receptor I or II	hypertelorism bifid uvula, cleft palate Craniosynostosis	Leier *et al.,* 1980

Disease	Symptoms	Protein	Fibrillin-1 in the affected tissue	Reference
Marfan syndrome	• cardiovascular, ocular (ectopia lentis) and skeletal defects • tall stature • no skin abnormalities	Mutations in *FBN1* gene	Reduced microfibrillar deposits	Kainulainen K *et al.,* 1994
Stiff Skin syndrome (SSS)	• **skin fibrosis** • **joint immobility** • **short stature**	Mutations in *FBN1* gene	Increased microfibrillar deposits	Loeys *et al.* 2010
Tight skin syndrome (in mice)	• **skin fibrosis** • Cardiovascular, lung and skeletal defects	Intragenic duplication of the exon 17-40 of *FBN1* gene	Increased microfibrillar deposits	Siracusa *et al.* 1996
Weill-Marchesani syndrome (WMS)	• **skin fibrosis** • **joint immobility** • **short stature** • glaucoma, • brachydactyly (short fingers) • ectopia lentis	Deletion in *FBN1* gene (Dominant form) Mutation in *ADAMTS10* gene (recessive form)	Not known	Faivre *et al.,* 2003
Systemic Sclerosis / localized scleroderma	• **skin fibrosis** • **joint immobility**	Fibrillin-1 auto-antibodies	SSc patients show a striking decrease in the *in vivo* microfibrillar network in affected and unaffected skin *In vitro* production, secretion and organisation of microfibrils by SSc fibroblasts are normal	Tan FK *et al.* 1999

Table 1.4 Fibrillin-1 in fibrotic disorders and comparison of these disorders with MFS (non-fibrotic) MFS is associated with tall stature, cardiovascular, ocular and skeletal defects. No skin abnormalities have been found in patients. *In vivo* studies have revealed reduced amount of fibrillin-1 microfibrils have been in affected tissue. Similar phenotypic findings in different disorders are shown in bold.

Mutation	Position of the residue in TB4	Disease	Reference
R1530C	------	Ectopia Lentis	B. Loeys *et al.,* 2001
C1564S	5th cysteine and forms 5-8 disulphide bond	SSS	B. Loeys *et al.,* 2010
C1564Y	Same as above	MFS	Biggin *et al.,* 2004
C1564F	Same as above	MFS	Arbustini *et al.,* 2005
W1570C	Highly conserved residue, hydrophobic core of domain	SSS	B. Loeys *et al.,* 2010
M1576T	------	MFS	Rommel *et al.,* 2005
C1577G	7th cysteine and forms 4-7 disulphide bond	SSS	B. Loeys *et al.,* 2010
V1580G	Close to the RGD loop	MFS	Kainulainen *et al.,* 1994
C1589F	8th cysteine, forms 5-8 disulphide bond	MFS	Tynan *et al.,* 1993
G1594N	Next to the F1595, involved in packing with F1626 of cbEGF23	SSS-Ectopia lentis	Loeys et al., 2010
E1605K	Last residue of TB4	MFS	Liu *et al.,* 1997
Duplication of cbEGF7-cbEGF24 domains in mice fibrillin-1 (17-40 exon duplication)	-----	Tsk (in mice)	Siracusa *et al.,* 1994

Table 3.1 Table showing missense mutations in the TB4 domain of fibrillin-1. Note that three substitutions have been described at residue 1564, which give rise to either SSS or MFS. In *Tsk* mice TB4 domain in fibrillin-1 is duplicated.

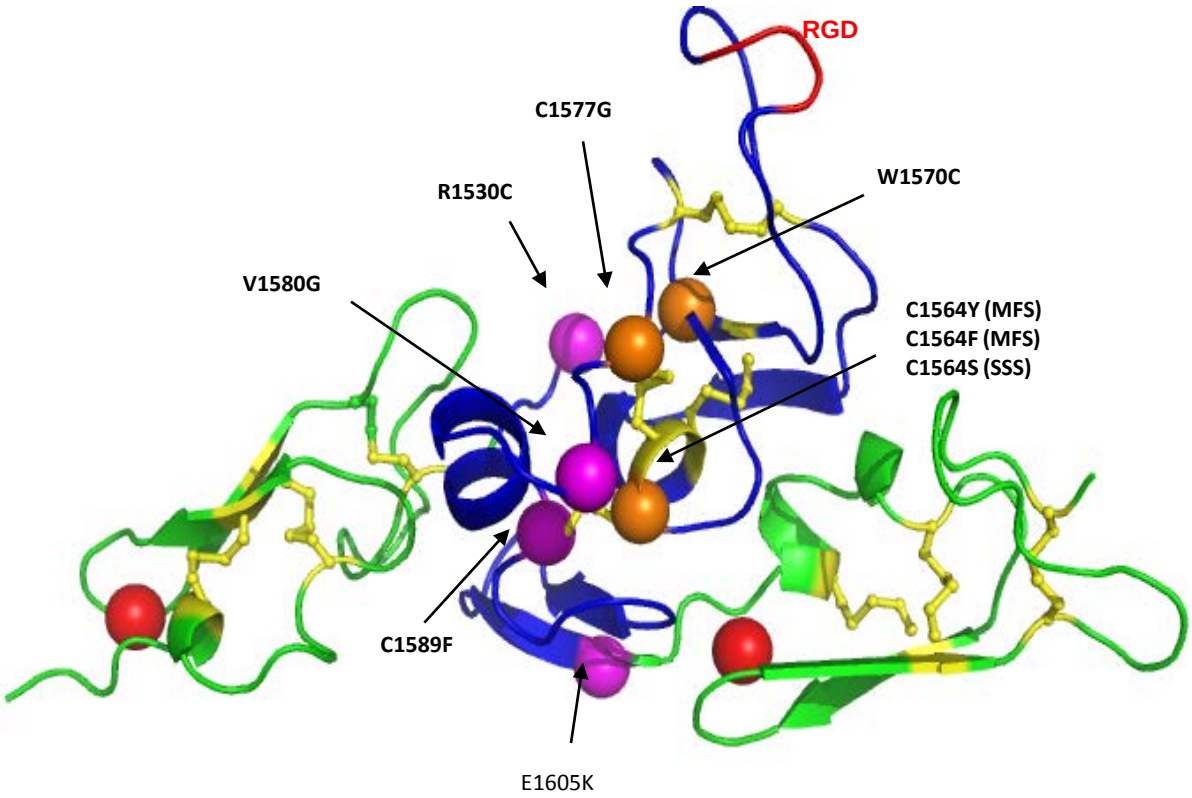

Figure 3.1 Crystal structure of cbEGF22-TB4-cbEGF23 (Lee *et al.,* 2004) showing the positions of disease-causing substitutions in TB4. Those associated with SSS are shown as orange spheres, whereas MFS-causing substitutions are shown as purple spheres. Both SSS substitutions W1570C and C1564S affect residues that are structurally important in the TB4 domain. W1570 is a highly conserved residue and plays an important structural role in stabilising the TB domain hydrophobic core and is important for the folding of the TB domain (Yuan *et al*., 1997; Lee *et al*., 2004). C1564 is the fifth cysteine residue and forms a buried 5-8 disulphide bond in the native TB4 domain. Figure was created using PyMOL software using the cbEGF22-TB4-cbEGF23 triple domain construct coordinates (Lee et al., 2004)

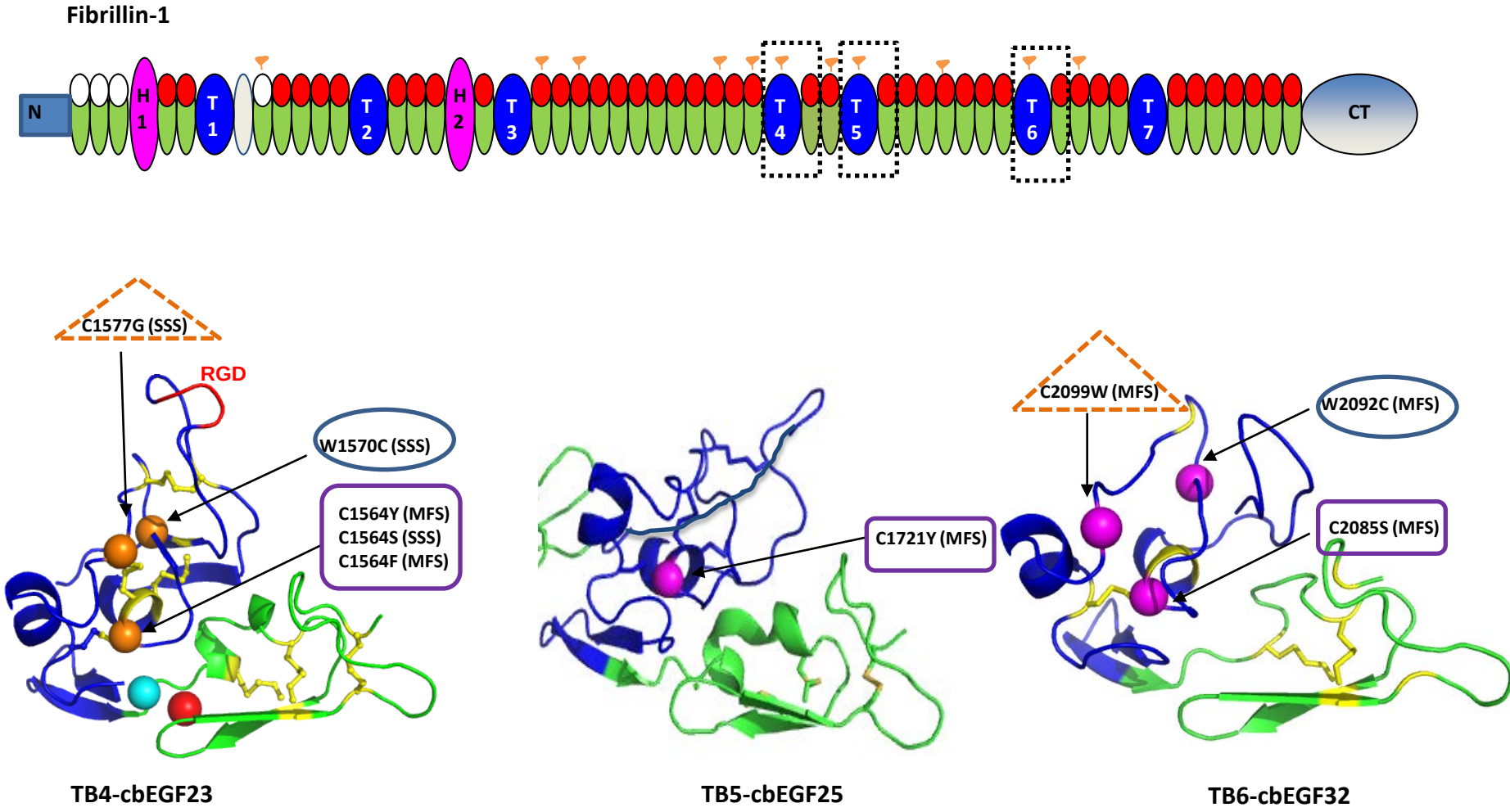

Figure 3.2. Diagram representing the domain structure of the fibrillin-1 protein showing analogous missense mutations in the 3D structures of TB4, TB5 and TB6 domains which result in different disease phenotypes. MFS-causing substitutions are shown as purple spheres and SSS-causing substitutions are shown as orange spheres. Substitutions occur at similar positions in these domains but result in different disease phenotypes. For example, substitution of the highly conserved tryptophan residue in TB4 domain (W1570C) results in SSS whereas in TB6 (W2092C) domain its substitution gives a classic MFS phenotype (residues in blue oval). Same in the case of the fifth cysteine residue (C1564S-TB4, C1721Y-TB6) of the TB domain (residues in purple square). The substitution (C1564S) at the 7th cysteine residue in TB4 domain, in TB6 domain the substitution C2099W is associated with MFS (dotted triangle). Figure was created using PyMOL software using the cbEGF22-TB4-cbEGF23 triple domain construct coordinates (Lee *et al*., 2004) and TB5-cbEGF25 structure is modelled on TB4-cbEGF23 crystal structure.

A.

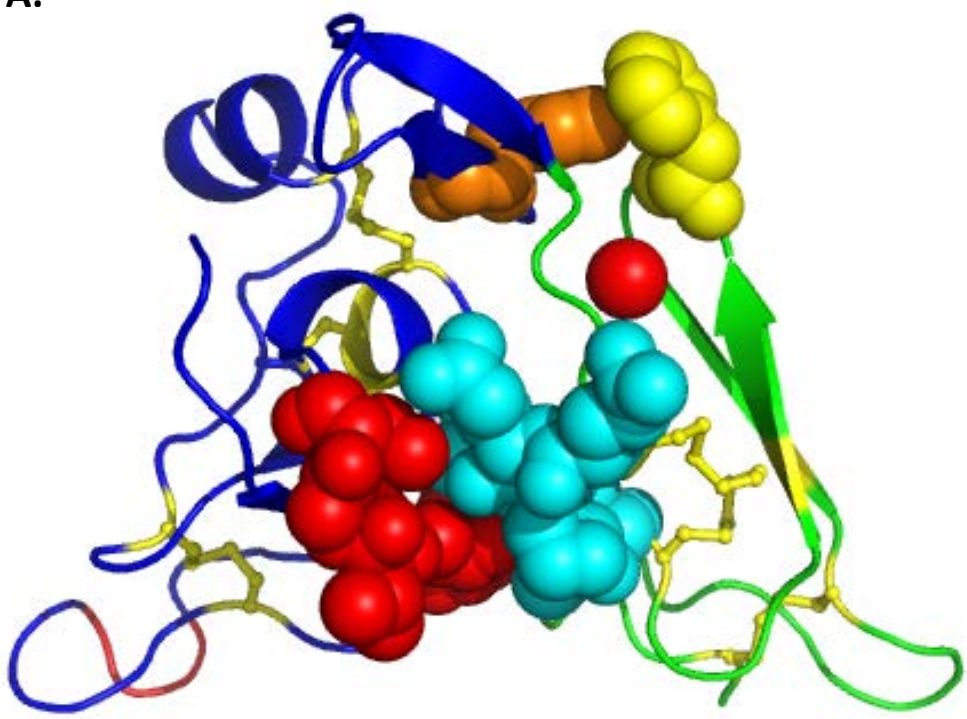

B.

TB4

DTRSGNCYLDIRPRGDNGDTACSNEIGVGVSKASCCCSLGKAWGTPCEMCPAVNTSEYKILCPGGEG
FRPNPITVILE

cbEGF23

DIDECQELPGLCQGGKCINTFGSFQCRCPTGYYLNEDTRVCD

Figure 3.3 (A) Hydrophobic interdomain interactions of TB4 and cbEGF23. The TB4 domain backbone is shown in blue, and that of the cbEGF23 domain in green. The colour coding of the space-filled sections of the structure is as in the sequence shown in (B). A bound calcium atom is displayed as a red sphere. It is postulated that the interdomain packing between two Phe residues (Phe1595 and Phe1626) orange and yellow respectively and the two hydrophobic stretches at the interdomain interface stabilises the calcium binding region and results in the observed high calcium affinity. Figure was created using PyMOL software using the cbEGF22-TB4-cbEGF23 triple domain construct coordinates (Lee *et al*., 2004).

(B) Sequences involved in in TB4 and cbEGF23 packing revealed by the crystal structure. Sequences highlighted in red and blue (shown in blue) were observed to pack closely together in the crystal structure. The two Phe residues in orange (Phe1595, TB4) and yellow (Phe1626, cbEGF23) were also observed to pack between the domains.

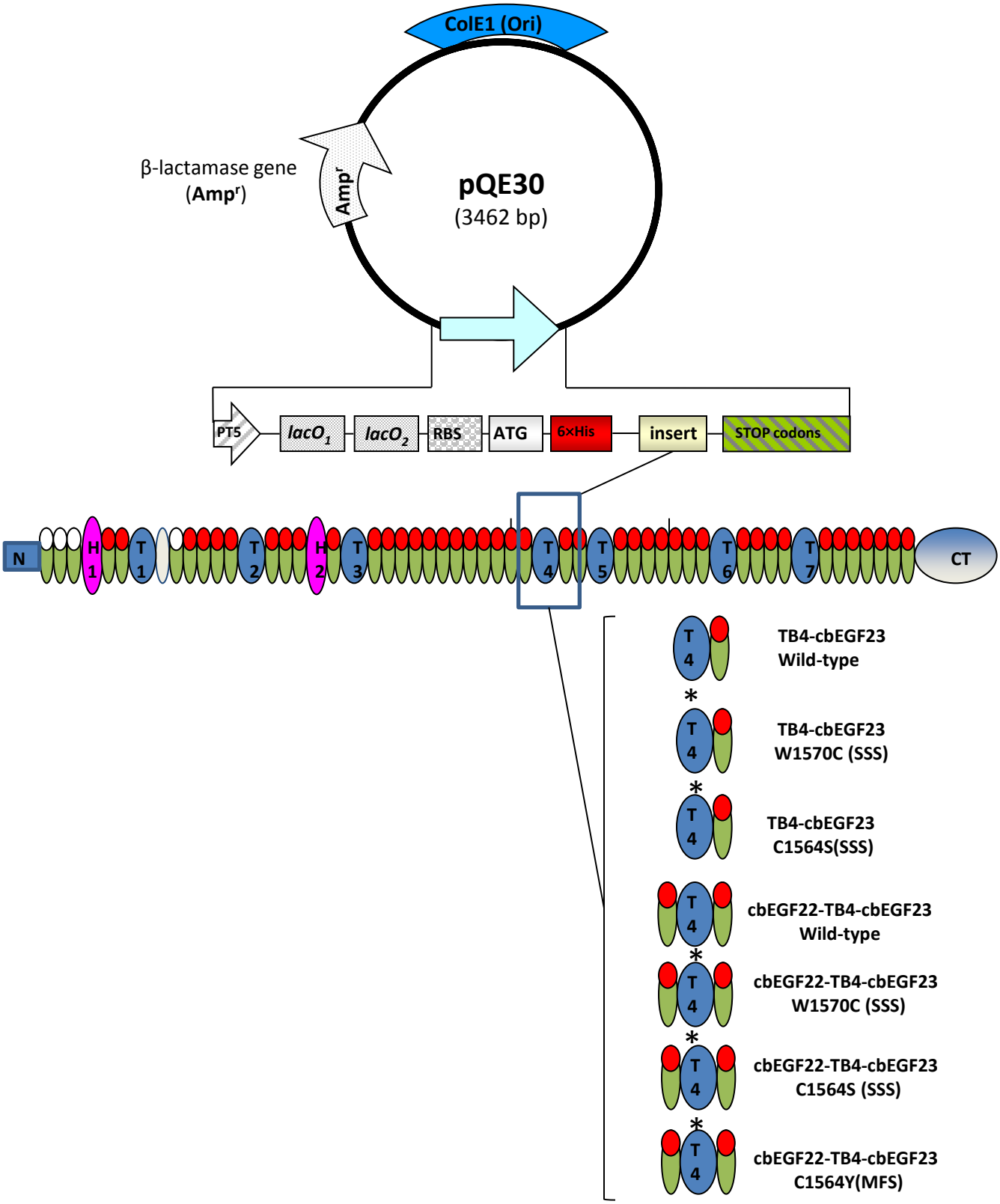

Figure 3.4 Schematic representation of fibrillin-1 constructs investigated in this study, including a diagram of pQE30 expression vector used for production of recombinant proteins. The pQE30 vector contains the ColE1 origin of replication, an ampicillin resistance gene (Amp^r), PT5 promoter, two *lac* operators (*lacO*$_1$ and *lacO*$_2$), a ribosome binding site (RBS), a sequence encoding a 6 x His tag and a multiple cloning site (MCS) into which DNA fragments encoding various fibrillin-1 domains have been inserted. Cartoons of fibrillin-1 proteins produced from this expression system are shown. Calcium ions are shown as red spheres. Black asterisk indicates substitutions introduced into the constructs.

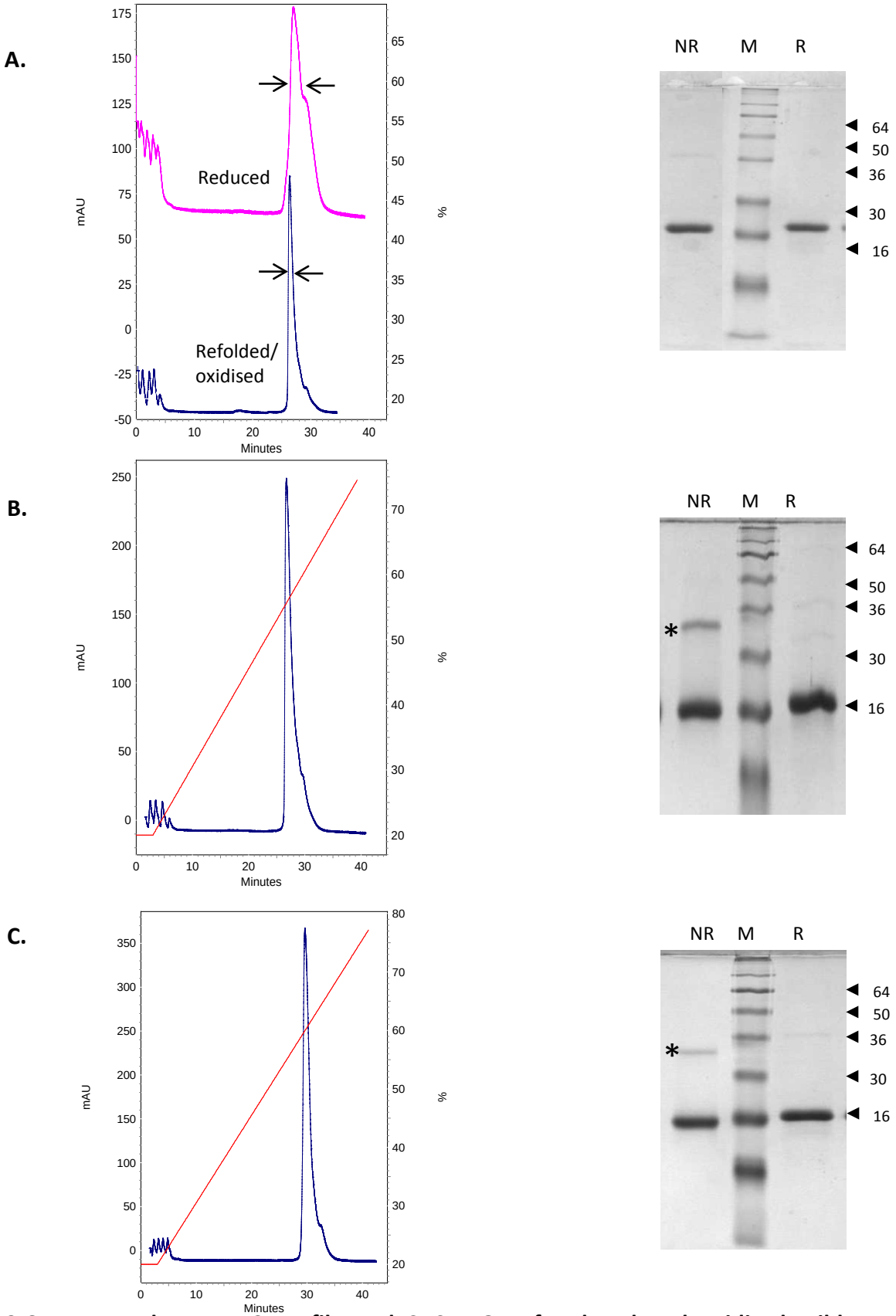

Figure 3.6 Reverse-phase HPLC profile and SDS-PAGE of reduced and oxidised wild-type (A), oxidised W1570C (B) and oxidised C1564S (C) TB4-cbEGF23 constructs. One sharp peak corresponding to oxidised protein was obtained in each case. SDS-PAGE analyses of refolded protein samples after the final HPLC purification step are next to each trace. Samples were denatured by boiling with reducing (R) or non-reducing (NR) loading buffer, then resolved on a 16% SDS PAGE and stained with Coomassie Blue. Molecular weights (kDa) of pre-stained markers(M) are indicated. The SDS PAGE of the refolded mutant proteins show a small amount of higher molecular weight material, which is possibly a dimer shown by an asterisk. This might form because of a free thiol in both the mutant constructs. One representative HPLC trace of reduced protein is show for wild-type. A similar difference between reduced and refolded HPLC profiles were observed for the mutant constructs (data not shown).

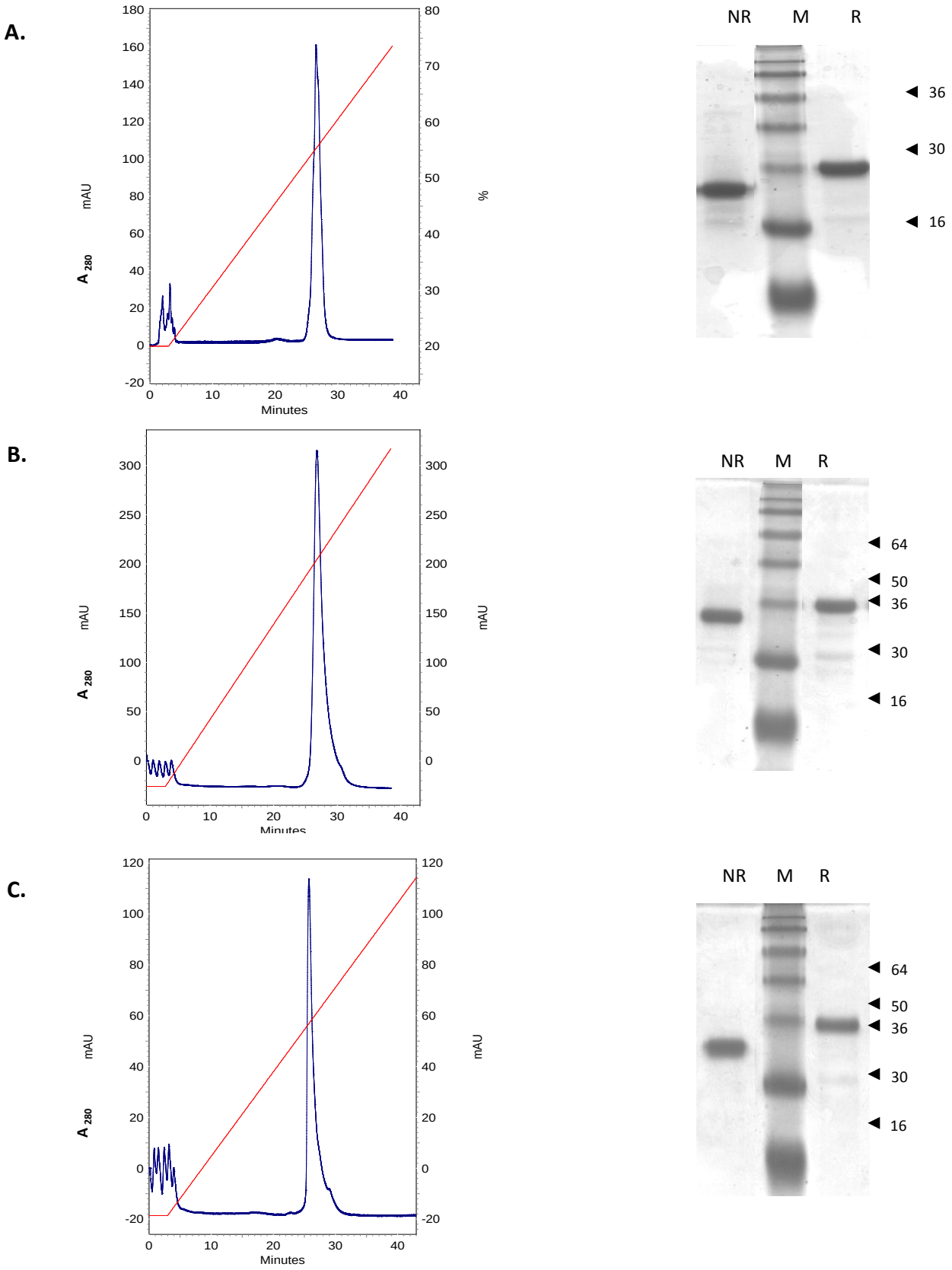

Figure 3. Reverse-phase HPLC profile and SDS-PAGE of refolded of cbEGF22-TB4-cbEGF23 wild-type (A), cbEGF22-TB4-cbEGF23 C1564S(B), cbEG22-TB4-cbEGF23 W1570C (C) constructs. One sharp chromatographic peak was obtained in each case. SDS-PAGE analyses of refolded protein samples after the final HPLC purification step are next to each trace. Samples were denatured by boiling with reducing (R) or non-reducing (NR) loading buffer, then resolved on a 16% polyacrylamide gel and stained with Coomassie Blue. Molecular weights (kDa) of pre-stained markers are indicated. Mutant protein samples show a small amount of higher molecular weight material, which is most likely dimer, shown by an asterisk, which might be forming because of a free thiol in both the mutant constructs. Under reducing conditions, a small amount of lower molecular weight material was observed indicated by a red arrow. This was also observed in wild-type.

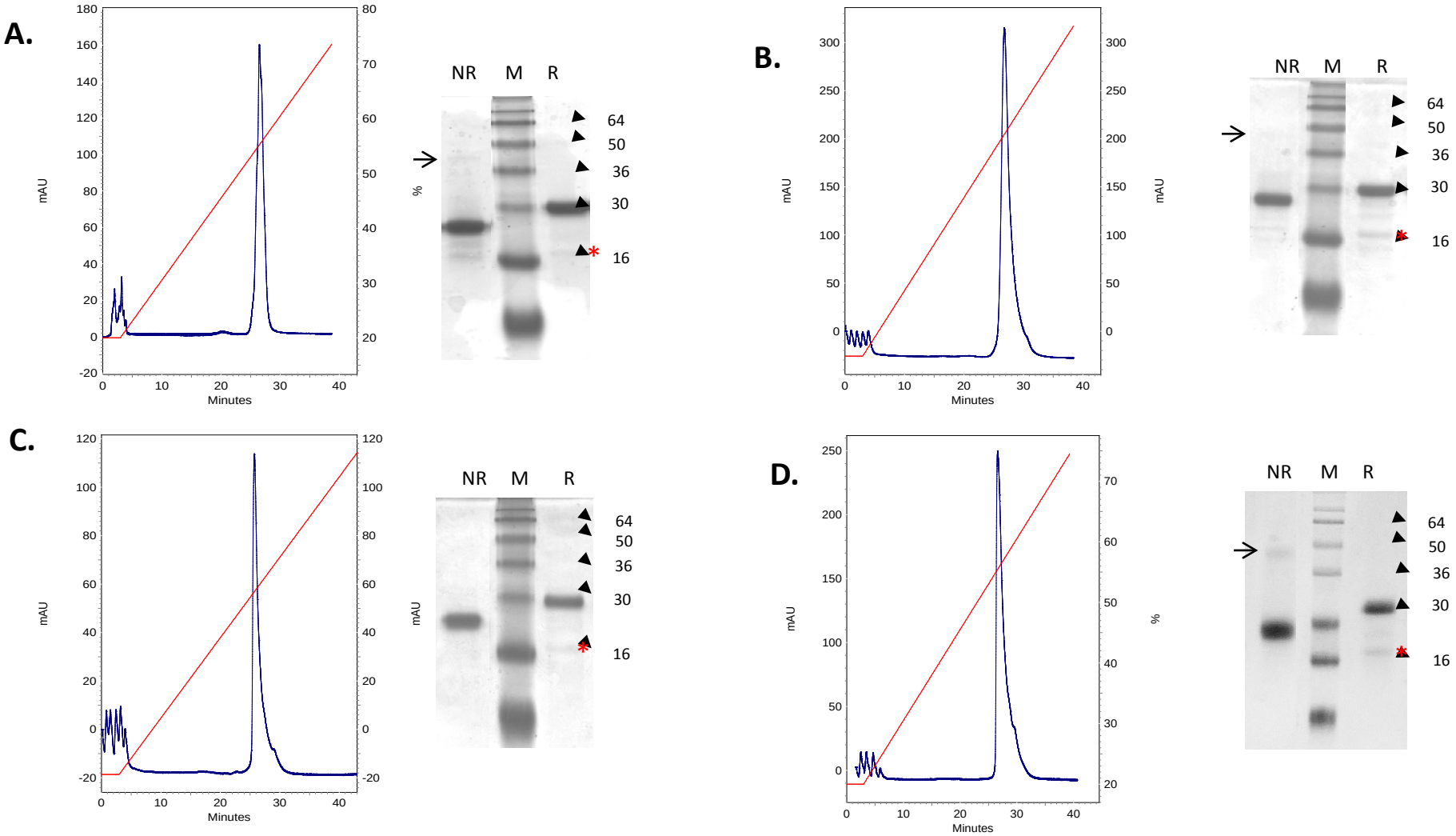

Figure 3.7 Reverse-phase HPLC profile and SDS-PAGE analysis of refolded wild-type (A), W1570C (SSS) (B) C1564S (SSS) (C) C1564Y (MFS) (D) cbEGF22-TB4-cbEGF23 constructs. One sharp chromatographic peak was obtained in each case. SDS-PAGE analyses of refolded protein samples after the final HPLC purification step are next to each trace. Samples were denatured by boiling with reducing (R) or non-reducing (NR) loading buffer, then resolved on a 16% polyacrylamide gel and stained with Coomassie Blue. Molecular weights (kDa) of pre-stained markers (M) are indicated. Mutant protein samples under NR conditions show a small amount of higher molecular weight material, which is most likely dimer (arrow). Under reducing conditions, a small amount of lower molecular weight material was observed indicated by a red asterix. This was also observed in the wild-type sample and may indicate an impurity or a small amount of degradation (<5%).

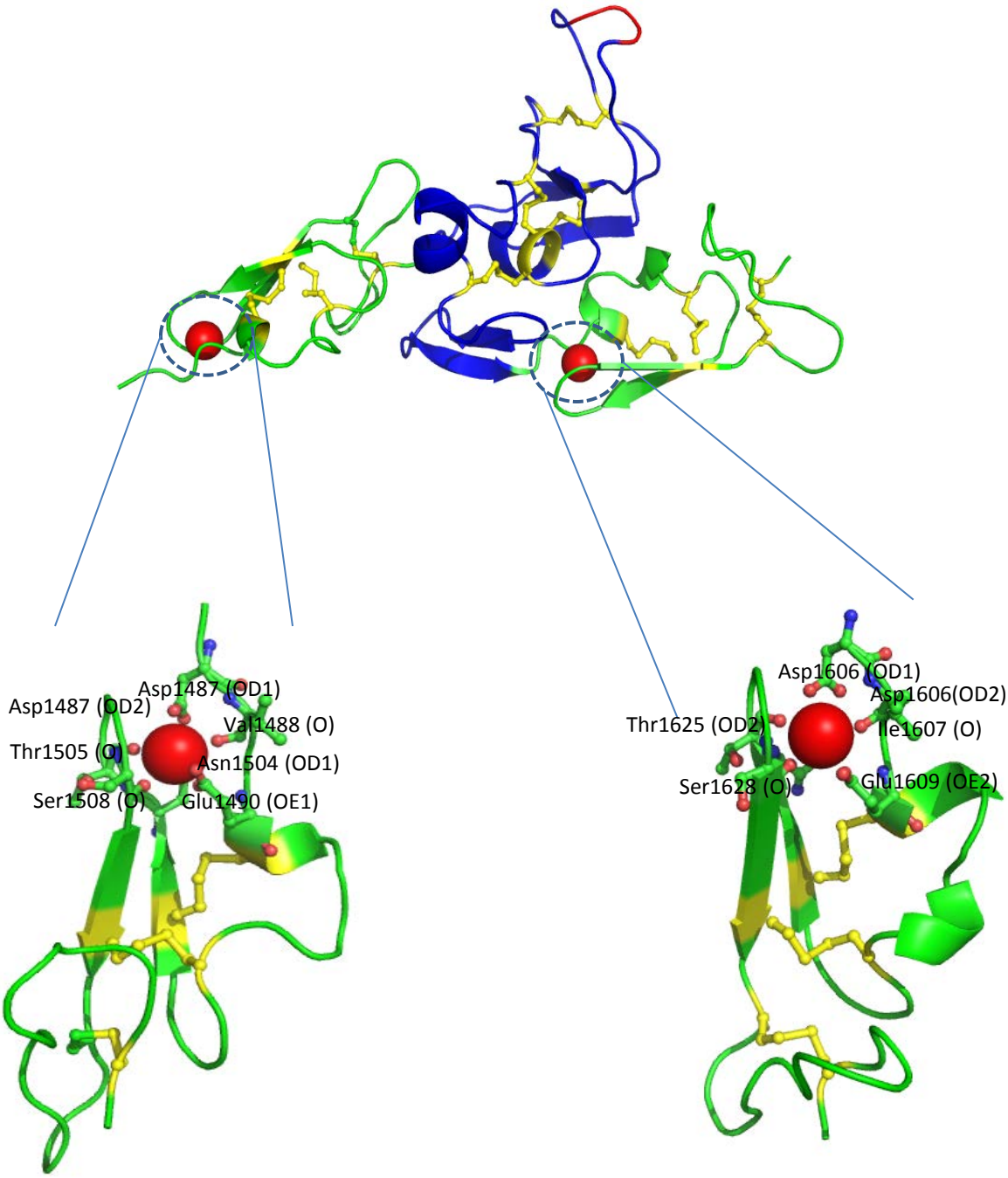

Figure 3.8 Ca^{2+} -binding ligands in cbEGF22 and cbEGF23 as determined by the crystal structure of cbEGF22-TB4-cbEGF23. Ca^{2+}-binding consensus residues forming the pentagonal bipyramidal Ca^{2+}-coordination sphere are shown in a ball-and-stick drawing. β strands are depicted as green arrows, and Ca^{2+}-binding oxygen atoms together with the Ca^{2+} ion are shown as red spheres. Dotted lines represent coordinating bonds between seven intradomain oxygen atoms and the Ca^{2+} ion. The conserved serine is indicated by an arrow. OD and OE indicate oxygen atoms in aspartate and glutamate side chains, respectively, while O indicates carbonyl oxygen (Taken from Lee *et al*., 2004).

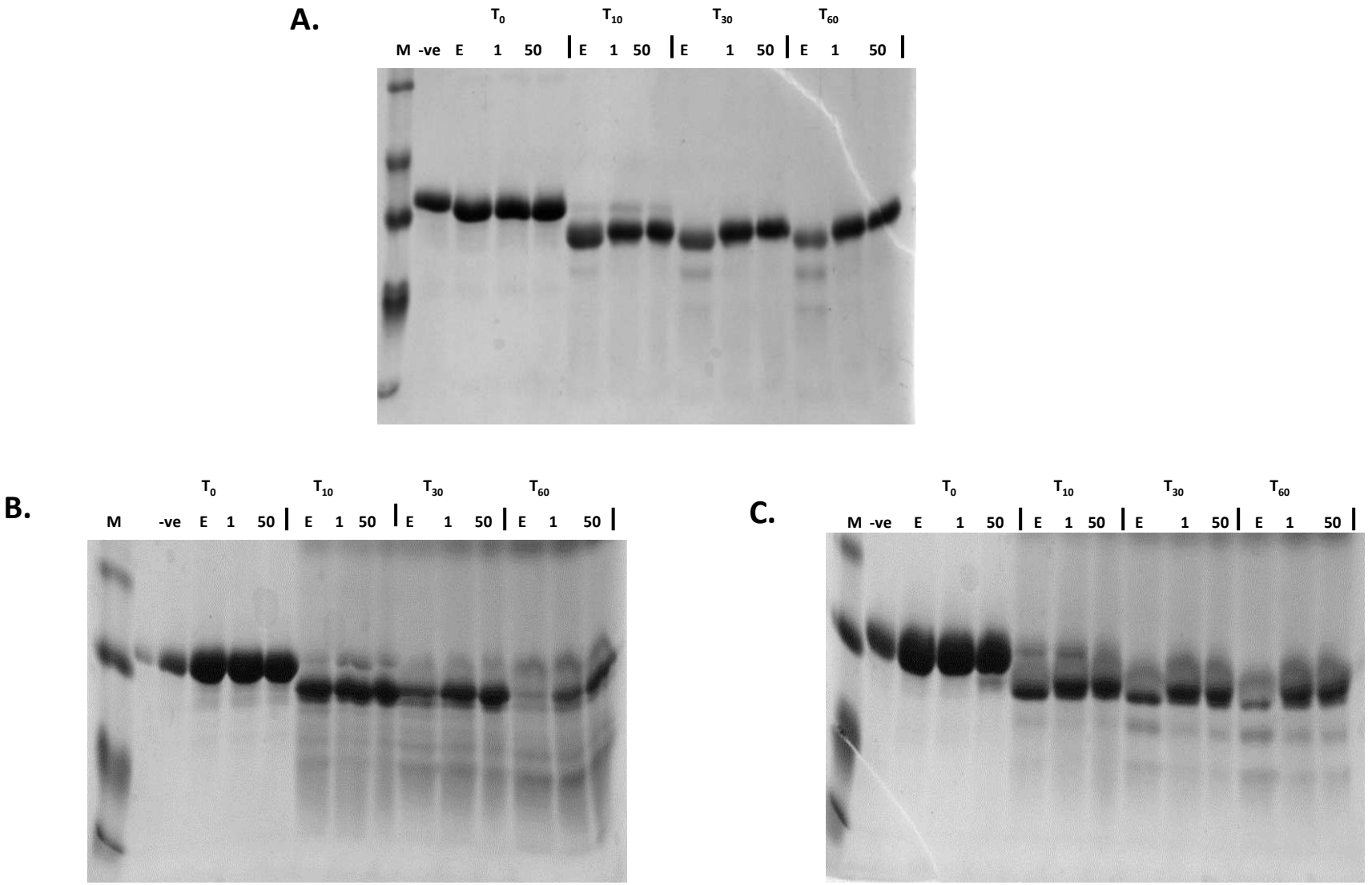

Figure 3.10 Reducing 16% SDS-PAGE of tryptic digests of TB4-cbEGF23 fragments performed in the presence and absence of Ca^{2+} at pH 7.5. Digestion of **(A)** wild type, **(B)** C1564S mutant and (C) W1570C mutant. Digestion occurred over 60 min with samples being removed at T_0 , T_{10},T_{30} and T_{60}. The negative control incubated for 60 min with no enzyme present to act as control. E= 10 mM EDTA, 1= 1 mM Ca^{2+} and 50 = 50 mM Ca^{2+}. Wild-type construct shows evidence of Ca^{2+} protection. Both mutants show evidence of Ca^{2+} protection.

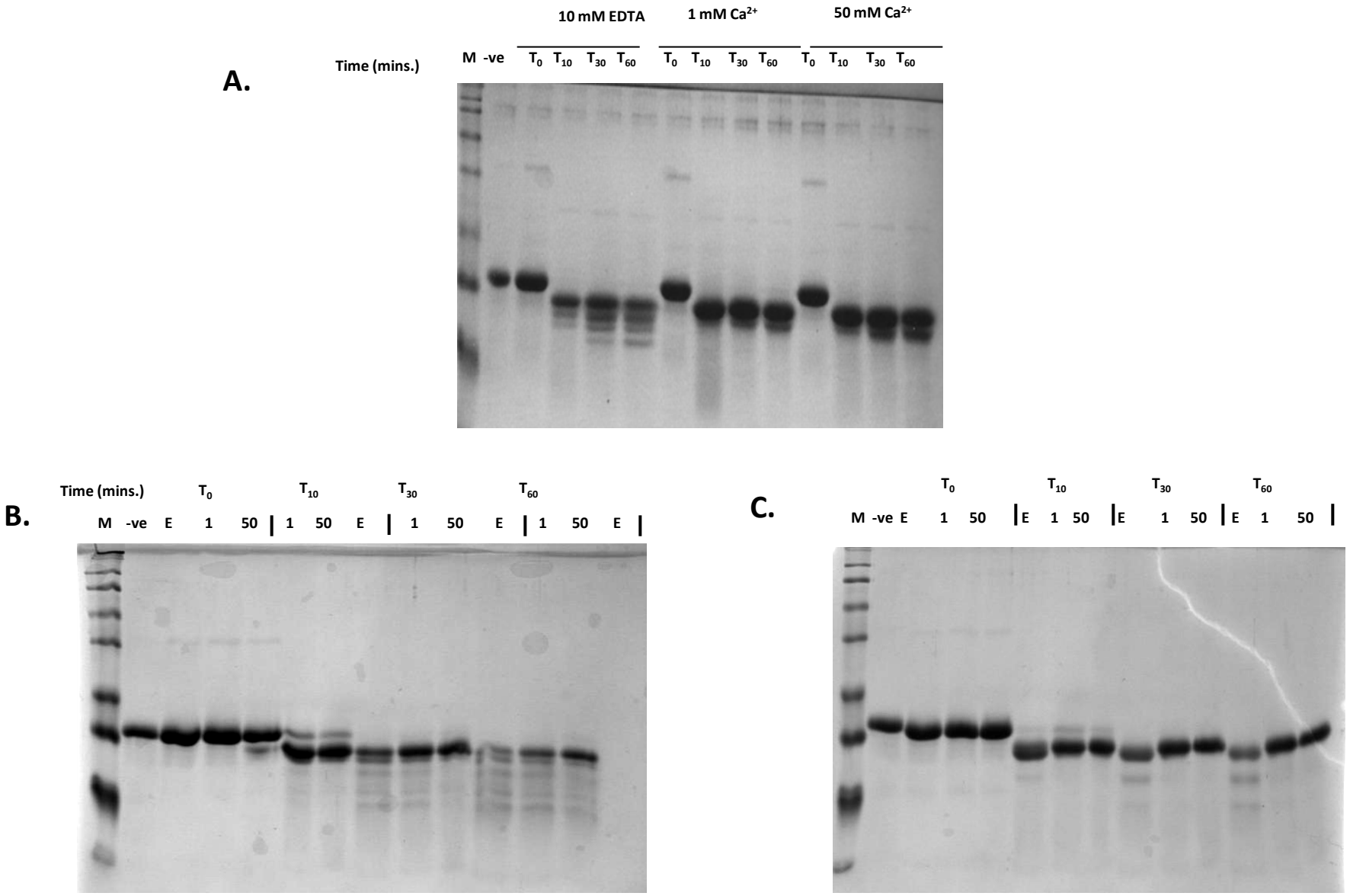

Figure 3.14 Reducing 16% SDS PAGE of tryptic digests of TB4-cbEGF23 fragments performed in the presence and absence of Ca^{2+} at pH 7.5. Digestion of (A) wild type, (B) C1564S mutant and (C) W1570C mutant. Digestion occurred over 60 minutes with samples being removed at T_0 , T_{10},T_{30} and T_{60}. The '-ve' control incubated for 60 min with no enzyme present to act as control. E= 10 mM EDTA, 1= 1 mM Ca^{2+} and 50 = 50 mM Ca^{2+}

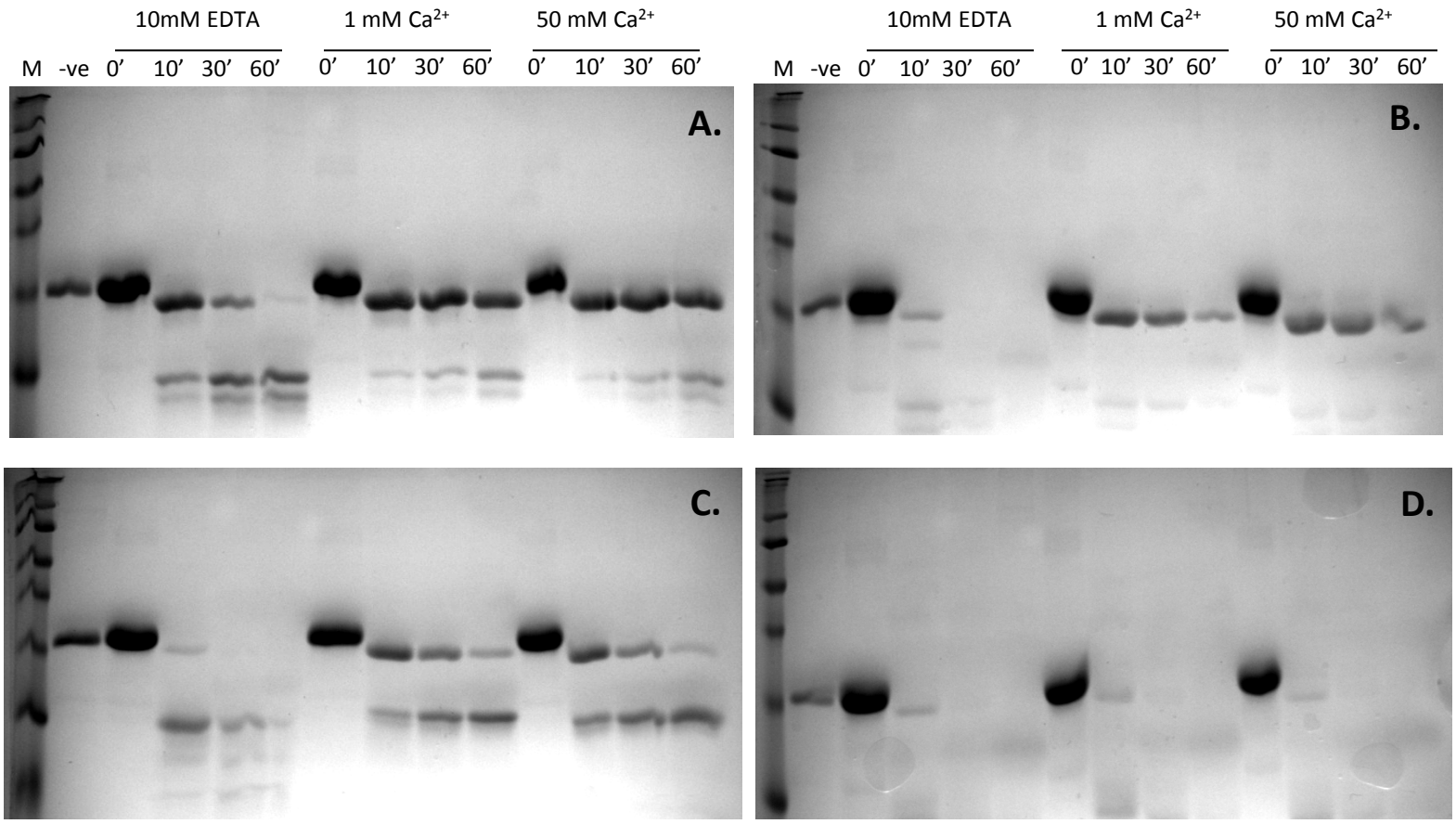

Figure 3.9 Reducing 16% SDS PAGE of tryptic digests of cbEGF22-TB4-cbEGF23 fragments performed in the presence and absence of Ca^{2+} at pH 7.5. Digestion of **(A**) wild type, **(B)** W1570C mutant and **(C)** C1564S mutant and **(D)** C1564Y mutant fragments. Digestion occurred over 60 min with samples being removed at T_0,T_{10},T_{30} and T_{60}. The '-ve' control incubated for 60 min with no enzyme present to assess degradation. E= 10 mM EDTA, 1= 1 mM Ca^{2+} and 50 = 50 mM Ca^{2+}. A, B,C show evidence of Ca^{2+} protection as there is less digestion in Ca^{2+} than without. D shows no evidence of Ca^{2+} protection and irrespective of Ca^{2+} is rapidly degraded suggesting more pronounced effect of mutation on domain fold. In B, C, the EDTA digests appear to degrade more rapidly that wild-type that wild-type, suggesting a Ca^{2+} independent effect on structure. This is consistent with known role of residues in stabilising TB4 fold.

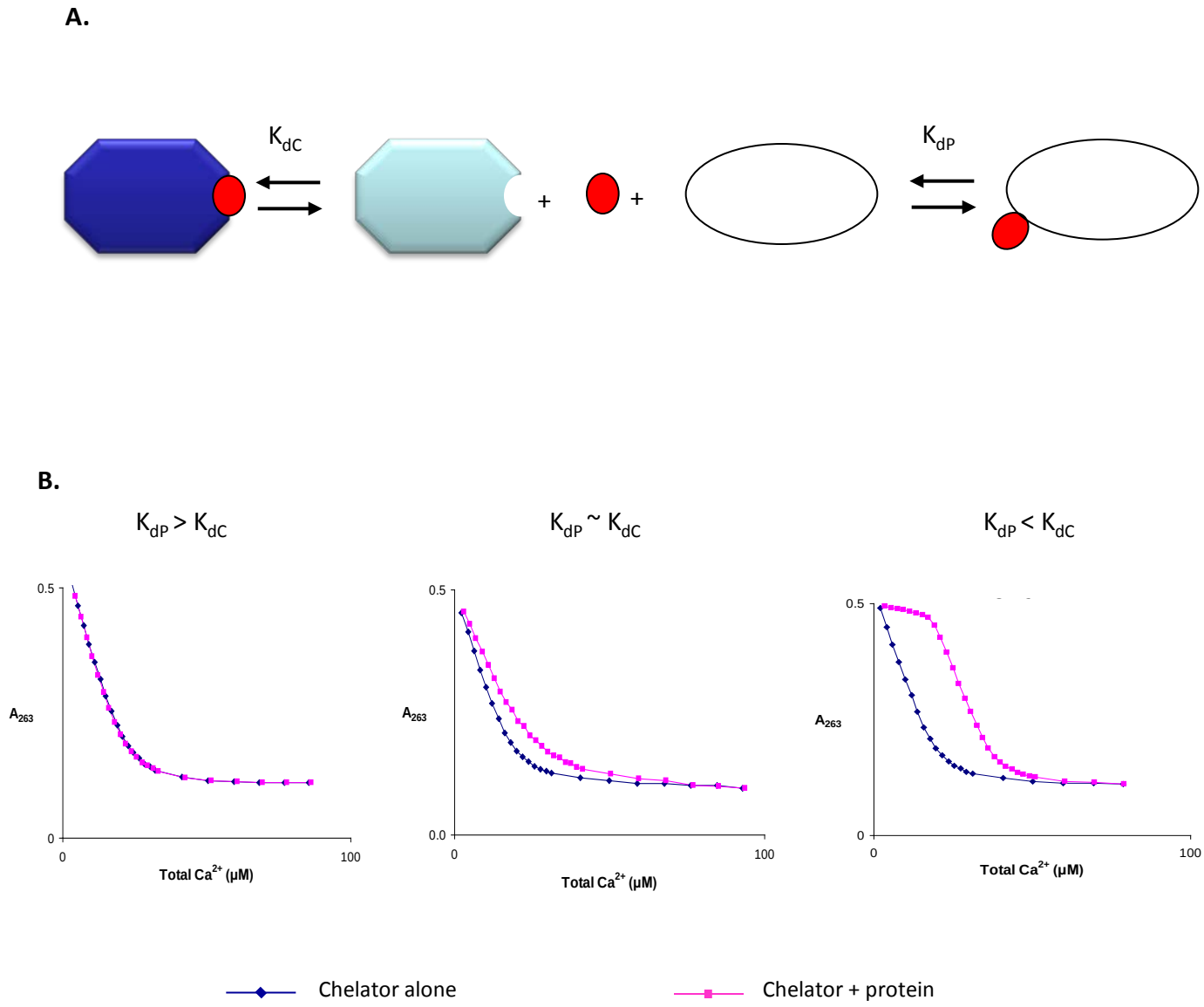

Figure 3.11 Illustration of chromophoric chelation to measure calcium-dissociation constants. (A) During calcium titrations the chromophoric calcium chelator (blue fill) changes absorbance on the binding of calcium (represented by different shades). In the presence of a calcium-binding protein (white oval) competition for the ion (red circle) occurs between the chelator and the protein. The strength of competition depends on the relative values of the calcium-dissociation constants of the chelator (K_{dC}) and the protein (K_{dP}). (B) Chelation curves typical of those obtained when calcium titrations are performed in the presence of calcium-binding proteins with lower ($K_{dP}>K_{dC}$), equivalent ($K_{dP}\sim K_{dC}$), and higher ($K_{dP}<K_{dC}$) affinity for calcium than the chelator are shown.

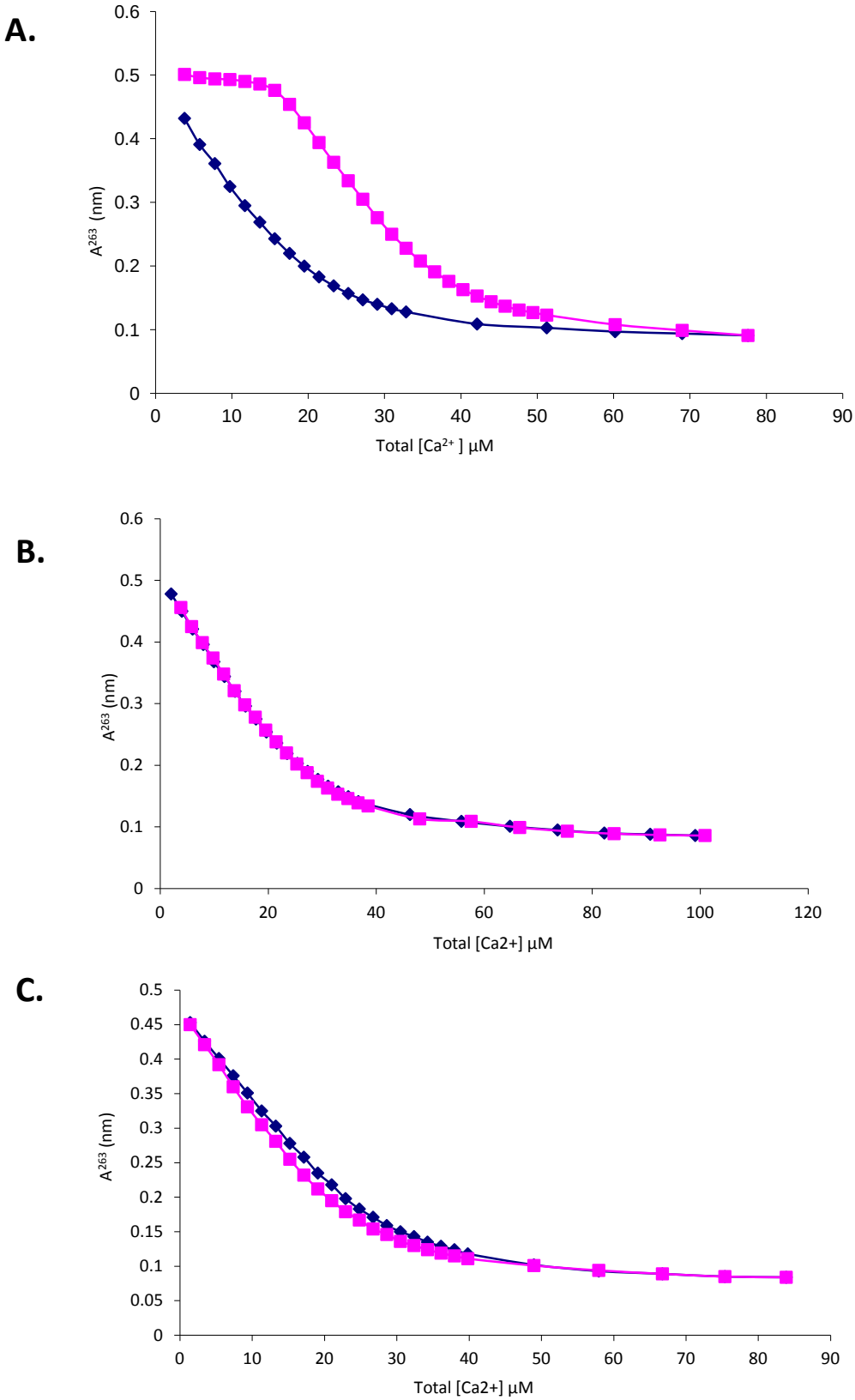

Figure 3.12 Br_2BAPTA competition chelation curves for the cbEGF22-TB4-cbEGF23 wild-type and mutants. Calcium chelation titration was carried out at pH 7.5 and constant ionic strength (I=0.15). The blue line represents the change in absorbance at 263 (A^{263}) of Br_2BAPTA upon incremental Ca^{2+} additions. The pink line represents the change in A^{263} of a mixture of Br_2BAPTA and **(A)** cbEGF22-TB4-cbEGF23 wild-type **(B)** cbEGF22-TB4-cbEGF23 W1570C mutant **(C)** cbEGF22-TB4-cbEGF23 C1564S mutant upon incremental Ca^{2+} additions. The curves for the mutant constructs show that there is no competition between the chelator and protein and therefore, there are no high affinity sites present in the mutant constructs.

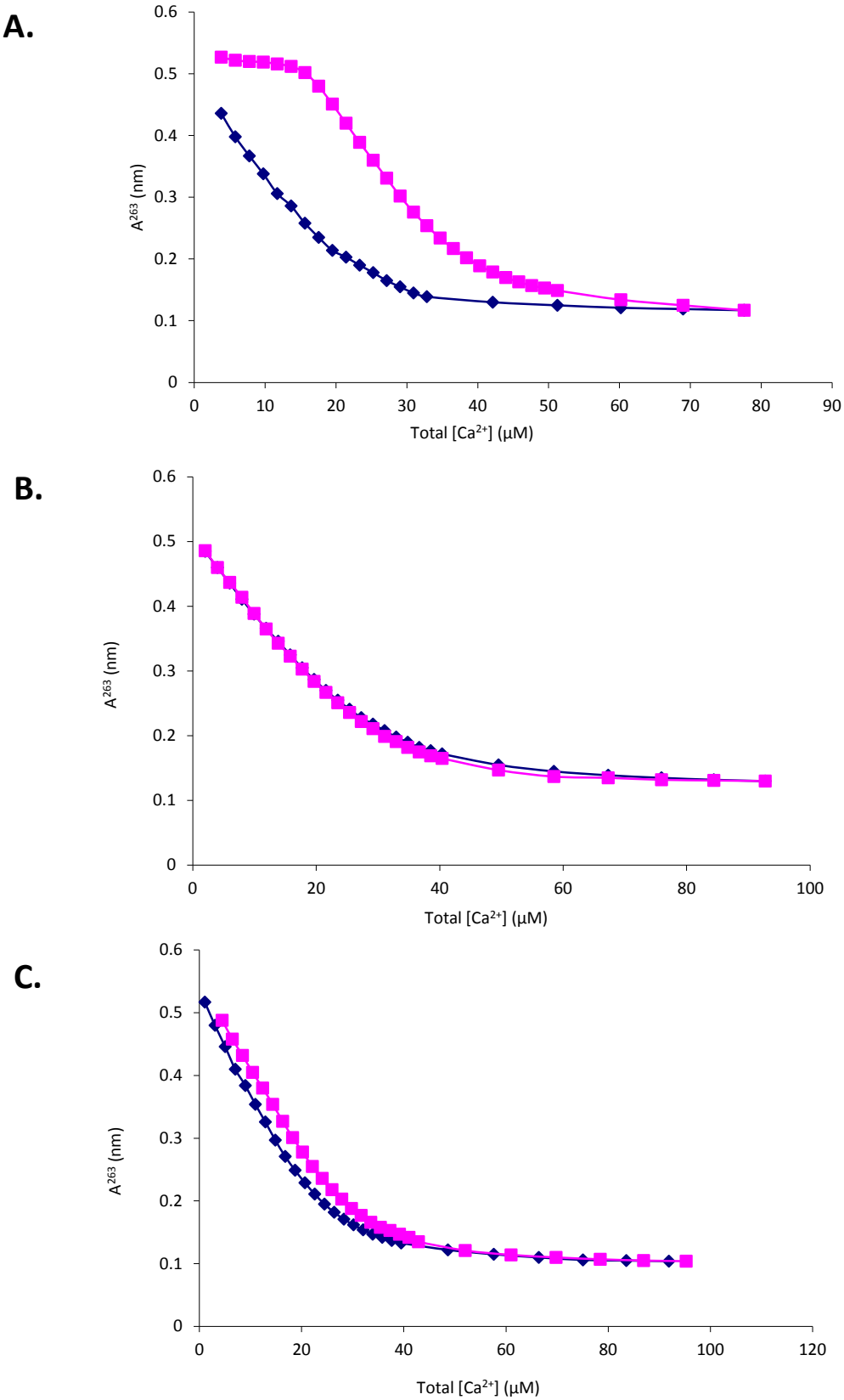

Figure 3.13 Br_2BAPTA competition chelation curves for the TB4-cbEGF23 wild-type and mutants. Calcium chelation titration was carried out at pH 7.5 and constant ionic strength (*I*=0.15).The blue line represents the change in absorbance at 263 (A^{263}) of Br_2BAPTA upon incremental Ca^{2+} additions. The pink line represents the change in A^{263} of a mixture of Br_2BAPTA and **(A)** cbEGF22-TB4-cbEGF23 wild-type **(B)** TB4-cbEGF23 W1570C mutant **(C)** TB4-cbEGF23 C1564S mutant upon incremental Ca^{2+} additions. The curves for the mutant constructs show that there is no competition between the chelator and protein, indicating the absence of high affinity calcium binding.

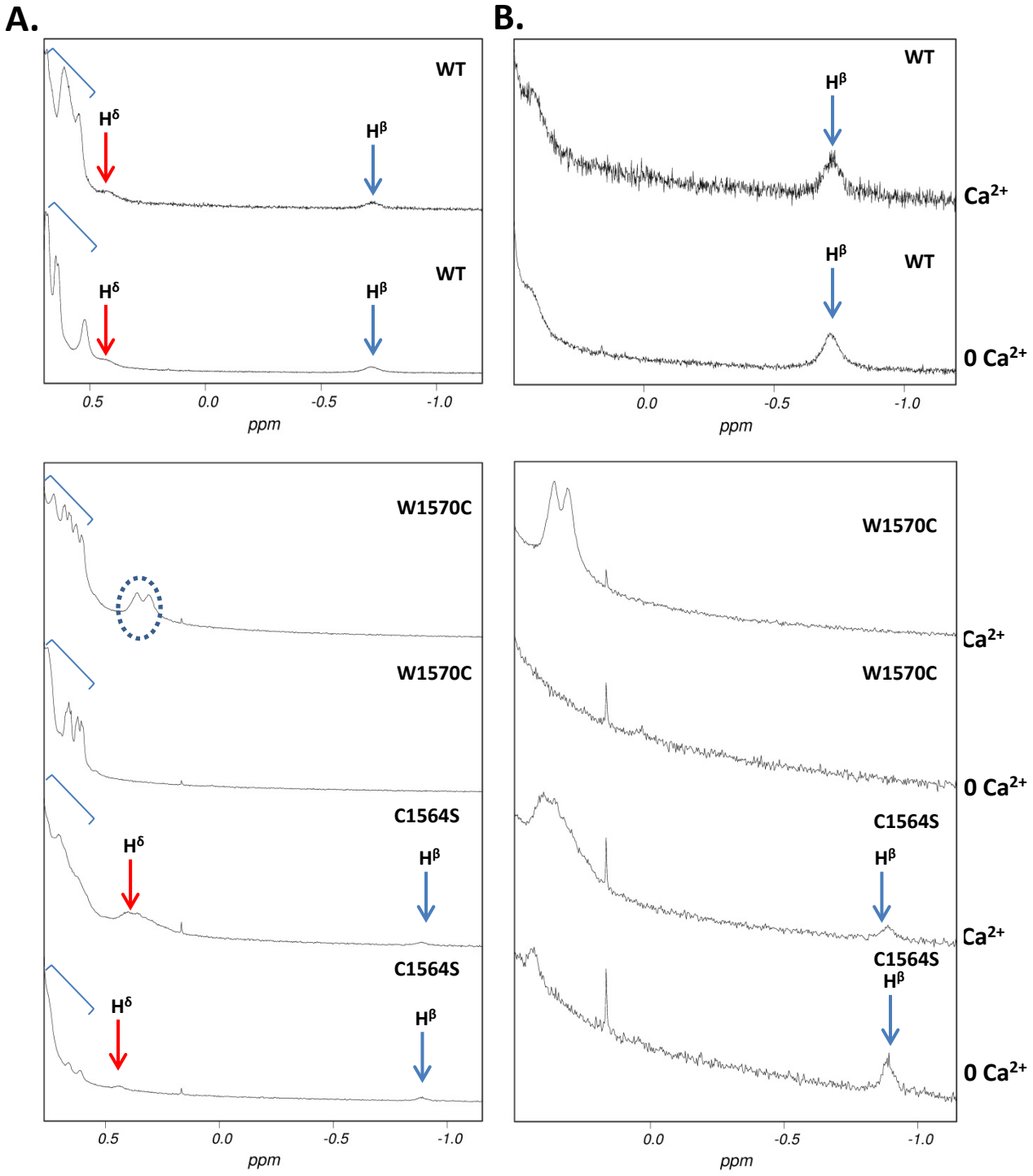

Figure 3.14 Upfield shift of aliphatic resonances in the 1D ^{1}H-NMR spectra of TB4-cbEGF23 WT, W1570C and C1564S fragments. Experiments were carried out in Tris-DCl pH 6.5, 150 mM NaCl. **A.** Resonances characteristic of upfield-shifted aliphatic groups (bracketed with blue lines), which are close to aromatic rings in the tertiary structure of the wild-type protein and are also seen for the mutants. **B.** The dramatically shifted proton resonances are indicated with a blue and red arrow, which are likely to arise from the H^{β} of conserved K1559 residue in TB4 which packs against the W1570 in TB4 domain. The absence of this peak in the W1570C spectrum is in agreement with this observation. The C1564S mutant shows similar peaks for the K1559 residue compared to the wild-type. The changes in these spectrum on addition of calcium also suggests that they may partly arise from cbEGF23 methyl and/or TB4-cbEGF23 interface. Encircled resonance in W1570C calcium spectrum suggests that it might be due to cbEGF23 methyl.

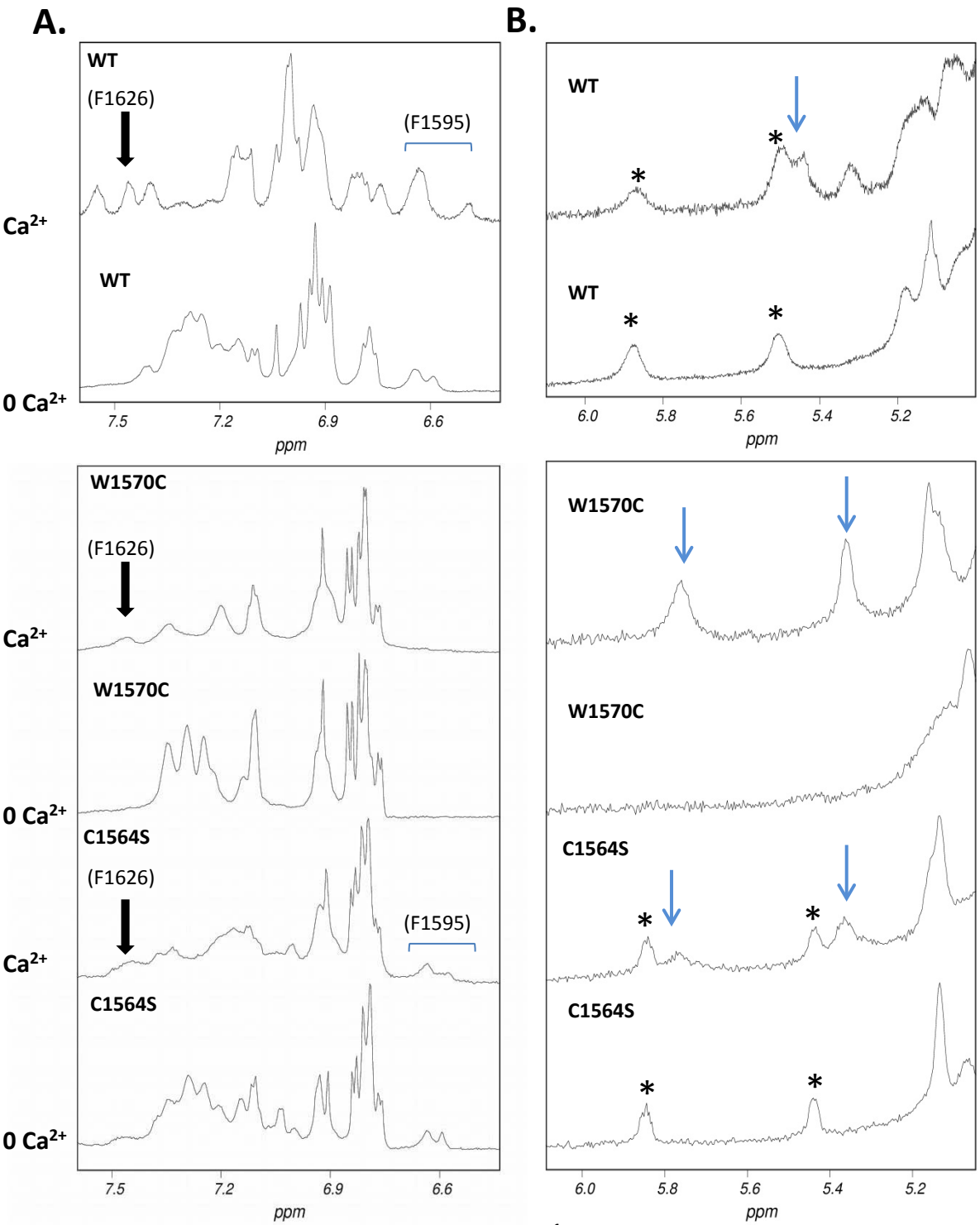

Figure 3. 15 Comparison of the aromatic region of the 1D ^{1}H-NMR spectra of TB4-cbEGF23 WT, W1570C and C1564S fragments in the presence and absence of calcium. A. On addition of Ca^{2+} to the wild-type, the downfield shifted F1626 resonances resulting from the formation of a Ca^{2+}-dependent interdomain interface can be seen at 7.5 ppm (black arrow), these resonances are also seen for the mutants in the presence of calcium. F1595 resonance around 6.6 ppm is seen in the wild-type indicating an interface formation. Similar resonances are seen in the same region for C1564S mutant but the shift is not as dramatic as that for the wild-type indicating a weak interface. There are no peaks seen in W1670C spectra for Phe1595 indicating no interface formation. **B.** There are calcium-dependent changes seen in the spectra of all the three constructs (indicated by blue arrows). Two downfield shifted markers of natively folded TB4, showing residues W1570 and C1534 in the β-sheet (indicated by asterisk) in wild-type and C1564S mutant spectra but not in W1570C spectra as expected.

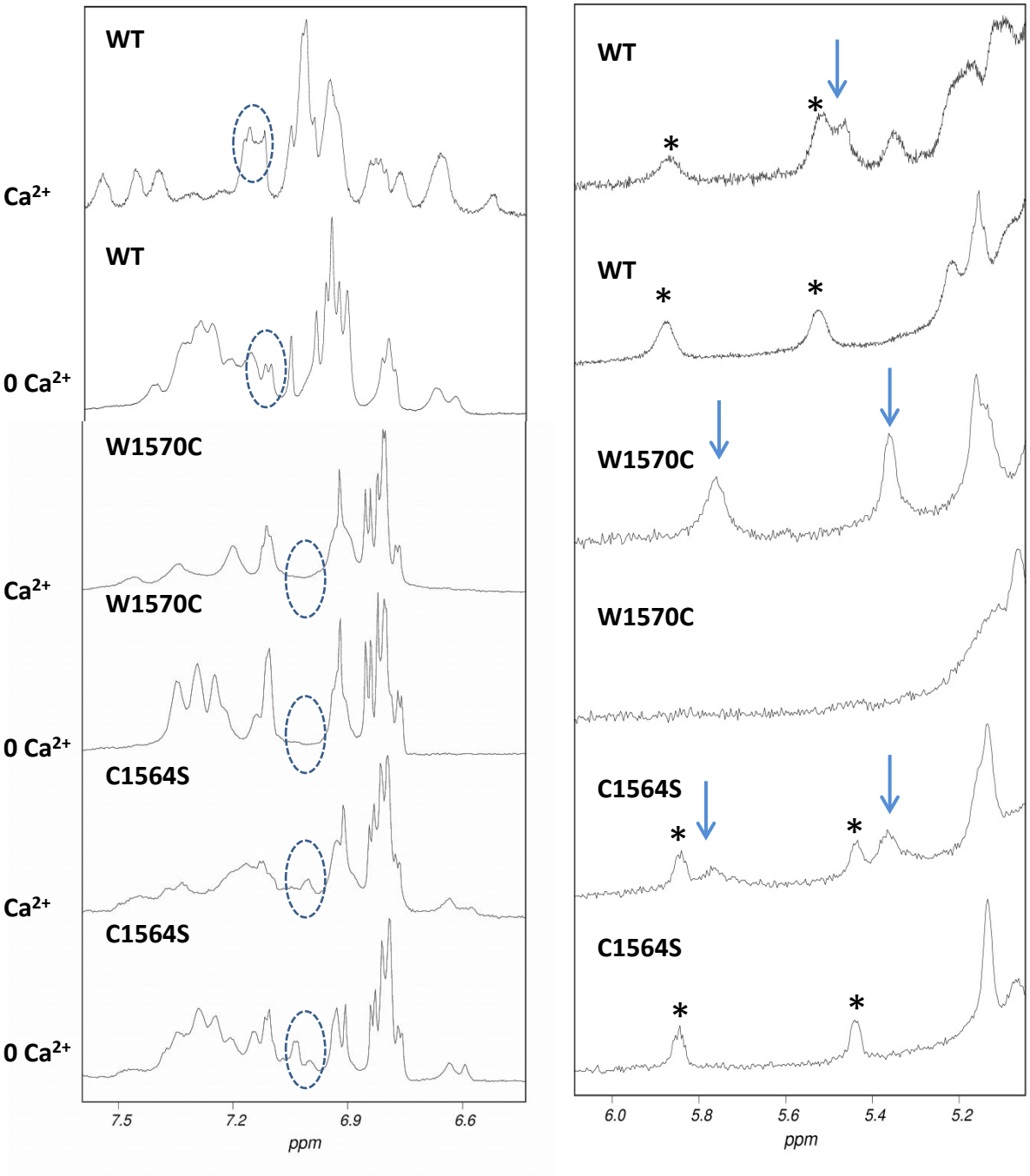
WT
Ca2+
WT
0 Ca2+
W1570C
Ca2+
W1570C
0 Ca2+
C1564S
Ca2+
C1564S
0 Ca2+
7.5
7.2
6.9
6.6
ppm
WT
WT
W1570C
W1570C
C1564S
C1564S
6.0
5.8
5.6
5.4
5.2
ppm

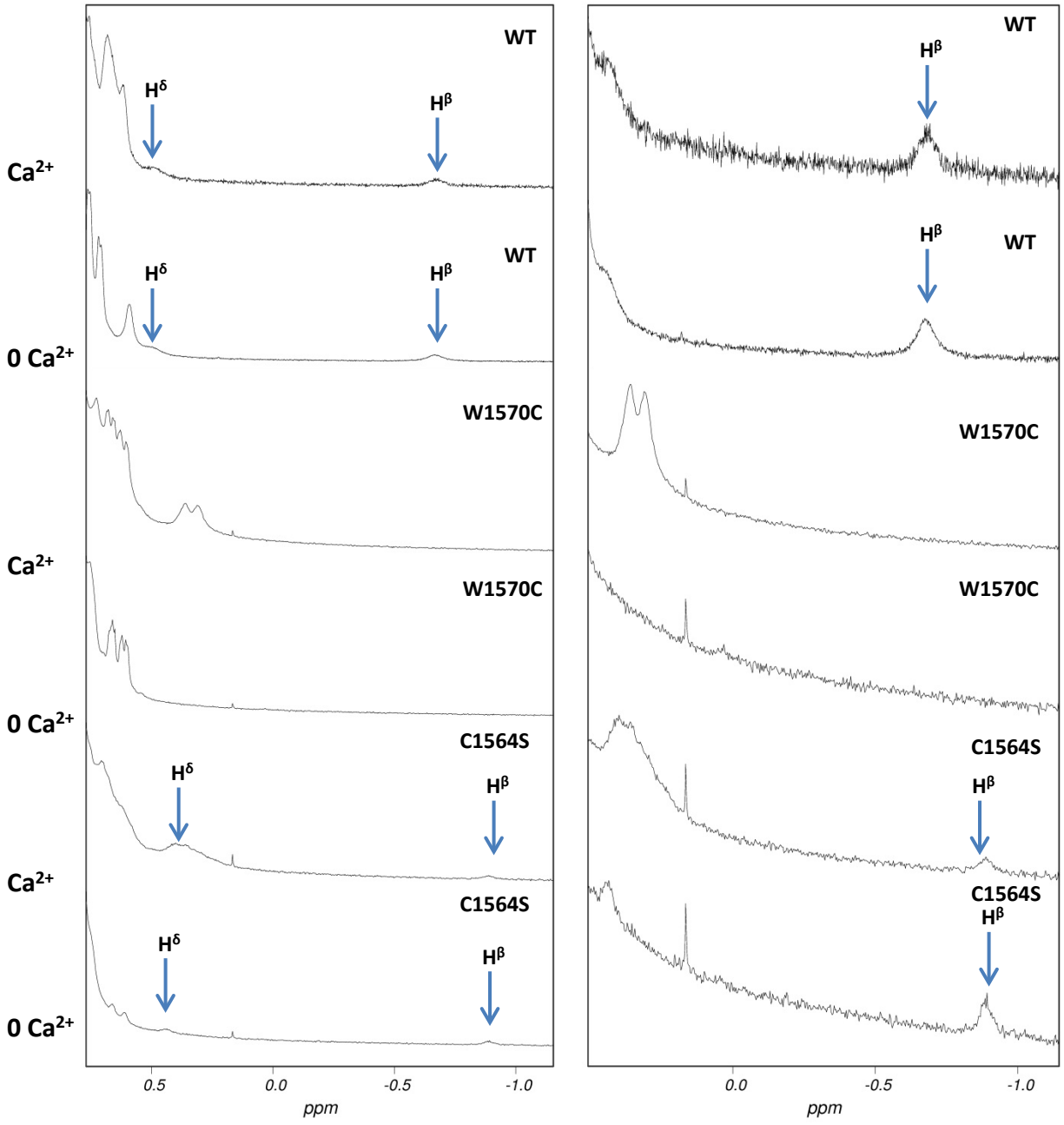

Figure 4. Upfield shift of aliphatic resonances in the 1D 1H-NMR spectra of TB4-cbEGF23 WT, W1570C and C1564S fragments. The dramtically shifted proton resonances are indicated with a blue arrow. This resonance is likely to arise from the H^{β} of conserved K1559 residue in TB4 which packs against the W1570 in TB4 domain. The absence of the peak in W1570C spectrum is in agreement with this. The C1564S mutant shows similar peaks for the K1559 residue compared to the wild-type. The other blue arrow indicates a shoulder assigned to H^{δ} of the same lysine.

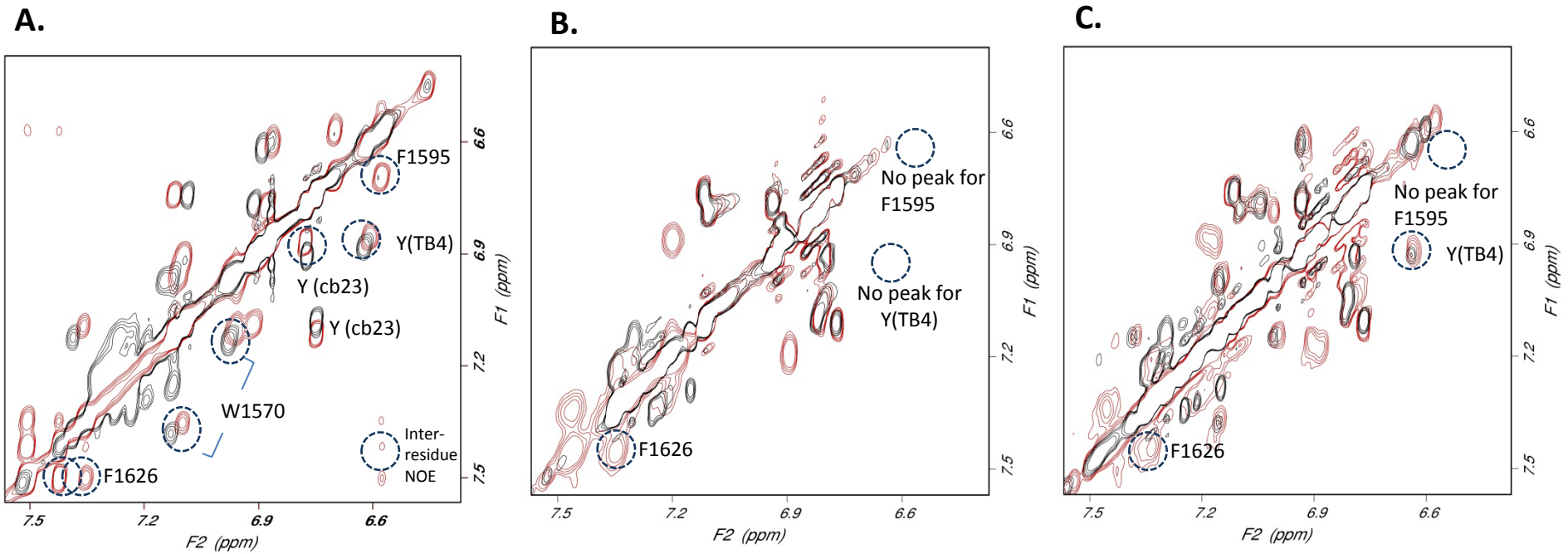

Figure 3.16 2D NOESY NMR spectrum of the aromatic region of wild-type (A), W1570C (B) and C1564S (C) TB4-cbEGF23 constructs in the presence of 5 mM calcium (red) or no calcium (black) at pH 6.5. There are Ca^{2+}-dependent shifts seen in the spectra of all the three constructs suggesting that cbEGF23 is binding Ca^{2+}. Peaks that have been assigned to W1570 residue in TB4 are missing in the W1570C mutant fragment, as expected. However, the presence of Ca^{2+} binding suggests the fold of cbEGF23 is intact although lack the packing interaction required to promote high affinity. The interface is absent in the case of mutants compared to the wild-type as the shift for the F1626 residue in cbEGF23 in the spectra is not as large as that for the wild-type, and there is no peak seen for the TB4 residue F1595, which packs with F1626. The shift for F1626 residue might just be because of calcium binding to cbEGF23 and not due to interface formation.

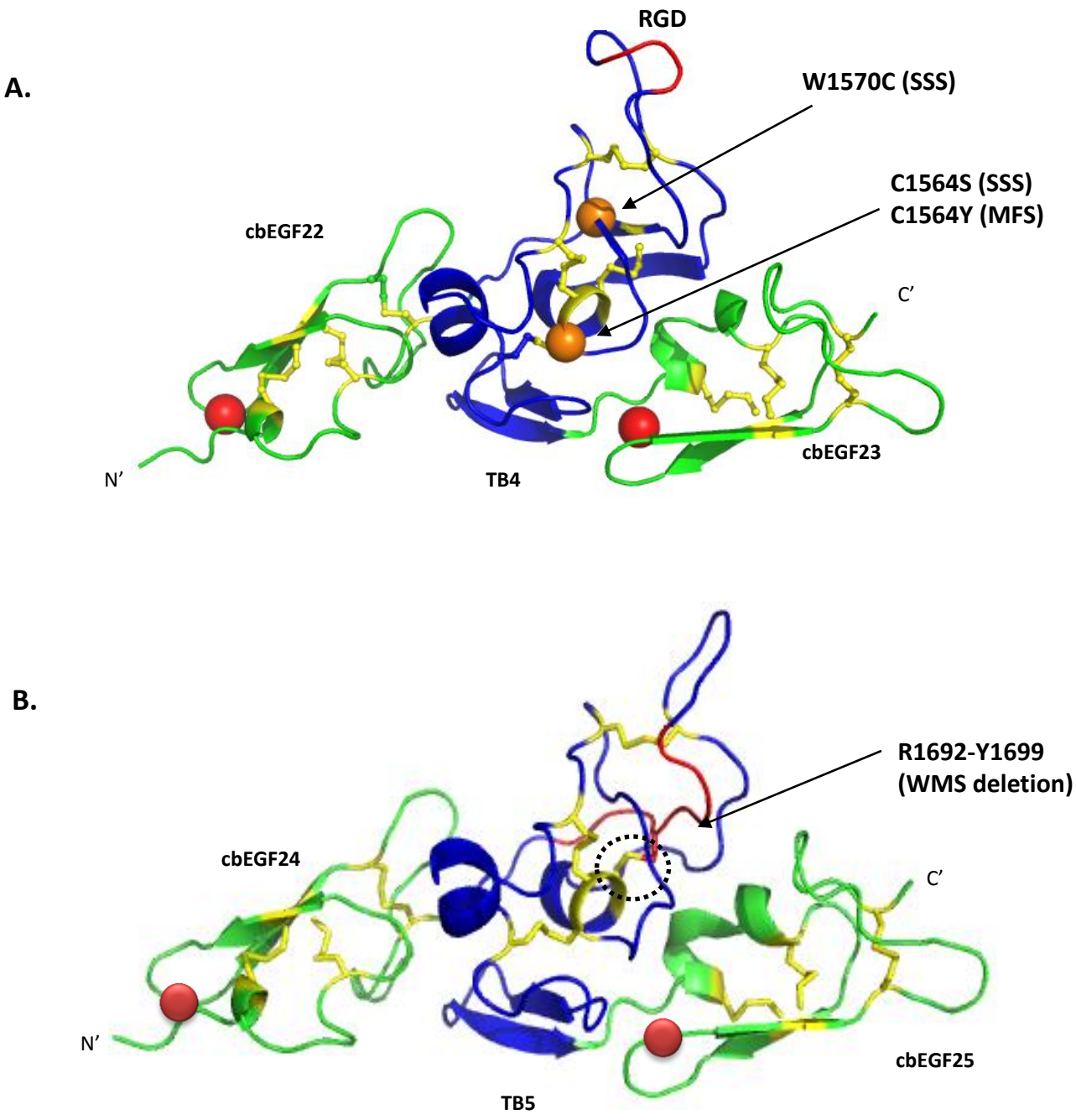

Figure 4.1. A. Crystal structure of cbEGF22-TB4-cbEGF23 (Lee *et al.,* 2004) showing the RGD motif and residues that are substituted in SSS and MFS (yellow spheres). **B.** cbEGF24-TB5-cbEGF25 homology model based on the crystal structure of cbEGF22-TB4-cbEGF23 showing eight amino acid deletion (R-S-L-C-Y-R-N-Y) found to cause WMS. The deletion is shown in red and the free cysteine created in TB5 as a result of the deletion is encircled. This homology model was created using Modeller 9v6 and rendered using PyMol. The cbEGF domains are in green and TB domains are in blue. Calcium ions bound to the cbEGF domains are shown as red spheres; disulphide bridges as yellow sticks; integrin-binding RGD motif is shown in red.

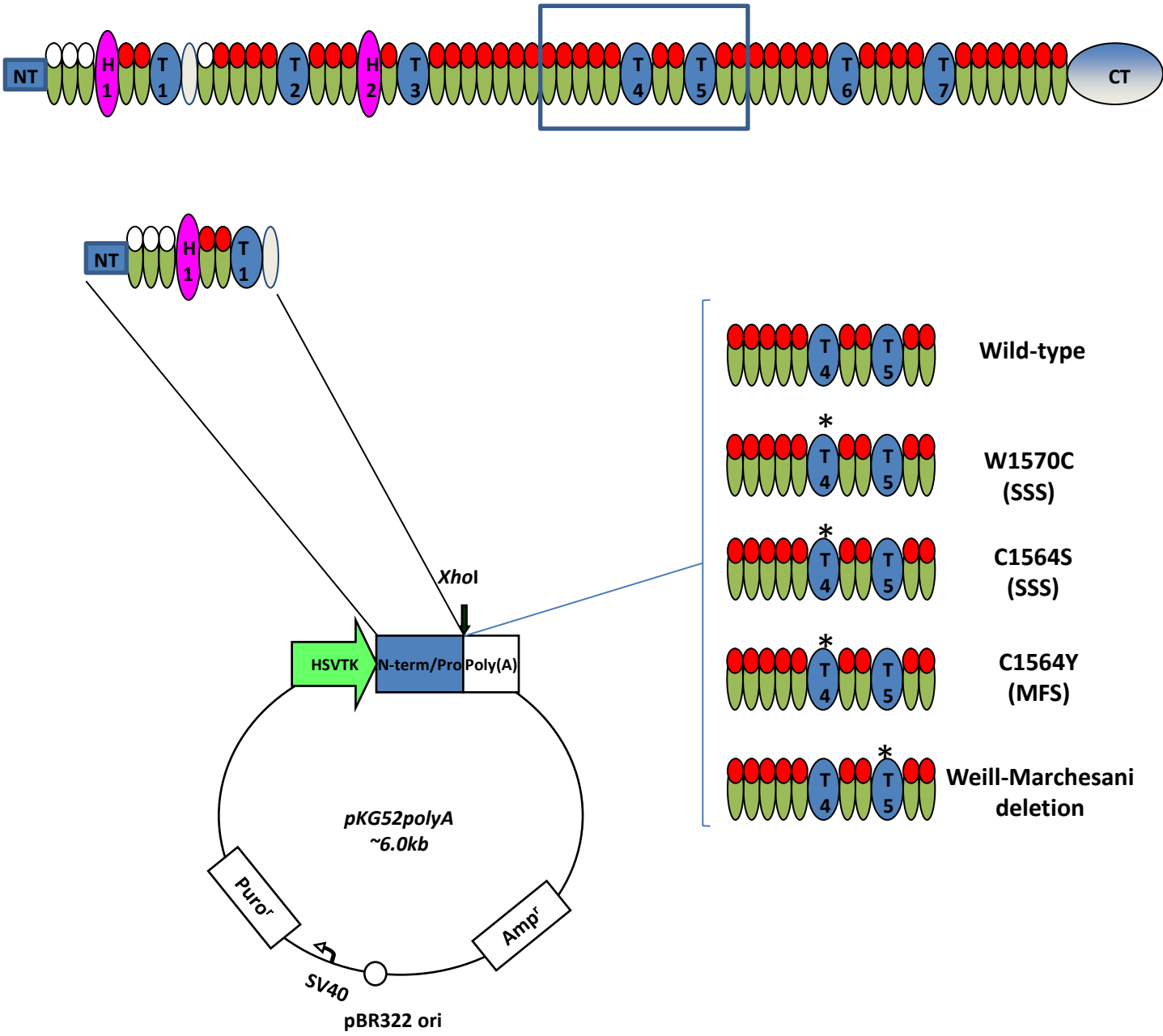

Figure 4.2 Schematic diagram of the construction of the NterPro-cbEGF18-26 fibrillin-1 recombinant fragments. Asterisks indicate substitutions W1570C (SSS), C1564S (SSS), C1564Y (MFS) in the TB4 domain and the Weill-Marchesani deletion in TB5 domain. DNA encoding the N-terminal stalk of fibrillin-1 has been previously been engineered into the mammalian expression vector pKG52polyA. A truncated fibrillin-1 recombinant fragment was used in expression studies to distinguish the mutant fibrillin-1 fragment from endogenous full length fibrillin-1 expressed by the host cell line. Detection of the truncated fragment was by Western blot analysis using fibrillin antibody raised against the unique Pro-rich region. NT : N-terminus; CT : C-terminus; H : Hybrid domain; T: TB domain

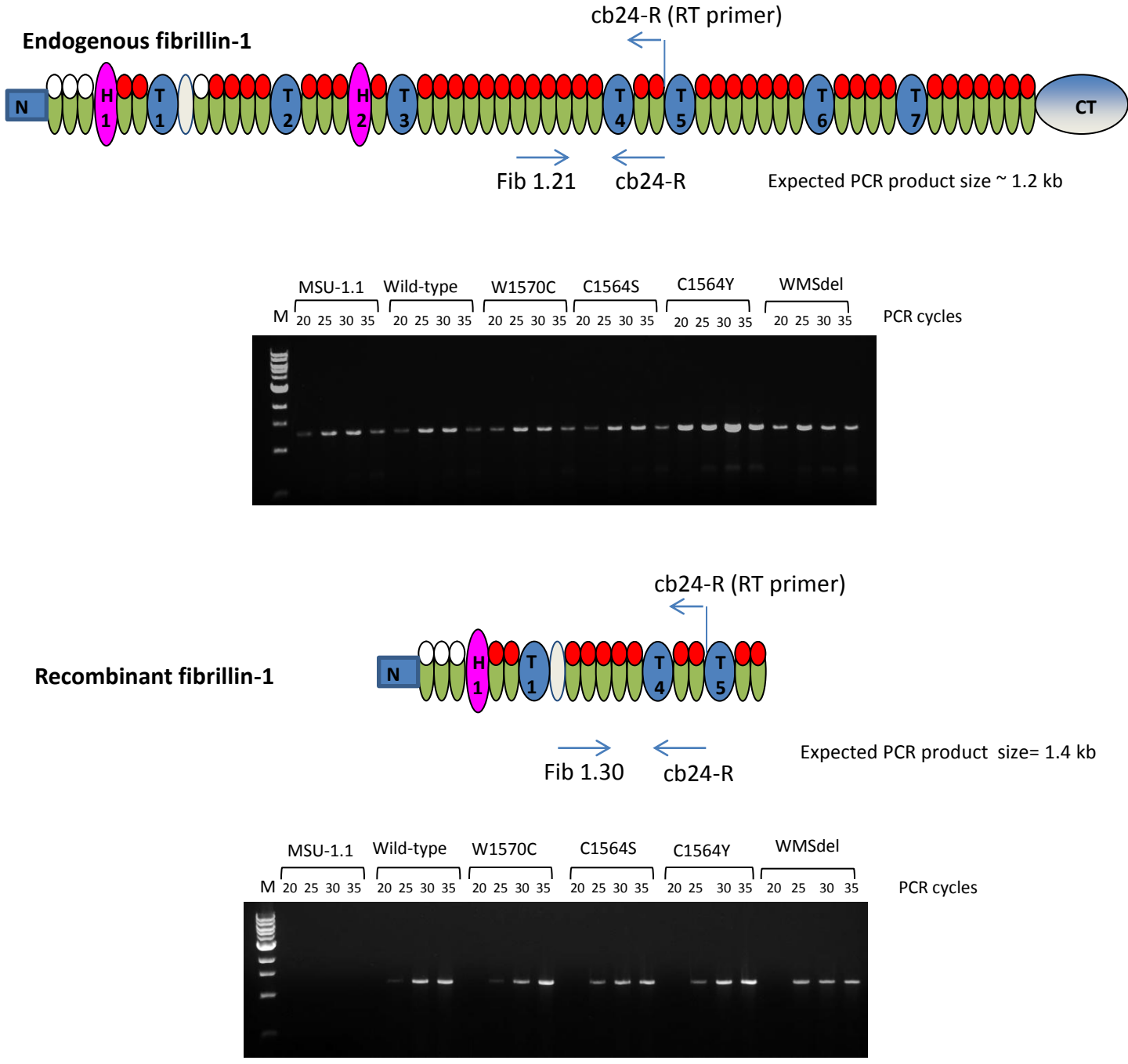

Figure 4.3 Estimation of the gene expression levels by semi-quantitative RT-PCR. Total RNA was reverse transcribed using a reverse primer that hybridises to cDNA encoding fibrillin-1. PCR amplification of the RT product was performed in two sets of PCR reactions with forward primers specific for the endogenous fibrillin-1 (top) or recombinant construct (bottom). A gradual increase in PCR cycle numbers indicates that all clones show similar expression of the recombinant cDNA. Endogenous fibrillin-1 was used as a control to provide evidence that all clones had undergone equivalent reverse transcription into cDNA. M = 100 bp DNA size marker (NEB).

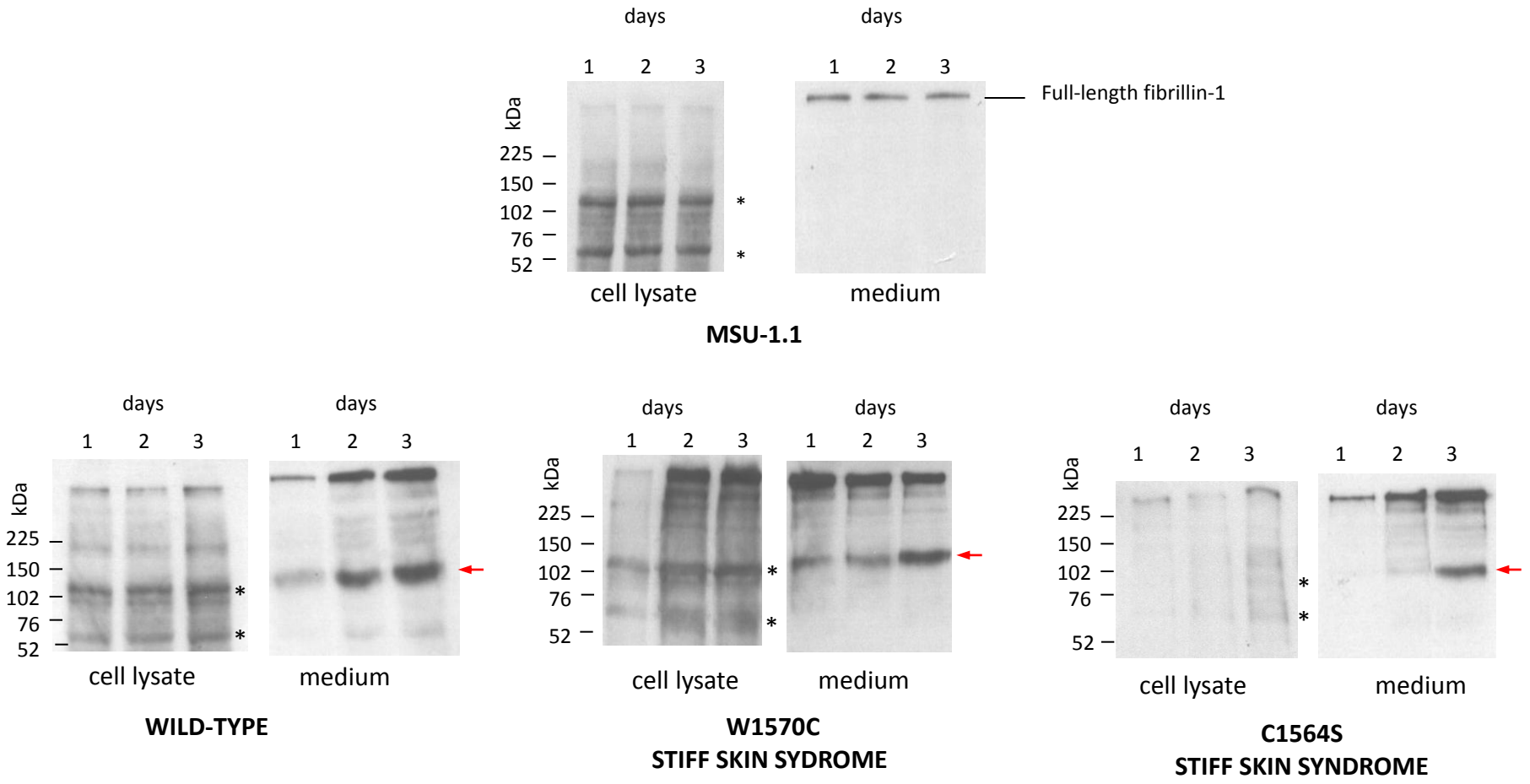

Figure 4.4 MSU-1.1 expression of the NterPro-cbEGF18–26 wild-type and mutant-containing fragments. Conditioned media samples were analysed on 4–15% gradient SDS–PAGE under reducing conditions followed by Western blot analysis and detection with anti-Pro antibody. Molecular masses (kDa) of marker proteins are indicated. Arrows indicate the ~110 kDa recombinant fragments. Position of endogenous full length fibrillin-1 (~320 kDa) is indicated. Each of the blots were run with MSU-1.1 cell lysate and medium samples as negative controls. The recombinant fragment was detected in the media samples of the wild-type and from W1570C and C1564S pools of clones.

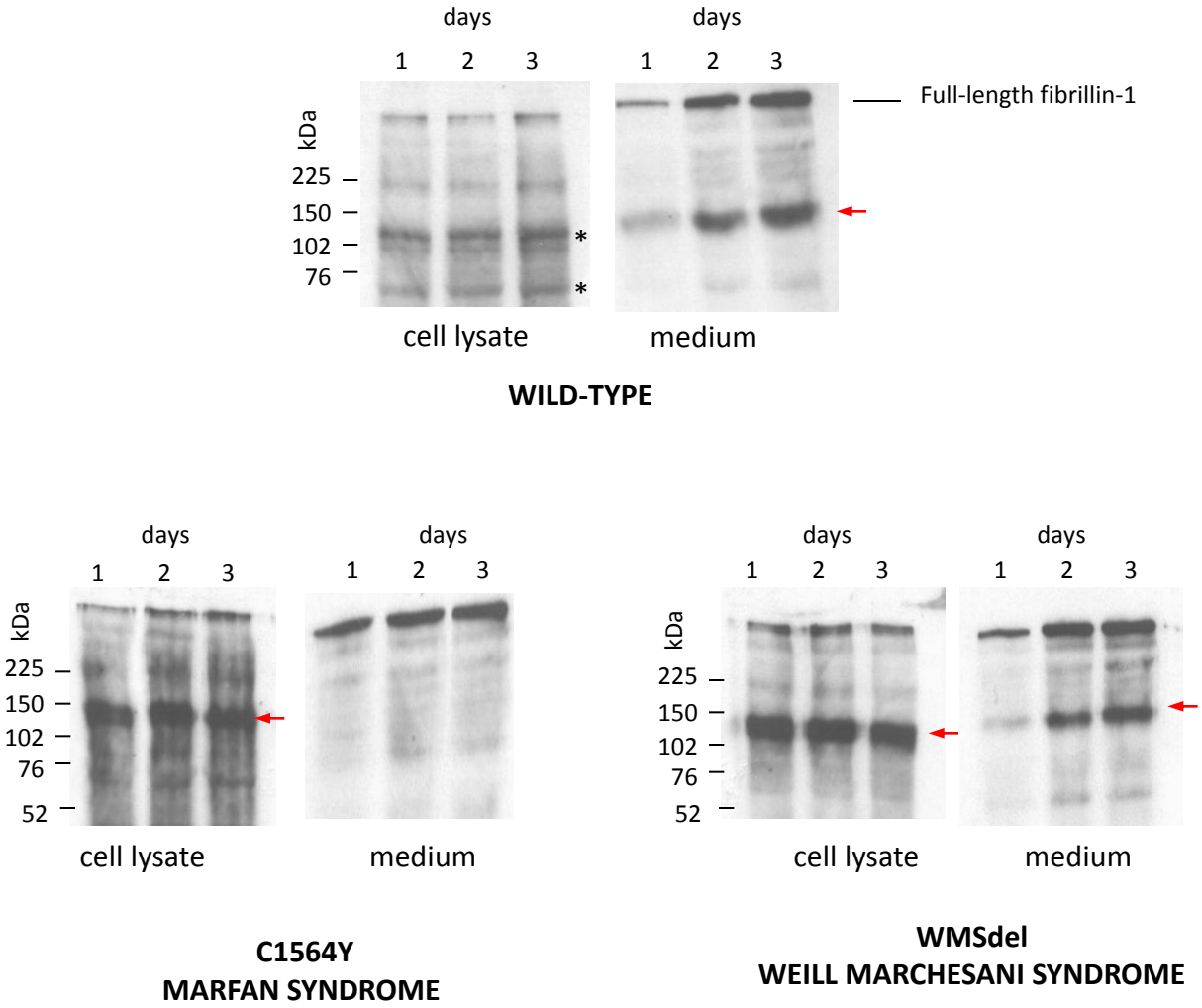

Figure 4.5 MSU-1.1 expression of the NterPro-cbEGF18–26 wild-type and mutant-containing fragments. Conditioned media samples were analysed on 4–15% gradient SDS–PAGE under reducing conditions followed by Western blot analysis and detection with anti-Pro antibody. Molecular masses (kDa) of marker proteins are indicated. Arrows indicate the ~110 kDa recombinant fragments. Position of endogenous full length fibrillin-1 (~320 kDa) is indicated. Each of the blots were run with MSU-1.1 medium and cell samples as loading controls. The recombinant fragment was not detected in case of the C1564Y Marfan mutant but immunoreactive material is present inside the cells whereas the Weill-Marchesani mutant was seen both inside and outside the cell.

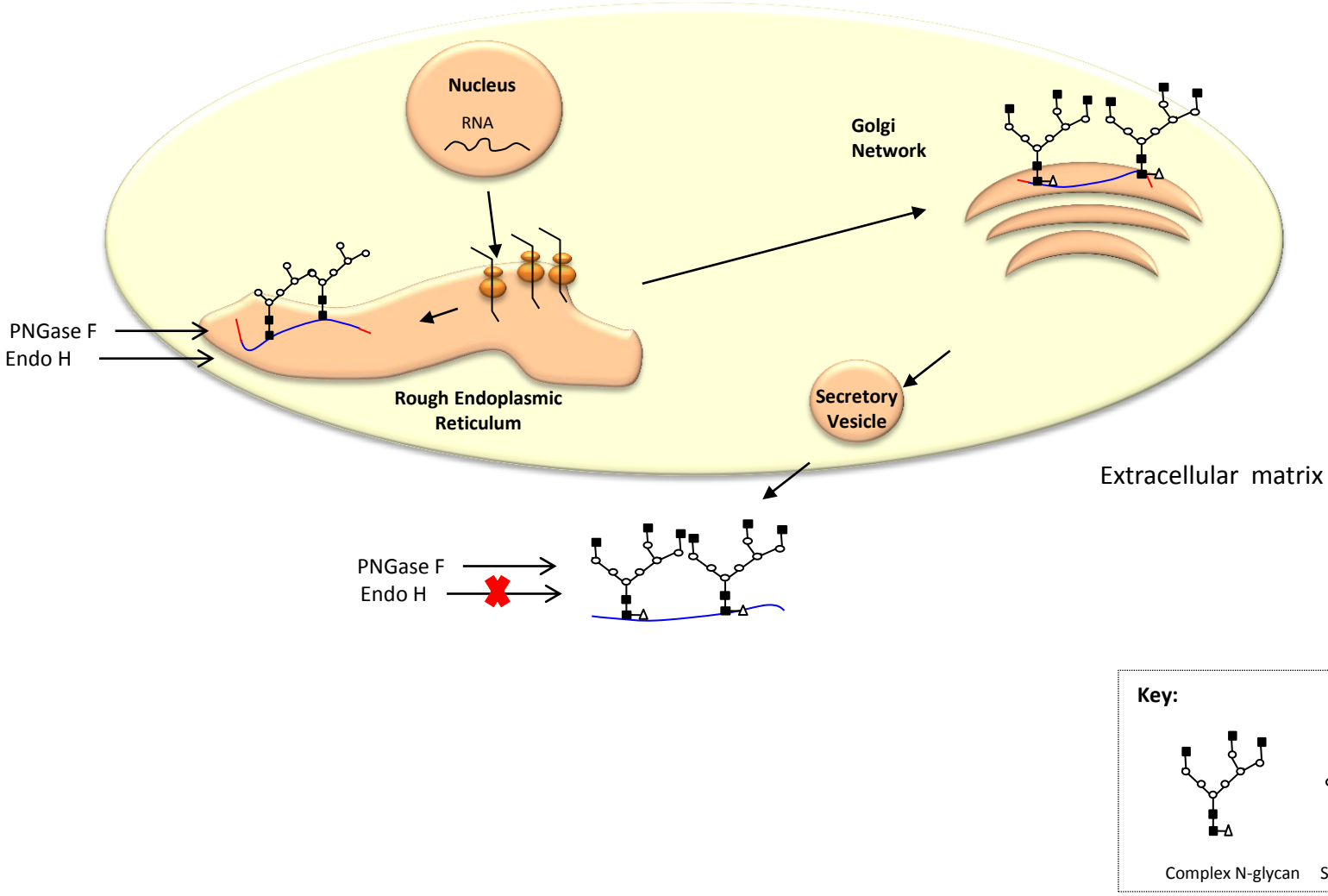

Figure 4.6 This diagram shows the difference between the two endoglycosidase enzymes, namely, PNGase F and Endo H on glycosylated protein. Protein in the endoplasmic reticulum generally has simple N-glycan modifications and on reaching Golgi apparatus more complex N-glycan modifications take place. The secreted protein will also, therefore, have complex N-glycan modifications. PNGase F removes all types of N-linked (Asn linked) glycosylation; high mannose, hybrid, bi, tri, and tetra antennary, whereas, Endo H removes only simple types of N-glycans on the protein. Therefore, protein secreted out of the cell would be resistant to Endo H enzyme action, but susceptible to PNGase F. Conversely, protein retained in the ER will be susceptible to both PNGase F and Endo H.

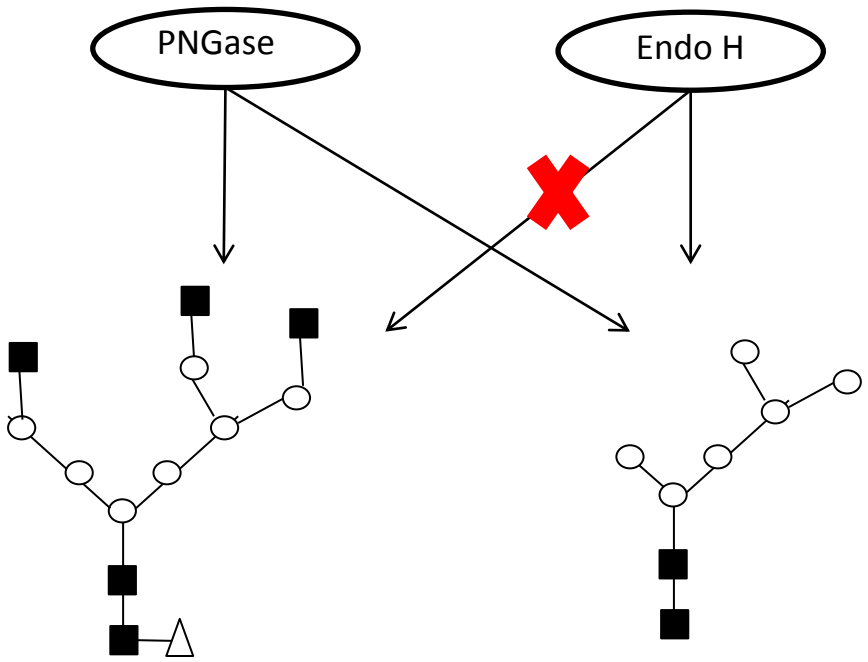
PNGase
Endo H
Complex N-glycan
Simple N-glycan

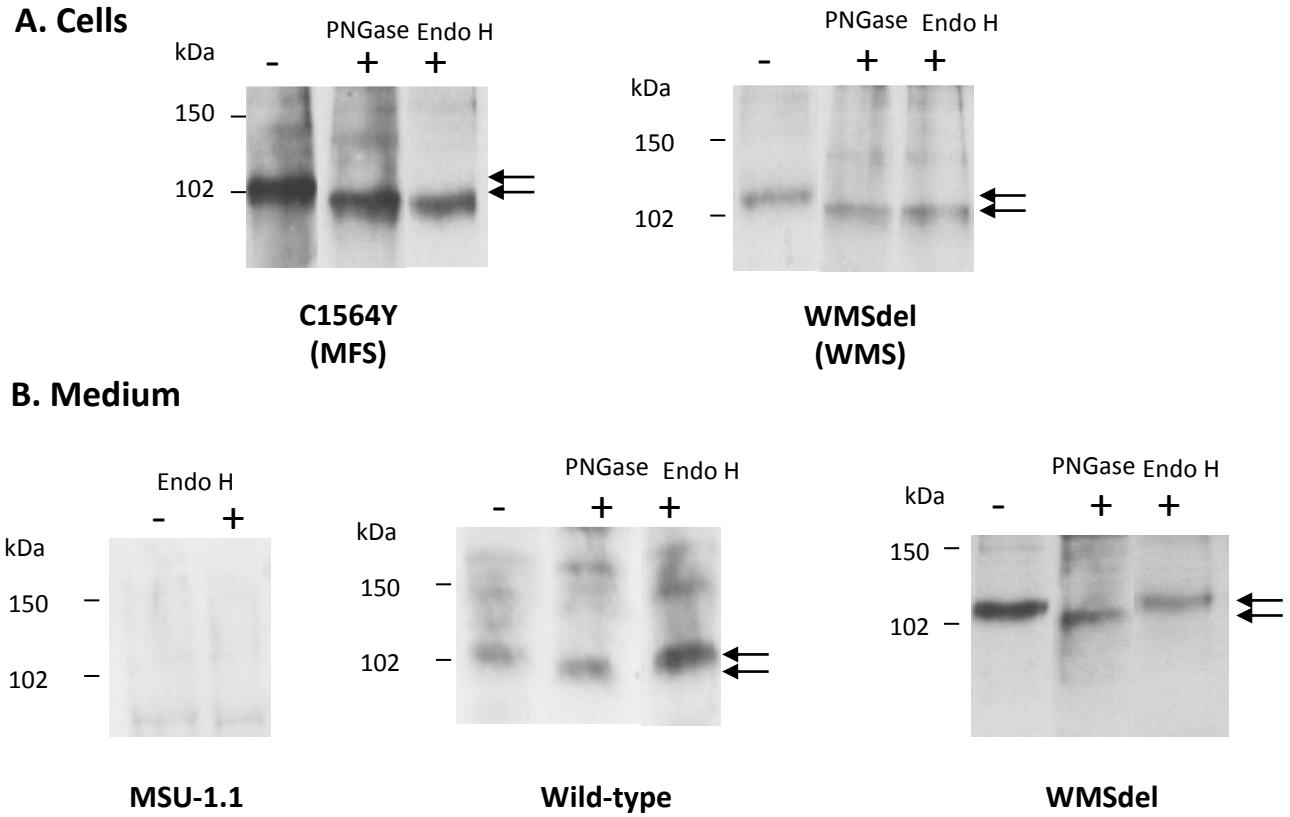

Figure 4.7 Analysis of N-linked glycosylation on retained and secreted recombinant fragments (A) Retained fragments in the cell. The retained NterPro-cbEGF18-26 C1564Y (MFS) and NterPro-cbEGF18-26 WMSdel fragments are sensitive to Endo H and PNGase F (indicated by arrows). The effect on migration indicated by arrows was similar for both enzymes. Equivalent amounts of the lysate fractions were loaded onto the 4–15% gradient gel for electrophoresis under reducing conditions, western blotting and detection by the anti-Pro antibody. **(B) Secreted recombinant fragment in the medium.** The wild-type NterPro-cbEGF18-26 secreted fragment is sensitive to PNGase F (indicated by arrows) but not Endo H and the same is observed for WMS deletion fragment. MSU-1.1 medium sample was used as a negative control. Molecular masses (kDa) of marker proteins are indicated.

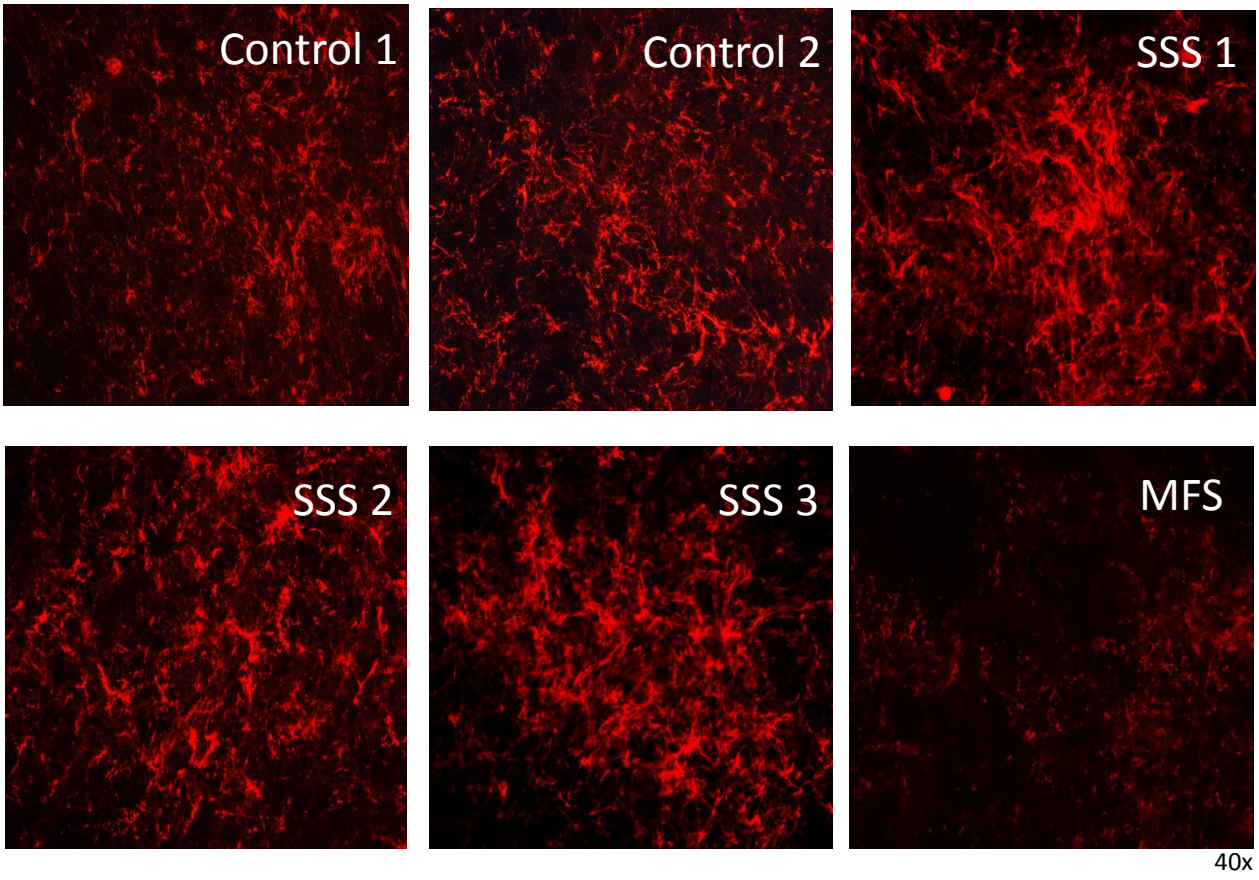

Figure 4.8 Immunofluorescence of fibrillin 1–containing microfibrils assembled by Stiff skin syndrome (SSS) fibroblasts, Marfan syndrome (MFS) fibroblasts, and control fibroblasts. Patient and control cell strains were seeded on chamber slides and allowed to grow for 72 hr. Fibrillin 1–containing microfibrils were visualised using a polyclonal antibody to proline-rich region of fibrillin-1 and a secondary antibody conjugated to texas red. Two control (neonatal and adult normal dermal fibroblasts) and three SSS patient cell strains show an elaborate network of microfibrils, whereas the MFS cell strain shows only a faint network of microfibrils, consistent with the dominant-negative pathogenesis of MFS.

B.

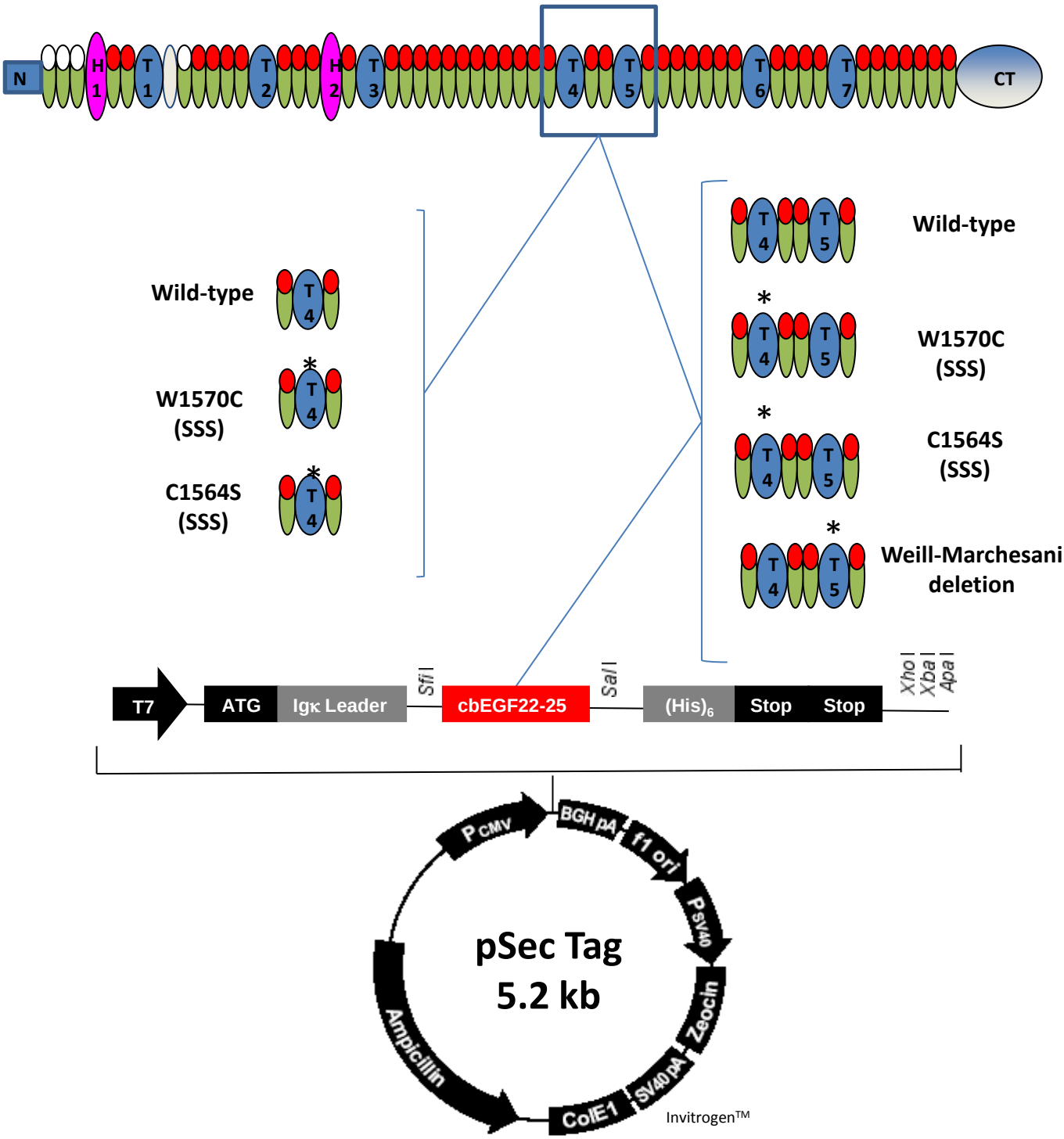

Figure 5.1 shows different fibrillin-1 fragments used in this study. Schematic diagram of construction of the cbEGF22-25 and cbEGF22-23 fibrillin-1 recombinant fragments. Asterisks indicate SSS substitutions W1570C and C1564S and in the TB4 domain and Weill-Marchesani deletion (WMSdel) in TB5 domain. DNA encoding the cbEGF22-25 of fibrillin-1 was engineered into the mammalian expression vector pSec Tag with a C-terminal His-tag and a CMV promoter. cbEGF22-25 fragments were expressed in mammalian expression system in HEK293S cells. Detection of the recombinant fragment was by western blot anlaysis using anti-His (C-term) antibody. The triple constructs were expressed in *E.coli* and *in vitro* refolded (as described in chapter 3).

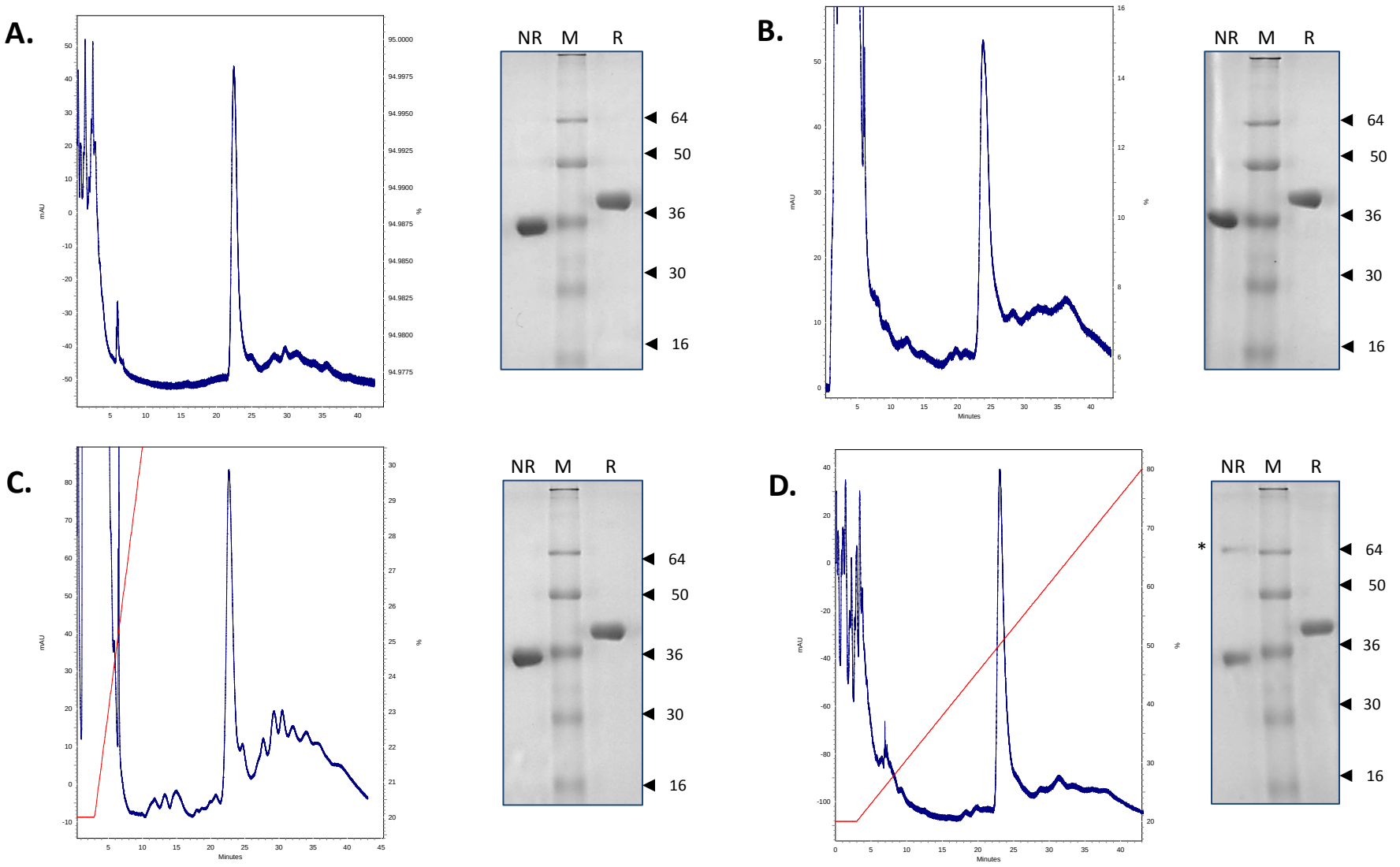

Figure 5.2 HPLC profile and SDS-PAGE of oxidised wild-type (A), W1570C (B), C1564S (C) and WMSdel (D) cbEGF22-25 constructs. One sharp peak obtained in each case. SDS-PAGE analyses of refolded protein samples after the final HPLC purification step are next to each trace. Samples were denatured by boiling with reducing (R) or non-reducing (NR) loading buffer, then resolved on a 12% SDS PAGE gel and stained with Coomassie Blue. Molecular weights (kDa) of pre-stained markers are indicated. The SDS PAGE of the refolded mutant protein in 'D' show a small amount of higher molecular weight material, which is possibly a dimer (asterisk). This might be forming because of a free thiol in the mutant construct.

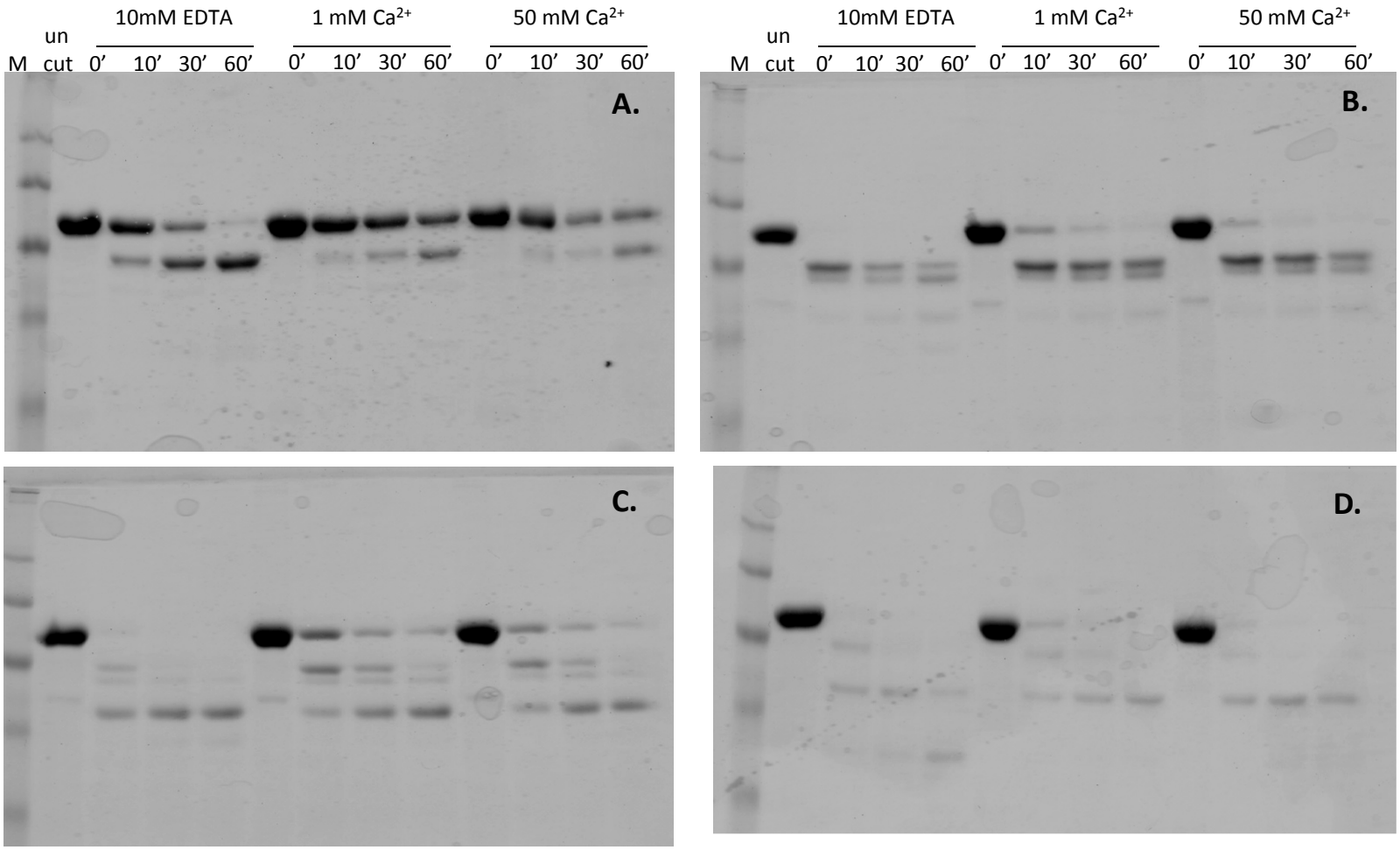

Figure 5.3 Reducing 16% SDS PAGE of tryptic digests of cbEGF22-25 fragments performed in the presence and absence of Ca^{2+} at pH 7.5. Digestion of (A) wild type, (B) W1570C mutant and (C) C1564S mutant and (D) Weill-Marchesani deletion mutant. Digestion occurred over 60 minutes with samples being removed at T_0 , T_{10},T_{30} and T_{60} . The ‘-ve’ incubated for 60 minutes with no enzyme present to act as control.

A.

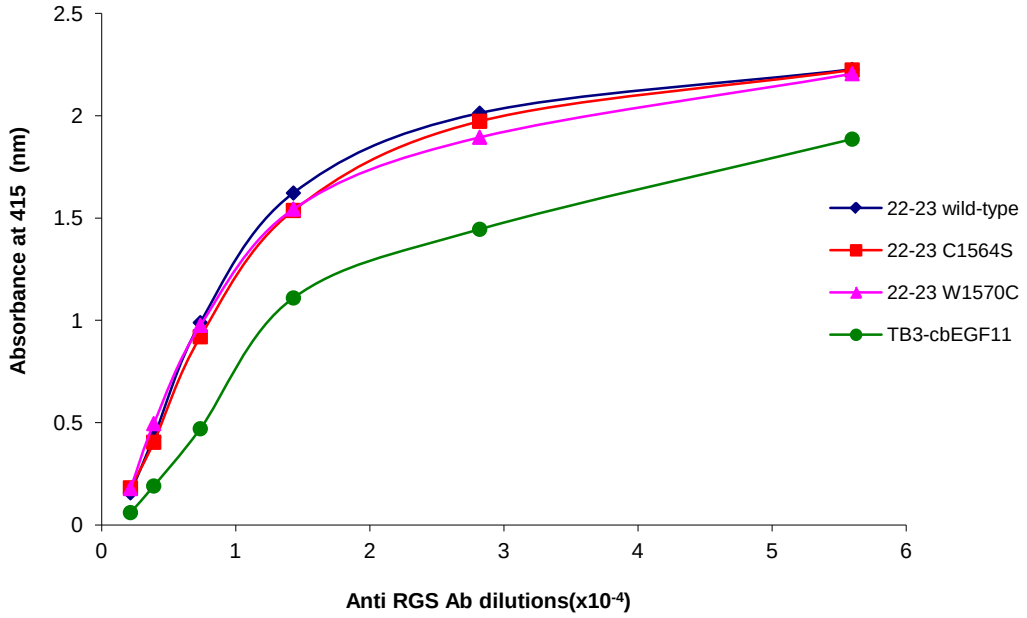

B.

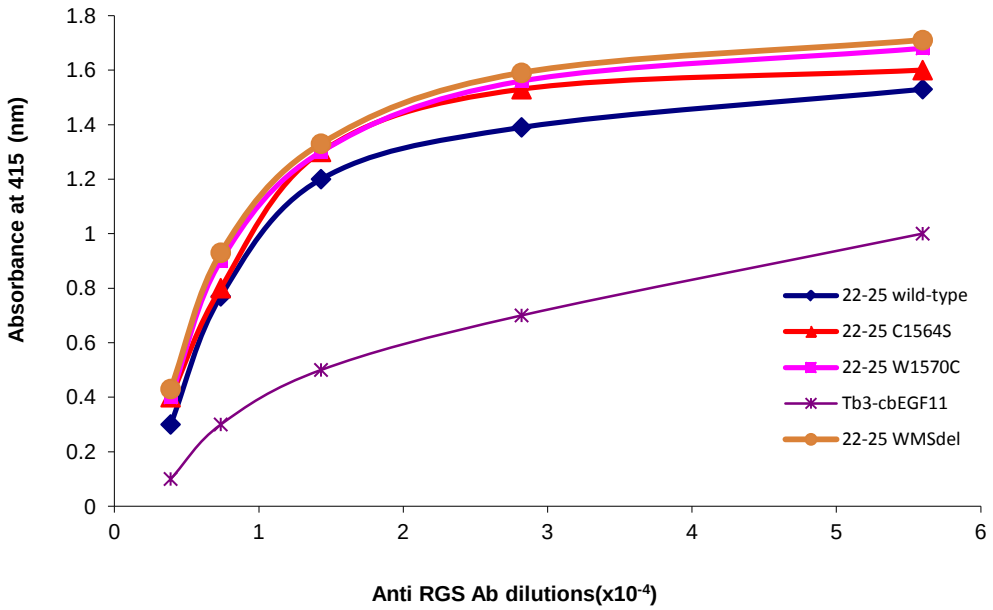

Figure 5.4 ELISA analysis of cbEGF22-TB4-cbEGF23 and cbEGF22-25 fragments binding to anti-RGS His antibody. Each protein sample was plated at 5 µM concentration and analysed using doubling dilutions of the primary antibody, each dilution measured in triplicate. RGS His antibody was used to determine the amount of each His-tagged protein that binds to the plate. **(A)** ELISA curves show that triple cbEGF22-TB4-cbEGF23 wild-type and mutant constructs bind to the wells similarly. **(B)** ELISA curves of the larger cbEGF22-25 fragment containing W1570C, C1564S substitutions and WMSdel bind at least as well as the wild-type fragment. A TB3-cbEGF11 construct purified in a similar manner to cbEGF22-TB4-cbEGF23 mutants showed that it does not bind to wells in a similar manner, as expected

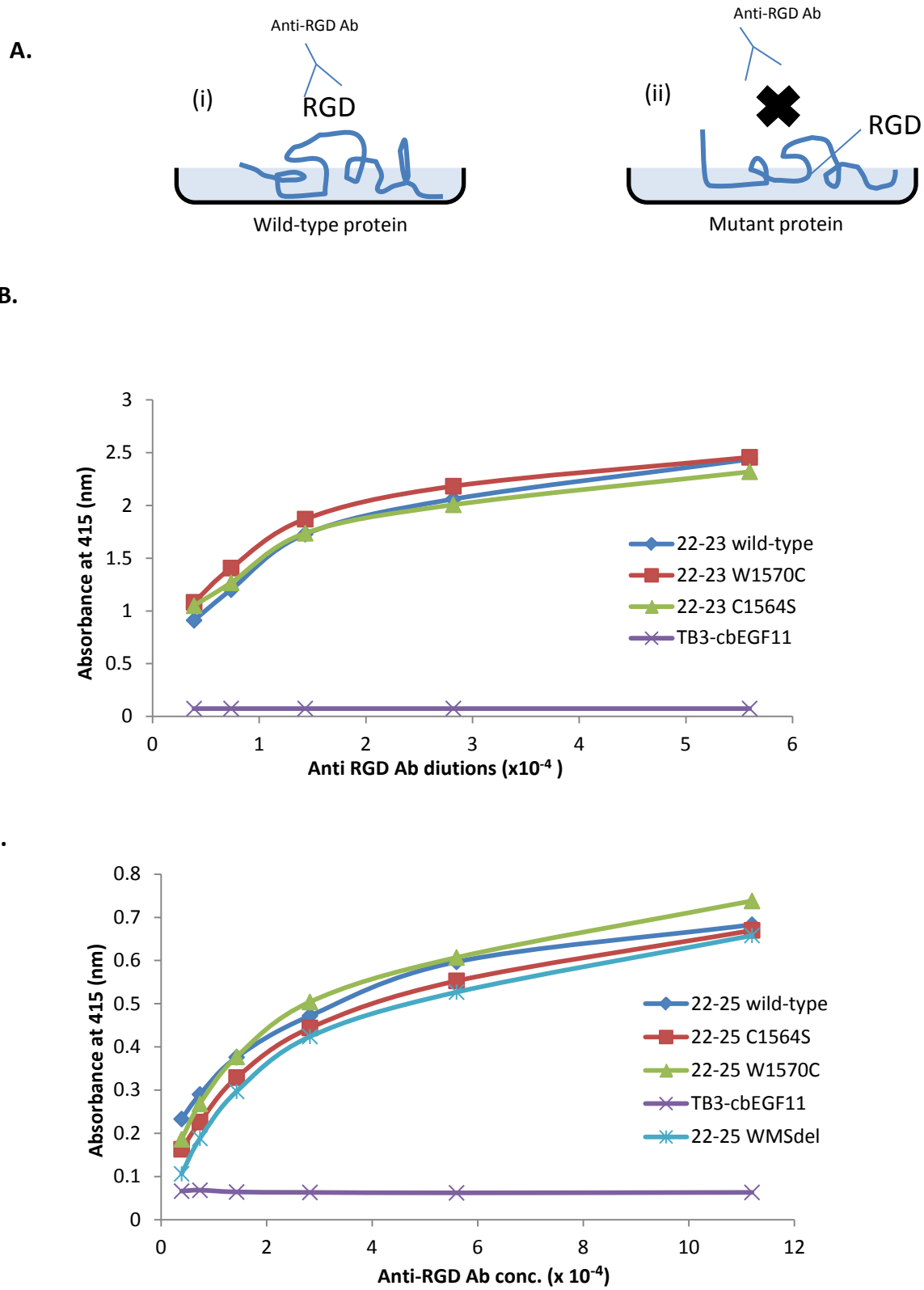

Figure 5.5. ELISA analysis of cbEGF22-TB4-cbEGF23 and cEGF22-25 fragments binding to anti-RGD antibody. Each protein sample was plated at 5 µM concentration and analysed using doubling dilutions of the primary antibody, each dilution measured in triplicate. Anti-RGD antibody was used to determine exposure of RGD-loop. **(A**) An anti-RGD antibody that recognises the RGD loop can be used to determine whether the RGD loop in TB4 domain is exposed in fragments containing mutations that affect TB4 domain structure. **(B)** ELISA curves show that triple cbEGF22-TB4-cbEGF23 wild-type and mutant constructs bind to the anti-fibrillin-1 RGD antibody similarly. **(C)** ELISA curves of the larger fragment containing W1570C, C1564S substitutions and WMSdel bind at least as well as the wild-type cbEGF22-25 fragment. A TB3-cbEGF11 construct purified in a similar manner to cbEGF22-TB4-cbEGF23 mutants showed no binding to the RGD antibody, as expected.

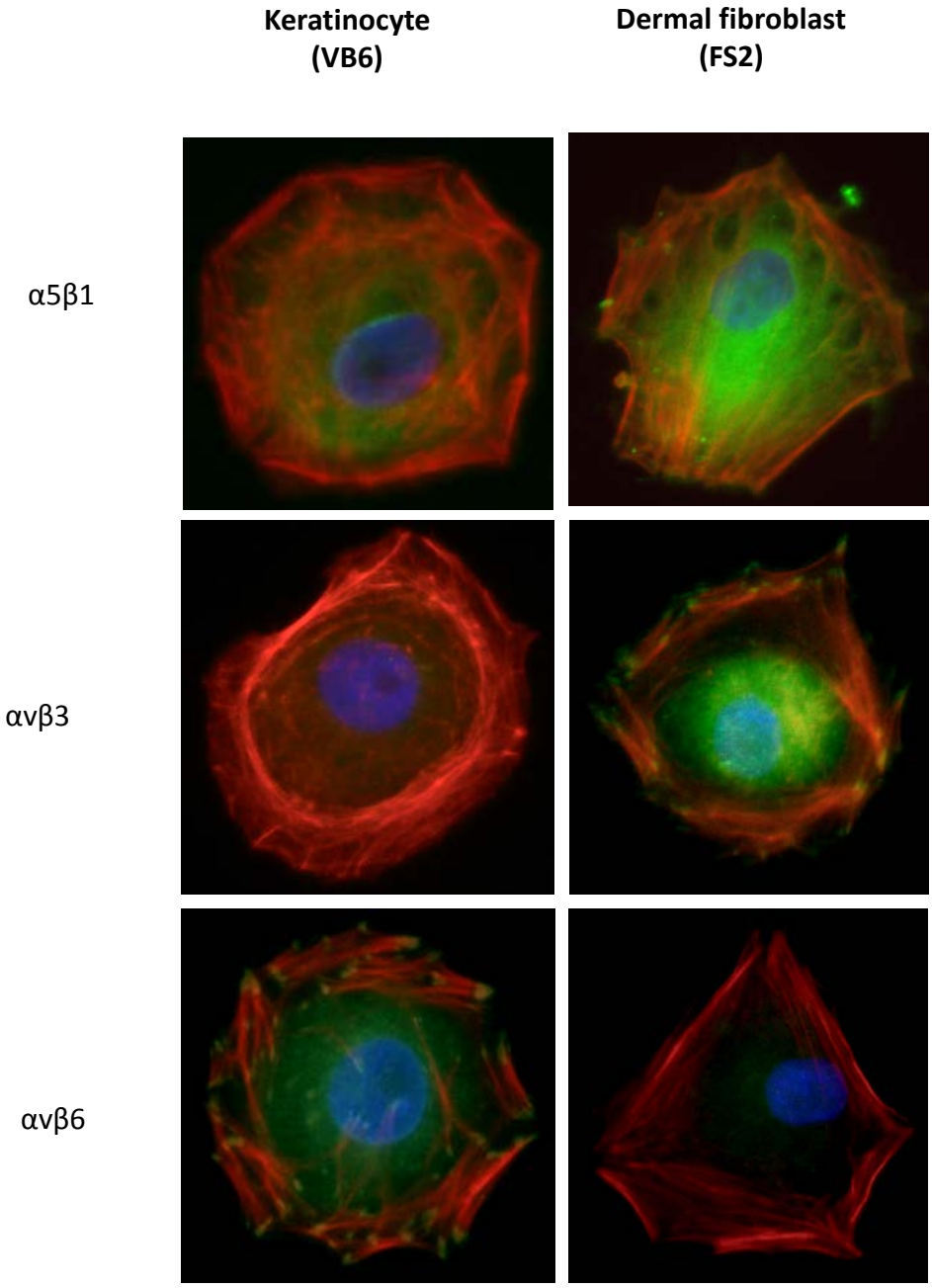

Figure 5.6 Expression of integrins in VB6 and FS2 cells. Immunocytochemistry using either VB6 or FS2 cells for the indicated integrin subtypes (green signal). An anti-actin antibody labels actin filaments (red signal). Nuclei are stained with DAPI (blue signal). VB6 cells only show positive staining for β6 integrin, both inside the cell and in punctate foci marking focal adhesions at the cell surface. FS2 cells show expression of both α5β1 and αvβ3 integrins, but only the latter localizes to focal adhesions.

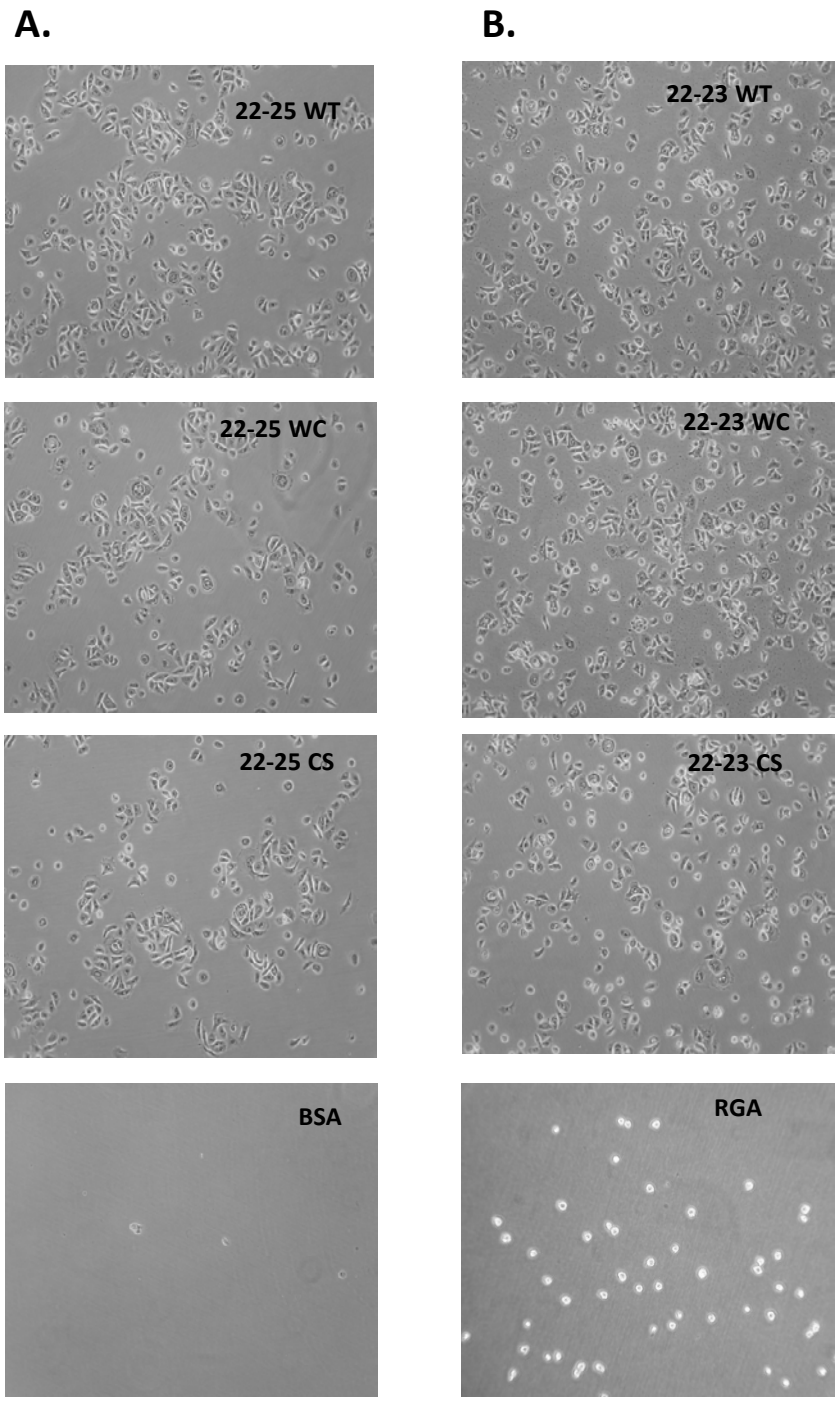

Figure 5.7 Cell attachment and spreading on human keratinocytes (VB6). Phase contrast images of VB6 cells on **A.** cbEGF22-25 and **B.** cbEGF22-TB4-cbEGF23 fibrillin-1 wild-type and mutant fragments. Wild-type construct was used as a positive control and BSA and RGA mutant as a negative control.

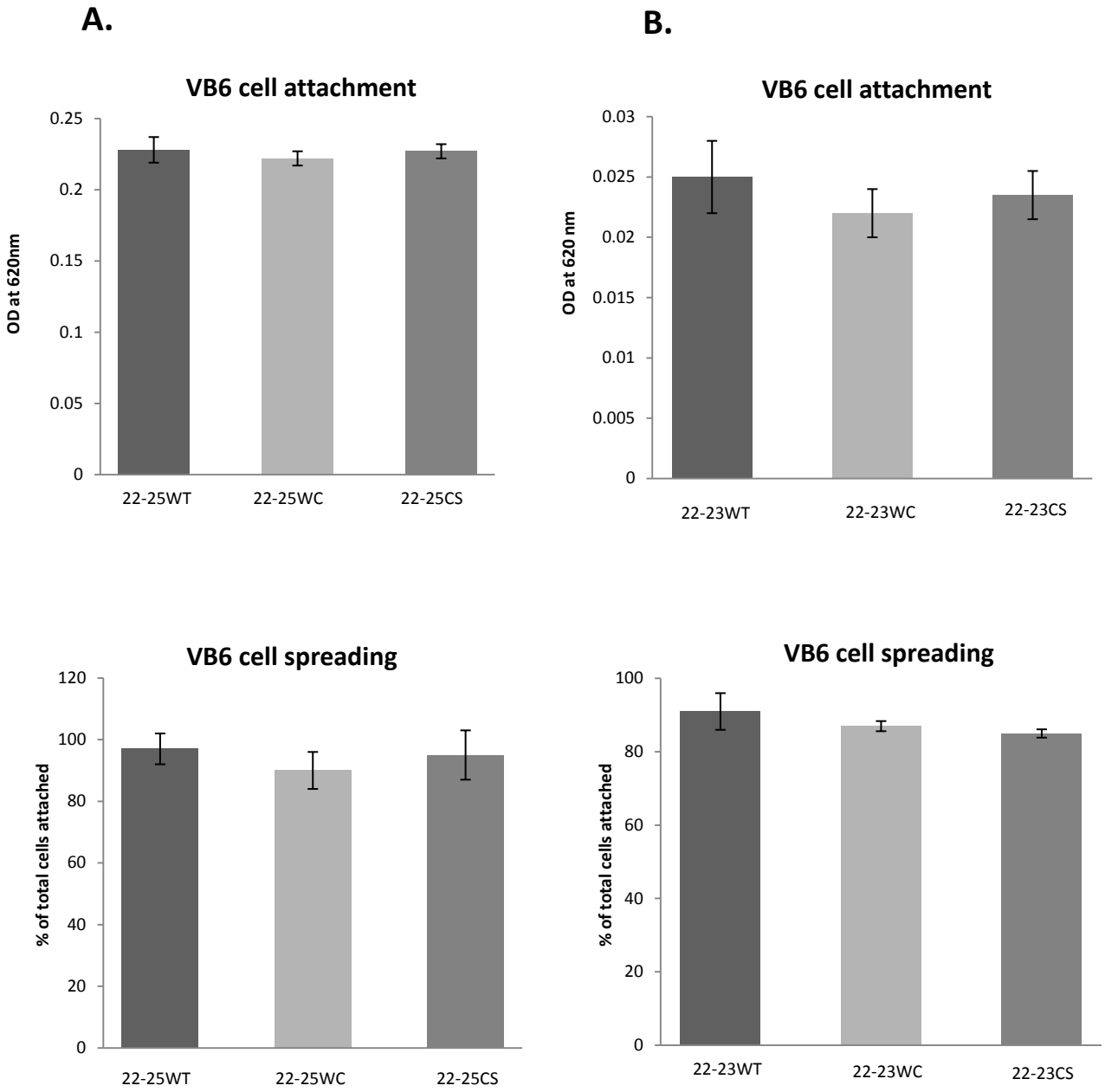

Figure 5.8 Quantitative analysis of cell attachment and spreading on human keratinocytes. Cell attachment (upper panel) and spreading (lower panel) of VB6 keratinocytes adherent on recombinant wild-type and mutant A. cbEGF22-25 (22-25) and B. cbEGF22-TB4-cbEGF23 (22-23) W1570C and C1564S protein constructs. Wild-type construct was used as a positive control and BSA and RGA mutant as negative control. Data are expressed as mean ±S.D. from three independent experiments (attachment, n=9; spreading, n=5 for each experiment).

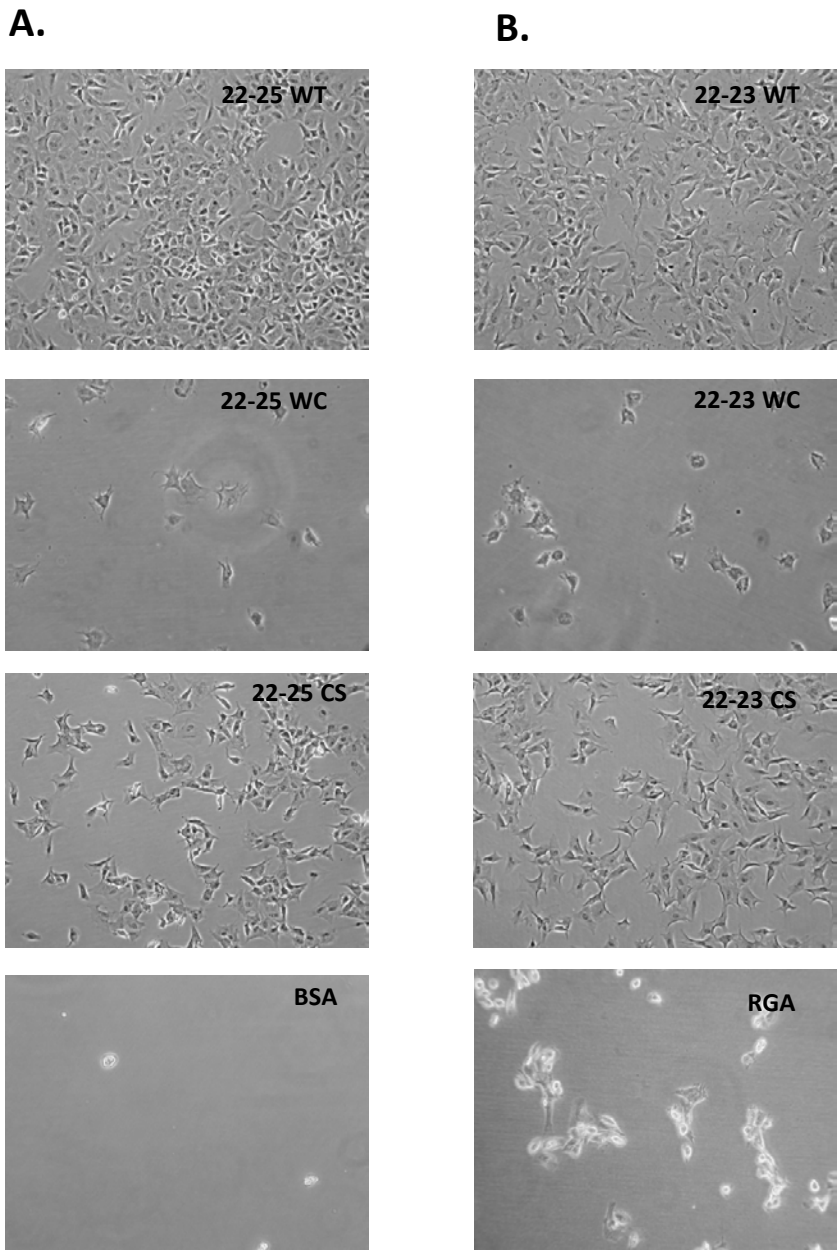

Figure 5.9 Cell attachment and spreading on human dermal fibroblasts (*expressing αvβ3 in the focal adhesions and α5β1).* Phase contrast images of FS2 cells on A. cbEGF22-25 and B. cbEGF22-TB4-cbEGF23 fibrillin-1 wild-type and mutant fragments. Wild-type construct was used as a positive control and BSA and RGA mutant as negative control.

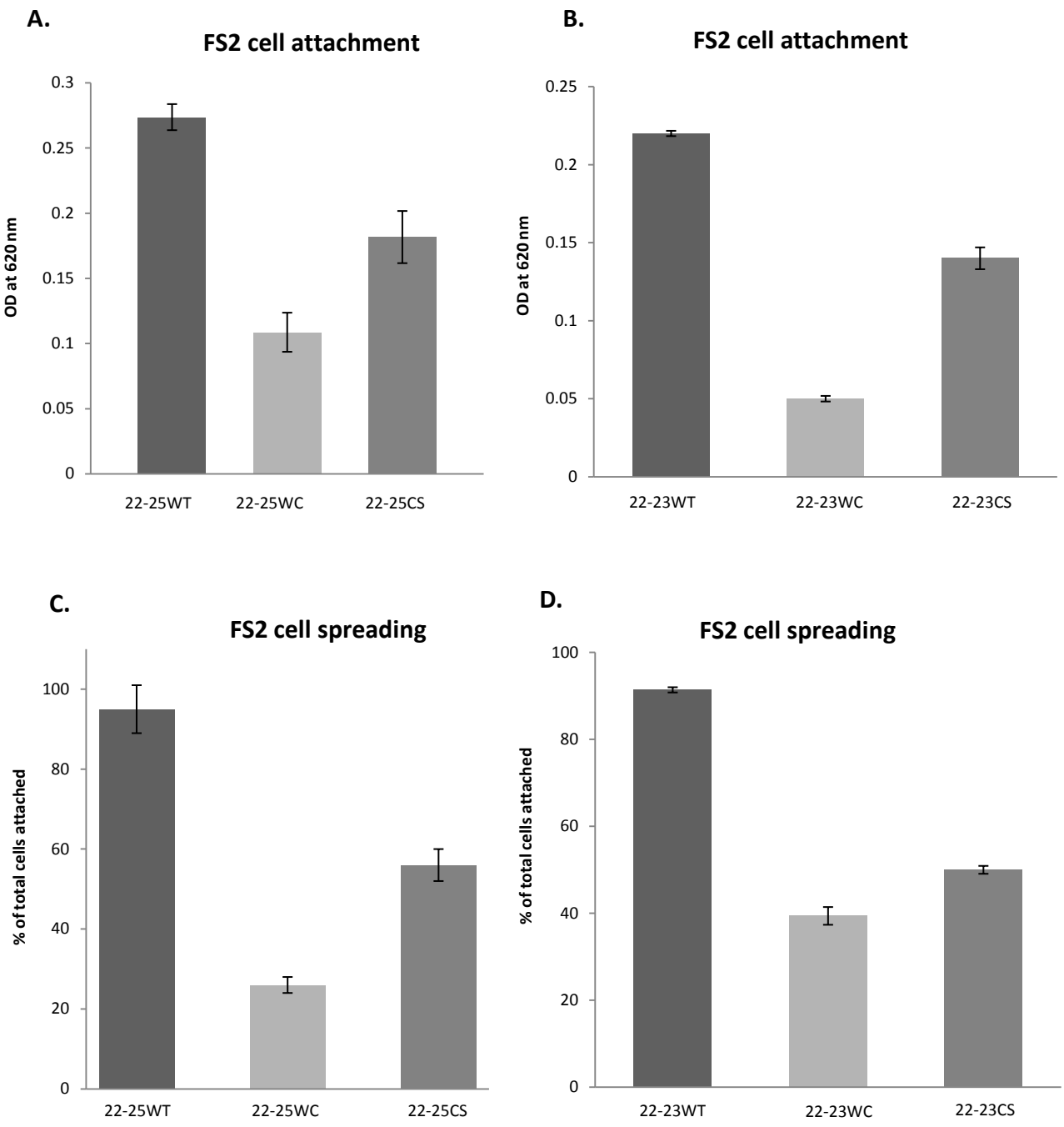

Figure 5.10 Quantitative analysis of cell attachment and spreading on human dermal fibroblasts. Cell attachment (upper panel) and spreading (lower panel) of FS2 dermal fibroblasts adherent on recombinant wild-type and mutant A. cbEGF22-25 (22-25) and B. cbEGF22-TB4-cbEGF23 (22-23) W1570C and C1564S protein constructs. Wild-type construct was used as a positive control and BSA and RGA mutant as negative controls. Data are expressed as mean ±S.D. from three independent experiments (attachment, n=9; spreading, n=5 for each experiment).

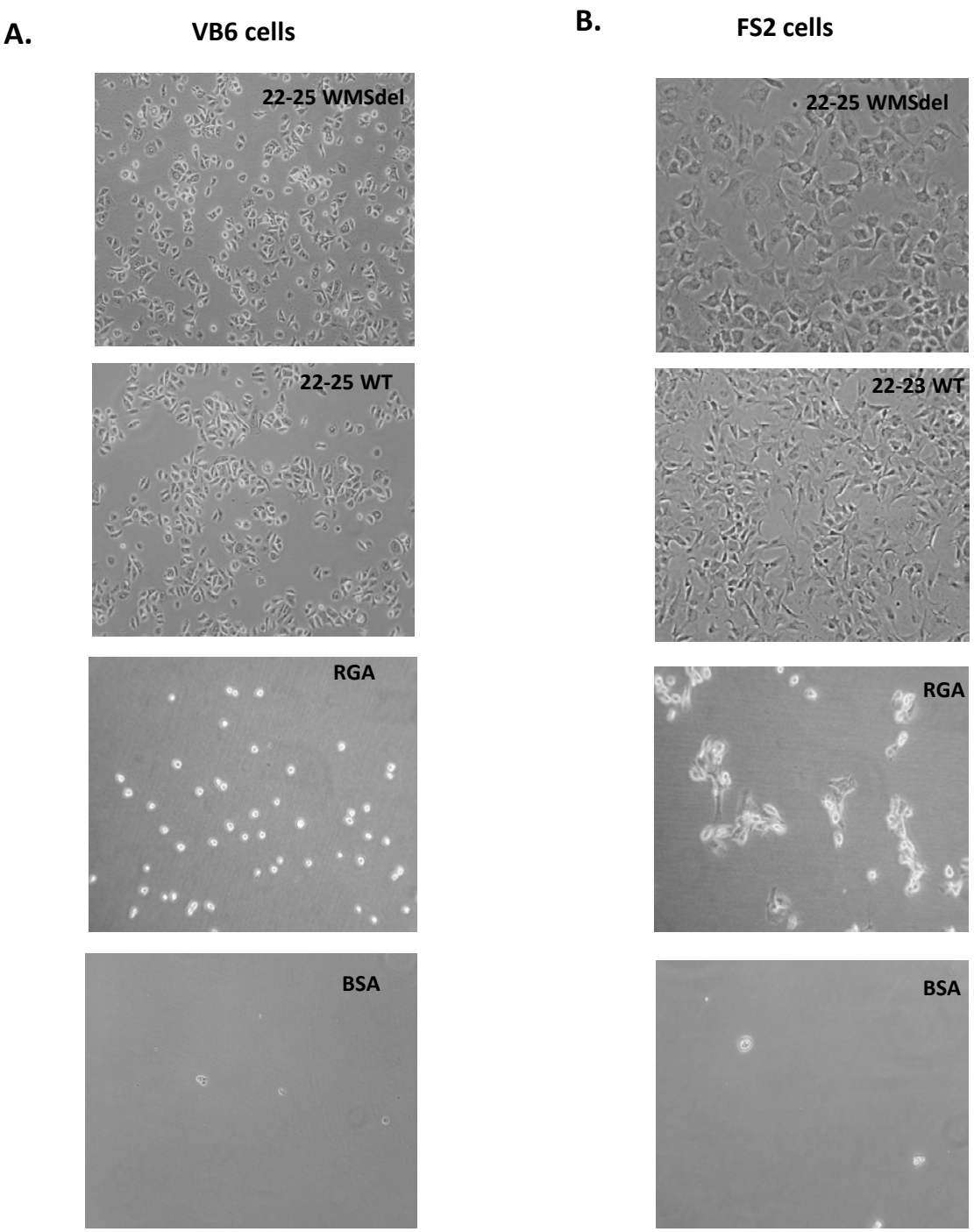

Figure 5.11 VB6 and FS2 cell spreading and attachment on the cbEGF22-25 construct containing the Weill-Marchesani deletion (WMSdel). Phase contrast images of VB6 (A) and FS2 (B) cells on cbEGF22-25 WMSdel and wild-type. Wild-type construct was used as a positive control and BSA and RGA mutant as negative control.

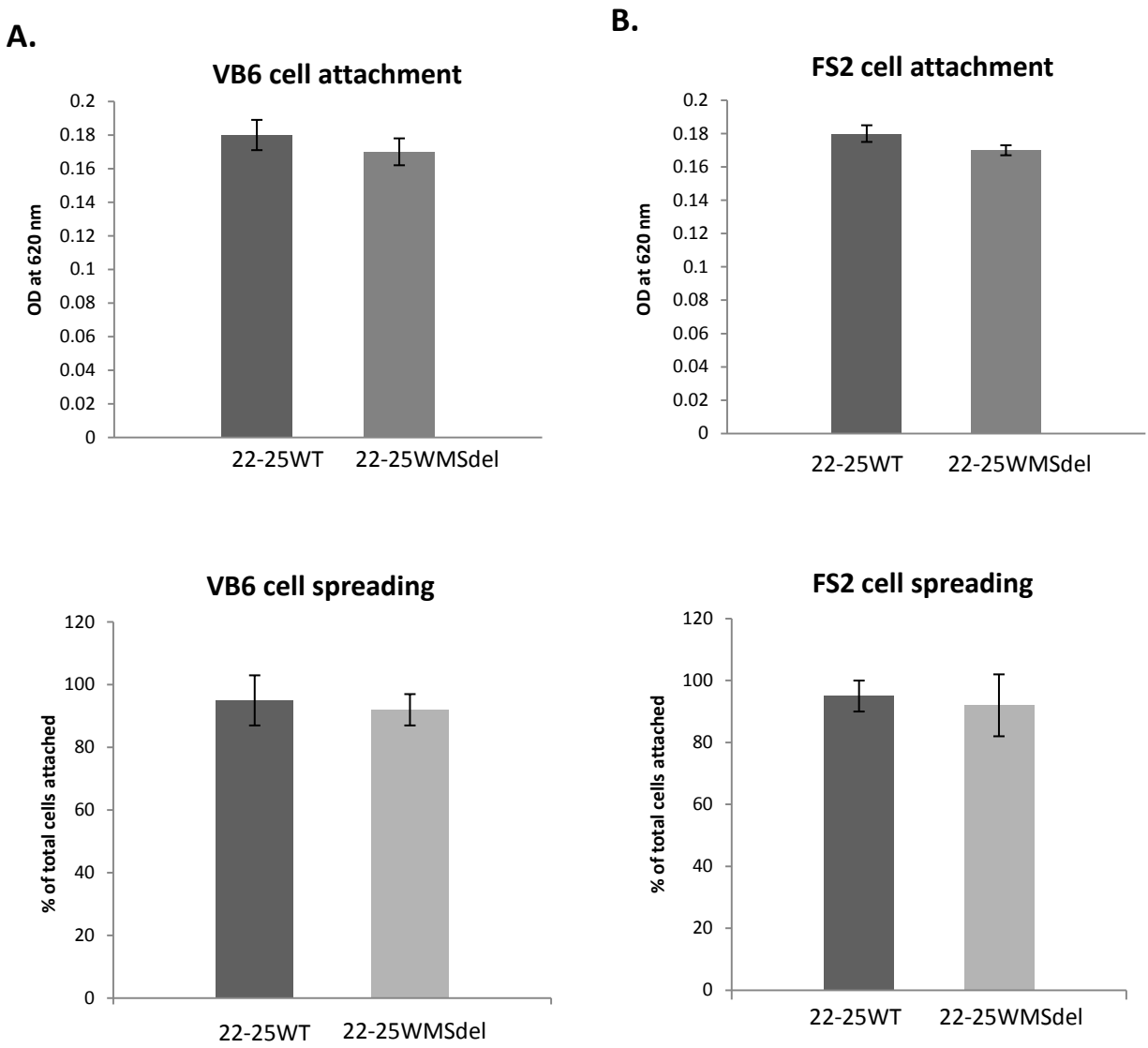

Figure 5.12 Quantitative analysis of cell attachment and spreading on VB6 and FS2 cells. **A.** VB6 cell attachment (upper panel) and spreading (lower panel) and **B.** FS2 dermal fibroblasts cell attachment and spreading on recombinant cbEGF22-25 wild-type and WMSdel constructs. Wild-type construct was used as a positive control and BSA and RGA mutant as negative controls. Data are expressed as mean ±S.D. from three independent experiments (attachment, n=9; spreading, n=5 for each experiment).

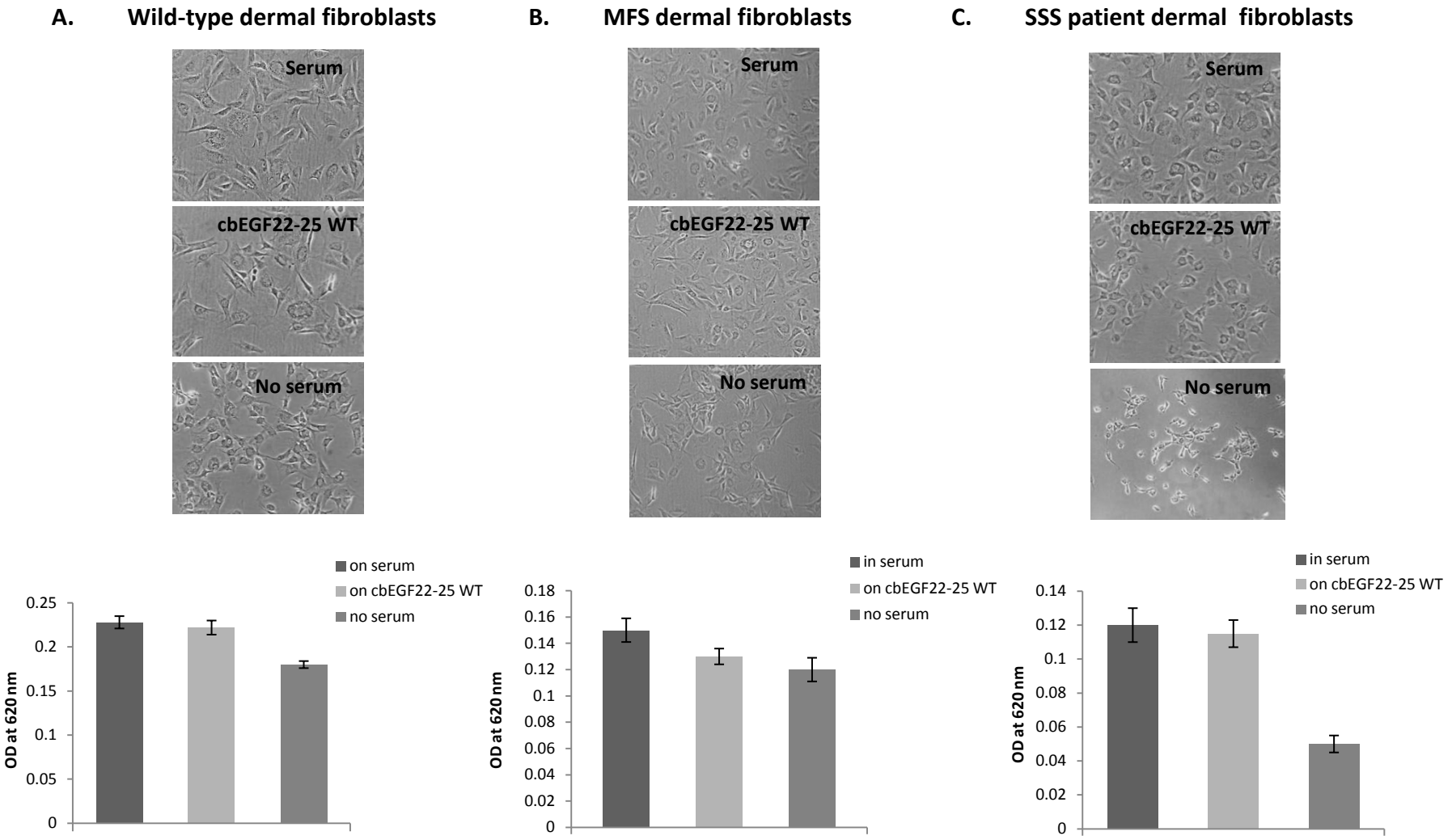

Figure 5.13 Phase contrast images of wild-type **(A)** MFS **(B)** and SSS patient dermal fibroblasts **(C)** in the presence and absence of serum, and on cbEGF22-25 fibrillin-1 wild-type fragment and quantitative analysis of cell attachment below the images. Data are expressed as mean ±S.D. (attachment n=9), from three independent experiments. Results shown here are from three different SSS patient cell lines. Neonatal and adult dermal fibroblast cells were used as controls and a MFS patient cell line containing the C1589F substitution in TB4 was used to compare.

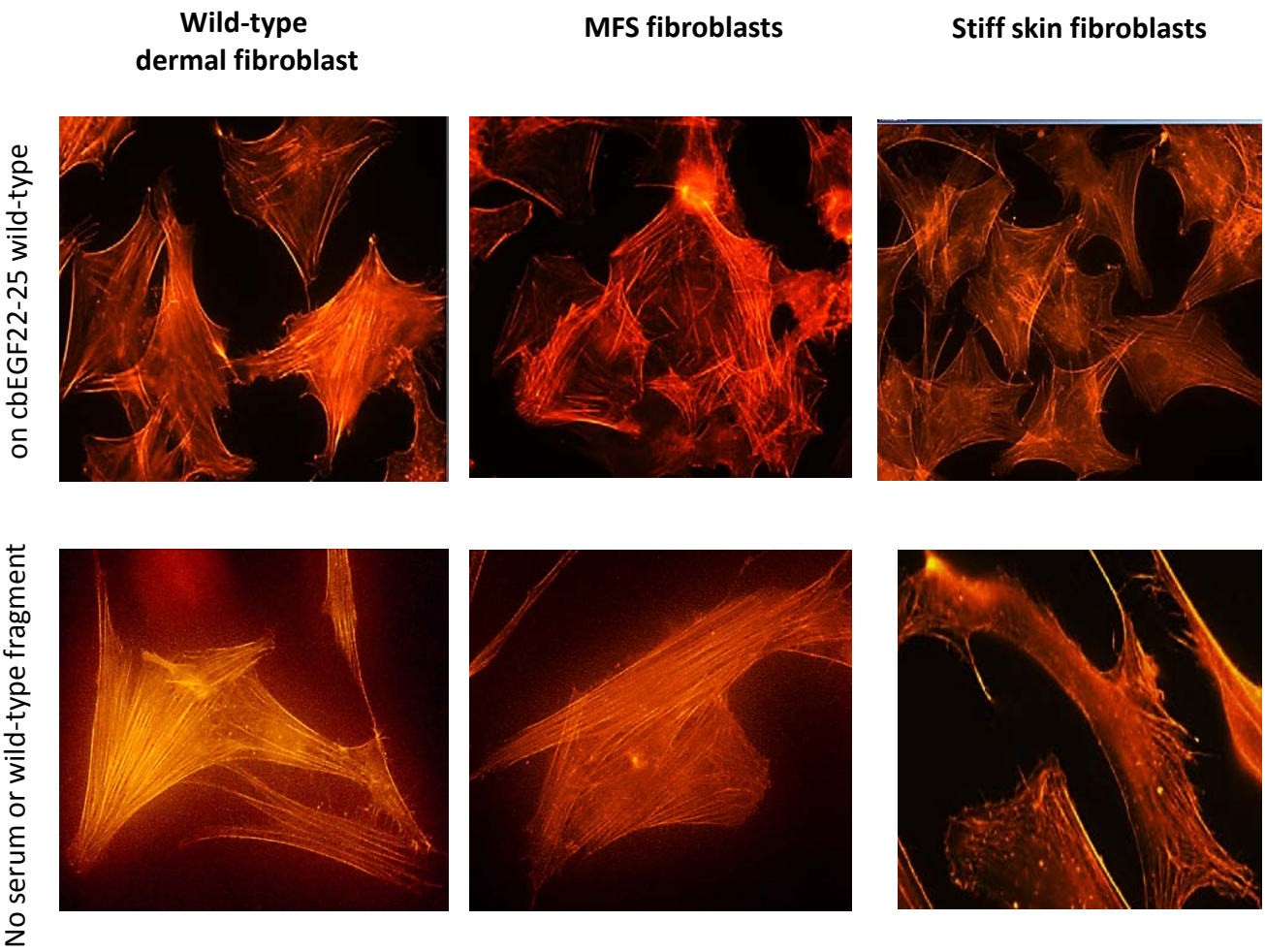

Figure 5.14 Difference in cell morphology between control, MFS and SSS patient dermal fibroblasts. Control, Marfan syndrome and Stiff Skin syndrome patient fibroblasts were seeded on chamber slides and allowed to grow for 72 hours. Cells were stained for F-actin using a fluorescently labelled phalloidin conjugate and show long filaments of F-actin, in the presence of a wild-type ECM ligand (cbEGF22-25 wild-type fibrillin-1 fragment), which is a marker of a well spread cell. In the absence of any exogenous ECM component, SSS patient cells expressing their own matrix fail to spread properly and show diffused F-actin staining, a reduction of polymerised F-actin as a result of a poorly spreading cell. Wild-type cells and MFS cells show normal actin staining on their own matrix after 72 hr.

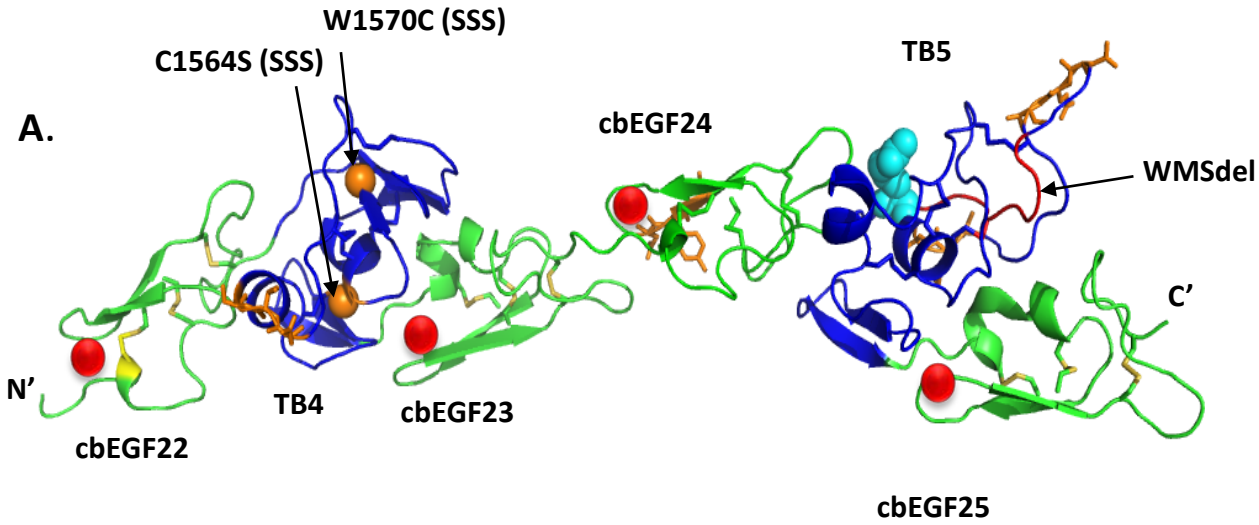

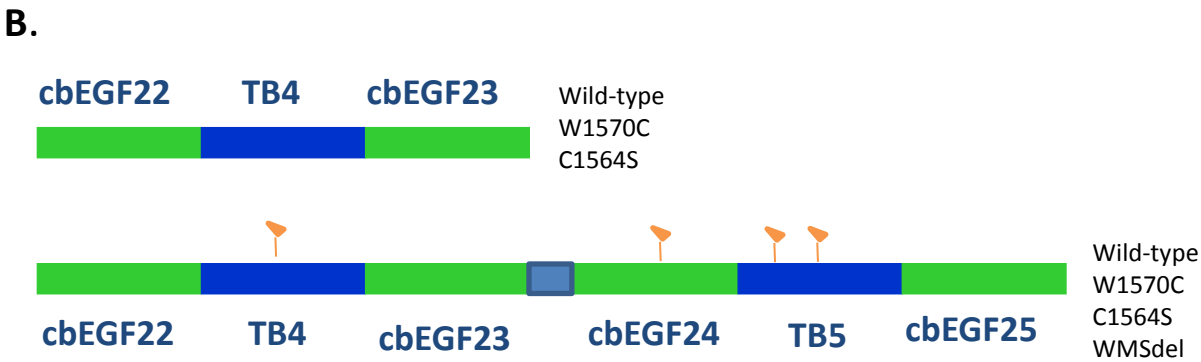

Figure 6.1 Fibrillin-1 cbEGF22-25 fragment. A. cbEGF22-25 homology model based on the crystal structure of cbEGF22-TB4-cbEGF23 showing SSS susbtitutions and WMS deletion. The cbEGF domains are in green and TB domains are in blue. Calcium ions bound to the cbEGF domains are shown as red spheres; disulphide bridges as yellow sticks; integrin-binding RGD motif is shown in red; potential N-linked glycosylation sites as orange sticks and heparin binding residues as cyan spheres (homology model created using Modeller 9v6 and rendered using PyMol). **B. Schematic representation of overlapping wild-type and mutant fragments.** Orange bars on these fragments show N-linked post-translational modifications as cbEGF22-25 fragments were produced in a mammalian expression system.

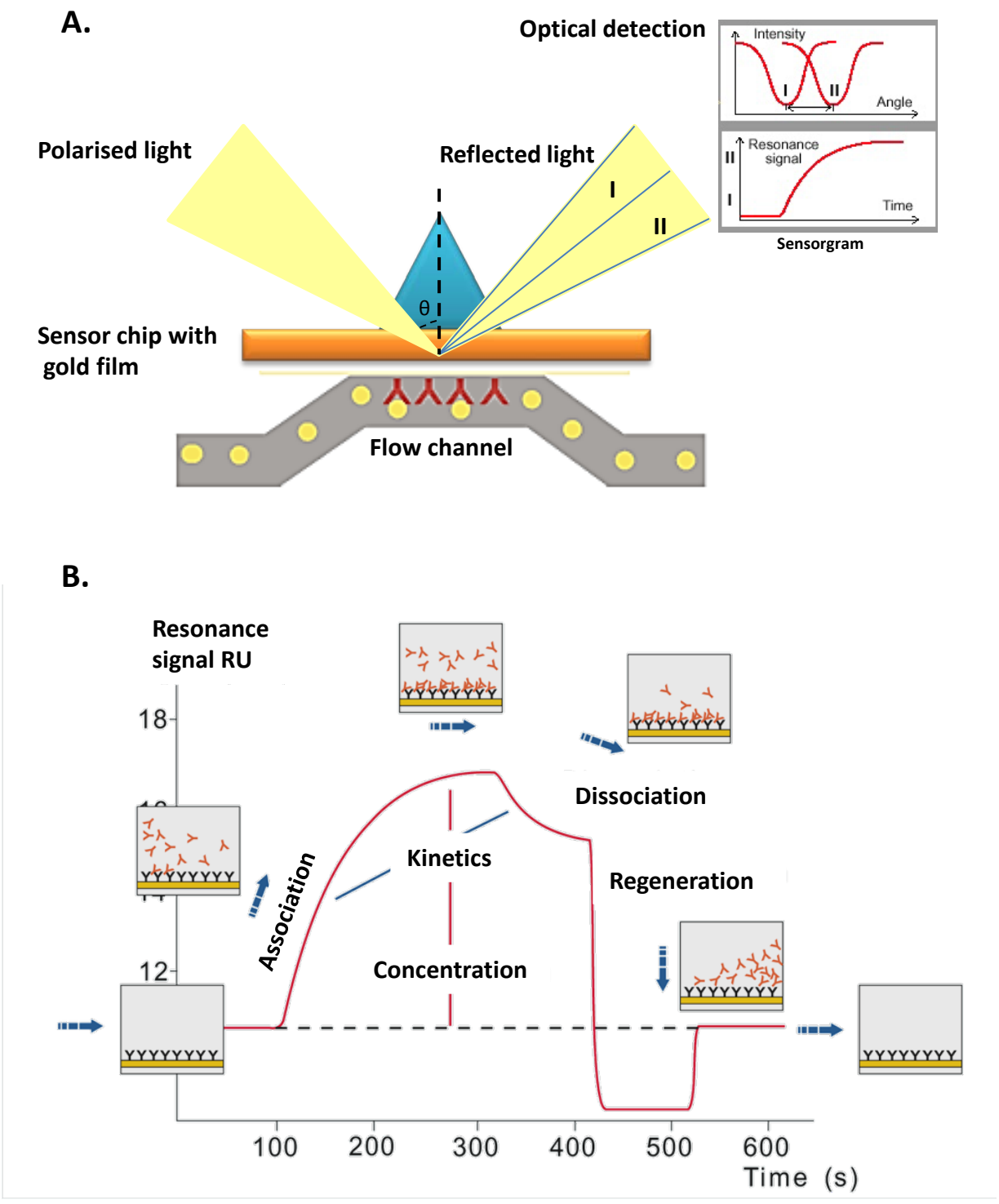

Courtesy Biacore International AB

Figure 6.2 A. The incident angle at which SPR occurs (SPR angle) is a function of the refractive index of the solution flowing over the sensor surface. As analyte-ligand complexes accumulate, the refractive index of the solution close to the gold film changes, and alters the momentum of the surface plasmons. The incident light angle at which resonance occurs consequently shifts. This shift is proportional to the mass of bound material, and recorded as a function of time, gives rise to a sensorgram. **B**. A typical sensogram obtained on binding is shown (Biacore International AB).

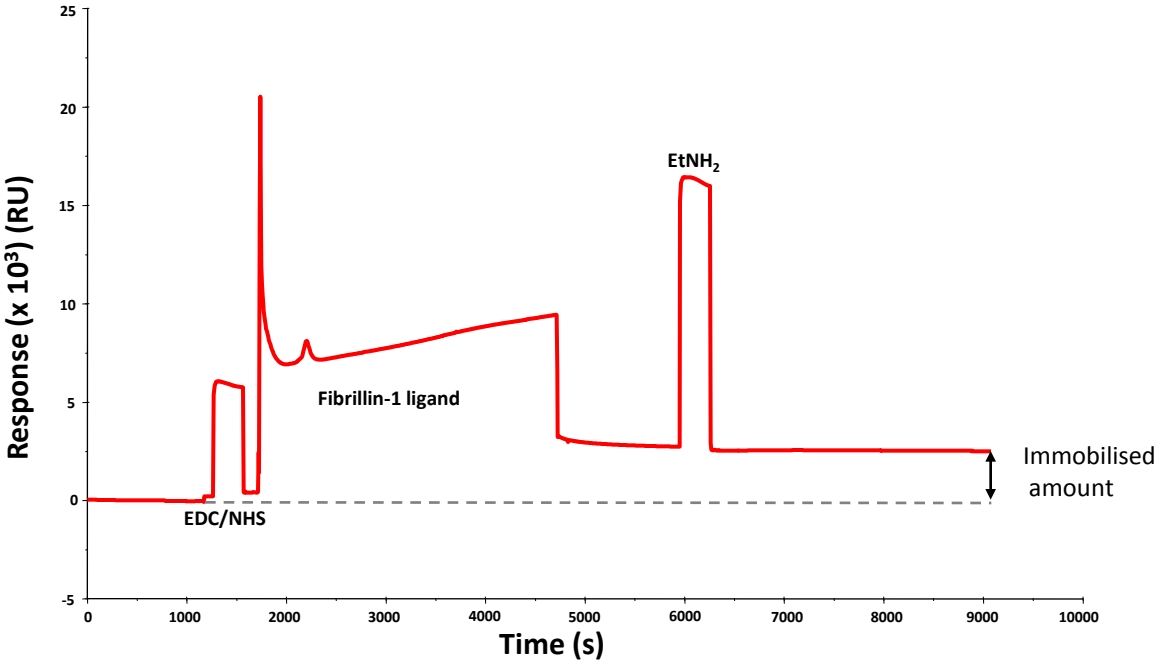

Figure 6.3. Amine coupling of cbEGF22-TB4-cbEGF23 to the surface of a CM5 sensor chip. The carboxymethyldextran matrix was first activated in a reaction with N-hydroxysuccinimide / N-ethyl-N'- (dimethylaminopropyl) carbodiimide hydrochloride (EDC/NHS). The protein was injected in 0.1 M NaOAc buffer pH 5.5 at the flow rate of 1 µl/min, and matrix subsequently deactivated with a pulse of ethanolamine ($EtNH_2$) (see Materials and Methods). Immobilisation of 1 ng/mm^2 of protein to the sensor surface leads to a response of ~1000 RU (Biacore International AB).

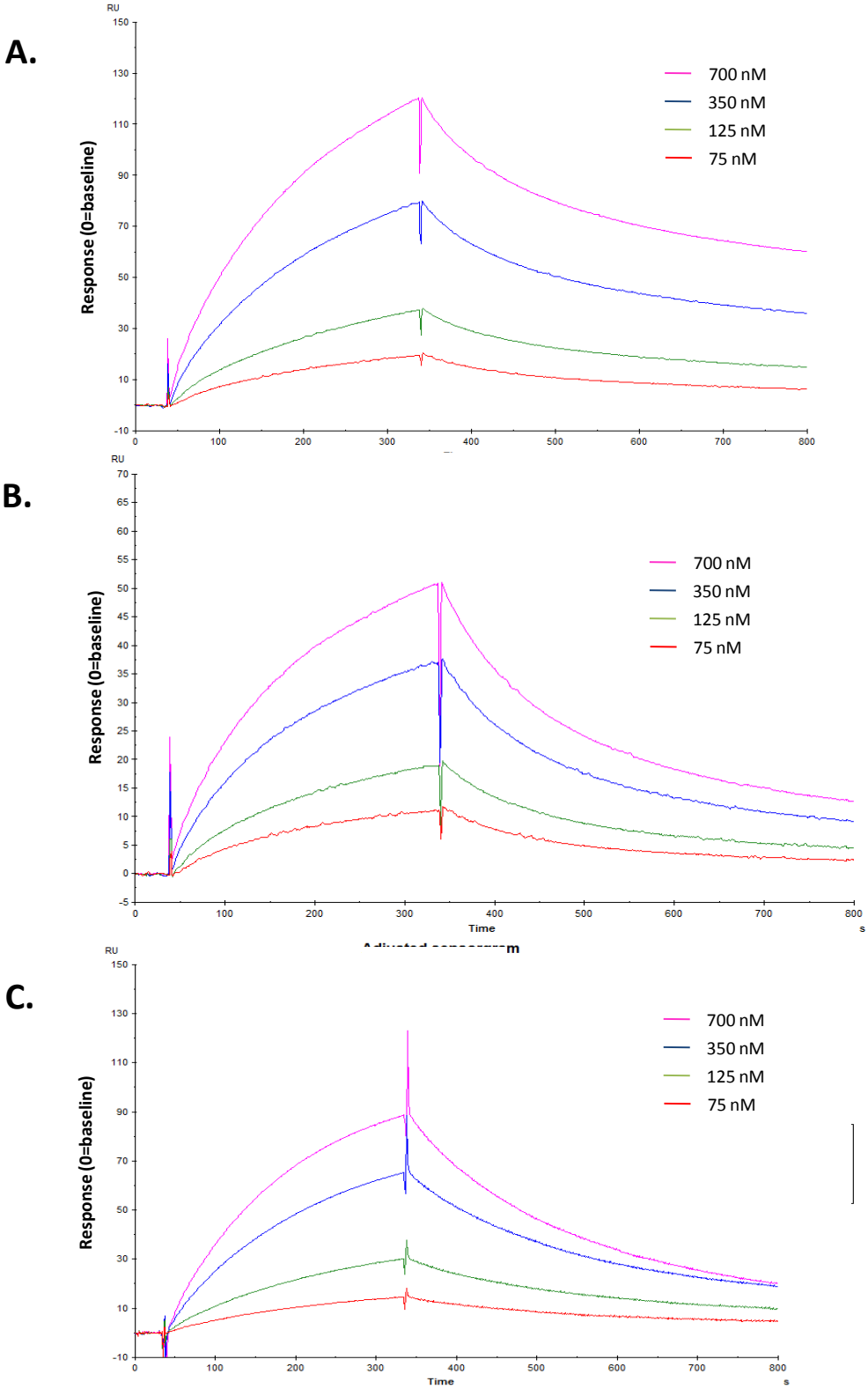

Figure 6.4. Comparison of the kinetics of αVβ6 binding to cbEGF22-TB4-cbEGF23 wild-type and SSS mutant fibrillin-1 fragments. Kinetics of dissociation**: ~**1000 RU of**,** cbEGF22-TB4-cbEGF23 wild-type (A), cbEGF22-TB4-cbEGF23 W1570C (B) and cbEGF22-TB4-cbEGF23 C1564S (C) were immobilised on the CM5 sensor surface, and recombinant αVβ3 integrin injected at 10 µl/min for 240 s. Sensorgrams shown were acquired with increasing concentrations of the integrin (75 – 700 nM), after subtracting the bulk response obtained with RGA mutant.

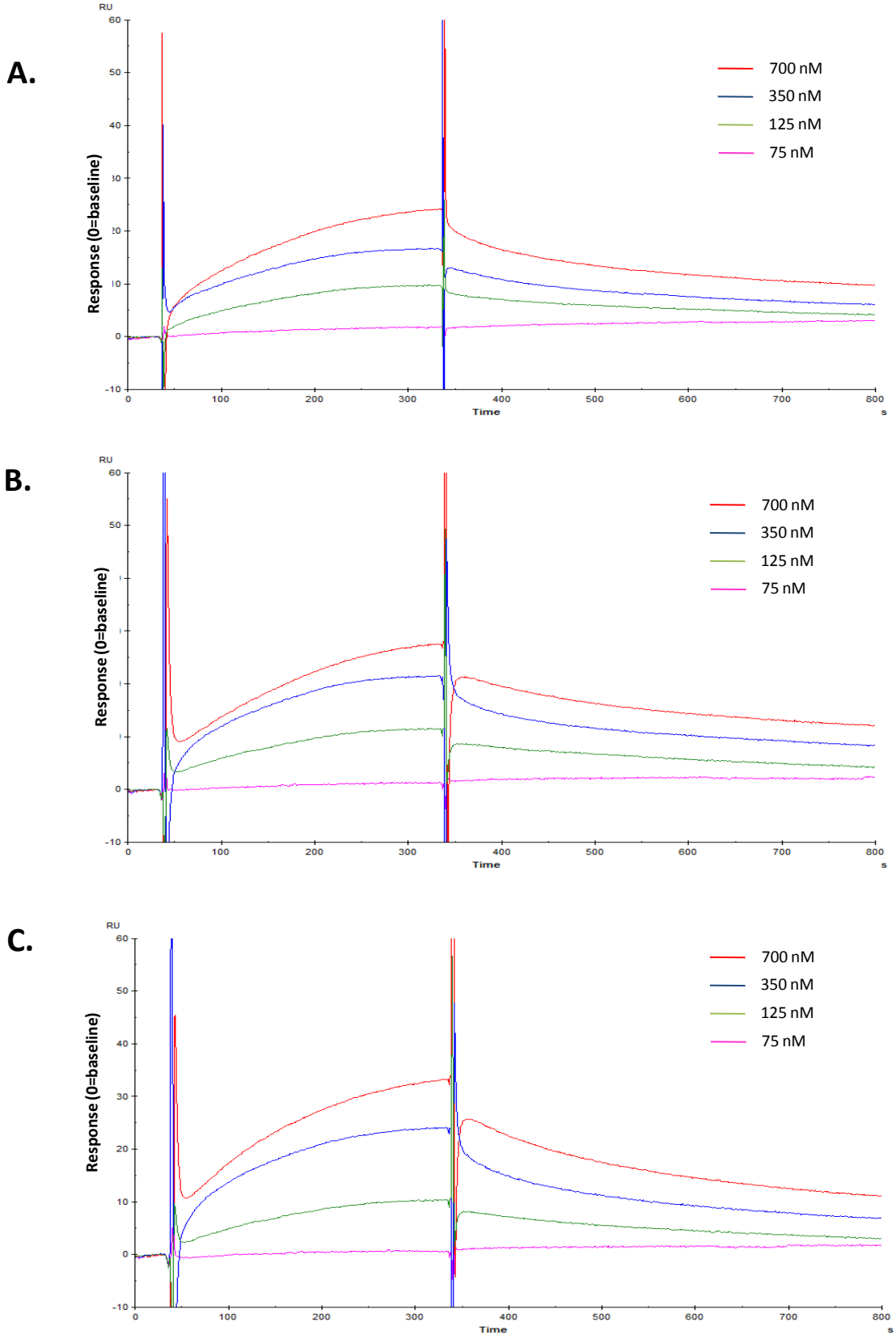

Figure 6.5. Comparison of the kinetics of αVβ6 binding to cbEGF22-25 wild-type and SSS mutant fibrillin-1 fragments. Kinetics of dissociation: ~1000 RU of, cbEGF22-25 wild-type (A), cbEGF22-25 W1570C (B) and cbEGF22-25 C1564S (C) were immobilised on the CM5 sensor surface, and recombinant αVβ3 integrin injected at 10 µl/min for 240 s. Sensorgrams shown were acquired with increasing concentrations of the integrin (75 – 700 nM), after subtracting the bulk response obtained with RGA mutant.

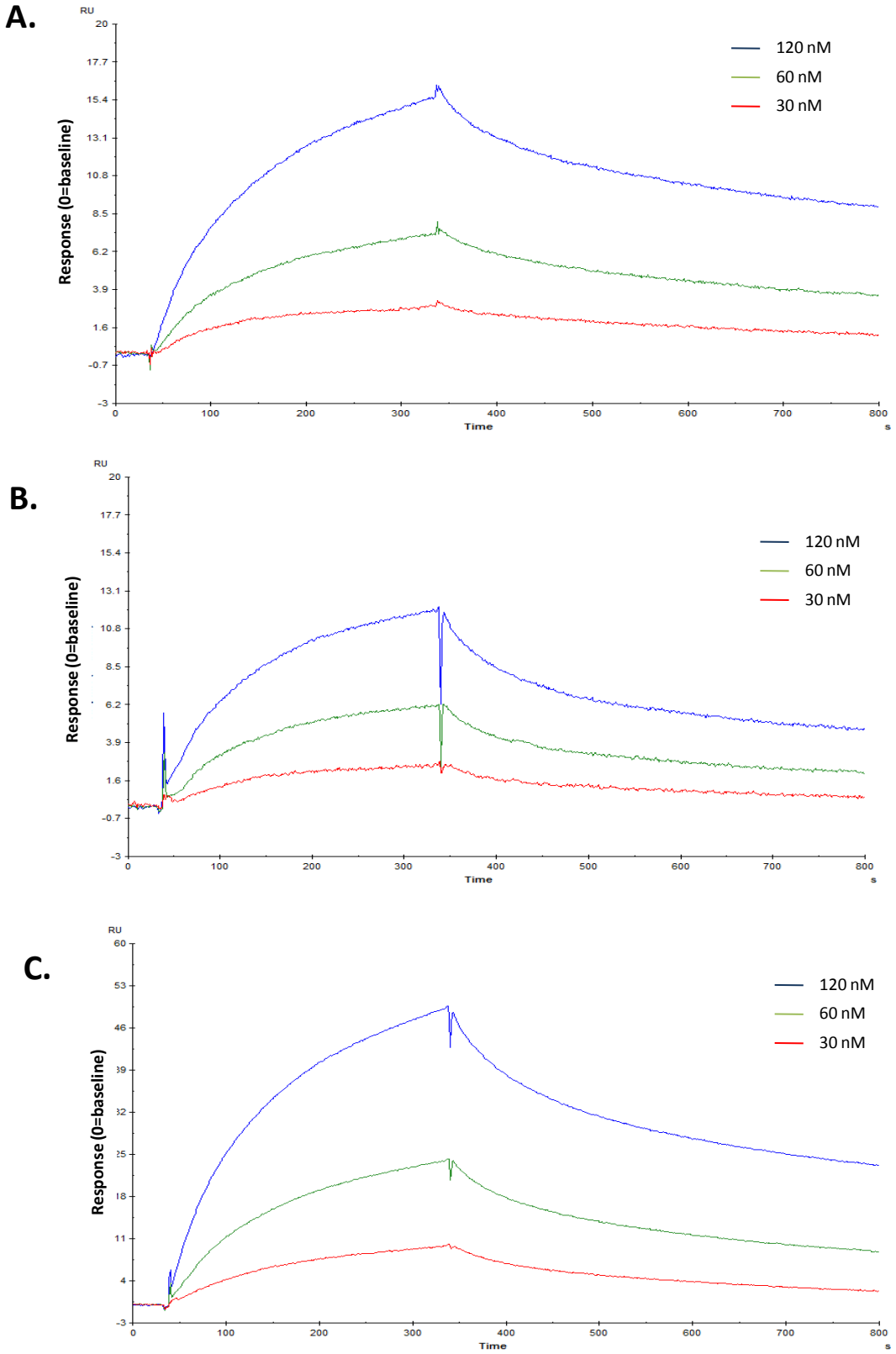

Figure 6.6. Comparison of the kinetics of αVβ3 binding to cbEGF22-25 wild-type and SSS mutant fibrillin-1 fragments. Kinetics of dissociation**: ~**1000 RU of**,** cbEGF22-25 wild-type (A), cbEGF22-25 W1570C (B) and cbEGF22-25 C1564S (C) were immobilised on the CM5 sensor surface, and recombinant αVβ3 integrin injected at 10 µl/min for 240 s. Sensorgrams shown were acquired with increasing concentrations of the integrin (30 – 120 nM), after subtracting the bulk response obtained with RGA mutant.

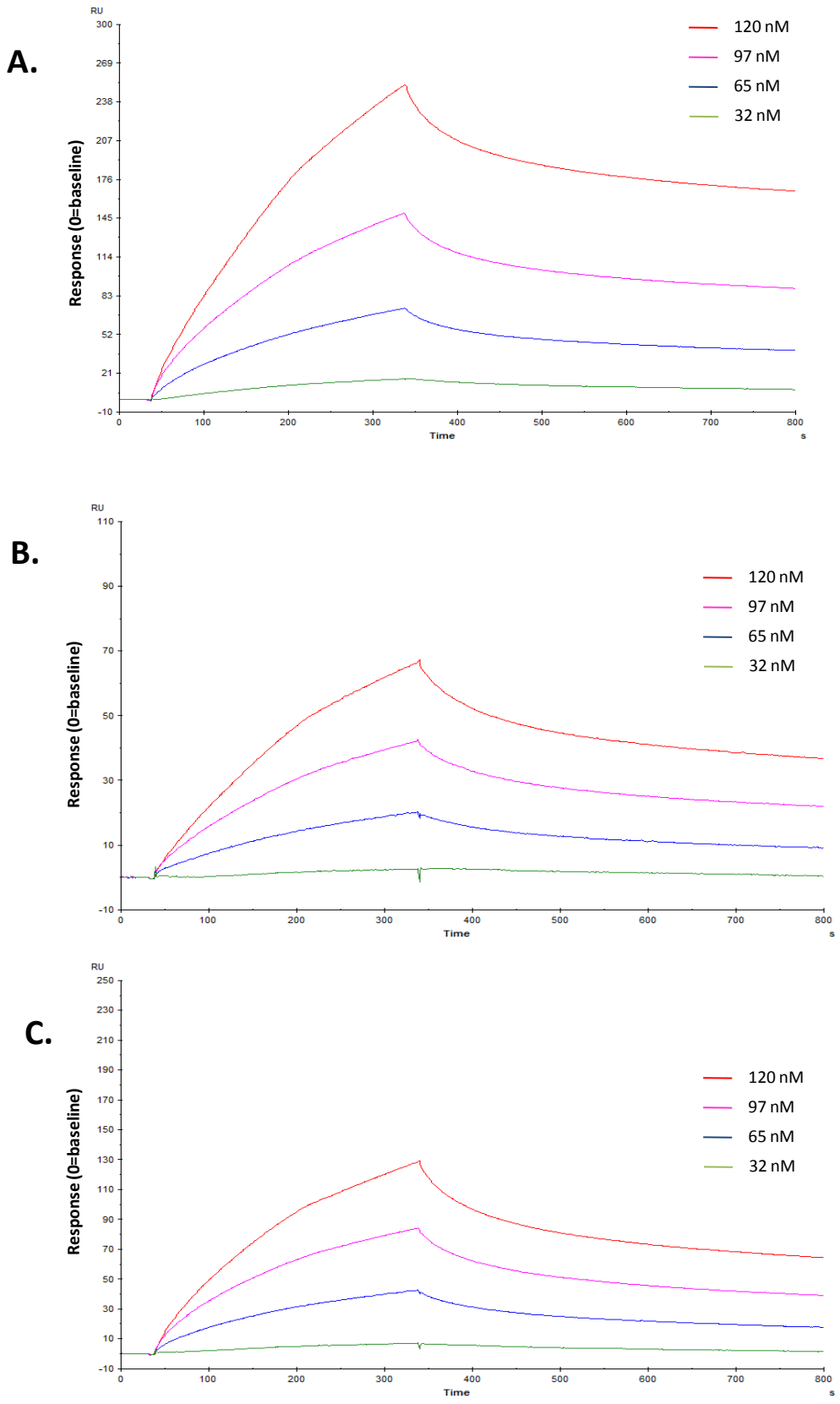

Figure 6.7. Comparison of the kinetics of αVβ3 binding to cbEGF22-TB4-cbEGF23 wild-type and SSS mutant fibrillin-1 fragments. Kinetics of dissociation: ~1000 RU of, cbEGF22-TB4-cbEGF23 wild-type (A), cbEGF22-TB4-cbEGF23 W1570C (B) and cbEGF22-TB4-cbEGF23 C1564S (C) were immobilised on the CM5 sensor surface, and recombinant αVβ3 integrin injected at 10 µl/min for 240 s. Sensorgrams shown were acquired with increasing concentrations of the integrin (32 – 120 nM), after subtracting the bulk response obtained with RGA mutant.

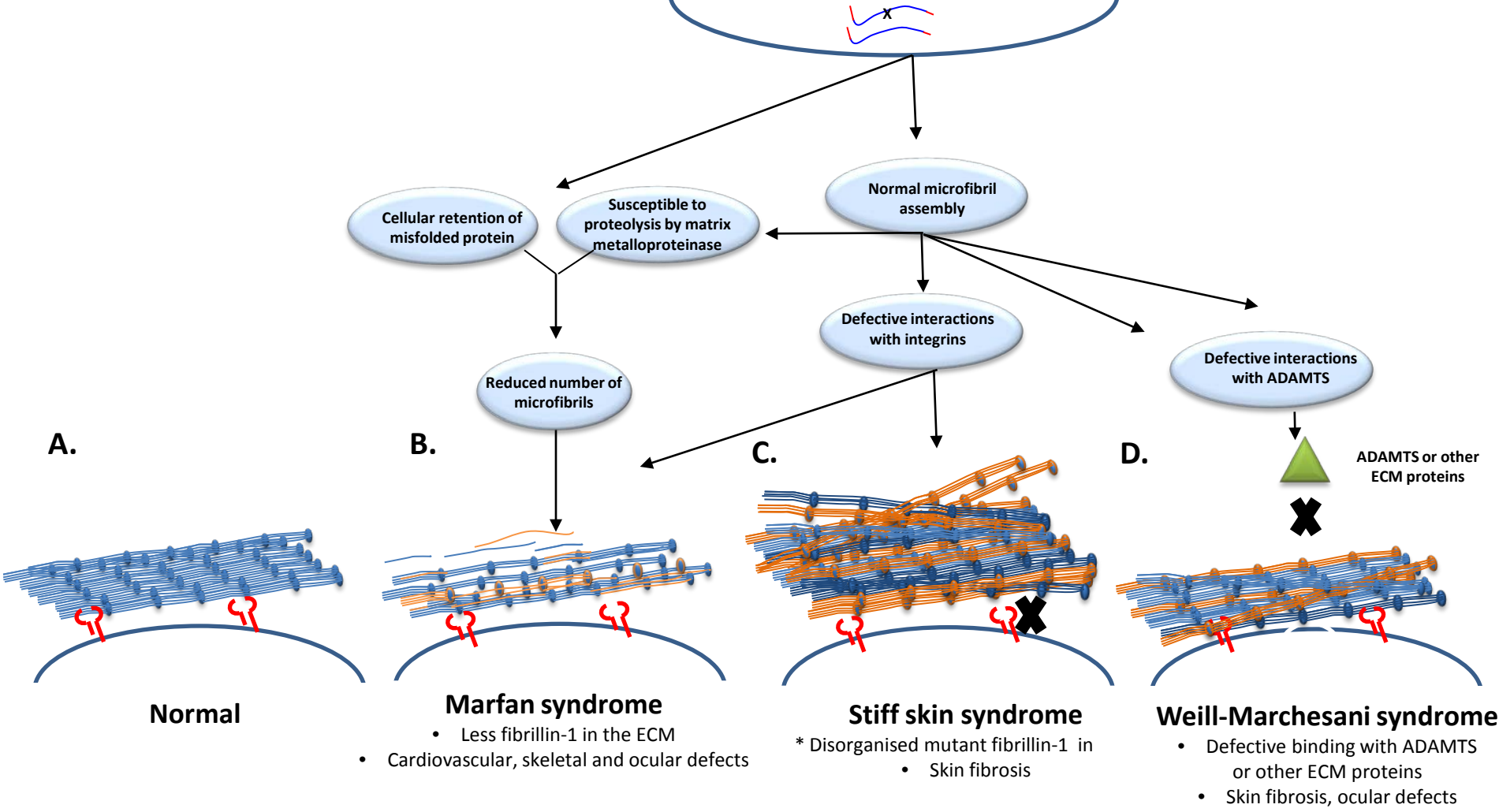

Figure 7.1 Different pathogenic mechanism that might be involved in MFS and SSS. A. There is normal interaction with integrins and other cell surface receptors. **B.** In MFS there is less fibrillin-1 in the ECM due to either delayed secretion, cellular retention or proteolytic degradation in ECM, leading to impaired microfibril assembly. The concentration of wild-type protein in the ECM in MFS might still be sufficient to interact with the integrins and other ECM molecules. **C.** In the case of the SSS, since the mutations are present in the integrin binding domain they affect interactions with integrins, which in turn induces increased integrin expression and/or bioavailability to participate in TGF-β activation, and this may contribute to downstream events leading to tissue fibrosis. **D.** WMS mutations in fibrillin-1 might indirectly affect integrin signalling and TGF-β activation *via* defective interactions with other proteins like syndecans and ADAMTS proteins. The importance of these different ECM interactions and the expression of these ECM molecules in different tissues may be responsible for their tissue-specific phenotype.

Disorder	Genes involved	Clinical phenotype	References
Marfan syndrome	FBN1 *(dominant)*	• **Dilatation or dissection of the aorta at the level of the sinuses of Valsalva** • **Ectopia lentis** • Dural ectasia • Skeletal abnormalities including long fingers and limbs, tall stature, joint hypermobility	Kainulainen K *et al.,* 1994
Stiff skin syndrome	FBN1 *(dominant)*	• **Short stature** • **Thickened skin** • **Progressive joint limitation and contractures**	Loeys *et al.* 2010
Weill-Marchesnai Syndrome	FBN1 *(dominant)* ADAMTS10 *(recessive)*	• **Short stature** • **Thickened skin** • **Ectopia lentis** • **Brachydactyly** • **Progressive joint limitation and contractures**	Faivre *et al.,* 2003
Ectopia lentis	FBN1 *(dominant)* ADAMTSL4 *(recessive)*	• **Ectopia lentis**	Kainulainen *et al.,* 1994
Geleophysic dysplasia Acromicric dysplasia	ADAMTSL2 *(recessive)* FBN1 ? *(dominant)*	• **Short stature** • **Thickened skin** • **Brachydactyly** • **Progressive joint limitation and contractures** • **Progressive cardiac valvular disease**	Spranger *et al.,* 1971 Faivre *et al.,* 2001

Table 7.1. List of disorders involving both fibrillin-1 and ADAMTS proteins. Similarities in clinical phenotype in different disorders have been highlighted in bold.

APPENDIX A

Oligonucleotide Primers

A. Primers for cloning cbEGF18-26 wild-type in pKG52 vector

Forward primer
5'- TAG TAG GTC GAC TT ACA GAC ATC AAT GAA TGT GAA ATT -3'

Reverse primer
5'- TAG TAG GTC GAC CTA TTA GTG ATG GTG ATG GTG ATG ATT GCA CTG TCC TGT GTG CTG CCA T CT CGA G -3'

Primers for cloning cbEGF22-25 wild-type in pSecTag vector

Forward primer
5'- TAG TAG GGC CCA GCC GGC CGA TGT GAA TGA ATG CCT GGA TC-3'

Reverse primer
5'-TAG TAG GTC GAC CTA TTA GTG ATG GTG ATG GTG ATG TGC TGA TTC ACA AAC CAA CAA CTT GTC-3'

B. Primers for mutagenesis

W1570C Forward primer:
5'- GGT AAA GCC TGT GGT ACT CCT TGT GAG ATG TG -3'

W1570C Reverse primer:
5'- AGG AGT ACC ACA GGC TTT ACC CAG AGA AC-3'

C1564S Forward primer:
5'- TCC TGC TGC TCT TCT CTG GGT AAA GCC TGG GG -3'

C1564S Reverse primer:
5'- ACC CAG AGA AGA GCA GCA GGA AGC TTT GGA AAC -3'

C1564Y Forward primer:
5'- TCC TGC TGC TAT TCT CTG GGT AAA GCC TGG GG -3'

C1564Y Reverse primer:
5'- ACC CAG AGA ATA GCA GCA GGA AGC TTT GGA AAC -3'

WMSdel Forward primer
5'-TGC ATG GAT ATG AGA TAT GCT GAC AAC CAG ACC TG-3'

WMSdel Reverse primer
5'-CA GGT CTG GTT GTC AGC ATA TCT CAT ATC CAT GCA ATT ATT TCC-3'

** DNA sequence mutated has been highlighted in yellow*

Table 1.1 shows the molar extinction coefficient (ε) and Molecular mass in Da of the TB4-containing wild-type and mutant construct used for protein quantitation.

Protein	Reduced	Refolded
cbEGF22-TB4-cbEGF23 WT BirA **ε**	21602.2 17780	21581.2 18980
cbEGF22-TB4-cbEGF23 W1570C BirA **ε**	21519.1 12950	21497.1 14325
cbEGF22-TB4-cbEGF23 C1564S BirA **ε**	21586.1 18450	21566.1 19700
3x cbEGF22-TB4-cbEGF23 C1564Y BirA **ε**	21662.2 19940	21642.2 21190
TB4cbEGF23 WT **ε**	15458.2 11460	15444.2 12335
TB4cbEGF23 W1570C **ε**	14871.5 11460	14858.5 12210
TB4cbEGF2323 C1564S **ε**	14804.5 5960	14789.5 6835

Calculation of Molar extinction coefficient (using ProtParam)

Extinction coefficients

The extinction coefficient (**ε)** indicates how much light a protein absorbs at a certain wavelength. It is useful to have an estimation of this coefficient for following a protein which a spectrophotometer when purifying it.

It has been shown (Pace et al. 1995) that it is possible to estimate the molar extinction coefficient of a protein from knowledge of its amino acid composition. From the molar extinction coefficient of tyrosine, tryptophan and cystine (cysteine does not absorb

appreciably at wavelengths >260 nm, while cystine does) at a given wavelength, the extinction coefficient of the native protein in water can be computed using the following equation:

ε (Protein) = **Number of (Tyr)** x **ε (Tyr)** + **Number of (Trp)** x **ε (Trp)** + **Number of (Cystine)** x **ε (Cystine)**

where **ε** (Tyr) = 1490, **ε** (Trp) = 5500, **ε** (Cystine) = 125;

The absorbance (optical density) can be calculated using the following formula:

Absorbance (Protein) = **ε** (Protein) / Molecular weight

APPENDIX B

DNA techniques

10 x PCR buffer:	100 mM KCl/ 60 mM $(NH_4)SO_4$/200 mM $MgCl_2$/1% Triton X-100/ 100 μg nuclease-free BSA.
10 x TBE buffer:	108.8 g Tris-HCl/ 55.4 g Boric acid/ 9.3 g EDTA.
3 M KOAc:	58.8 g KOAc/ 23 ml acetic acid/ to 200 ml total volume with H_2O.
5 x ligase buffer:	10 mM rATP (25 μl) 1 M Tris pH 7.5 (12.5 μl) 1 M $MgCl_2$ (2.5 μl) 1 M DTT (3.5 μl) H_2O (6.5 μl)
1% agarose:	0.5 g agarose (Roche) in 50 ml heated TBE buffer with 3 μl ethidium bromide.
6 x glycerol loading	0.25% (w/v) bromophenolblue/ 30 mM EDTA (pH 8.0)/ buffer: 30% (w/v) glycerol.

Bacterial growth

2xTy medium:	16 g Triptone/ 10 g yeast extract/ 5 g NaCl/ to 1 l total volume with H_2O, pH to 7.0-7.2
KA Plates:	Agar plates with 100 μg/ml ampicillin and 25 μg/ml kanomycin.
Ampicillin:	50 mg/ml stock solution, stored at –20 °C.
Kanamycin:	50 mg/ml stock solution, stored at –20 °C.

Protein purification

6 M guanidine buffer:	60 g guanidine-HCl/ 10 ml 0.5 M $NaPO_4$ pH 7.4, H_2O to 100 ml, add 25 μl EtSH
HPLC Buffer A:	0.1% Trifluoroacetic acid in milli-Q H_2O (pH 2.5-3).

HPLC Buffer B: 80% Acetonitrile / 0.1% Trifluoroacetic acid / milli-Q H_2O. (pH 2.5-3).

Milli-Q H_2O: Ultra pure water.

SDS-PAGE

16% polyacrylamide: 8 ml 40% acrylamide/ 4 ml 5 x separating buffer/ 8 ml resolving gel: milliQ-H_2O/ 300µl APS/ 30 µl TEMED.

6% polyacrylamide 1.5 ml 40% acrylamide/ 2 ml 5 x stacking buffer/ 6.5 ml stacking gel: milliQ-H_2O/ 200 µl APS/ 20 µl TEMED.

5 x separating buffer: 46 g Tris/ 1 g SDS/ 200 ml H_2O, pH to 8.8 with HCl

5 x stacking buffer: 30.25 g Tris/ 1 g SDS/ 200 ml H_2O, pH to 6.8 with HCl

5 x running buffer: 90 g glycine/ 18.75 g Tris/ 5 g SDS/ 1 l H_2O

Laemmli's sample 10% glycerol/ 3% SDS/ 50 mM Tris-Cl pH 6.8, trace BPB,buffer: 5% EtSH

Coomassie stain: 1.25 g Coomassie Blue R/ 10% MeOH/ 10% acetic acid

De-stain solution: 10% MeOH/ 10% acetic acid

Protein analysis

Calcium-free buffer: 1 M Tris-HCl pH 7.5 made with milli-Q H_2O containing chelex 100 Ca^{2+} chelating resin (Bio-Rad)

D_2O buffer: 100% ^2H_2O containing 5 mM Tris-DCl adjusted to pH 6.5 using DCl and NaOD.

APPENDIX C

Recombinant integrins used for SPR

Recombinant αvβ3 and α5β1 integrins were a kind gift of Dr Takagi, Osaka Japan and were prepared as described in Takagi *et al.,* 2002 (αvβ3) and Takagi *et al.,* 2001 (α5β1). Soluble α5β1 and αvβ3 integrin were prepared with heterodimer extracellular fragments in which interactions between - and -subunit cytoplasmic domains were replaced with an artificial clasp.

Soluble recombinant αvβ6 integrin was a kind gift by Dr. N. Abrescia, CIC bioGUNE, Spain and purified as described in Weinacker *et al.,* 1994. The truncated integrin only contained the extracellular domains which interacts with ECM ligands. FPLC (i) and SDS-PAGE (ii) profiles of purified αvβ6 recombinant integrin, which was used in SPR binding assays. αv* indicates the band that corresponds to the highly glycosylated αv (purity ~70-80%). The molecular marker is from Fermentas (Page Ruler unstained Protein ladder).

(i) (ii)